Title
Mechanisms of gestation length timing in mice

Author
McIntyre, Tara

Publication Date
2024

Peer reviewed|Thesis/dissertation

Mechanisms of gestation length timing in mice

by
TARA MCINTYRE

DISSERTATION
Submitted in partial satisfaction of the requirements for degree of
DOCTOR OF PHILOSOPHY

in

Biomedical Sciences

in the

GRADUATE DIVISION
of the
UNIVERSITY OF CALIFORNIA, SAN FRANCISCO

Approved:

DocuSigned by:
Susan Fisher
3D7FD5EAA89E411...

Susan Fisher
Chair

DocuSigned by:
Adrian Erlebacher
[illegible]

Adrian Erlebacher

DocuSigned by:
Hiten D. Madhani
[illegible]

Hiten Madhani

DocuSigned by:
Daniel Lim
FC7A2B6D45EF428...

Daniel Lim

Committee Members

To Greg, for your love and patience.

Acknowledgments

First and foremost, this endeavor would not have been possible without the exceptional guidance and support provided by my mentor, Dr. Adrian Erlebacher. My decision to pursue my graduate work in Adrian's lab was initially influenced by his reputation as a rigorous, thoughtful, and careful scientist. While he undoubtedly lived up to this reputation, what truly set my doctoral journey apart were three additional facets of his mentoring style. First, Adrian's scientific boldness, exemplified by his readiness to follow the science wherever it may lead, has not only enhanced the depth of my graduate work but also made me into a more versatile and well-rounded scientist. Second, while Adrian consistently granted me the autonomy and liberty to explore ideas independently (for which I was grateful), he was also always available to talk through a problem, help think through an analysis, or strategize the execution of a complicated experiment. This type of mentorship was critical in building my confidence as a scientist. Finally, Adrian's unwavering belief in my abilities pushed me to heights I never knew I could achieve. These qualities were not only an incredible source of motivation over the years but have undoubtedly made me into the scientist I am today.

I am sincerely thankful for my thesis committee, Drs. Susan Fisher, Hiten Madhani, and Daniel Lim. These three individuals consistently shared their expertise in reproductive biology, epigenetics, and KDM6B, provided thoughtful feedback on my manuscript, and helped guide me during times of uncertainty or confusion. Susan has not only been the most wonderful thesis chair, but also an inspiration and role model for women in science. I will never forget the hug she gave me after I told her I was pregnant. I look up to Hiten for many reasons but one of which is his sincere dedication to his trainees. He never hesitated to connect me with colleagues to help me with a technique, particular analysis, or think through a scientific idea. His words of

encouragement and support gave me the confidence and motivation I needed to get through tough times (I will always look back on his response to the final draft of my manuscript as a source of motivation and happiness). I met Dan for the first time during a turning point in the project and will forever be grateful for his guidance and advice. He always put me and my career first and I owe him for that.

I am eternally grateful for the scientific mentors who shaped my interest in research and encouraged me to pursue a Ph.D., including Peter Rabinovitch (University of Washington), Ursula Garrigues (ZymoGenetics), Tao Sai (Genentech), and Margaret Feeney (UCSF). The Rabinovitch lab introduced me to the world of research, Ursula Garrigues taught me how to run my first ELISA, and Tao Sai instilled in me a sense of scientific efficiency. I extend my sincerest gratitude to Margaret Feeney, who provided me with the opportunity to spend 3 years post-undergraduate growing into my role as a scientist, falling in love with maternal-fetal tolerance and building the confidence to apply to PhD programs. I would also like to thank Drs. Prasanna Jagannathan, Pamela Odorizzi, and Mary Prahl for their patience, guidance, and steadfast support during my tenure in the Feeney Lab. Upon leaving the Feeney Lab, Dr. Jagannathan wrote me a letter that I kept in my desk drawer in the Erlebacher Lab and re-read frequently as a source of motivation ("You have hands like Jesus!"). And last, but certainly not least, thank you to Rachel Budker, my partner in crime, best friend, and inspiration. Those days in the Feeney lab together were some of my favorites. My dream is to work together again someday.

I am so thankful for my collaborators whose time and efforts have significantly enriched and shaped the content of this work. To start, Dr. Alexis Combes has been a collaborator since the project's inception, offering not only invaluable assistance in the design and execution of the single-cell experiments, but also serving as a thoughtful and supportive mentor. Other members

and collaborators of the Combes lab were also integral to the project, including Brittany Davidson, Bushra Samad, and Kenneth Hu. Thank you for your patience, diligence, and dedication.

The day-to-day experience of my PhD journey would have been markedly different without the companionship of my fellow Erlebacher lab members, a group of remarkably hardworking, intelligent, and inspiring individuals. Specifically, I would like to thank Dr. Gabrielle Rizzuto, who I was first introduced to as my rotation mentor and has since become one of my closest friends. Through memes, music, our shared love of Ladle and Leaf, books, and obvious shared love of science, our friendship deepened over a very short period of time. She has been a continual source of support and encouragement throughout my PhD and was always there when I needed her –celebrating every triumph or offering solace on challenging days. Despite being miles and miles apart now, she continues to make me laugh, inspires me to be a better scientist, and is the most thoughtful listener. Second, I would like to thank Johan Siewiera, who has been an invaluable resource, mentor, and friend throughout my PhD. Johan taught me how to dissect my first pregnant uterus, isolate prostaglandins from tissue, measure progesterone levels, and so much more. After I submitted my manuscript, he emailed me a Churchill quote that said: "Now this is not the end. It is not even the beginning of the end. But it is, perhaps, the end of the beginning." Thank you.

Beyond the Erlebacher lab, I am fortunate to have friends with whom I can laugh with during times of joy and find solace during times of despair. Thank you Casey, Camillia, Lindsey and Denise from my UCSF PhD cohort, with whom I have shared countless glasses of wine and many wonderful meals.

My time at UCSF would not have been successful without the support of my friends. Whether it was the shared joy of savoring delicious meals, embarking on memorable travel adventures, immersing ourselves in music, or engaging in heartfelt conversations, my friends played important roles both in supporting my academic endeavors while also reminding me of the richness of life outside of lab. Thank you: Xana & Charlie, Chris & Carrie, Marshall & Elisabeth, Katie & Jon, Blair & Tom, Taylor, India, Britt & Ryan, Joe & Andrea, CJones, Owen, Sarah, and Viken & Maria.

I would not be where I am today without the love and support from my families. Thank you to the Sanfords, who have always made me feel like one of their own and believe in me more than I believe in myself. Thank you to my older sister, Katie, who has shown me what it's like to balance a successful career and raise a beautiful family, inspiring me in both personal and professional aspects of my life. Thank you to my younger sister, Ellie, whose support is a comforting mix of empathy, humor, and unwavering encouragement, making her a pillar of strength in my life. Thank you to my brother Joe, whose passion for life and learning has inspired me to dream bigger and ask more questions. And finally to my parents – thank you for the sacrifices you made to afford me the best opportunities, for your unwavering support of my dreams, and for showing me what it means to live a rich, curious and fulfilling life. You somehow managed to teach me so much without ever telling me what to do. I love you.

Lastly, I dedicate this dissertation to my husband Greg. You've been by my side for every step of this journey, consistently offering comfort in times of need and joyously celebrating every success, big or small. You made countless sacrifices over the past six years, all to support this dream of mine. I want you to know that those sacrifices did not go unnoticed, and that I am

forever appreciative of your selflessness. Your enduring commitment has made this not just my journey but our shared triumph.

Advisor's Statement

Regarding inclusion of material with multiple authors

Chapter 3 has been previously published as "Circumvention of luteolysis reveals parturition pathways in mice dependent upon innate type 2 immunity" in Immunity 56(3):606-619 (2023), with Dr. Johan Siewiera as first author and Tara McIntyre as second author. As stated below in the "Contributions" section, as well as at the beginning of Chapter 3, Tara McIntyre performed the experiments in Figures 3.7A-E and 3.14A-F (Figures 7A-E and S7A-F in the published article) and made significant intellectual contributions to the work.

Adrian Erlebacher, M.D., Ph.D.

Dissertation Advisor

Contributions

Chapters 1, 4, 5, and 6 were written by Tara McIntyre. Chapter 6 also incorporates unpublished data generated by Dr. Akanksha Onkar (Figure 6.2).

Chapter 2 was adapted from the following manuscript, written by Tara McIntyre and Adrian Erlebacher, and currently under review:

McIntyre, T. I., Davidson, B., Samad, B., Valdez, O., Qiu, L., Hu, K., Combes, A. J., & Erlebacher, A. (2024). An epigenetic timer of gestation length in mice.

Additional author contributions for Chapter 2 are described in the Author Contributions section at the end of the chapter.

Chapter 3 was adapted from the following article, written primarily by Johan Siewiera and Adrian Erlebacher, and published in *Immunity*:

Siewiera J, McIntyre TI, Cautivo KM, Mahiddine K, Rideaux D, Molofsky AB, Erlebacher A. Circumvention of luteolysis reveals parturition pathways in mice dependent upon innate type 2 immunity. Immunity. 2023 Mar 14;56(3):606-619.e7. doi: 10.1016/j.immuni.2023.01.005. Epub 2023 Feb 6. PMID: 36750100; PMCID: PMC10023352.

Additional author contributions for Chapter 3 are described in the Author Contributions section at the end of the chapter. I performed the experiments shown in Figures 3.7A-E and 3.14A-F.

Epigraph

Time is the wisest of all things that are; for it brings everything to light.

Thales

Mechanisms of gestation length timing in mice

Tara McIntyre

Abstract

Timing mechanisms in biology remain poorly understood. As one prime example, little is known about the mechanisms that specify how long the gestating uterus will remain quiescent before entering labor. Our lack of insight into this fundamental question, which applies to all mammalian species, also limits investigation into potential causes of preterm labor, a major human pregnancy complication. My dissertation work provides evidence that gestation length in mice is determined by an epigenetic timer that runs autonomously within the fibroblasts of the pregnant uterus. The timer is set during the peri-implantation period when select loci establish appropriate levels of the repressive histone mark H3K27me3. These loci then progressively lose H3K27me3, thereby scheduling the uterine cell state transitions and associated gene expression changes of late gestation that are the proximal mediators of luteolysis (progesterone withdrawal) and labor onset. Initial overwinding of the timer via genetic ablation of the histone demethylase KDM6B delays these transitions and extends gestation length. My findings also demonstrate requirements for KDM6 demethylases in inflammation-induced preterm labor, and suggest potential requirements for KDM6B in the uterus-intrinsic pathways of parturition that are distinct from luteolysis. These results unexpectedly implicate epigenetic pathways in fibroblasts as a top-level determinant of both normal and pathological parturition mechanisms. We anticipate that further dissection of the ways such fibroblast programming controls gestation length may suggest novel approaches for improving human pregnancy outcomes.

Table of Contents

Chapter 1: Fibroblasts and their role in pregnancy and parturition 1

Parturition mechanisms across species 1

Fibroblasts in the non-pregnant uterus 3

Fibroblasts during pregnancy: decidualized and undecidualized 6

A role for decidual activation in PTL, but not normal labor 7

A role for PDGFRα^{+} fibroblasts in mouse and human parturition 9

Overview of dissertation: a central role for fibroblasts in pregnancy and parturition 12

Figures 14

Chapter 2: An epigenetic timer of gestation length in mice 16

Summary 16

Introduction 16

Results 19

KDM6B is required for on time parturition in mice 19

On time parturition requires KDM6B function within uterine fibroblasts 20

H3K27me3 dynamics in uterine fibroblasts reveal KDM6B-dependent and -independent processes 22

A H3K27me3-dependent timer schedules fibroblast gene induction at mid-to-late gestation 24

Peri-implantation H3K27me3 tuning sets the gestational timer 26

Discussion 29

Acknowledgments 32

Author contributions 32

Figures 33

Methods and Materials 61

Chapter 3: Circumvention of luteolysis reveals parturition pathways in mice dependent upon innate type 2 immunity 77

Summary 77
Introduction 78
Results 80
IL-33 is required for on-time parturition when only uterus-intrinsic pathways are available to drive labor onset. *80*
PDGFRα^{+} interstitial fibroblasts in the myometrium, undecidualized endometrium and mesometrial triangle are the main sources of IL-33 in the pregnant uterus. *82*
Il33 deletion in uterine interstitial fibroblasts delays labor onset. *84*
Prior to labor onset, ILC2s expand in the mesometrial triangle and become highly activated in an IL-33-dependent fashion. *85*
ILC2 depletion or loss of ILC2 responsiveness to IL-33 delays labor onset. *87*
Decidual Ptgs2 induction is downstream of IL-33 in the prepartum uterus, but is non-essential for on time labor onset. *88*
Eosinophil turnover increases in the prepartum uterus and IL-5 is required for on time labor onset via uterus-intrinsic parturition pathways. *89*
Discussion 93
Limitations of the Study 98
Acknowledgements 99
Author Contributions 99
Figures 100
Methods and Materials 122
Chapter 4: H3K27me3 demethylases are required for inflammation-induced PTL 131
Introduction 131
Results 135
A potential role for KDM6A and KDM6B in LPS-induced uterus-intrinsic PTB pathways *135*
A role for KDM6B in LPS-induced luteolysis PTB pathways *136*

Early administration of LPS delays parturition in wild-type mice *137*

Administration of ATRA induces PTL in control, but not Kdm6b cKO mice *137*

Discussion 138

Figures 142

Methods and Materials 146

Chapter 5: Histone demethylase KDM6A is critical for murine decidualization and pregnancy 149

Introduction 149

Results 151

Kdm6a cKO mice exhibit early pregnancy loss *151*

Ablation of Kdm6a in the uterus leads to a defect in decidualization *152*

Stromal proliferation is intact, but differentiation is compromised in Kdm6a cKO DSCs *153*

Discussion 154

Figures 158

Methods and Materials 162

Chapter 6: Conclusions and Future Directions 165

Figures 176

References 179

List of Figures

Figure 1.1 Comparison of human and mouse pregnancy. 14

Figure 1.2 Spatially distinct subpopulations of fibroblasts in the mouse uterus. 15

Figure 2.1 *Kdm6b cKO* mice experience delayed parturition due to delayed luteolysis. 33

Figure 2.2 A KDM6B-influenced gene expression program within uterine fibroblasts controls parturition timing. 34

Figure 2.3 H3K27me3 dynamics in the fibroblasts of the pregnant mouse uterus involve KDM6B-dependent and -independent processes. 35

Figure 2.4 H3K27me3 erosion is detectable as early as GD8.5. 36

Figure 2.5 Progressive, locus-specific erosion of H3K27me3 in uterine fibroblasts is associated with the induction of linked genes at mid-to-late gestation. 37

Figure 2.6 H3K27me3 accumulation in uterine fibroblasts between GD0.5 and GD5.5 sets the gestational timer. 38

Figure 2.7 An epigenetic timer of gestation length in mice (proposed model). 39

Figure 2.8 Additional characterization of *Kdm6b cKO* mice. 40

Figure 2.9 Additional characterization of *Ltf-iCre Kdm6b*$^{f/f}$ and *Pdgfra-cre Kdm6b*$^{f/f}$ mice and scRNA-Seq analysis of the pregnant mouse uterus. 41

Figure 2.10 Purity analysis of uterine fibroblasts prior to and after Dynabead-based negative selection, assessed by flow cytometry. 43

Figure 2.11 Additional H3K27me3 CUT&RUN analyses. 44

Figure 2.12 Additional analysis of associations between gene expression and H3K27me3 dynamics in uterine fibroblasts. 45

Figure 2.13 Additional analysis of associations between gene expression and H3K27me3 dynamics in uterine fibroblasts. 46

Figure 2.14 Peri-implantation H3K27me3 dynamics in uterine fibroblasts. 47

Figure 3.1 IL-33 deficiency delays labor onset in mice when parturition occurs through uterus-intrinsic pathways. 100
Figure 3.2 Myo/endo and mesometrial triangle PDGFRα^{+} stromal cells are the main sources of IL-33 in the pregnant uterus 101
Figure 3.3 Cell type-specific requirements for *Il33* expression in parturition. 102
Figure 3.4 IL-33 dependent uterine ILC2 expansion and activation shortly before labor onset. 103
Figure 3.5 Distribution of ILC2s in the late gestation uterus. 105
Figure 3.6 Delayed labor onset in mice with depleted or IL-33-unresponsive ILC2s. 106
Figure 3.7 Eosinophil dynamics in the prepartum uterus and delayed labor onset in IL-5-deficient mice 107
Figure 3.8 Defects in uterus-intrinsic parturition pathways in *Il33*$^{-/-}$ mice. 109
Figure 3.9 Contributions of immune, endothelial and epithelial cells to uterine IL-33 production. 110
Figure 3.10 Characterization of stromal cells in the prepartum uterus 112
Figure 3.11 Identification of cell types in the GD7.5 and GD18.5 uterus with historical expression of *Pgr* 113
Figure 3.12 Identification of ST2-expressing cells in the uterus; analysis of uterine ST2^{+} T cell densities. 115
Figure 3.13 IL-33 enhances COX-2 expression in the late gestation decidua, but COX-2 activity is not a critical component of uterus-intrinsic parturition pathways. 117
Figure 3.14 Additional analysis of eosinophil dynamics and phenotypes in the late gestation uterus. 119
Figure 4.1 KDM6A and KDM6B are required for LPS-induced PTL. 142
Figure 4.2 KDM6B is required for LPS-induced PTL. 143
Figure 4.3 LPS injection in mid-gestation delays gestation length. 144
Figure 4.4 ATRA injection induces PTL in WT but not *Kdm6b cKO* mice. 145
Figure 5.1 Post-implantation failure in *Kdm6a cKO* mice. 158
Figure 5.2 KDM6A immunostaining of post-implantation uteri. 159

Figure 5.3 Impaired expression of decidualization genes in *Kdm6a cKO* DSCs. 160
Figure 5.4 Immunofluorescence detection of CD31 expression in control and *Kdm6a cKO* GD6.5 implantation sites. 161
Figure 6.1 Expression patterns of fibroblast genes potentially involved in epithelial COX-1 induction. 176
Figure 6.2 KDM6B deficiency in uterine fibroblasts delays labor onset in mice when parturition occurs through uterus-intrinsic pathways. 177
Figure 6.3 Expression patterns of genes potentially linked to uterus-intrinsic pathways of parturition. ..178

List of Tables

Table 2.1 Details of the association analyses.....48

Table 2.2 Genes with a nearby H3K27me3 peak that increase with advancing gestation and are differentially expressed by *Kdm6b cKO* and ctrl cells. 51

Table 2.3 Genes with triple characteristics (peri-implantation H3K27me3 winding, post-implantation H3K27me3 erosion, and increased RNA expression). 59

Table 2.4 Details of scRNA-Seq.....60

Table 3.1 RNA-seq analysis of the prepartum B6 and *Il33*$^{-/-}$ uterus.....121

Table 3.2 qRT-PCR primers.....121

List of Abbreviations

ATRA – all-trans retinoic acid

BMP – bone morphogenetic protein

B6 - C57BL/6 mice

COX-1 – cyclooxygenase 1

COX-2 – cyclooxygenase 2

dS – pre-decidualized stromal cell

DMPA - depot medroxyprogesterone acetate

DT – diphtheria toxin

DSC – decidualized stromal cell

ESC - endometrial stromal cell

ELISA – enzyme-linked immunosorbent assay

EZH1 – enhancer of zeste homolog 1

EZH2 – enhancer of zeste homolog 2

E2 - Estrogen

F1 – B6CBAF1/J mice

GD – gestation day

HC – histone category

H3K27me3 – histone H3 trimethyl lysine 27

IIS – inter-implantation site

iDTR – Cre-inducible DT receptor

IGFBP – insulin-like growth factor binding protein

IS – implantation site

ILC2 – group 2 innate lymphoid cell

IL-33 - interleukin-33

LPS - lipopolysaccharide

MPA – medroxyprogesterone acetate

MT – mesometrial triangle

Myo/endo – myometrium/endometrium

NFκB – Nuclear factor kappa

NSAID – nonsteroidal anti-inflammatory drugs

PDGFRα - platelet-derived growth factor receptor α

PG - prostaglandin

PGD_2- prostaglandin D_2

PGE_2 – prostaglandin E_2

$PGF_{2\alpha}$- prostaglandin $F_{2\alpha}$

PRC2 – polycomb repressive complex 2

PTB – preterm birth

Ptgs1 - prostaglandin-endoperoxide synthase 1

Ptgs2 - prostaglandin-endoperoxide synthase 1

PR – progesterone receptor

PTL – preterm labor

P4 - Progesterone

P4-tx – progesterone-treated

RAR – retinoic acid receptor

RXR – retinoid X receptor

RNA-Seq – RNA sequencing

scRNA-Seq - single-cell RNA sequencing

SEM – standard error of mean

SMC – smooth muscle cell

smFISH - single-molecule fluorescent in situ hybridization

TGF-β – transforming growth factor-β

Th2 – T helper 2 cells

TLR4 - Toll-like receptor 4

Treg – regulatory T cells

UMAP – uniform manifold approximation and projection

xVAS – mated to vasectomized males

20α-HSD - 20α-hydroxysteroid dehydrogenase

Chapter 1: Fibroblasts and their role in pregnancy and parturition

Parturition mechanisms across species

The processes that determine the timing of birth remain one of biology's greatest unsolved mysteries. While significant progress has been made in understanding the individual roles of prostaglandins[1-3], smooth muscle cell expression of gap junction proteins that promote cell-cell electrical coupling[4-7], and contraction-inducing hormones like oxytocin[8,9], a significant knowledge gap remains. That is, the nature of the "clock" that times the sequential induction of these events remains poorly defined. This gap spans across species from mice to humans and has severely impeded the development of therapies to forestall or prevent preterm birth, a leading cause of perinatal morbidity and mortality[10].

A major challenge in deciphering the mechanisms required for parturition in humans stems from the high degree of divergence across species in the endocrine control of labor onset (Figure 1.1). In mice, labor is triggered by progesterone (P4) withdrawal. For this to occur, the luminal epithelial cells of the uterus induce expression of cyclooxygenase 1 (COX-1), encoded by prostaglandin-endoperoxide synthase 1 (*Ptgs1*), an enzyme that is responsible for the biosynthesis of prostaglandins from arachidonic acid. COX-1, together with downstream enzymes, synthesizes the prostaglandin $PGF_{2\alpha}$. Although $PGF_{2\alpha}$ is a powerful pro-contractile agent like oxytocin, its immediate effect is to cause the corpus luteal cells of the ovary to induce *Akr1c18,* which encodes the P4 catabolizing enzyme 20α-hydroxysteroid dehydrogenase (20α-HSD). This process, known as luteolysis, leads to a systemic drop in P4 concentrations and rapid maturation of the myometrium. P4 withdrawal is both necessary and sufficient for on time mouse parturition given that treatment with the P4 receptor blocker RU486 causes early P4 withdrawal and premature labor, whereas P4 supplementation delays labor onset[11,12].

In contrast to rodents, other placental mammals including guinea pigs and higher primates do not experience P4 withdrawal prior to parturition onset. In these species, the corpus luteum involutes early in pregnancy and the placenta instead produces high levels of P4 throughout labor onset and delivery[13-15]. Supplementation with exogenous P4 does not extend the length of gestation in guinea pigs and has varying efficacy at delaying preterm birth in humans[16,17]. Thus, P4 withdrawal is not the trigger for labor in these species, although mechanisms of "functional" P4 withdrawal have been proposed, including: downregulation of progesterone receptors (PR)[18-20], altered expression of PR coregulators, and/or indirect PR antagonism by transcription factors[21]. Thus, the differences in P4 regulation across species has posed challenges for translating mouse findings to humans. To overcome this challenge, a potential solution involves redirecting research efforts towards the pathways and mechanisms upstream of luteolysis and/or functional P4 withdrawal, since these pathways are more likely to be conserved across species.

Prostaglandin production represents one shared component of parturition pathways in both rodents and humans. The discovery of prostaglandins dates back to the 1930s when researchers observed that substances from seminal fluid induced a rapid decrease in blood pressure and contraction of uterine and intestinal smooth muscle[22-24]. Since then, prostaglandins have been shown to contribute to numerous physiological processes, although much interest has focused on their role in the initiation and progression of parturition[25-27]. Their significance was underscored by key observations such as heightened synthesis during labor[28], the induction of labor upon administration to women, and delayed labor from the inhibition of their synthesis[29,30]. In mice, luteolysis and parturition requires upregulation of luminal epithelial COX-1 and subsequent $PGF_{2\alpha}$ production[1-3]. Guinea pigs, which give birth without a need for luteolysis (like

humans), upregulate PTGS1 prior to labor onset and are delayed when administered the PTGS inhibitor piroxicam at doses inhibiting PTGS1 but not PTGS2[31]. A recent study on term human myometrium specimens showed upregulation of PTGS1, and not PTGS2[32], raising the possibility that cell types or pathways upstream of COX-1, which remain almost entirely undefined, may be shared amongst all species.

Growing evidence from our lab and others suggests potential roles for fibroblasts expressing platelet-derived growth factor receptor α (PDGFRα) as crucial upstream mediators of both luteolysis and luteolysis-independent parturition pathways. In the non-pregnant uterus, these fibroblasts are found intercalated between the smooth muscle cell (SMC) bundles of the myometrium, as well as within the stromal layer of the endometrium. During pregnancy, uterine PDGFRα$^+$ fibroblasts are found within three main locations: 1) the undecidualized endometrium, constituting the lining of the inter-implantation sites as well as the inner lining of the anti-mesometrial portions of implantation sites; 2) the mesometrial triangle, a histologically distinct segment of the myometrium adjacent to the decidua basalis; and 3) the myometrium, the smooth muscle layer (see Figures 2.1E and 3.2C for histology of these areas). Here, we review the makeup and locations of these fibroblasts within the non-pregnant and pregnant uterus and discuss the molecular, cellular, and immunological evidence in support of these fibroblasts as a cell type important for the timing of birth.

Fibroblasts in the non-pregnant uterus

The uterus is a remarkable, yet overlooked, organ. Not only does it undergo dynamic cyclical changes in its non-pregnant state, but also completely transforms during pregnancy to support and grow the fetus. These distinct functions require an intricate arrangement of tissue

layers and cell types, each serving specific functional roles. In both mice and humans, the uterine wall consists of three distinct layers: the endometrium, myometrium, and perimetrium. The endometrium is made up of glandular and luminal epithelial cells lining a complex bed of fibroblasts, pericytes, and well-developed vasculature. The myometrium is primarily composed of uterine smooth muscle cells (SMCs), along with interstitial fibroblasts and vascular tissue. The perimetrium is the outermost serosal layer of the uterus, made up of mesothelium and a layer of connective tissue. While the uterine fibroblasts residing in the myometrium and endometrium have historically been considered a homogenous cell population with a shared set of functions, recent data suggests their heterogeneity and likelihood of engaging in specialized programs tailored to the needs of the uterus.

The use of single-cell RNA sequencing (scRNA-Seq) on both the mouse[33,34] and human[35,36] uterus has revealed significant heterogeneity within the uterine fibroblast compartment, thereby revolutionizing our understanding of this cell type. Kirkwood et al. described three PDGFRα^{+} fibroblast subpopulations in the mouse endometrium (F1, F2, and F3; Figure 1.2A). Not only were these fibroblasts transcriptionally unique, but the authors used immunofluorescence to show that these populations were also spatially distinct. NGFR^{high} CXCL14^{low} "F1s" were found to be localized to the sub-epithelial stromal layer while the NGFR^{low}CXCL14^{high} "F2s" were adjacent to the F1s. In contrast, NGFR^{-}CLEC3B^{+} "F3s" were found to reside within the basal endometrial layer near the myometrium.

Saatcioglu et al. nicely confirmed the findings of Kirkwood et al., reporting two populations of fibroblasts they designated as "inner" (corresponding to Kirkwood et al.'s F1/F2) or "outer" (corresponding to Kirkwood et al.'s F3) depending on the proximity to the endometrial lumen[34]. Moreover, my own work (see Chapter 2) confirms the existence of these

"inner" and "outer" fibroblasts in both the non-pregnant and pregnant mouse myometrium. In addition to the markers shown by Kirkwood et al, we note that the inner sub-epithelial fibroblasts uniquely express the marker *Hsd11b2*, while the outer myometrial interstitial fibroblasts express *Lum, Col8a1,* and *Mmp3* (Figure 1.2B).

The authors of these studies note that the transcriptional profiles of these fibroblasts suggest functions in immune response regulation, wound healing responses, and extracellular matrix organization, implying that these cells are involved in a multitude of processes[33,34]. My work described further in Chapter 2 highlights a prominent role for these fibroblasts in the timing of labor onset, but we anticipate further studies will uncover even more roles for these cells in endometrial tissue function.

Novel distributions of uterine fibroblast subpopulations have also been found in humans using superficial endometrial biopsies. Vento-Tormo's group has published two separate scRNA-Seq studies on the non-pregnant endometrium, the most recent of which integrates all of the published endometrial scRNA-seq studies performed to date[35,36]. These studies report clusters of endometrial stromal cells (eS), "pre-decidualized" stromal cells (dS) that appear during the secretory phase prior to implantation, and fibroblasts expressing complement C7. Pairing transcriptomic data with spatial analysis, the fibroblast_C7 cluster was found to be enriched in the basal layer of the endometrium, while the eS and dS clusters were found closer to the uterine lumen. The fibroblast_C7 cells express many of the same genes as the "outer" fibroblasts found in the mouse, including: COL3A1, COL1A1, FBLN1, APOE, DPT, and COL14A1. Conversely, the eS and dS cells express many of the same genes as the "inner" fibroblasts found in the mouse, including: ISLR, SPON2, FBLN2, MFAP4, CDH11, FN1, WT1, DIO2, NKD2, and WNT4. While most of the mouse markers were equally expressed between eS and dS, NGFR

and BMP7 were exclusively expressed by eS cells, while RGS2 was exclusively expressed by dS cells. Together, these results suggest that distinct fibroblast subpopulations are found in both the mouse and human uterus, and that these subtypes at least partially overlap spatially and transcriptionally. We anticipate these datasets will provide a rich foundation for future studies exploring these fibroblast subtype's unique roles in endometrial tissue function.

Fibroblasts during pregnancy: decidualized and undecidualized

During pregnancy, endometrial fibroblasts undergo a process called "decidualization," transforming into decidual stromal cells (DSCs) under the influence of the steroid hormones estrogen (E2) and P4. The newly formed decidua regulates local immune responses and provides structural support to the placenta[37,38]. In most species, including the mouse, decidualization is initiated upon embryo implantation, with morphological changes becoming apparent starting on gestation day (GD) 5.5. Murine DSCs express *Bmp2, Prl8a2,* and *Wnt4*, and are the predominant cell population within the implantation site until GD8.5, after which the decidua partially regresses concurrent with placental growth. While decidualization occurs in implantation sites, fibroblasts within the inter-implantation sites remain undecidualized.

Decidualization in humans is a spontaneous process, initiated independently of embryo implantation during the secretory phase of the cycle. Once triggered, pre-decidual cells appear around the spiral arteries of the uterus[39,40]. In the event of successful implantation, this decidualization reaction spreads beyond the perivascular regions to complete the formation of the maternal decidua. The morphological changes associated with decidualization are driven by transcriptomic and proteomic changes[36,41] and enable this new tissue layer to perform functions

akin to the murine decidua, including regulation of syncytiotrophoblast invasion and dampening local maternal immune responses.

Similar to the fibroblasts in mouse inter-implantation sites, subsets of endometrial fibroblasts also remain undecidualized during human pregnancy. Indeed, one of the first scRNA-Seq studies of the human maternal-fetal interface identified 3 distinct subsets of fibroblasts (dS1, dS2, and dS3)[41]. Among these, one cluster (dS3) contained fully decidualized stromal cells expressing the classic DSC markers IGFBP1 and PRL[42,43], whereas the other two clusters expressed high levels of PDGFRα. Multiplexed single-molecule fluorescent in situ hybridization (smFISH) showed that the PDGFRα$^+$ dS1 cells were present in the decidua spongiosa, closest to the myometrium, whereas the dS2 cells were located in the decidua compacta towards the uterine lumen. This data is in line with our earlier discussion on mouse fibroblast subpopulations residing in distinct "inner" and "outer" uterine layers. Of note, a separate study of the maternal-fetal interface published simultaneously confirmed the findings of Vento-Tormo et al. That is, they also found three subsets of stromal cells/fibroblasts, only one of which was an IGFBP1$^+$PRL$^+$ DSC cluster[44]. Together these studies indicate that the maternal-fetal interface contains decidual stromal cells in addition to large populations of undecidualized fibroblasts, the latter of which are severely understudied as a result of the field's focus on the role of DSCs.

A role for decidual activation in PTL, but not normal labor

Over the years, research on the mechanisms driving labor onset has predominantly centered on the decidual layer, primarily due to the compelling idea of "decidual activation." This hypothesis, pioneered by MacDonald and Casey in the 1980s, proposes that the decidua, the specialized lining of the uterus during pregnancy, undergoes a critical proinflammatory process

prior to the onset of parturition. This process most notably includes increased levels of the prostaglandins PGE_2 and $PGF_{2\alpha}$, proinflammatory cytokine secretion, and leukocyte infiltration[45,46]. However, subsequent studies performed over the past 40 years suggests that decidual activation plays a more important role in preterm labor (PTL) than normal parturition. This distinction is important considering that the triggers for each of these pathways are different[47].

A role for the decidua in PTL has been shown extensively in both mice and humans. In humans, it has long been known that intra-amniotic inflammation, resulting from microbial invasion of the amniotic cavity, leads to decidual inflammation and PTL[48-55]. Microbial products are sensed by pattern recognition receptors, such as toll-like receptors (TLRs), which leads to the production of chemokines (e.g., IL-8, IL-1, CCL-2), cytokines (e.g., IL-1β, TNF-α), and prostaglandins from within the decidua to trigger PTL[56,57]. In mice, injection of lipopolysaccharide (LPS) as a model for inflammation-induced PTB rapidly induces intrauterine inflammation, decidual COX-2 expression, premature luteolysis and PTB[58]. Administration of COX-2 inhibitors reduces the rate of PTL, thus implicating decidual COX-2 as the crucial cyclooxygenase for this process[59]. More recent studies combining the use of animal models and omics technologies have strengthened this concept to better establish causality between intra-amniotic infection, decidual inflammation, and PTL[60-63]. In addition to decidual infection/inflammation, decidual senescence has also been shown to act upstream of decidual activation and PTL. In mice, uterine deletion of *Trp53*, encoding the tumor suppressor protein 53, leads to spontaneous preterm birth (PTB) in 50% of mice[64]. This PTB phenotype occurs in the absence of P4 withdrawal, and instead is attributable to upregulation of COX-2 and prostaglandins within the decidua.

With regards to normal labor, decidual activation appears to play a more important role in labor progression than its onset. Whereas decidual COX-2 plays an important role in PTL, normal labor onset in mice requires induction of epithelial COX-1. This is most prominently demonstrated by the fact that COX-1$^{-/-}$ mice exhibit delayed luteolysis and parturition, whereas pharmacological inhibition of COX-2 does not prolong mouse labor unless it is given at doses that also inhibit COX-1 activity[3]. COX-1 induction is moreover highly localized to the luminal epithelial cells that line the anti-mesometrial portions of the implantation sites and inter-implantation sites, and is undetectable in the decidua[3]. Temporally, COX-1 is also induced far earlier in gestation than COX-2. While COX-1 protein levels significantly increase ~3-5 days prior to labor onset in the mouse[65,66], COX-2 levels are hardly detectable until their induction *during* parturition[65,66]. This is all consistent with epithelial COX-1 being essential for normal labor onset in mice, with less of a role for decidual activation or COX-2.

Thus, PTL pathways in mice are distinct from normal parturition pathways, especially with regards to the tissue layers and cyclooxygenase isoforms required for PG production. How the underlying etiology of labor differentially induces COX-1 or COX-2-derived PGs, and how these various COX-derived PGs differ in terms of their downstream functions, remains a topic of future investigation. Nonetheless, decidual activation appears to be more relevant to PTL parturition pathways, and not normal parturition. With regards to the latter, decidual activation is likely a byproduct of a labor-inducing event happening elsewhere.

A role for PDGFRα^{+} fibroblasts in mouse and human parturition

The critical and novel hypothesis presented in this dissertation is that PDGFRα^{+} fibroblasts, residing primarily in the myometrium, undecidualized endometrium, and

mesometrial triangle, play significant roles in the onset of mouse luteolysis and parturition onset. This idea that PDGFRα$^+$ fibroblasts can regulate the activity of a smooth muscle organ is not an entirely novel concept. Interstitial cells expressing PDGFRα$^+$ within the gastrointestinal tract[67-69] and the muscularis of the bladder[70-72] have been shown to closely associate with nerve fibers, express signal transduction and effector molecules required for receiving and translating neural inputs, as well as form gap junctions with SMCs to allow for their electrical coupling. More recently, PDGFRα$^+$ cells distributed in mouse and monkey reproductive tracts have been shown to express high levels of *Gja1*, encoding the gap junction connexin 43, suggesting that these cells are capable of forming gap junctions to one another and/or with neighboring SMCs[73]. Moreover, the locations of PDGFRα$^+$ cells are remarkably similar between monkeys and mice, raising the possibility that these cells have important shared functions across species.

Recent studies employing single-cell technologies also support the hypothesis that PDGFRα$^+$ fibroblasts are involved in parturition. Zhao et al. performed scRNA-seq on the pregnant mouse uterus in late gestation and reported five different stromal cell populations, including one decidualized stromal cell population[74]. Using bioinformatics and one functional experiment, the authors showed an important role for local retinoic acid (RA) synthesis in parturition. Administration of all-trans RA (ATRA) to mice starting on GD16.5 decreased expression of extracellular matrix genes *in vitro* and induced early labor onset *in vivo.* They found that this PTL pathway was in large part driven by retinoic acid produced by uterine interstitial fibroblasts expressing high levels of *Pdgfra* and *Hsd11b2*, as evidenced by this cluster's robust upregulation of *Aldh1a2*, one of the aldehyde dehydrogenase isoforms responsible for synthesizing retinoic acid from retinal. As previously mentioned, these *Hsd11b2*-expressing fibroblasts are subepithelial fibroblasts (Figure 1.2) residing in the undecidualized

endometrial layer of the pregnant uterus (see Chapter 2). While Zhao et al. did not address whether administration of ATRA induced preterm birth through early induction of COX-1 and luteolysis, this is a question I address further in Chapter 4. Lastly, similar to my own findings, Zhao et al. report upregulation of *Gja1* and *Oxtr* in their stromal populations (in addition to the SMC clusters) in late gestation. Since previous studies have primarily attributed *Oxtr* and *Gja1* upregulation to the SMCs[7,75-77], its upregulation in fibroblasts suggest a potentially unique role for this hormone in parturition beyond just inducing uterine contractions. This uterine fibroblast expression of *Gja1* and *Oxtr* has also been shown by another group[78].

In contrast to mice, the contribution of PDGFRα$^+$ fibroblasts to human parturition remains unclear. Performing these studies is challenging given that myometrial tissue is difficult to obtain, as well as the added layer that multiple time points are required to infer gene expression dynamics. Given these obstacles, most studies performed to date have identified candidate genes required for labor onset by comparing nonlabor to labor specimens[79-81], which provides limited insight into candidate genes upstream of the parturition cascade. Indeed, my own work shown in Chapter 2, as well as others[60], shows that the labor cascade begins much earlier than was once assumed with most gene changes occurring well before the onset of murine labor. To our knowledge, only two studies have employed a well-designed temporal approach to study transcriptional changes during parturition. Both studies compared human term myometrium to non-pregnant uteri, with Wu et al.[32] using bulk RNA-seq and Ji et al. using scRNA-seq[82]. Comparing these human datasets to my own work presented in Chapter 2 on mouse PDGFRα$^+$ fibroblasts revealed that many of the same genes were upregulated in late gestation in both mice and humans, including: OXTR, INHBB, CSF1, GPX3, IL1R2, STC2, TGFBI, SERPINE2, VCAM1, and FOXO1. While this suggests that late gestation PDGFRα$^+$

fibroblasts may be undergoing similar transcriptional programs leading up to labor onset in mice and humans, more human temporal transcriptomic profiling approaches are needed to fully parse out these species-to-species comparisons. These temporal studies should leverage non-pregnant, early gestation, and mid-gestation samples to get a full picture of the transcriptional dynamics that occur throughout pregnancy.

Overview of dissertation: a central role for fibroblasts in pregnancy and parturition

Parturition involves a series of physiological events that culminate in the initiation and progression of labor. The process involves release of certain signaling molecules, such as prostaglandins and oxytocin, which stimulate uterine contractions and gradual dilation of the cervix. However, despite understanding how each of these events contribute to the labor cascade, many aspects of parturition remain unclear, particularly how the uterus "knows" it is time to deliver. The core hypothesis presented in my dissertation is that undecidualized PDGFRα$^+$ fibroblasts play significant roles in the timing of mouse parturition. The bulk of my findings are presented in Chapter 2, with additional data on roles for fibroblasts in other pathways of parturition in Chapters 3, 4, and 5.

In **Chapter 2,** experiments on mice lacking the histone demethylase KDM6B reveal the existence and operation of a H3K27me3 timer within uterine PDGFRα$^+$ fibroblasts that schedules luteolysis and labor onset in mice. As the first mechanism of its kind underlying gestation length in any mammalian species, it opens up a wealth of potential questions and parturition pathways that we discuss further in Chapter 6.

While Chapter 2 addresses luteolysis-dependent parturition pathways in mice, **Chapter 3** implicates PDGFRα$^+$ fibroblasts as upstream mediators of uterus-intrinsic parturition pathways,

which operate independent of luteolysis and are thought to be analogous to parturition pathways in humans. The work described in this chapter was primarily the output of a postdoctoral fellow in the lab, Dr. Johan Siewiera, to which I contributed by performing the analyses on eosinophils as downstream mediators of this pathway. This data not only emphasizes the distinct physiological mechanisms at play in luteolysis versus uterus-intrinsic parturition pathways in mice, but also the upstream role for PDGFRα$^+$ cells in both. **Chapter 6,** which includes conclusions and future directions, speculates on how my results in Chapter 2 may be upstream of and linked to the uterus-intrinsic pathways described in Chapter 3.

In addition to studying luteolysis-dependent and independent parturition pathways in mice, I also performed experiments using various mouse models of preterm birth (PTB), which are presented in **Chapter 4**. These experiments reveal that KDM6B is essential in PDGFRα$^+$ fibroblasts to initiate inflammation-induced PTL, providing insight into pathological parturition mechanisms potentially relevant to the clinical problem of preterm labor.

Chapter 5 presents data on the other H3K27me3 demethylase, KDM6A, and its important role in early mouse decidualization. When combined with the discoveries presented in Chapters 2 and 4, these findings reveal the essential role of regulated H3K27me3 gene silencing in the uterine adaptation to pregnancy and parturition.

Collectively, the results presented in this dissertation broaden our mechanistic understanding of mouse pregnancy and parturition by introducing novel roles for PDGFRα$^+$ fibroblasts and the epigenetic pathways they employ to regulate critical events during pregnancy.

Figures

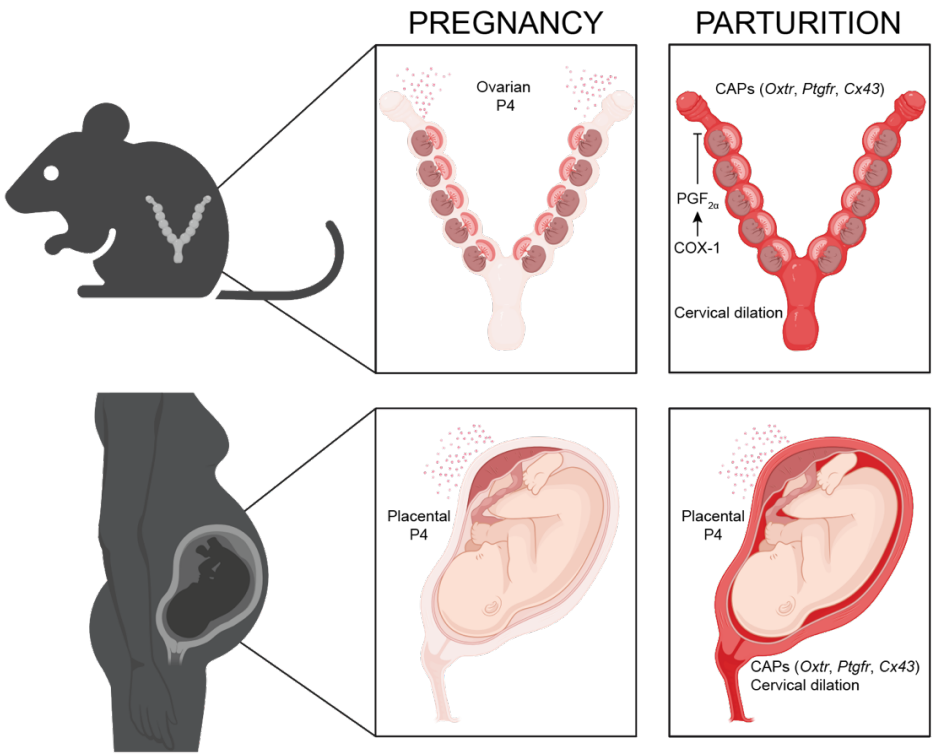

Figure 1.1 Comparison of human and mouse pregnancy.

In mice, labor is initiated when uterine luminal epithelial cells induce expression of cyclooxygenase 1 (COX-1). COX-1, together with downstream enzymes, leads to synthesis of prostaglandin $F_{2\alpha}$ ($PGF_{2\alpha}$) which acts on the ovarian corpus luteum to catabolize P4. P4 withdrawal results in induction of contraction-associated proteins (CAPs), dilation of the cervix, and uterine contractions. In human pregnancy, the trigger for labor induction is unclear, but involves prostaglandins and other pro-inflammatory mediators. Note the other fundamental differences between human and mouse pregnancies including: uterine shape, number of implantation sites, and the site of P4 generation during pregnancy. Figure was made with BioRender.com.

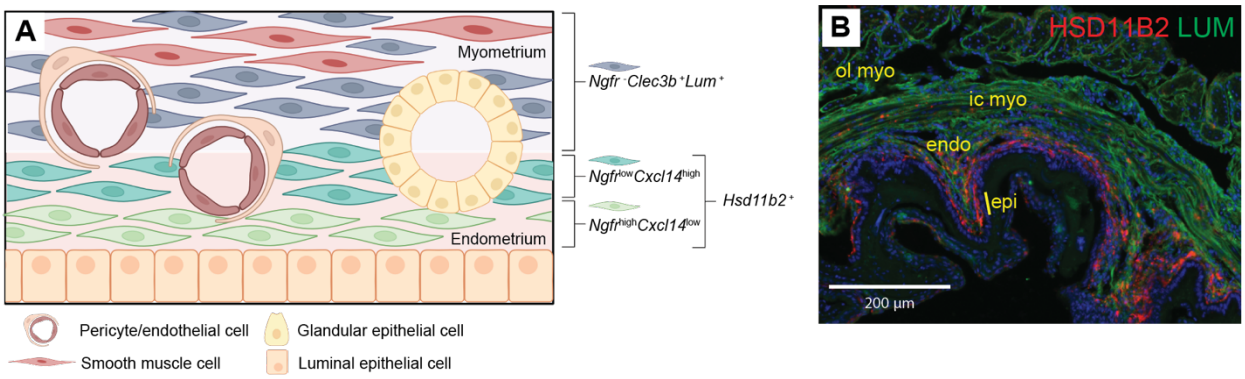

Figure 1.2 Spatially distinct subpopulations of fibroblasts in the mouse uterus.

(A) Schematic of mouse uterine fibroblast populations as defined by Kirkwood et al, Saatcioglu et al, and McIntyre et al (Chapter 2). "Inner" fibroblasts express *Hsd11b2* and can be further subsetted by their expression of *Ngfr* and *Cxcl14*. "Outer" fibroblasts found in the basal layer of the myometrium express *Clec3b* and *Lum*. (B) HSD11B2 and LUM immunostaining of the myometrium/endometrium region of a GD14.5 implantation site (representative of *n*=3 B6 mice). ol myo, outer longitudinal smooth muscle layer of the myometrium; ic myo, inner circular smooth muscle layer of the myometrium; endo, endometrium; epi, epithelium. Figure 1.2A was made with BioRender.com. Immunostaining in Figure 1.2B was performed by Omar Valdez.

Chapter 2: An epigenetic timer of gestation length in mice

Summary

Timing mechanisms in biology remain poorly understood. As one prime example, little is known about the mechanisms that specify how long the gestating uterus will remain quiescent before entering labor. Here, we provide evidence that gestation length in mice is determined by an epigenetic timer that runs autonomously within the fibroblasts of the pregnant uterus. The timer is set during the peri-implantation period when select loci establish appropriate levels of the repressive histone mark H3K27me3. These loci then progressively lose H3K27me3, thereby scheduling the uterine cell state transitions and associated gene expression changes of late gestation that are the proximal mediators of labor onset. Initial overwinding of the timer via genetic ablation of the histone demethylase KDM6B delays these transitions and extends gestation length. Further dissection of the ways such uterine programming controls gestation length may have relevance to human pregnancy complications such as preterm labor.

Introduction

Molecular timers are thought to regulate a wide range of biological phenomena. At present, those that control rates of continuous developmental programs or progressive processes such as aging are beginning to be elucidated in detail[83,84] (for recent examples see refs.[85-90]). Much less is known about timers that schedule discrete events in the future, after periods of relative stasis. Labor onset potentially represents one such event, as the gravid uterus transitions out of its non-contractile, quiescent state only upon reaching the end of gestation[91,92]. It has long been postulated that labor onset timing is controlled by clocks that variously run with the fetus,

placenta or decidua, the specialized endometrial tissue that encases the conceptus[93-96], but despite many years of investigation the details of such clocks have yet to be uncovered. This raises the possibility that a gestation length timer, if it exists at all, operates in a different tissue compartment entirely.

In mice, parturition (the act of giving birth) is currently appreciated to be initiated by events that take place within the uterus (Figure 2.1A). Specifically, in the few days prior to delivery, uterine luminal epithelial cells begin producing prostaglandin $PGF_{2\alpha}$ as a result of their induction of the prostaglandin synthesis enzyme COX-1 (encoded by *Ptgs1*)[1-3,97]. $PGF_{2\alpha}$, in turn, acts upon the corpora luteal cells of the ovary, which, up until this point, have been producing large quantities of progesterone (P4) in order to maintain high serum concentrations of this pregnancy-sustaining steroid hormone. Upon $PGF_{2\alpha}$ exposure, however, corpora luteal cells induce expression of *Akr1c18*, which encodes the P4-catabolizing enzyme 20α-hydroxysteroid dehydrogenase (20α-HSD), thus inducing the catabolism of newly synthesized P4 and hence a rapid decline in serum P4 concentrations. This process, called luteolysis, causes rapid maturation of the myometrium, the smooth muscle layer of the uterus, allowing it to assume its highly contractile state necessary to expel the conceptus. Critically, these components of the labor cascade have been known since the 1990s[1,3] but there has been little progress in identifying the upstream signals that induce uterine epithelial COX-1 expression, nor has it been clear whether the production of such signals might in turn be controlled by some kind of gestation length timer.

Previously, we implicated demethylation of histone H3 trimethyl lysine 27 (H3K27me3), a repressive histone mark, as contributing to the parturition cascade in mice[98]. Specifically, we found that GSK-J4, an inhibitor of the two known H3K27 demethylases KDM6A and KDM6B[99-101], delayed delivery when mice were injected with this drug in late gestation while also

supplemented with P4 to circumvent luteolysis and thus mimic the hormonal environment that prevails during human parturition[91]. This finding was in line with our additional observation that the stromal cells of the decidua basalis, the uterine tissue layer that overlays the surface of the placenta, experience a global reduction in H3K27me3 levels starting after GD12.5, as well as with the suggestion in the literature that a process of "decidual activation" stimulates labor progression in humans[102,103]. However, GSK-J4 administration also delayed parturition when the mice were otherwise allowed to deliver naturally, i.e., via luteolysis. In this case, it was difficult to understand how H3K27me3 demethylation in the decidua would affect birth timing, since COX-1 expression is induced at the end of gestation by uterine epithelial cells throughout the entire uterus, including in the segments of undecidualized uterus positioned between each implantation site as well as at each implantation site's anti-mesometrial pole, distant from the decidua basalis[3]. This disconnect thus raised the possibility that H3K27me3 demethylation might function to promote natural labor onset in a cell type that did not reside within the decidua.

Here, we have taken a genetic approach to evaluate how H3K27me3 demethylation contributes to parturition in mice when it is allowed to occur naturally, via luteolysis. We find that undecidualized uterine fibroblasts, residing within the undecidualized endometrium and myometrium, are the key cell type that experiences H3K27me3 demethylation. Moreover, we find that such demethylation occurs in a highly locus-specific fashion and has the characteristics of a gestation length timer, as it begins in early gestation, occurs progressively, and predicts the gene expression changes seen in mid and late gestation uterine fibroblasts that ensure on time parturition. When the timer is "overwound" in early gestation due to genetic loss of KDM6B, mice experience a delay in luteolysis and a delay in labor onset.

Results

KDM6B is required for on time parturition in mice

To study the role of KDM6A and KDM6B in mouse parturition, we generated *Pgr-cre Kdm6a*$^{f/f}$ and *Pgr-cre Kdm6b*$^{f/f}$ mice (hereafter referred to as *Kdm6a cKO* and *Kdm6b cKO* mice) to inactivate their encoding genes within the progesterone receptor (PR)-expressing cells of reproductive tissues[104]. While *Kdm6a cKO* mice showed early pregnancy failure and were not studied further, *Kdm6b cKO* mice were fertile and sustained their pregnancies to term. However, these mice delivered 1-3 days later than *Kdm6b*$^{f/f}$ and *Pgr-cre Kdm6b*$^{wt/wt}$ controls, which both consistently delivered on gestation day (GD) 19.5 as is typical for mice on a C57BL/6 (B6) background (Figure 2.2.1B). This delay in turn was associated with a delay in luteolysis since *Kdm6b cKO* mice maintained high serum P4 concentrations past GD18.5, in contrast to control mice (Figure 2.1C), and showed impaired ovarian induction of *Akr1c18*, which encodes 20α-HSD (Figure 2.1D). Additionally, prepartum uteri of *Kdm6b cKO* mice were characterized by delayed *Ptgs1* mRNA induction (Figure 2.8A), reduced epithelial cell expression of COX-1 protein (Figure 2.1E), and reduced $PGF_{2\alpha}$ concentrations (Figure 2.1F). Importantly, we also found that parturition timing in mice subjected to reciprocal *Kdm6b cKO* and *Kdm6b*$^{f/f}$ ovary transplants tracked with the genotype of the transplant recipient, thus ruling out a requirement for KDM6B within the ovaries themselves (Figure 2.8B). Indeed, injecting *Kdm6b cKO* mice with a $PGF_{2\alpha}$ analog on GD18.5 induced both *Akr1c18* (Figure 2.1D) and delivery within 24 hours (Figure 2.1B), consistent with these mice retaining normal ovarian responsiveness to $PGF_{2\alpha}$. Lastly, *Kdm6b cKO* mice showed normal implantation timing, and the differences we could detect in fetal growth rates, placental growth rates, and litter sizes compared to *Kdm6b*$^{f/f}$ mice were either minimal or within the limits known not to affect birth timing (Figure 2.8C-F)[105,106].

These observations suggested that the parturition delay of *Kdm6b cKO* mice was not due to delayed implantation nor was it secondary to an effect on the conceptus. Rather, these results collectively indicated that on time uterine COX-1 induction, and thus on time luteolysis and on time labor onset, requires a uterus-intrinsic role for KDM6B.

On time parturition requires KDM6B function within uterine fibroblasts

We next used *Ltf-iCre*[107] and *Pdgfra-cre*[108] drivers to identify which PR-expressing uterine cell type (epithelial cells or fibroblasts; Figure 2.9A-B) required KDM6B for on time parturition. Surprisingly, *Ltf-iCre Kdm6b*$^{f/f}$ mice delivered at the same time as *Kdm6b*$^{f/f}$ and *Ltf-iCre Kdm6b*$^{wt/wt}$ controls, demonstrating that KDM6B was dispensable within uterine epithelial cells (Figure 2.2A). By contrast, *Pdgfra-cre Kdm6b*$^{f/f}$ mice phenocopied *Kdm6b cKO* mice in that they showed a 1-3 day parturition delay, delayed luteolysis, and reduced uterine epithelial *Ptgs1* expression (Figures 2.2A-B and 2.9C). These results thus not only revealed a previously unappreciated role for uterine PDGFRα^+ fibroblasts in mouse parturition, but also the existence of a KDM6B-regulated pathway in these cells that allows them to induce COX-1 expression in nearby luminal epithelial cells. The phenotype of *Pdgfra-cre Kdm6b*$^{f/f}$ mice also clarified an incidental finding of *Kdm6b cKO* mice, namely the presence in late gestation of ectopic decidual tissue (i.e., deciduomas) in the uterine segments positioned between implantation sites (henceforth referred to as inter-implantation sites, or IIS; Figure 2.9D-H). That is, since *Pdgfra-cre* mice did not develop deciduomas, these structures were not the cause of delayed parturition in *Kdm6b cKO* mice.

In the mouse uterus, PDGFRα^+ fibroblasts constitute the fibroblasts that intercalate between the smooth muscle cell (SMC) bundles of the myometrium, as well as those that

comprise the stromal layer of the undecidualized endometrium[73,109]. During pregnancy, this endometrial tissue, with its surface of luminal epithelial cells, constitutes not only the inner lining of IIS but also, starting at mid-gestation[110], the inner lining of the anti-mesometrial portions of implantation sites (IS; hence our use of the term IS "myo/endo" to refer to this endometrial tissue and its overlying myometrium; Figure 2.1E shows the histology of this area). Thus, to gain insight into how KDM6B activity within uterine fibroblasts regulates parturition timing, we used scRNA-Seq to longitudinally profile *Kdm6b cKO* and control *Kdm6b*$^{f/f}$ PDGFRα^{+} fibroblasts both in IIS, from GD5.5 (i.e., ~1.5 days after implantation) to GD18.5, and in IS myo/endo, from GD12.5 to GD18.5 (Figures 2.2C and 2.9I).

Remarkably, control fibroblasts within both IIS and IS myo/endo continuously shifted their position on the Uniform Manifold Approximation and Projection (UMAP) from GD8.5 to GD18.5, suggesting that their transcriptomic state constantly evolves during this period (Figure 2.2D). The cells' positioning was also slightly different between IIS and IS myo/endo, especially on GD12.5 and GD14.5, suggesting the influence of anatomic site-specific factors, although both locations experienced a conserved pattern of gene upregulation with advancing gestation (Figure 2.9J). The transcriptomic state of *Kdm6b cKO* fibroblasts also continuously evolved, but starting on GD12.5 cell positioning diverged from anatomic location-matched controls (Figure 2.2D). Together, these observations suggested the existence of a KDM6B-influenced gene expression program embarked upon by many, if not all, uterine fibroblasts in mid-to-late gestation. As might be expected, execution of this program coincided with *Ptgs1* induction by uterine epithelial cells. Our scRNA-Seq analysis in fact revealed that this induction was part of a generalized transition in uterine epithelial cell state that commenced around GD14.5 and that was delayed in *Kdm6b cKO* mice (Figure 2.9K-M).

H3K27me3 dynamics in uterine fibroblasts reveal KDM6B-dependent and -independent processes

Since KDM6B is a H3K27 demethylase, the above results also implicated H3K27me3 dynamics in the control of parturition timing. Accordingly, we performed CUT&RUN on purified uterine fibroblasts from *Kdm6b cKO* and control *Kdm6b*$^{f/f}$ mice (Figure 2.10) to determine how H3K27me3 distributions evolved across the cells' respective genomes from GD5.5 to GD18.5. Importantly, a separate analysis revealed that peak profiles in *Kdm6b cKO* and *Pdgfra-cre Kdm6b*$^{f/f}$ uterine fibroblasts were almost identical (Figure 2.11A), indicating that loss of KDM6B in uterine epithelial cells did not affect H3K27me3 dynamics in fibroblasts. Moreover, H3K27me3 distributions, while different between *Kdm6b cKO* and control cells, were respectively identical in cells derived from IIS or IS myo/endo (Figure 2.11B). This latter observation meant not only that we could perform an aggregate differential peak analysis using genotype and time (gestation day) as sole covariates, but also that peak distributions evolve uniformly within all fibroblasts across the uterus of both *Kdm6b cKO* and control mice. Accordingly, we found that 56.3% of the 64,923 identified peaks varied significantly with respect to genotype and 11.4% varied with respect to time (Figure 2.3A-B). Consistent with the function of KDM6B as a histone demethylase, many peaks showed pronounced elevations in *Kdm6b cKO* fibroblasts (Figure 2.3A). In addition, ~2.2x more peaks lost intensity (i.e., eroded) with advancing gestation than gained intensity (Figure 2.3B).

We also noted that time-dependent changes in peak intensities occurred monotonically, and that initial differences in peak intensity between *Kdm6b cKO* and controls were maintained with advancing gestation. Accordingly, and as confirmed by K-means clustering (Figure 2.11C-D), the peak patterns fell into a simple 3x3 matrix defining 9 histone categories (HC1-9) with

time and genotype as variables: eroding, steady, or increasing over time and/or higher, equivalent or lower in *Kdm6b cKO* cells (Figures 2.3C and 2.11E; Figure 2.3D shows representative peak tracks for 4 of these categories). These patterns unexpectedly revealed that peak erosion, a process that affected 4,554 peaks, occurred largely, if not entirely, via a KDM6B-independent process. Rather, KDM6B deficiency affected, for a number of loci, what appeared to be a H3K27me3 setpoint already apparent on GD5.5. We also found that peak erosion and genotype-dependent peak elevation were highly localized and frequently abutted peaks that remained constant over gestation or were similar between strains (Figure 2.11F).

We next sought to gain greater insight into the timing of peak erosion. This question could not be addressed through the application of an *FDR* threshold to the CUT&RUN data since such application detected very few peaks as eroding within each of three segmented time periods available for analysis (GD5.5 to GD8.5, GD8.5 to GD14.5, and GD14.5 to GD18.5), despite the many peaks significantly eroding (*FDR*<0.1) over the entire GD5.5 to GD18.5 period according to the aggregate analysis. Thus, we instead applied a P_{raw}<0.05 significance threshold to this segmented time point analysis. Remarkably, large percentages of the peaks detected as eroding from GD5.5 to GD18.5 (*FDR*<0.1, aggregate analysis) were also detected as eroding (P_{raw}<0.05) from GD5.5 to GD8.5 (17.8%-26.1%) and/or from GD8.5 to GD14.5 (30.5%-35.4%; Figure 2.4A). This concordance was unlikely due to the presence of false positives since ~100-200x fewer peaks that were detected as eroding by the aggregate analysis were conversely detected as increasing when subjected to the segmented time period analysis (Figure 2.4B). While this segmented analysis also suggested that peak erosion leveled off somewhat from GD14.5 to GD18.5, in turn suggesting that the underlying process might have ceased by GD14.5, we cannot rule out the strong possibility that we were unable to detect peak erosion past GD14.5 merely

because many eroded peaks had already by this point reached low concentrations. Together, these results indicated that uterine fibroblast are subjected to a H3K27me3 erosion program at select loci that is initiated soon after implantation and that likely continues throughout the rest of gestation, or at least through GD14.5.

A H3K27me3-dependent timer schedules fibroblast gene induction at mid-to-late gestation

We next assessed whether H3K27me3 dynamics in uterine fibroblasts might regulate parturition timing by determining the extent to which the 9 histone categories codified above predicted linked gene expression, both with respect to the changes that unfold with advancing gestation as well as with respect to the differences that were evident between genotypes. To accomplish this, we first assigned the appropriate time- and genotype-dependent histone category (i.e., HC1-9) to every gene with a H3K27me3 peak within 10 kb of its transcription start site (see Methods and Materials for a description of how we assigned genes with multiple peaks). Repeating the procedure separately for the genes assigned to each of these 9 histone categories, we then tallied the number whose mRNA expression in uterine fibroblasts from mid to late gestation (GD12.5, 14.5, 16.5, and 18.5, considering each time point separately but combining scRNA-Seq data respectively from IS myo/endo and IIS) differed in comparison to early gestation (combined scRNA-Seq data from GD5.5 and 8.5 IIS), and/or differed between gestation day-matched control and *Kdm6b cKO* cells. That is, for each mid-to-late gestation time point, we tallied the number of peak-associated genes whose expression matched any of the 10 genotype- and/or time-dependent patterns defined by the circular Venn diagrams shown in Figure 2.5A, and then mapped the distributions of these tallies across the 9 histone categories. This created a series of tiles representing the experimentally-determined association between gene

expression and locus-specific histone dynamics. We then calculated fold-enrichment scores by dividing these tallies by the number of genes expected to be present in each tile if gene expression and locus-specific histone dynamics were unrelated processes. Figure 2.5B displays these fold-enrichment scores in heat-map form, with the red coloring of a tile indicating a significant association between locus-specific H3K27me3 dynamics and the expression pattern of linked genes (see Table 2.1 for absolute gene counts and the values of these fold-enrichment scores).

This analysis revealed that genes nearby a HC1 peak were strongly enriched (up to 2.4-fold) for ones whose expression in control fibroblasts increased at the mid-to-late gestation time points compared to early gestation, as well as for ones that were differentially expressed between gestation day-matched *Kdm6b cKO* and control fibroblasts (Figure 2.5B; Table 2.1). Indeed, genes nearby HC1 peaks were highly enriched for both of these time and genotype-dependent expression characteristics (up to 4.6-fold). The same associations were also apparent when we used GD12.5 rather than GD5.5/8.5 as our baseline (Figure 2.5C; Table 2.1), suggesting that this program drove a continuous, unfolding process. Finally, we uncovered similar associations when we separately analyzed IS myo/endo (Figure 2.12A; Table 2.1) and IIS (Figure 2.12B; Table 2.1), consistent with the shared programs of H3K27me3 erosion and gene upregulation noted for both anatomic locations (Figures 2.9J and S2.11B). By contrast, no such associations were apparent for SMCs and pericytes, two other stromal cell types that our scRNA-Seq data suggested would be present in our CUT&RUN fibroblast preparations at levels of 3-17% each (Figure 2.13A-B; Table 2.1). Together, these observations thus linked the transcriptional upregulation of genes whose expression is associated with on time labor onset (i.e., ones that are differentially expressed in *Kdm6b cKO* and control fibroblasts) with their proximity to H3K27me3 peaks that

experience both progressive erosion over time and setpoint elevation in the absence of KDM6B.

Considering the canonically repressive function of H3K27me3, its progressive erosion thus appeared as a timing mechanism that limited expression of HC1-associated genes until the point at which, at mid-to-late gestation, H3K27me3 levels had fallen below a certain threshold. For the induced genes that were expressed at lower levels in *Kdm6b cKO* fibroblasts, this idea comports with the additional idea that the H3K27me3 setpoint elevation caused by KDM6B deficiency would increase the time required to reach this threshold, thus delaying gene induction and labor onset. Indeed, many of the induced genes with lower expression in *Kdm6b cKO* fibroblasts at one point in mid-to-late gestation either normalized their expression at later time points or even showed higher expression than controls (Table 2.2). For genes showing elevated expression in *Kdm6b cKO* fibroblasts as an initial outcome (Table 2.2), such expression presumably reflects the dual influence of H3K27me3 and other transcriptional regulators directly or indirectly regulated by KDM6B. The strong association between HC1, gene upregulation, and differential gene expression between genotypes was also evident when we performed the reciprocal analysis that tallied the genes that showed both upregulated expression in control fibroblasts at any point from GD12.5-18.5 and gestation-day matched differential expression between *Kdm6b cKO* and control fibroblasts (Figures 2.5D and 2.13C-D).

Peri-implantation H3K27me3 tuning sets the gestational timer

Having gained evidence for a gestation length timer in uterine fibroblasts that is based upon the progressive, locus-specific erosion of H3K27me3, we next assessed how these loci initially establish their H3K27me3 setpoint in early gestation. Accordingly, we determined how H3K27me3 distributions changed from GD0.5 (which is ~12 h post-copulation) to GD5.5. This

experiment employed highly fertile B6CBAF1/J mice[111] to ensure consistent reproductive endocrine performance (of note, the minor differences in H3K27me3 distributions between B6CBAF1/J and B6 uterine fibroblasts were unrelated to pregnancy histone dynamics; Figure 2.14A).

Remarkably, 2,289 H3K27me3 peaks (of the total 64,923) increased from GD0.5 to GD5.5 (Figure 2.6A-B), with 1,037 of them being gene-associated. About 20% of these peaks subsequently eroded, which is ~2.8-fold more than expected given the independent genome-wide frequencies of these two processes (Figure 2.14B). This association thus linked the "winding" and "unwinding" of the timer and identified genes whose scheduled de-repression in late gestation might be particularly important in controlling labor onset timing. Indeed, genes already implicated in parturition control in either mice[112-116] or, interestingly, humans[81,117-122] were amongst the 47 with the triple characteristics of 1) a nearby H3K27me3 peak that increases from GD0.5 to GD5.5; 2) subsequent erosion of this peak; and 3) increased RNA expression in late gestation (Table 2.3). For example, genes with these three characteristics included *Oxtr*, which encodes the receptor for oxytocin, a potent uterotonic hormone*, Inhbb*, which encodes an activin subunit and whose deficiency is known to delay parturition onset in mice by 1-2 days[116], and *Csf1*, which encodes the macrophage growth factor CSF-1, in line with the expansion of macrophages previously reported to occur in the pre-partum uterus[103,123,124]. Interestingly, these three genes were also HC1-associated and their induction was impaired in *Kdm6b cKO* mice (Figure 2.6C).

Next, we investigated possible mechanisms of H3K27me3 elevation in early pregnancy. Remarkably, peak distributions on GD5.5 were virtually identical to those in female mice that had been mated to vasectomized males (xVASX; 17 differential peaks out of 64,923 [*FDR*<0.1])

(Figure 2.6D). Such mating induces the state of "pseudopregnancy," in which implantation does not occur but females still experience seminal fluid exposure, elevated serum P4 and prolactin concentrations, and the nidatory estrogen surge[125,126]. Moreover, non-pregnant mice injected with P4 (P4-tx) showed H3K27me3 distributions in uterine fibroblasts that much more closely resembled those seen on GD5.5 than on GD0.5 (1,590 versus 19,324 differential peaks, respectively [*FDR*<0.1]). Together, these data suggested that setting the H3K27me3 gestational timer was independent of implantation and instead was likely driven, at least in part, by the rise in serum P4 concentrations that occurs following copulation.

Lastly, we noted that 2,399 peaks declined in intensity from GD0.0 to GD5.5 (Figure 2.14C). Although such "pruning" was less dramatic than peak "winding" in terms of fold change and statistical significance (Figure 2.6B), it was also observed following xVASX mating and also showed a link to subsequent peak erosion, albeit less overtly (Figure 2.14B). Together, these observations suggested that the locus-specific establishment of H3K27me3 levels during the peri-implantation period should be considered a more general "tuning" process that optimally schedules the induction of linked genes in mid-to-late gestation. Provocatively, peaks that were elevated in *Kdm6b cKO* fibroblasts on GD5.5 were over-represented in the sets of peaks that either increased or decreased from GD0.0 to GD5.5, as well as in the set of peaks that eroded after GD5.5 (Figure 2.14D-E). Together, these observations suggested the possible complex, locus-specific modulation of KDM6B activity during the peri-implantation period, and a link between such modulation and the process that selects peaks for erosion.

Discussion

We present evidence that gestation length in mice is controlled by an epigenetic timer that operates within the fibroblasts of the pregnant uterus (Figure 2.7). Under the influence of systemic pregnancy hormones like P4, the timer is set in the peri-implantation period through the establishment of appropriate H3K27me3 levels at select loci. Then, starting soon after implantation, H3K27me3 begins to progressively erode at 4,554 loci, limiting the expression of associated genes until late gestation, when their induction initiates the labor cascade. In contrast to other biological timers described to date that drive continuous developmental events (reviewed in ref.[84]), this timer is programmed once and then appears to run silently and autonomously in the background to trigger a discrete event more distantly in the future. The timer we have uncovered also contrasts with the set of epigenetic clocks currently described that are thought to run over long time scales to control processes such as aging (reviewed in ref.[83]), in that the modification (H3K27me3 demethylation in our case) occurs in a highly localized fashion rather than globally across the genome.

While epithelial COX-1 induction and luteolysis are known to be the proximal triggers of parturition in mice, triggers of human parturition have remained obscure. Importantly, human parturition has variously been speculated to involve signals emanating from the fetus, placenta, or decidua that directly induce myometrial maturation[91,93-96]. What times the generation of these signals, or if they are truly relevant, is unknown. Our observation that uterine fibroblasts play a more upstream role in controlling gestation length in mice raises the possibility that parturition timing in humans might also be directed by this uterine compartment. This idea is supported by our observation that some of the genes in uterine fibroblasts we identify as being H3K27me3-regulated are implicated in human parturition, as well as our recent finding that uterine

fibroblasts, through their stimulation of innate type 2 immune processes, play an important role in triggering labor onset when mice are hormonally manipulated to model their human counterparts[109]. Conversely, the results presented here suggest that our previous observation of H3K27me3 demethylation in the stromal cells of the late gestation mouse decidua [98], which occurs in a predominantly global fashion, is not a causative trigger of labor onset, and that the delay in labor onset we observed in mice treated with the KDM6A/B inhibitor GSK-J4 is likely due to the effect of this drug on KDM6A activity within uterine fibroblasts.

Our work leaves unresolved the exact mechanism whereby uterine fibroblasts induce COX-1 expression in uterine epithelial cells. One possibility invokes a role for activin, since, as mentioned above, *Inhbb*$^{-/-}$ mice show a 1-2 day parturition delay[116]. Importantly, however, we note that the impaired induction of *Inhbb* in *Kdm6b cKO* fibroblasts in late gestation might in part be due to the delayed luteolysis of *Kdm6b cKO* mice given that administration of the progesterone antagonist RU486 increases *Inhbb* expression in total myometrial tissue [60]. This caveat also applies to our observation of impaired *Oxtr* induction. A second possibility comes from a recent study showing that retinoic acid injection causes preterm labor in mice, thus implicating a role for retinoic acid in labor onset[74]. Although this study did not address whether retinoic acid directly induces *Ptgs1* expression in uterine epithelial cells, COX-1 induction by retinoic acid has been shown in other contexts[127,128]. Provocatively, *Aldh1a2*, one of the aldehyde dehydrogenase isoforms responsible for synthesizing retinoic acid from retinal, is induced by uterine fibroblasts in late gestation and is expressed at lower levels in *Kdm6b cKO* compared to control fibroblasts (Table 2.2). This gene, however, bears a static HC5 H3K27me3 peak at its promoter (Table 2.2) suggesting that its regulation by the H3K27me3 timer would have to occur indirectly, possibly through the induction of an intermediate transcription factor. It is also unclear

how other genes we detect as being regulated by H3K27me3 erosion might contribute to labor onset. For example, our data suggesting that H3K27me3 erosion leads to *Oxtr* upregulation in late gestation uterine fibroblasts suggests that oxytocin, whose role in mouse parturition has remained unclear[129,130], may act on uterine fibroblasts in addition to myometrial SMCs, a previously undescribed function for this hormone. Similarly, our finding that the H3K27me3 timer controls *Csf1* expression by uterine fibroblasts suggests a role for macrophages in parturition, and highlights the likely involvement of non-fibroblastic, non-epithelial cell types in the labor cascade in mice, potentially as intermediaries between uterine fibroblasts and epithelial cells. We also note that uterine fibroblasts might express additional H3K27me3-regulated genes that contribute to the labor cascade that were not detected as such in this study due to scRNA-Seq's limited depth.

Lastly, our results raise questions regarding mechanisms of locus-specific H3K27me3 erosion and peri-implantation H3K27me3 tuning, including how P4 and KDM6B contribute to the latter process. Indeed, while the H3K27me3 elevations observed in *Kdm6b cKO* mice suggest a role for KDM6B in peak tuning, our results are also consistent with the possibility that these elevations are present prior to copulation. Nonetheless, the elevations allowed us to ascribe functional significance to subsequent peak erosion. It is also unclear why erosion takes over as the dominant feature of H3K27me3 dynamics after implantation given that high serum P4 levels persist up until the end of gestation, but it is possible that the switch somehow involves locus-specific replicational dilution of H3K27me3 or the activation of KDM6A, in line with the parturition delay we previously observed in GSK-J4-treated mice that were otherwise allowed to deliver via luteolysis [98]. We anticipate that insight into these questions will bear upon investigations into whether and how perturbations to the uterine microenvironment in early

gestation could alter birth timing and whether perturbations to analogous processes in humans could contribute to the pathogenesis of preterm labor.

Acknowledgments

We thank S. Fisher, H. Madhani, and D. Lim for helpful discussions and suggestions, S. Bustamante Eguiguren for assistance with histology, and L. Maliskova, N. Kochhar and W. Eckalbar of the UCSF Genomics Core for assistance with CUT&RUN library preparation and data analysis. Figure 2.2D and Figure 2.7 were created with BioRender.com. This work was supported by the Burroughs Wellcome Fund Preterm Birth Initiative (Grant #1019789 to A.E.), grants from the National Institutes of Health (NIH) (R01AI150191 and R01AI143187 to A.E. and F31HD106714 to T.I.M.), and the UCSF Bakar ImmunoX Initiative (to B.D., A.J.C., and A.E).

Author contributions

Conceptualization: T.I.M. and A.E. Methodology: T.I.M., K.H., A.C., A.E. Investigation: T.I.M., B.D., O.V., L.Q. Visualization: T.I.M. and A.E. Funding acquisition: T.I.M. and A.E. Project administration: A.E. Supervision: A.E. Writing – original draft: T.I.M. Writing – review & editing: T.I.M. and A.E.

Figures

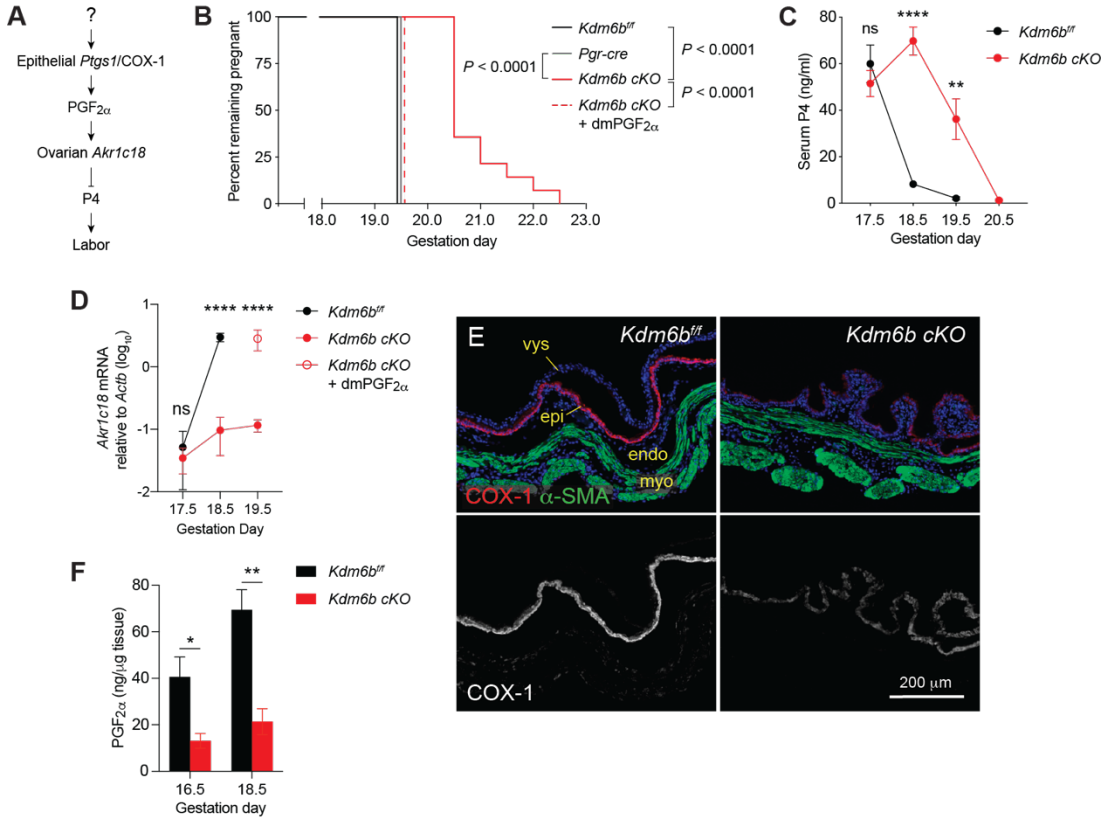

Figure 2.1 *Kdm6b cKO* mice experience delayed parturition due to delayed luteolysis.

(A) Schematic showing the series of events in late gestation that trigger labor onset in mice. (B) Parturition timing in *Kdm6b cKO* and control *Kdm6b*$^{f/f}$ and *Pgr-cre* mice. *Kdm6b*$^{f/f}$ mice were littermates of *Kdm6b cKO* mice. Groups were compared by the log-rank test (n=8-16 mice/group). (C) Serum P4 concentrations and (D) *Akr1c18* mRNA expression in the ovaries. **, P<0.01; ****, P<0.0001 by Student's t-test (n=3-6 mice/group; mean+/-SEM). ns, not significant. As indicated in (B) and (D), some mice were injected with the stable $PGF_{2\alpha}$ analog 16,16-dimethyl $PGF_{2\alpha}$ ($dmPGF_{2\alpha}$) on GD18.5. (E) COX-1 immunostaining of the anti-mesometrial portion of GD16.5 implantation sites (representative of n=3 mice/group). α-smooth muscle actin (α-SMA) identifies SMCs in the myometrium (myo). epi, uterine epithelium; endo, endometrium, vys, visceral yolk sac. (F) Uterine $PGF_{2\alpha}$ concentrations. *, P<0.05; **, P<0.01 by Student's t-test (n=5 mice/group; mean+/-SEM).

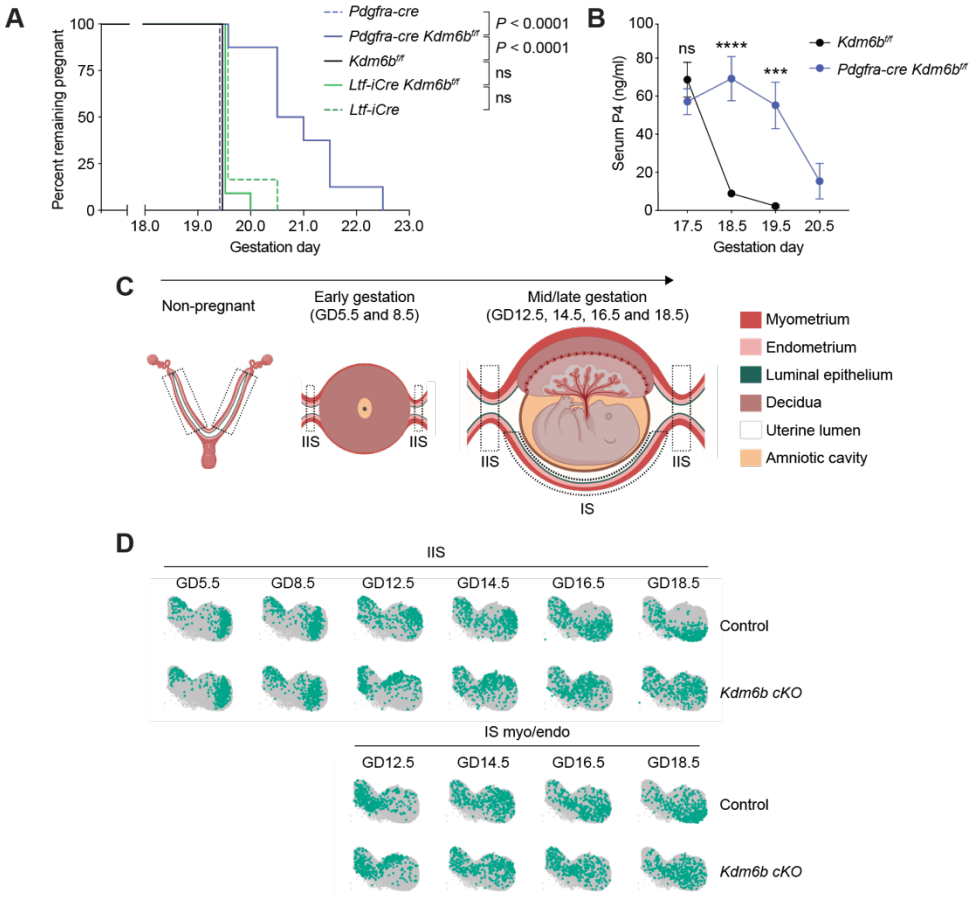

Figure 2.2 A KDM6B-influenced gene expression program within uterine fibroblasts controls parturition timing.

(A) Parturition timing in mice with cell type-specific *Kdm6b* deficiencies. *Kdm6b*$^{f/f}$ mice were littermates of *Pdgfra-cre Kdm6b*$^{f/f}$ mice. Groups were compared by the log-rank test (n=6-11 mice/group). (B) Serum P4 concentrations. ***, P<0.001; ****, P<0.0001 by Student's t-test (mean+/-SEM, n=4 mice/group). (C) Schematic of non-pregnant uterus and early and mid/late gestation implantation sites (IS) and inter-implantation sites (IIS). Dashed lines demarcate the dissected tissues analyzed by scRNA-Seq and/or CUT&RUN (see Figure 2.3). (D) UMAP projection of fibroblasts combined from every time point, genotype, and anatomic location (gray), highlighted by the gestation day, genotype, and anatomic location indicated (green). Projections were down sampled to show the same number of cells (n=400) for each group.

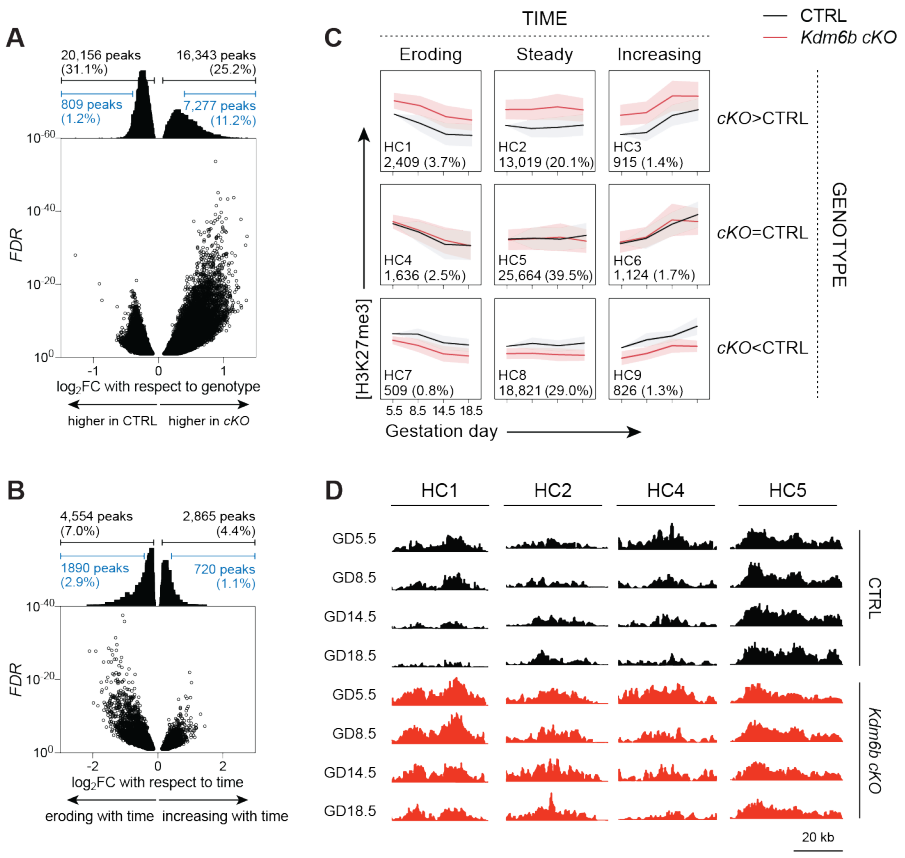

Figure 2.3 H3K27me3 dynamics in the fibroblasts of the pregnant mouse uterus involve KDM6B-dependent and -independent processes.

Peak concentrations and distributions were determined by CUT&RUN (*n*=3 specimens for each genotype and time point) and then subjected to an aggregate differential peak analysis that specified genotype and gestation day (time; GD5.5-18.5) as independent covariates (*FDR*<0.1 each). (A-B) Volcano plot analysis of H3K27me3 peaks that varied significantly with respect to genotype or time. Percentages are of the total 64,923 peaks. The pronounced elevation in H3K27me3 concentrations at certain loci in *Kdm6b cKO* compared to control *Kdm6b*$^{f/f}$ fibroblasts (abbreviated as "*cKO*" and "CTRL" respectively) was especially apparent when applying a fold-change cutoff (e.g., a 0.4 cutoff, blue). No fold-change skewing was apparent for time-dependent changes, despite more peaks eroding with time than increasing with time. (C) The 9 ways H3K27me3 levels vary by time and genotype. For example, the 2,409 peaks in histone category 1 (HC1) both erode with advancing gestation and are significantly higher in *Kdm6b cKO* compared to control fibroblasts. For each histone category graph, we show the mean concentrations (with SD as shaded areas) for all member peaks after first normalizing to their respective concentrations in GD5.5 control fibroblasts. Each graph also shows the number of member peaks and the percentage these peaks comprise of all 64,923 peaks. (D) Representative pileups of the *n*=3 replicates/group for HC1, 2, 4, and 5 (Figure 2.11E shows examples of all histone categories).

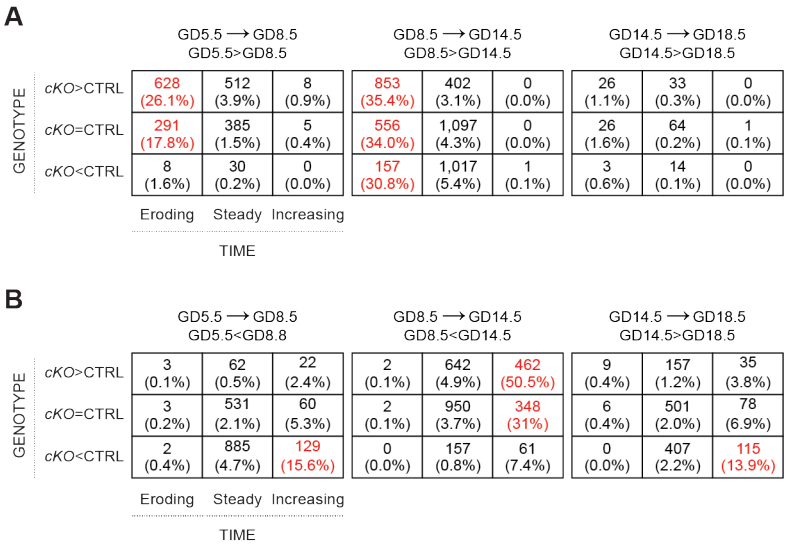

Figure 2.4 H3K27me3 erosion is detectable as early as GD8.5.

(A, B) Tallies of the number of peaks within the 9 histone categories (defined by the results of the aggregate analysis that employed a *FDR*<0.1 significance threshold; see Figure 2.3C) that were scored as either eroding (A) or increasing (B) during the three indicated time periods when we instead applied a P_{raw}<0.05 significant threshold. The percentages these tallies comprise of the number of peaks within their respective parent histone category (Figure 2.3C) are also shown (red denotes cases where the percentages exceeded 10%).

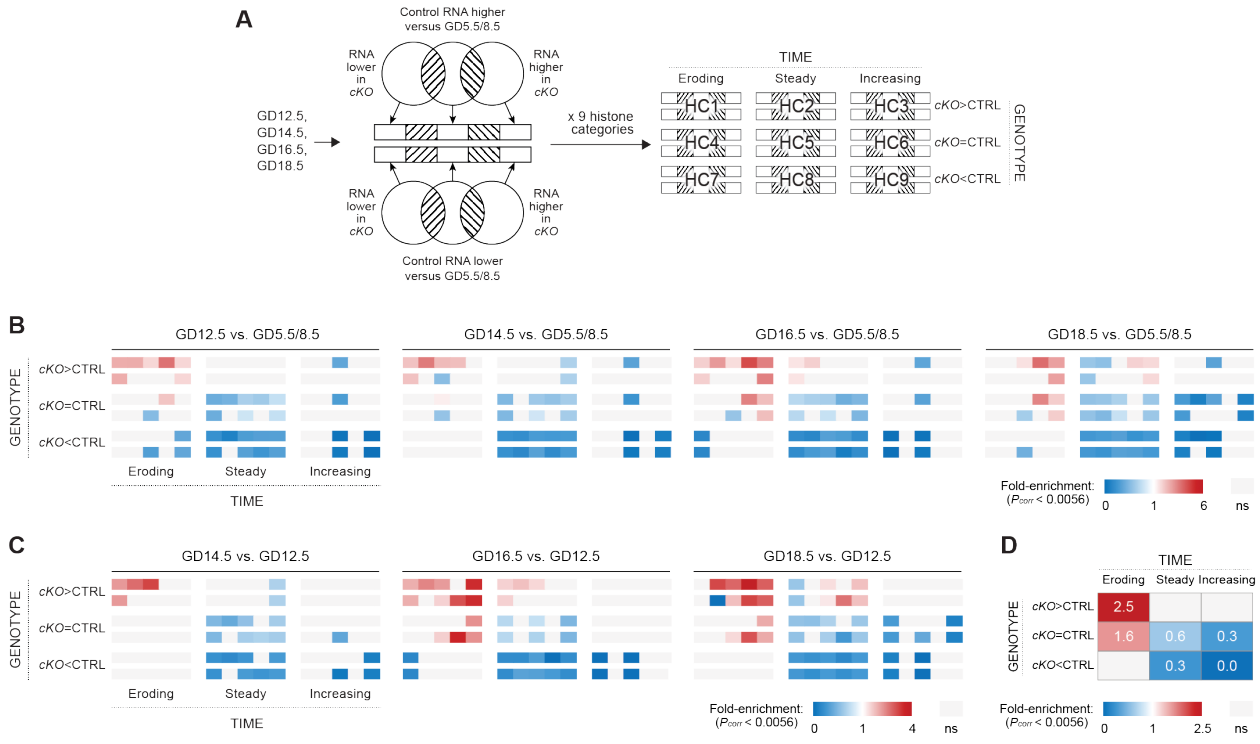

Figure 2.5 Progressive, locus-specific erosion of H3K27me3 in uterine fibroblasts is associated with the induction of linked genes at mid-to-late gestation.

(A) Workflow to identify associations between gene expression and locus-specific H3K27me3 dynamics. Note that the non-hatched boxes represent the total number of genes in a category, not just those that fell outside the hatched areas of overlap. (B) Heat-map representation of log fold differences (i.e., fold-enrichment scores) between the number of genes in each histone/gene expression category and the number expected by chance based upon the underlying, independent distributions of histone category memberships and gene expression patterns. Colored tiles indicate scores that are statistically significant (two-tailed Fisher's exact test, using a Bonferroni-corrected *P*-value threshold of 0.0056 to account for the 9 histone category comparisons made per time point). ns, not significant. Values for fold-enrichment scores, together with absolute gene counts, are shown in Table 2.1. (C) A similar analysis as panel (B), but using gene expression on GD12.5 rather than GD5.5/8.5 as the baseline reference point. (D) The distribution across HC1-9 of all genes showing both increased expression in control IS myo/endo and IIS fibroblasts for at least one time point from GD12.5-18.5 compared to GD5.5/8.5 IIS and differential expression between *Kdm6b cKO* and gestation day-matched control fibroblasts. Fold-enrichment scores were determined as in (B); colored tiles indicate scores that are statistically significant (two-tailed Fisher's exact test as above).

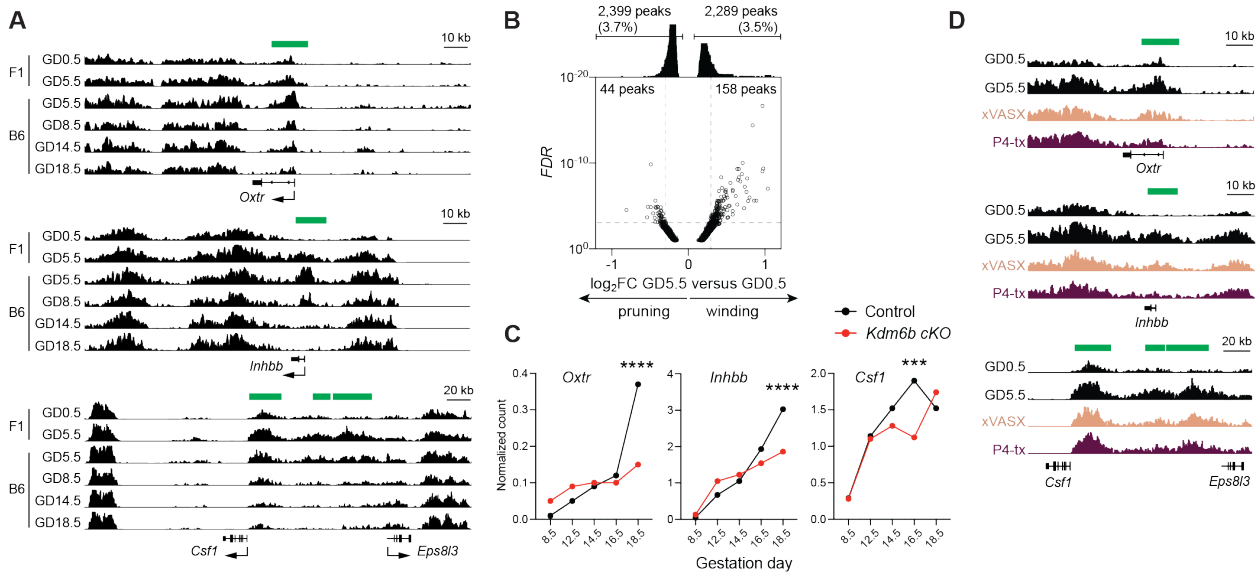

Figure 2.6 H3K27me3 accumulation in uterine fibroblasts between GD0.5 and GD5.5 sets the gestational timer.

(A) H3K27me3 distributions at the *Oxtr*, *Inhbb,* and *Csf1* loci (pileups of *n*=3 independent replicates/group). Green bars denote peaks that significantly increase from GD0.5-5.5 and then erode from GD5.5-18.5 (*FDR*<0.1). Transcription start sites are indicated. Note the similarities in peak profiles on GD5.5 for B6CBAF1/J (F1) and B6 mice. (B) Volcano plot analysis of the 4,688 H3K27me3 peaks that varied significantly between GD0.5 and GD5.5 (*FDR*<0.1). Percentages are of the total 64,923 peaks. (C) Normalized mRNA counts for *Oxtr, Inhbb,* and *Csf1* in control and *Kdm6b cKO* fibroblasts from GD8.5, GD12.5, GD14.5, GD16.5, and GD18.5 (from the scRNA-Seq analysis and including data from both IS myo/endo and IIS). ***, *FDR*<0.001, ****, *FDR*<0.0001 by a two-sided Wilcoxon rank-sum test. (D) H3K27me3 distributions at the *Oxtr, Inhbb*, and *Csf1* loci on GD0.5, GD5.5 (following natural mating), the equivalent of GD5.5 following xVASX mating, and 1 day after injecting non-pregnant mice with P4 for 3 days (pileups of *n*=3 independent replicates/group). Green bars denote the peaks shown in panel (A). Compared to GD0.5, these peaks are significantly higher in GD5.5, xVASX, and P4-tx mice (*FDR*<0.1). For *Oxtr* and *Inhbb*, they are also higher in the GD5.5 compared to P4-tx groups, but not significantly different between GD5.5 and xVASX groups. *Csf1* peak concentrations are not significantly different between GD5.5, xVASX, and P4-tx groups.

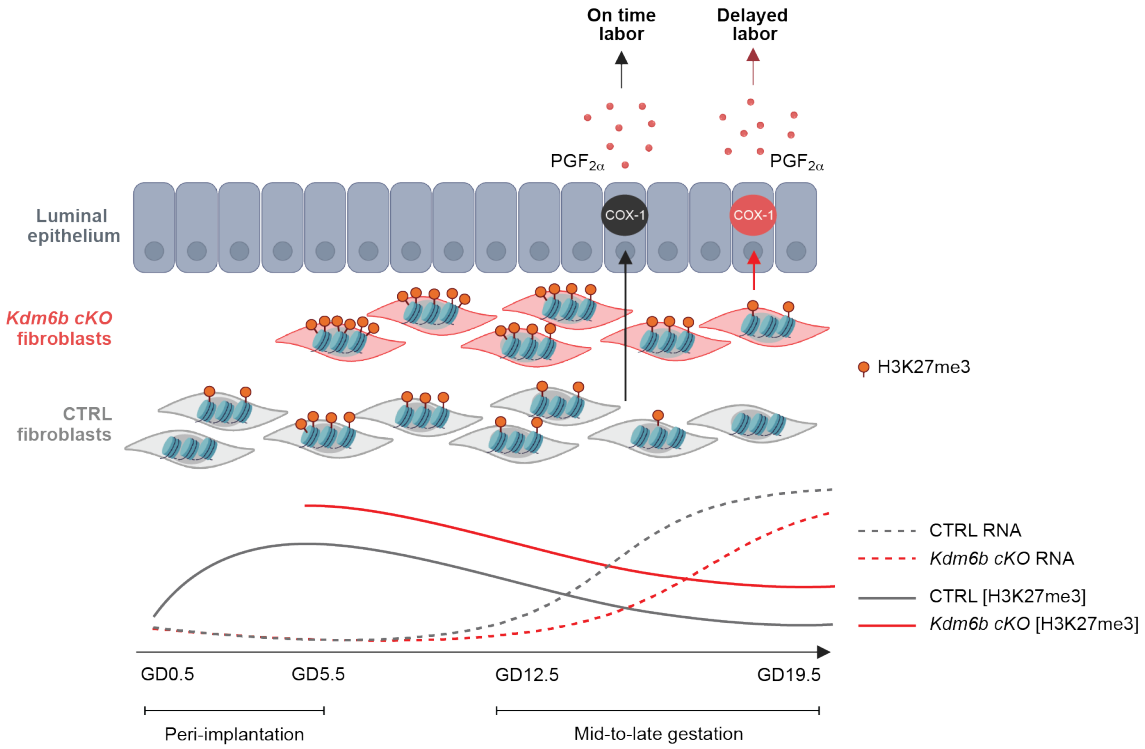

Figure 2.7 An epigenetic timer of gestation length in mice (proposed model).

The timer is set during the peri-implantation period when levels of the repressive histone mark H3K27me3 are established at select loci in uterine fibroblasts. This process most overtly involves H3K27me3 accumulation (depicted), but also, to a lesser extent, H3K27me3 pruning. After GD5.5, progressive erosion of H3K27me3 at these loci controls the timing of a uterine-wide gene induction program in fibroblasts that becomes evident in mid-to-late gestation. This program in turn directly or indirectly induces COX-1 expression by uterine epithelial cells, which then triggers labor onset. In mice with uterine KDM6B deficiency, peak erosion occurs at the normal rate, but the timer starts with an elevated setpoint thus increasing the time before H3K27me3 can reach levels otherwise already reached during normal pregnancy. This delays and dysregulates the gene induction program in uterine fibroblasts, in turn leading to delayed COX-1 induction and thus delayed labor onset.

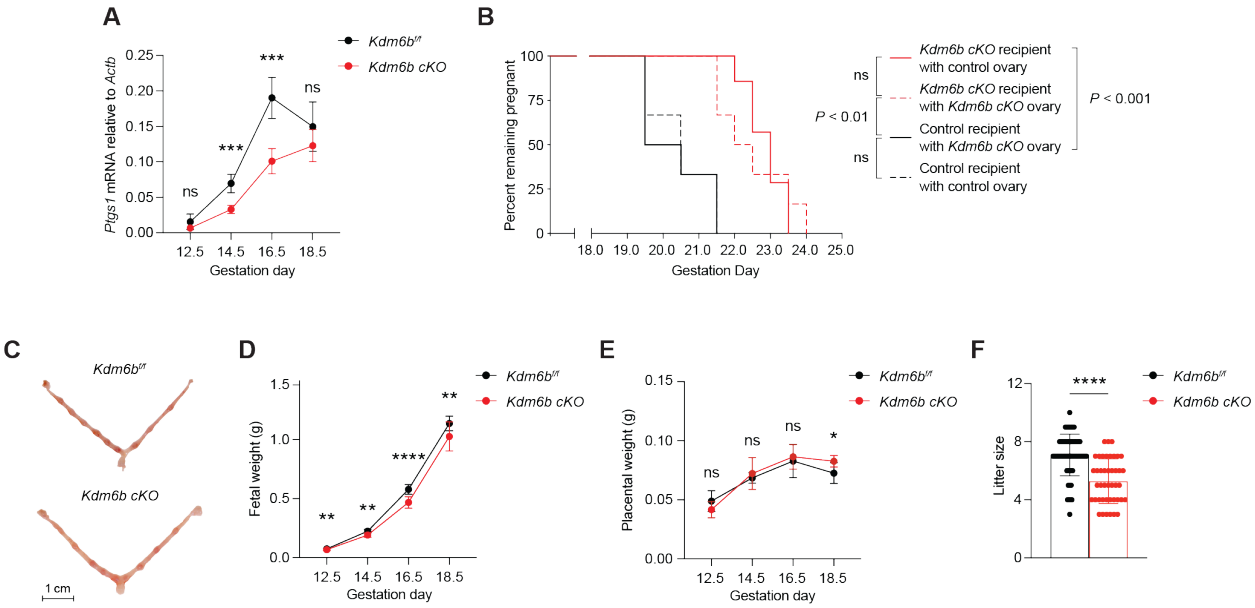

Figure 2.8 Additional characterization of *Kdm6b cKO* mice.

(A) *Ptgs1* mRNA expression by purified uterine luminal epithelial cells. ***, $P<0.001$ by Student's *t*-test (n=3-6 mice/group; mean+/-SEM). (B) Parturition timing of mice following ovary transplantation. In addition to reciprocal ovary transplants (*Kdm6b*$^{f/f}$ → *Kdm6b cKO* and *Kdm6b cKO* → *Kdm6b*$^{f/f}$), we also performed *Kdm6b cKO* → *Kdm6b cKO* and *Kdm6b*$^{f/f}$ → *Kdm6b*$^{f/f}$ transplants in order to control for the effect of transplantation per se. Groups were compared by the log-rank test (n= 6-7 mice/group). Females were mated with B6 males 2-4 weeks post surgery. Delayed parturition tracked with the genotype of the transplant recipient and not the genotype of the transplanted ovaries. (C) Morphology of pregnant uteri on GD5.5 (representative images of n=4-6 mice/group). (D-E) Fetal (n=7-21 pregnancies/group) and placental (n=5-11 pregnancies/group) weights in mid-to-late gestation. Weights were first averaged over all pups within a litter; graph shows mean+/-SD of these averages. *, $P<0.05$; **, $P<0.01$; ****, $P<0.0001$ by Student's *t*-test. (F) Litter sizes (n=49-61 mice/group). ****, $P<0.0001$ by Student's *t*-test.

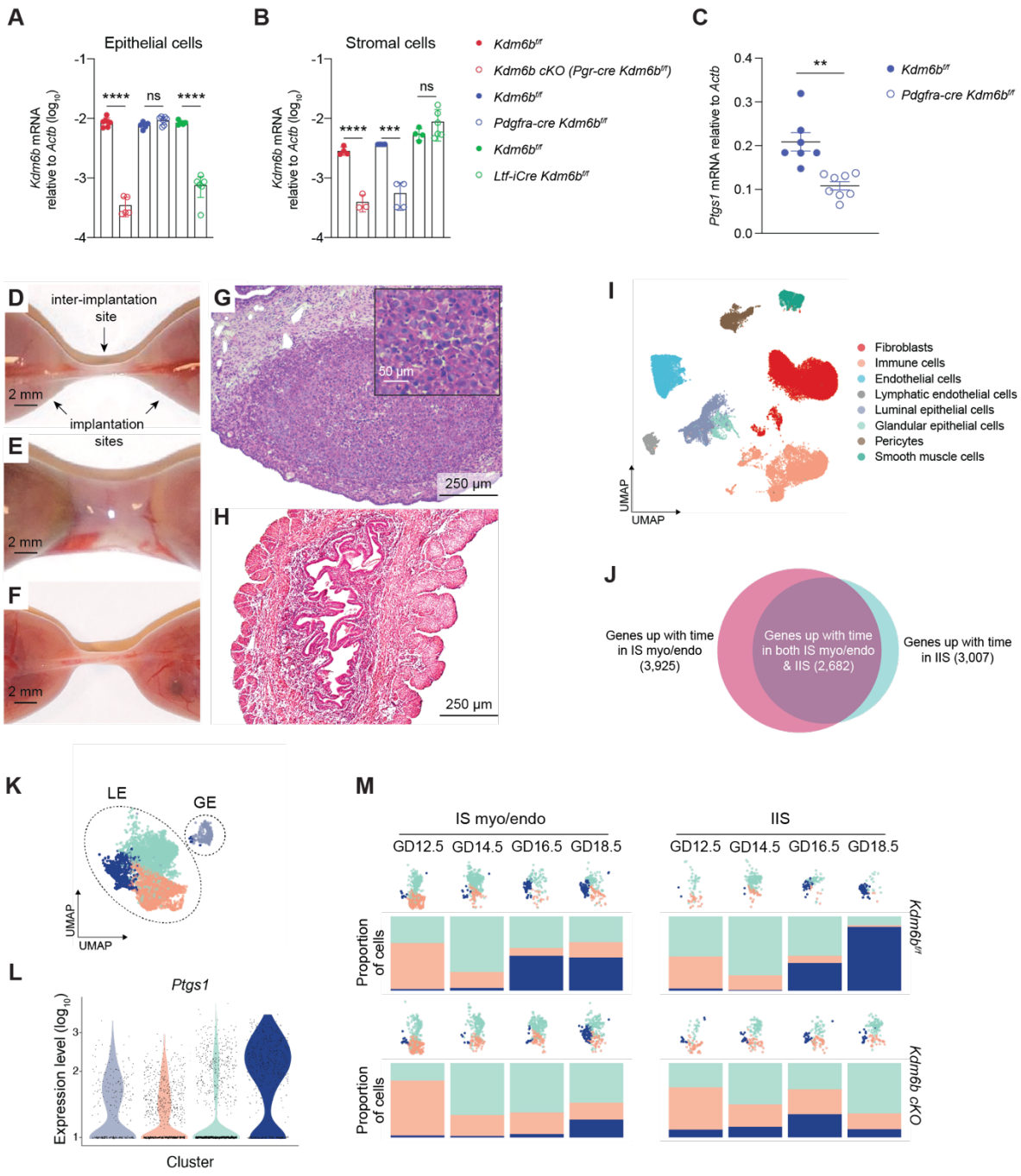

Figure 2.9 Additional characterization of *Ltf-iCre Kdm6b*$^{f/f}$ and *Pdgfra-cre Kdm6b*$^{f/f}$ mice and scRNA-Seq analysis of the pregnant mouse uterus.

(Figure caption continued on the next page)

Figure 2.9. (Figure caption continued from the previous page) (A-B) qRT-PCR determination of *Kdm6b* mRNA expression in (A) uterine epithelial cells and (B) uterine fibroblasts from the indicated strains on GD16.5. ***, $P<0.001$; ****, $P<0.0001$ by two-sided Student's *t*-test (n=3-7 mice/group; mean+/-SEM). Filled circles represent respective littermate controls for the mice represented by open circles. Note the targeting of *Kdm6b* deletion to epithelial cells in *Ltf-iCre Kdm6b*$^{f/f}$ mice, to stromal cells in *Pdgfra-cre Kdm6b*$^{f/f}$ mice, and to both cell types in *Kdm6b cKO* mice. (C) qRT-PCR determination of *Ptgs1* mRNA expression in purified uterine epithelial cells on GD16.5. **, $P<0.01$ by two-sided Student's *t*-test (n=7-8 mice/group; mean +/- SEM). (D-H) Ectopic deciduoma formation in the IIS of pregnant *Kdm6b cKO* mice. (D-F) Whole-mount images of GD16.5 uteri from (D) *Kdm6b*$^{f/f}$ control; (E) *Kdm6b cKO*; and (F) *Pdgfra-cre Kdm6b*$^{f/f}$ mice. Note the swelling of the IIS in the *Kdm6b cKO* specimen. Such swellings were apparent in all *Kdm6b cKO* mice examined and none of the control or *Pdgfra-cre Kdm6b*$^{f/f}$ mice. (G-H) H&E-stained cross-sectional images of *Kdm6b cKO* (G) and *Kdm6b*$^{f/f}$ (H) IIS. Note the aggregation of decidual stromal-like cells in the *Kdm6b cKO* IIS. (I) IIS (GD5.5, 8.5, 12.5, 14.5, 16.5, 18.5) and the IS myo/endo (GD12.5, 14.5, 16.5, 18.5; see Figure 2.2C) were processed using the 10X Genomics platform. UMAP embedding of combined data from control cells over all time points (n=54,273 cells). Eight major cell clusters were identified through graph-based clustering. (J) Venn diagram displaying the number of genes in either the IIS, IS myo/endo, or both, that experienced increased expression in control fibroblasts for at least one time point from GD12.5-18.5 compared to the combined expression data from GD5.5 and 8.5 IIS. (K) UMAP embedding of data from late gestation uterine epithelial cells pooled from GD12.5, 14.5, 16.5, and 18.5 control mice. Graph-based clustering identified three clusters of luminal epithelial cells (LE) and one cluster of glandular epithelial cells (GE). Glandular epithelial cells were identified by virtue of their expression of *Prss29*. Colors of the UMAP clusters correspond to the populations shown in (L) and (M). (L) Violin plot of *Ptgs1* expression amongst the epithelial clusters in control mice. (M) Bar plots, with associated UMAPs, showing the proportion of cells for each luminal epithelial cluster, separated by gestation day, genotype, and location (IS myo/endo and IIS plots respectively show n=188-774 and n=72-262 cells). Note that the transition of the control epithelium to a *Ptgs1*-expressing phenotype occurs throughout the entire uterus (both IS myo/endo and IIS), and that this transition is delayed in the *Kdm6b cKO* epithelium.

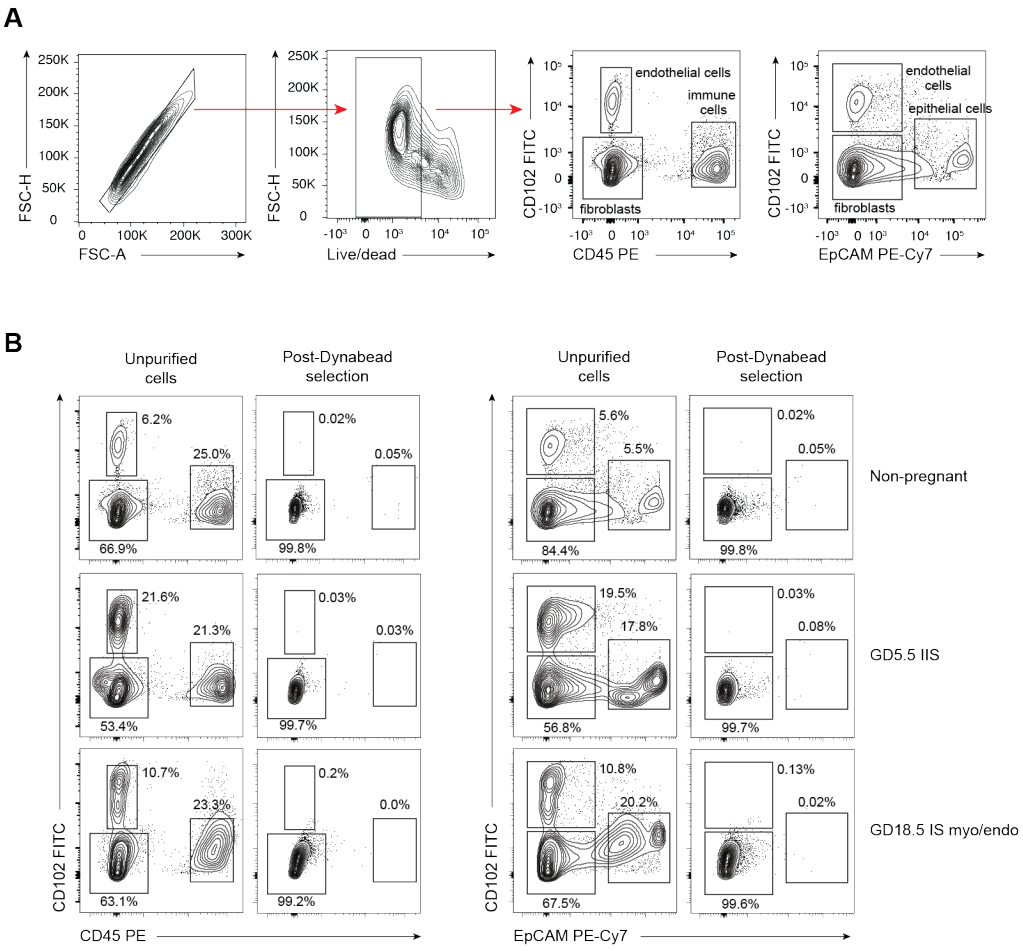

Figure 2.10 Purity analysis of uterine fibroblasts prior to and after Dynabead-based negative selection, assessed by flow cytometry.

(A) Gating strategy. (B) Prevalence of endothelial cells ($CD102^+$), immune cells ($CD45^+$), epithelial cells ($EpCAM^+$), and fibroblasts ($CD102^-$ $CD45^-$ $EpCAM^-$) in cell suspensions prepared from non-pregnant uteri, GD5.5 IIS and GD18.5 IS myo/endo prior to and after negative selection (representative of n=3/group).

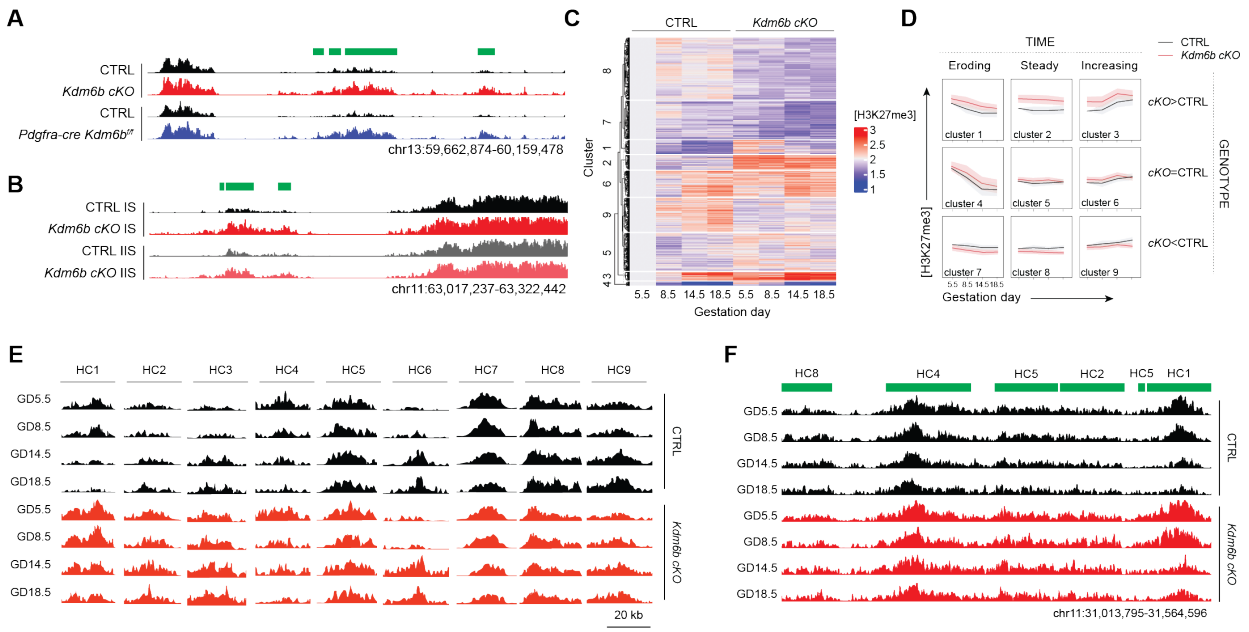

Figure 2.11 Additional H3K27me3 CUT&RUN analyses.

(A) Genomic area showing H3K27me3 tracks for *Kdm6b cKO* (*Pgr-cre Kdm6b*$^{f/f}$) and *Pdgfra-cre Kdm6b*$^{f/f}$ uterine fibroblasts on GD14.5, together with tracks from respective littermate controls (*Kdm6b*$^{f/f}$ for both; pileups of n=3 independent replicates per group). Peaks significantly higher in the *Kdm6b cKO* and *Pdgfra-cre Kdm6b*$^{f/f}$ cells compared to their respective controls (*FDR*<0.1) are denoted by green bars. Genome-wide peak profiles were virtually identical between *Kdm6b cKO* and *Pdgfra-cre Kdm6b*$^{f/f}$ cells (54 differential peaks, *FDR*<0.1). (B) Genomic area showing H3K27me3 tracks for *Kdm6b cKO* and *Kdm6b*$^{f/f}$ control uterine fibroblasts isolated from either the IS myo/endo or IIS on GD14.5 (pileups of n=3 independent replicates per group). Peaks significantly higher in both *Kdm6b cKO* IS myo/endo and IIS compared to controls (*FDR*<0.1) are denoted by green bars. Peak profiles were virtually identical between control IS myo/endo and IIS fibroblasts (18 differential peaks, *FDR*<0.1) as well as between *Kdm6b cKO* IS myo/endo and IIS fibroblasts (125 differential peaks, *FDR*<0.1). (C) Heat-map visualization of K-means clustering of H3K27me3 peak patterns in uterine fibroblasts. Prior to clustering, H3K27me3 concentrations were normalized to GD5.5 control levels. (D) Summary visualization of the 9 categories of H3K27me3 dynamics identified by K-means clustering. For each cluster, we show the mean concentrations (with SD as shaded areas) for all member peaks after first normalizing to the respective concentration for that peak in GD5.5 control fibroblasts. Note that this approach arrives at the same 9 histone categories identified by the aggregate analysis performed in DiffBind (Figure 2.3C). (E) Representative peak pileups (n=3 replicates per group) for all 9 histone categories. HC1, 2, 4 and 5 peaks are the same as those shown in Figure 2.3D. (F) A genomic area demonstrating the highly localized nature of genotype- and time-dependent variations in peak concentrations, as peaks experiencing such differences frequently abutted peaks that either remained constant over time and/or were unchanged between strains (pileups of n=3 independent replicates). Chromosome location and histone categories are shown.

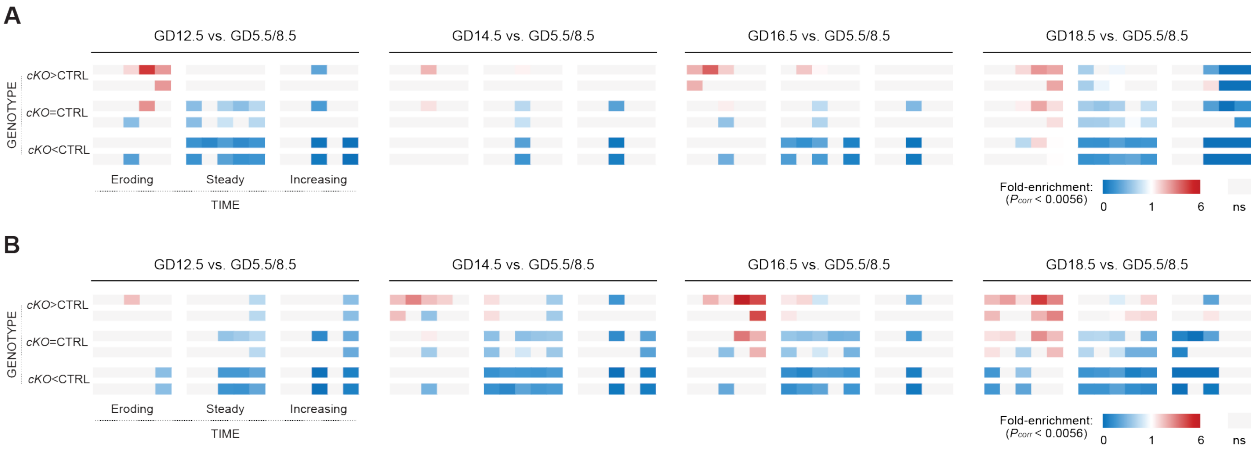

Figure 2.12 Additional analysis of associations between gene expression and H3K27me3 dynamics in uterine fibroblasts.

(A-B) Associations between gene expression and locus-specific H3K27me3 dynamics in uterine fibroblasts, separated by anatomic location. This analysis took the same approach as in Figure 2.5A-B but separately analyzed mRNA expression in IS myo/endo (A) and IIS (B) fibroblasts. Colored tiles indicate scores that are statistically significant (two-tailed Fisher's exact test, using a Bonferroni-corrected *P*-value threshold of 0.0056 to account for the 9 histone category comparisons made per time point). ns, not significant. Note the similar enrichment patterns at both anatomic locations. Values for fold-enrichment scores, together with absolute gene counts, are shown in Table 2.1.

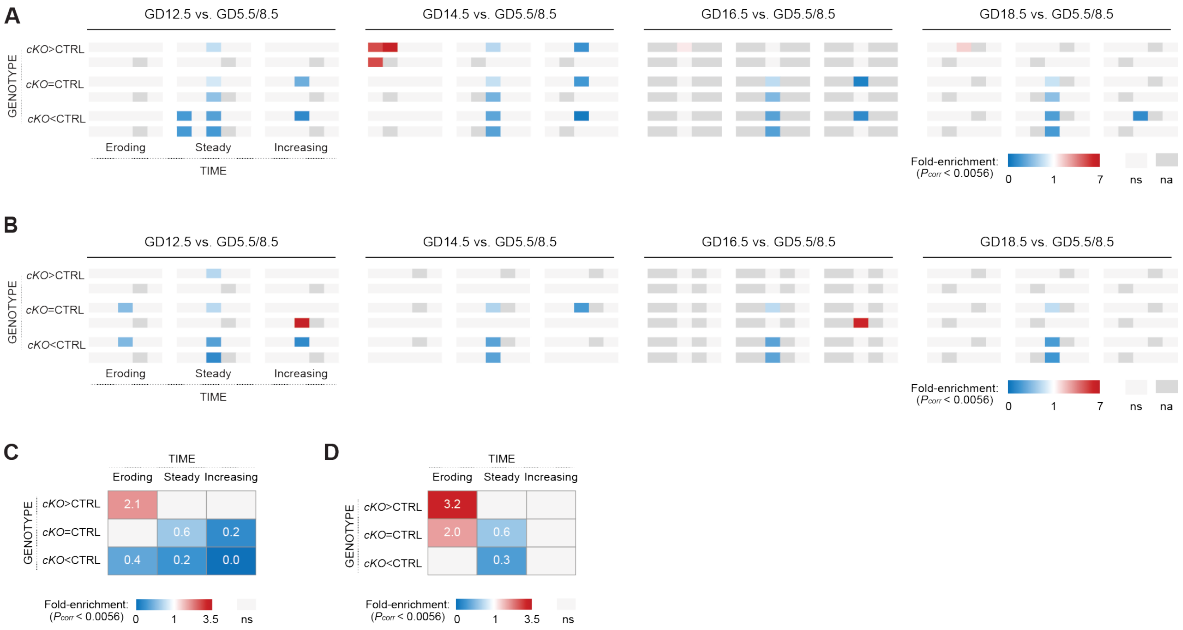

Figure 2.13 Additional analysis of associations between gene expression and H3K27me3 dynamics in uterine fibroblasts.

(A-B) Associations between gene expression in uterine SMCs and pericytes and locus-specific H3K27me3 dynamics in uterine fibroblasts. This analysis took the same approach as in Figure 2.5A-B but analyzed mRNA expression in IS myo/endo and IIS SMCs (A) or pericytes (B). Colored tiles indicate scores that are statistically significant (two-tailed Fisher's exact test, using a Bonferroni-corrected *P*-value threshold of 0.0056 to account for the 9 histone category comparisons made per time point). ns, not significant. Note the lack of a consistent association between mRNA expression in both SMCs and pericytes and H3K27me3 dynamics, as determined by our CUT&RUN analysis of uterine fibroblasts. This observation implied that the apparent association between gene expression in uterine fibroblasts and H3K27me3 dynamics shown in Figure 2.5B was not due to an incidental similarity in gene expression patterns between uterine fibroblasts and these other two cell types, which were present in our uterine fibroblast preparations used for CUT&RUN at levels of 3-17%. To the contrary, the isolated example of enrichment on GD14.5 between HC1 and genes that increased in expression with advancing gestation in control SMCs and that were also expressed at lower levels in *Kdm6b cKO* SMCs was caused by 5 genes that possessed these same expression characteristics in uterine fibroblasts. For (A) and (B), values for fold-enrichment scores, together with absolute gene counts, are shown in Table 2.1. (C-D) The distribution across HC1-9 of all genes showing both increased expression in control myo/endo IS and IIS fibroblasts for at least one time point from GD12.5-18.5 compared to GD5.5/8.5 IIS and either lower (C) or higher (D) expression in *Kdm6b cKO* fibroblasts compared to gestation day-matched control fibroblasts. Fold-enrichment scores were determined as in Figure 2.5B; colored tiles indicate scores that are statistically significant (two-tailed Fisher's exact test as above). ns, not significant. See Figure 2.5D for the combination of both expression characteristics (increased expression in control fibroblasts and either higher or lower expression in *Kdm6b cKO* fibroblasts compared to gestation day-matched control fibroblasts).

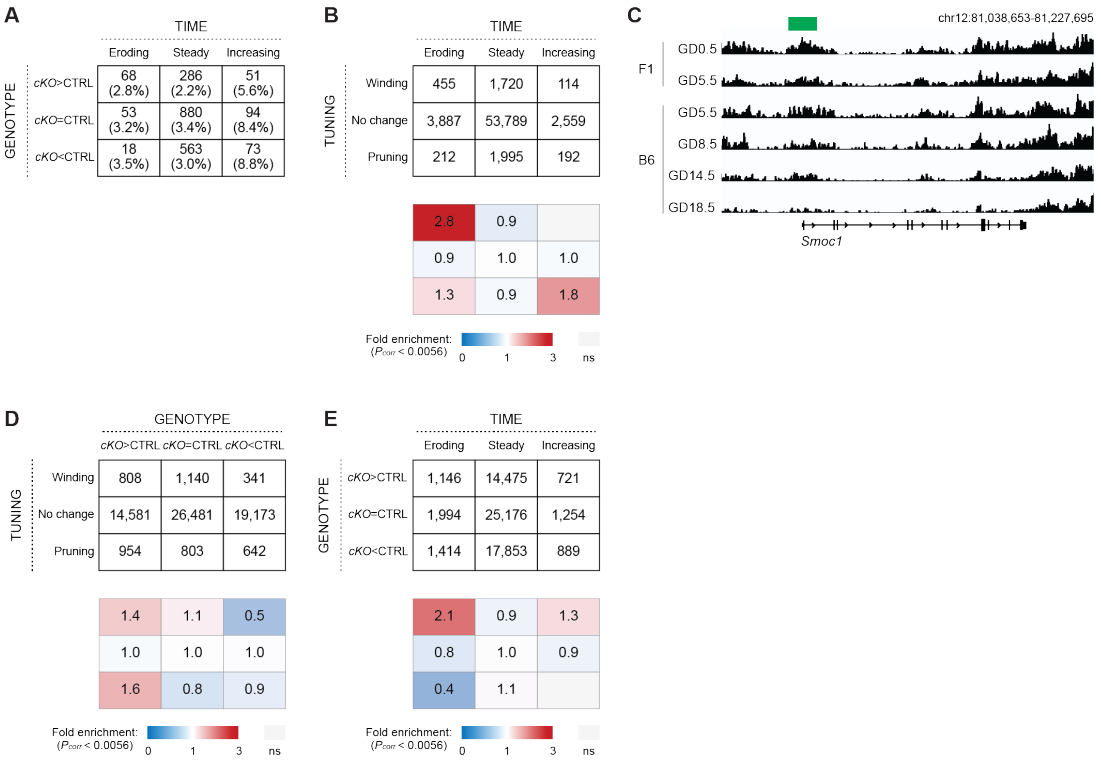

Figure 2.14 Peri-implantation H3K27me3 dynamics in uterine fibroblasts.

(A) Comparison of H3K27me3 distributions in B6 and B6CBAF1/J uterine fibroblasts on GD5.5. Differential peak analysis of B6 and B6CBAF1/J uterine fibroblasts identified 2,086 differential peaks (*FDR*<0.1). To determine how these differences might relate to time- and genotype-dependent H3K27me3 dynamics observed post-GD5.5 (all from cells on a B6 background), we assessed how these 2,086 peaks were distributed across the 9 histone categories defined in Figure 2.3C. Accordingly, the matrix shows how many differential peaks between B6 and B6CBAF1/J uterine fibroblasts were also differentially expressed with respect to time and genotype, both in absolute terms and as a percentage of the parent histone category. (B) Inter-relationships between H3K27me3 dynamics in the peri-implantation period and H3K27me3 dynamics after GD5.5. The top set of matrices show the number of peaks that fall within the indicated categories; the bottom set of matrices show fold difference compared to the number of peaks expected if independent processes controlled H3K27me3 dynamics pre- and post-GD5.5. Colored tiles indicate scores that are statistically significant (two-tailed Fisher's exact test, using a Bonferroni-corrected *P*-value threshold of 0.0056 to account for the 9 histone category comparisons made for each pair of parameters). (C) Example of a locus experiencing H3K27me3 pruning (pileups of *n*=3 independent replicates/group). The green bar denotes a peak identified as showing significant loss from GD0.5-5.5 followed by erosion from GD5.5-18.5 (*FDR*<0.1 in both cases). (D-E) Inter-relationships between KDM6B status and H3K27me3 dynamics in the peri-implantation period (D) and after GD5.5 (E). The matrices were generated and formatted as panel (B).

Table 2.1 Details of the association analyses.

Details of the association analyses. Values for fold-enrichment scores are shown within each tile (only for those determined as significant) and absolute gene numbers are shown below each tile, related to Figures 2.5B, 2.5C, 2.12A, 2.12B, 2.13A, and 2.13B.

Absolute gene counts and values for fold-enrichment scores plotted as heat-maps in Fig. 5B

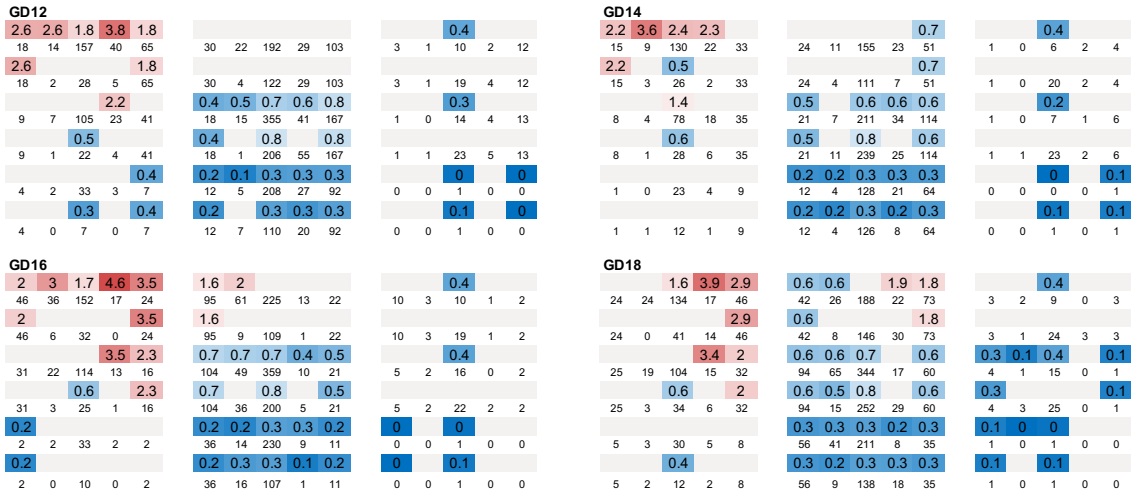

Absolute gene counts and values for fold-enrichment scores plotted as heat-maps in Fig. 5C

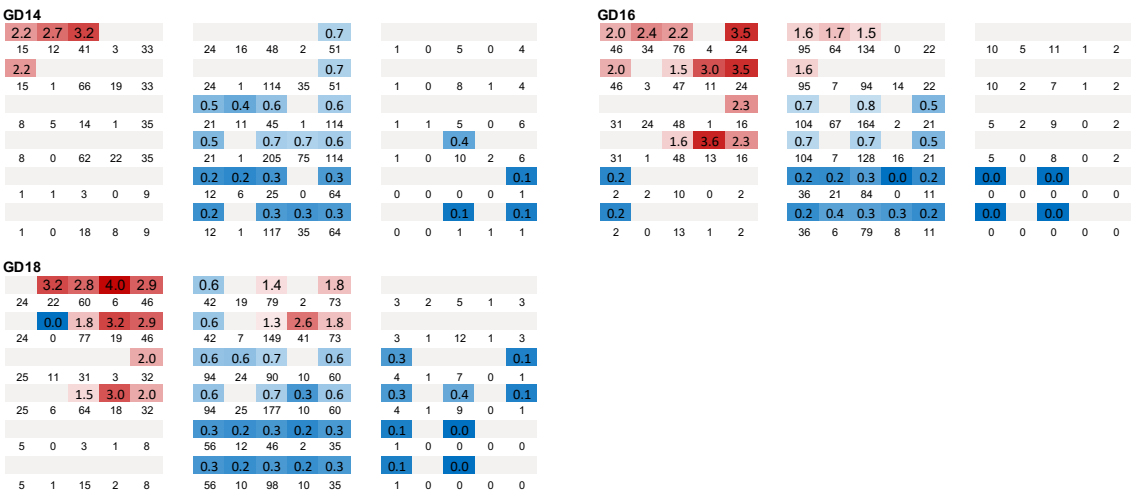

Absolute gene counts and values for fold-enrichment scores plotted as heat-maps in Fig. S5A

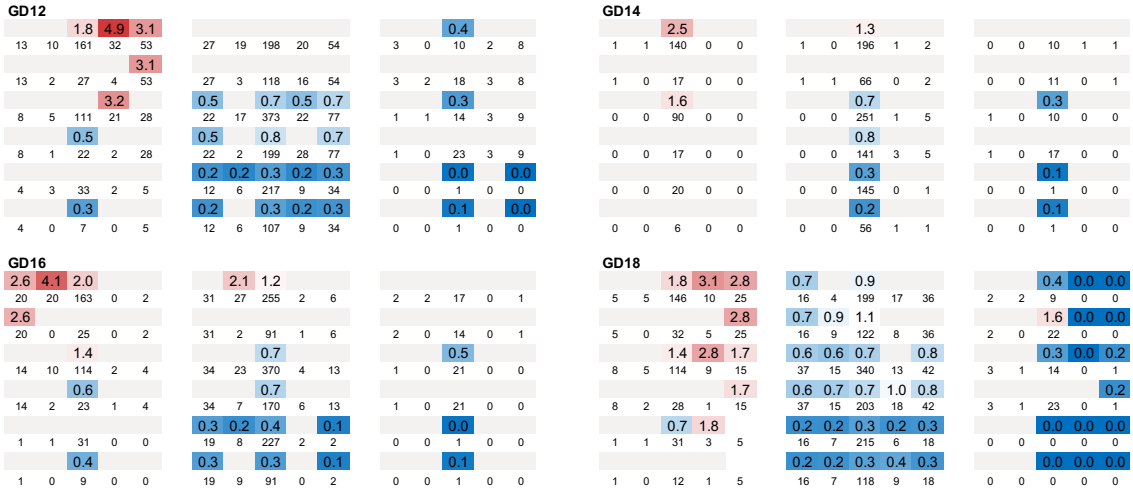

Absolute gene counts and values for fold-enrichment scores plotted as heat-maps in Fig. S5B

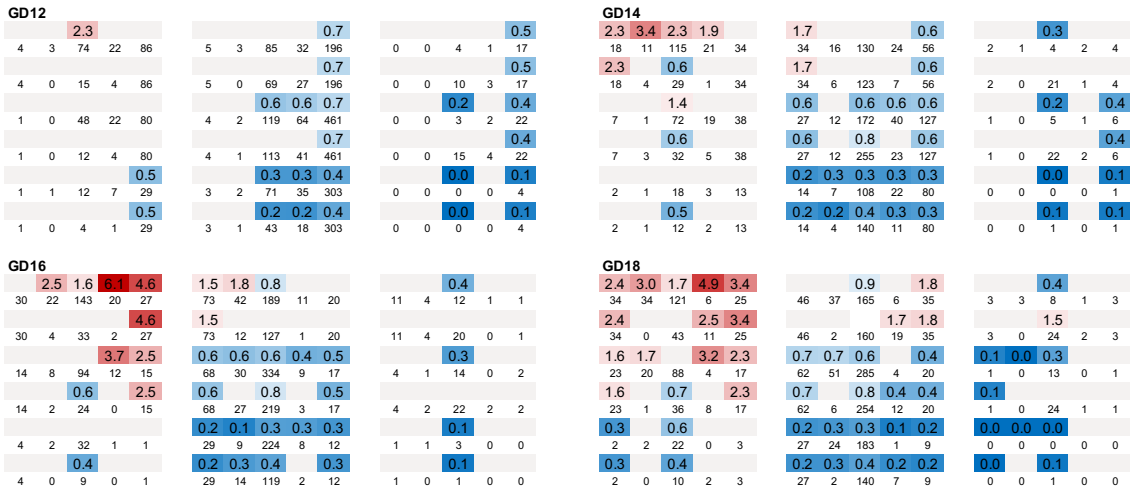

Absolute gene counts and values for fold-enrichment scores plotted as heat-maps in Fig. S6A

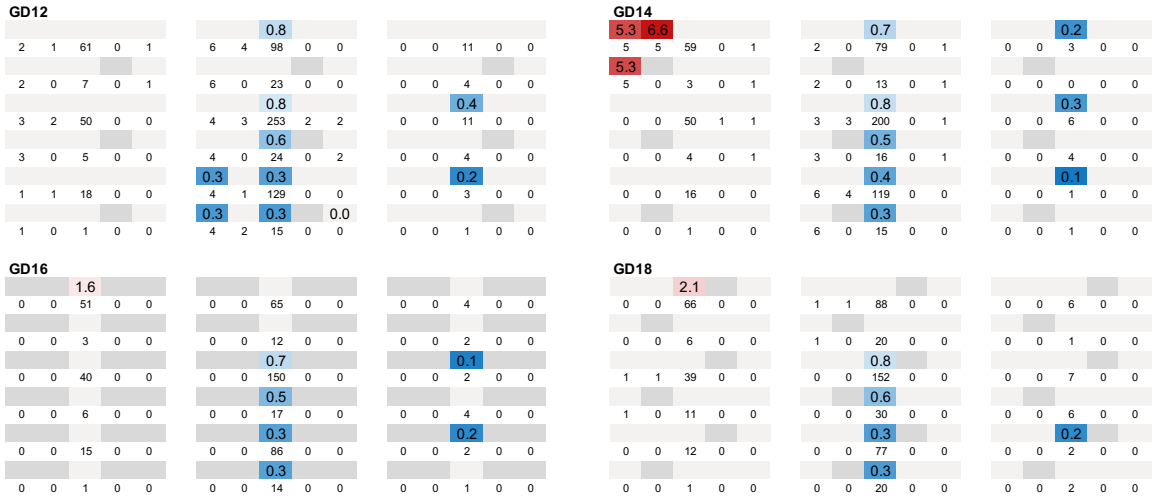

Absolute gene counts and values for fold-enrichment scores plotted as heat-maps in Fig. S6B

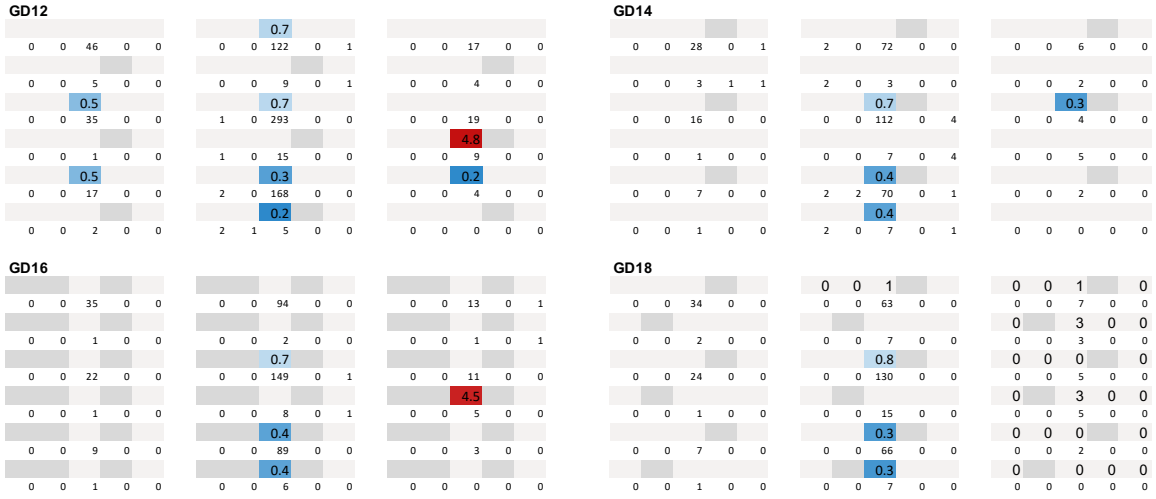

Table 2.2 Genes with a nearby H3K27me3 peak that increase with advancing gestation and are differentially expressed by *Kdm6b cKO* and ctrl cells.

Genes with a nearby H3K27me3 peak (+/- 10 kb from the TSS) and that bear the dual characteristics of 1) increased gene expression in ctrl fibroblasts on any day in mid-to-late gestation compared to GD5.5/8.5; and 2) differential gene expression on this day between *Kdm6b cKO* and ctrl cells.

				H3K27me3 peak dynamics*								RNA expression†							
				Aggregate time (GD5.5 to 18.5)		Aggregate genotype (*Kdm6b cKO* vs. ctrl)						Ctrl IS/IS fibroblasts vs. ctrl GD5.5/8.5 IIS fibroblasts (log_2FC)				*Kdm6b cKO* vs. ctrl IS/IS fibroblasts (log_2FC)			
Chr	Peak start	Peak end	Peak width	log_2FC	*FDR*	log_2FC	*FDR*	HC	Gene	Peak distance to TSS	Annotation	GD12.5	GD14.5	GD16.5	GD18.5	GD12.5	GD14.5	GD16.5	GD18.5
chr1	119416777	119431478	14702	-1.297	1.78E-20	0.212	5.58E-02	1	***Inhbb***	0	Promoter (<=1kb)	0.35	0.49	0.77	1.02	0.19	0.11	ns	-0.25
chr1	12689148	12695384	6237	-1.348	9.18E-13	0.369	6.46E-03	1	***Sulf1***	0	Promoter (<=1kb)	0.09	ns	ns	ns	0.17	ns	ns	0.08
chr1	130462231	130480398	18168	-0.340	9.09E-04	0.313	1.04E-05	1	***Cd55***	0	Promoter (<=1kb)	0.55	0.41	0.57	0.67	ns	ns	ns	-0.09
chr1	189396967	189413727	16761	-0.566	4.81E-08	0.515	1.27E-13	1	***Kcnk2***	0	Promoter (<=1kb)	0.25	0.14	0.17	0.28	ns	0.10	0.12	ns
chr1	40060281	40078513	18233	-0.407	1.43E-03	0.555	3.43E-11	1	***Il1r2***	0	Promoter (<=1kb)	0.09	0.25	0.35	0.33	ns	ns	-0.11	-0.09
chr1	54730270	54749720	19451	-0.247	6.89E-02	0.685	4.52E-13	1	***Ankrd44***	0	Promoter (<=1kb)	0.03	ns	ns	ns	0.05	ns	ns	ns
chr1	74092712	74110992	18281	-0.223	8.41E-02	0.382	4.86E-05	1	***Tns1***	0	Promoter (<=1kb)	0.25	0.35	0.39	0.36	ns	ns	-0.08	0.07
chr1	79852894	79920698	67805	-0.226	8.14E-03	0.320	2.70E-08	1	***Serpine2***	0	Promoter (<=1kb)	0.36	0.32	0.36	0.39	0.08	0.12	0.15	0.06
chr1	86616603	86701207	84605	-0.537	7.81E-07	0.174	4.03E-02	1	***Nppc***	0	Promoter (<=1kb)	ns	ns	0.07	0.24	ns	ns	ns	-0.16
chr1	91239541	91245531	5991	-0.528	1.59E-03	0.288	1.58E-02	1	***Ube2f***	-4773	Distal Intergenic	0.14	0.15	0.25	0.25	0.05	ns	-0.09	ns
chr1	98048906	98112617	63712	-0.240	4.56E-02	0.280	1.52E-03	1	***Pam***	0	Promoter (<=1kb)	0.37	0.12	0.17	0.19	ns	0.09	0.11	ns
chr10	109891037	109937453	46417	-0.547	5.84E-12	0.237	5.41E-05	1	***Nav3***	0	Promoter (<=1kb)	0.03	ns	ns	ns	0.07	0.04	ns	0.06
chr10	21904500	21948017	43518	-0.488	1.89E-06	0.497	3.26E-13	1	***Sgk1***	0	Promoter (<=1kb)	0.15	0.14	0.27	0.24	ns	ns	-0.24	ns
chr10	24703026	24730671	27646	-0.575	4.86E-07	0.337	2.64E-05	1	***Enpp1***	0	Promoter (<=1kb)	0.03	ns	ns	ns	0.03	ns	ns	ns
chr10	95388854	95405991	17138	-1.487	2.37E-12	0.448	2.54E-03	1	***Socs2***	8836	3' UTR	0.48	0.42	0.49	0.41	ns	0.08	ns	ns
chr10	54078824	54083751	4928	-0.600	9.75E-04	0.598	4.05E-07	1	***Man1a***	-2215	Promoter (2-3kb)	0.21	0.26	0.26	0.19	ns	ns	ns	0.08
chr10	59616982	59634046	17065	-0.460	1.01E-06	0.303	3.47E-06	1	***Mcu***	-290	Promoter (<=1kb)	0.09	ns	0.04	0.04	0.04	0.04	ns	ns
chr10	82967908	82984234	16327	-0.299	1.84E-02	0.547	2.01E-10	1	***Chst11***	-1264	Promoter (1-2kb)	0.26	0.30	0.43	0.40	0.06	ns	-0.14	ns
chr10	93620020	93644298	24279	-0.246	2.28E-02	0.322	1.95E-05	1	***Ntn4***	0	Promoter (<=1kb)	ns	ns	0.04	0.11	ns	ns	ns	-0.04
chr12	80508949	80527103	18155	-0.832	2.58E-09	0.321	1.69E-03	1	***Galnt16***	0	Promoter (<=1kb)	0.18	0.10	0.16	0.14	-0.06	ns	ns	ns
chr11	21375094	21380450	5357	-0.421	2.22E-02	0.364	7.75E-03	1	***Ugp2***	-3893	Distal Intergenic	0.18	0.22	0.32	0.25	-0.07	ns	-0.12	ns
chr11	22853349	22859837	6489	-0.719	7.82E-04	0.454	1.67E-03	1	***B3gnt2***	0	Promoter (<=1kb)	0.16	0.10	0.13	0.09	0.05	ns	ns	ns
chr11	31353859	31382560	28702	-0.796	1.29E-17	0.180	1.53E-02	1	***Stc2***	0	Promoter (<=1kb)	0.12	ns	ns	ns	-0.08	ns	ns	ns
chr11	35121591	35138710	17120	-1.390	1.59E-27	0.452	9.30E-07	1	***Slit3***	367	Promoter (<=1kb)	0.35	0.21	0.10	0.10	ns	ns	0.11	ns
chr11	49781864	49803666	21803	-0.309	3.83E-03	0.267	5.39E-04	1	***Gfpt2***	0	Promoter (<=1kb)	0.15	0.20	0.25	0.16	ns	ns	-0.11	ns
chr11	50587006	50602007	15002	-0.226	7.58E-02	0.477	1.12E-07	1	***Adamts2***	-77	Promoter (<=1kb)	0.70	0.63	0.70	0.74	ns	ns	ns	-0.05
chr11	54094712	54098536	3825	-0.363	3.96E-02	0.322	2.06E-02	1	***P4ha2***	-1559	Promoter (1-2kb)	0.47	0.30	0.41	0.23	-0.07	0.09	ns	ns
chr11	54886840	54900122	13283	-1.078	5.03E-12	0.683	6.11E-11	1	***Gpx3***	-2331	Promoter (2-3kb)	0.90	0.99	1.02	1.08	ns	ns	0.07	0.03
chr11	89276504	89327612	51109	-0.180	7.39E-02	0.175	1.60E-02	1	***Nog***	0	Promoter (<=1kb)	ns	0.12	0.08	0.07	ns	ns	-0.08	ns
chr12	33960094	33963191	3098	-1.075	9.85E-07	0.421	3.47E-03	1	***Twist1***	2423	Promoter (2-3kb)	0.07	ns	0.01	ns	0.04	ns	ns	ns
chr12	73879138	73895721	16584	-1.191	1.62E-14	0.767	1.06E-13	1	***Hif1a***	-5654	Intron (ENSMUST	0.32	0.36	0.44	0.39	0.09	ns	-0.09	ns
chr12	89799310	89847579	48270	-0.177	6.12E-03	0.101	3.43E-02	1	***Nrxn3***	0	Promoter (<=1kb)	ns	0.17	0.19	0.15	ns	0.09	ns	0.12
chr13	114764747	114810032	45286	-0.395	3.48E-04	0.238	3.11E-03	1	***Mocs2***	-8204	Distal Intergenic	0.11	0.11	0.13	0.12	ns	0.08	ns	ns
chr13	41470466	41507096	36631	-0.213	9.96E-02	0.826	4.24E-21	1	***Nedd9***	0	Promoter (<=1kb)	0.11	0.22	0.25	0.22	ns	ns	-0.11	ns
chr13	64371563	64396968	25406	-0.267	1.65E-03	0.281	1.86E-06	1	***Ctsl***	-673	Promoter (<=1kb)	0.28	0.24	0.28	0.31	0.03	0.11	0.08	ns
chr14	23522649	23533745	11097	-0.400	3.84E-02	0.872	7.24E-10	1	***Kcnma1***	9541	3' UTR	0.30	0.26	0.20	0.14	0.05	ns	ns	ns
chr3	107760378	107787841	27464	-0.743	1.11E-09	0.618	7.35E-14	1	***Csf1***	0	Promoter (<=1kb)	0.42	0.50	0.60	0.54	ns	ns	-0.16	ns
chr14	47354453	47374484	20032	-0.263	1.14E-02	0.267	3.84E-04	1	***Lgals3***	0	Promoter (<=1kb)	0.30	0.31	0.39	0.48	0.06	ns	ns	-0.12
chr3	52232980	52261367	28388	-0.315	3.68E-03	0.207	1.12E-02	1	***Foxo1***	-6969	Exon (ENSMUST0	0.19	0.16	0.27	0.38	0.07	0.12	0.08	-0.09
chr14	72712195	72716797	4603	-0.320	7.38E-02	0.369	1.26E-02	1	***Fndc3a***	-2192	Promoter (2-3kb)	0.13	0.11	0.20	0.26	0.09	ns	ns	ns
chr15	10202568	10220342	17775	-0.802	1.06E-11	0.623	4.13E-15	1	***Prlr***	0	Promoter (<=1kb)	0.25	0.38	0.19	0.11	ns	ns	0.09	0.16
chr15	36283480	36288104	4625	-0.329	4.60E-02	0.656	2.39E-08	1	***Rnf19a***	-333	Promoter (<=1kb)	0.10	0.20	0.24	0.22	ns	ns	ns	0.11
chr15	55437171	55442626	5456	-0.589	2.13E-03	0.330	1.66E-02	1	***Col14a1***	-6200	Exon (ENSMUST0	0.58	0.22	0.19	0.08	ns	0.12	0.15	ns
chr15	64384537	64415227	30691	-0.299	1.15E-04	0.214	1.41E-04	1	***Asap1***	-1618	Promoter (1-2kb)	ns	ns	0.10	0.11	0.04	ns	ns	-0.06
chr15	66969761	66982889	13129	-0.348	9.46E-03	0.482	1.21E-07	1	***Ndrg1***	-121	Promoter (<=1kb)	ns	0.14	0.28	0.28	ns	ns	-0.16	ns
chr4	137771273	137787174	15902	-0.810	8.21E-06	0.240	7.81E-02	1	***Alpl***	0	Promoter (<=1kb)	0.14	ns	ns	ns	0.06	0.05	0.05	ns
chr15	92578497	92606949	28453	-0.972	1.26E-13	0.630	1.64E-12	1	***Pdzrn4***	0	Promoter (<=1kb)	ns	0.30	0.21	0.16	ns	-0.20	-0.11	ns
chr16	33821932	33829457	7526	-1.020	2.12E-06	0.657	1.96E-06	1	***Itgb5***	-208	Promoter (<=1kb)	0.52	0.42	0.50	0.53	ns	ns	0.07	ns
chr16	57732496	57746247	13752	-0.194	9.56E-02	0.710	1.08E-21	1	***Col8a1***	8490	Intron (ENSMUST	0.27	ns	ns	ns	-0.09	ns	ns	ns
chr16	87336364	87352708	16345	-0.417	1.59E-04	0.302	8.10E-05	1	***N6amt1***	-1477	Promoter (1-2kb)	0.04	ns	ns	0.03	0.04	ns	ns	ns
chr17	28411124	28416533	5410	-1.540	2.13E-13	0.535	1.16E-04	1	***Fkbp5***	1971	Promoter (1-2kb)	0.19	0.13	0.14	0.06	ns	ns	ns	0.08
chr17	47921326	47924596	3271	-1.014	2.23E-05	0.565	2.81E-04	1	***Foxp4***	0	Promoter (<=1kb)	0.02	ns	ns	ns	0.04	ns	ns	ns
chr17	71165691	71182712	17022	-0.224	2.39E-02	0.355	1.26E-07	1	***Lpin2***	0	Promoter (<=1kb)	0.02	0.07	0.10	0.06	0.04	ns	ns	ns
chr17	71306840	71338093	31254	-0.458	2.73E-05	0.422	1.01E-08	1	***Emilin2***	0	Promoter (<=1kb)	0.43	0.42	0.58	0.62	ns	ns	ns	-0.06
chr17	7790478	7839895	49418	-0.199	3.52E-02	0.185	6.84E-03	1	***Fndc1***	0	Promoter (<=1kb)	0.20	0.07	0.07	0.06	-0.13	ns	ns	ns
chr18	43436672	43456779	20108	-0.439	2.89E-04	0.327	9.98E-05	1	***Dpysl3***	0	Promoter (<=1kb)	0.09	ns	0.16	0.12	0.09	ns	ns	ns
chr18	52533402	52536490	3089	-0.616	3.60E-03	0.273	7.67E-02	1	***Lox***	-3535	Intron (ENSMUST	0.77	0.48	0.54	0.64	0.08	0.14	0.17	ns
chr5	96782134	96795453	13320	-0.502	3.97E-03	0.291	2.27E-02	1	***Anxa3***	0	Promoter (<=1kb)	0.68	0.67	0.84	0.94	ns	ns	ns	-0.08
chr6	112480706	112494706	14001	-0.643	3.49E-06	0.263	1.02E-02	1	***Oxtr***	0	Promoter (<=1kb)	ns	ns	ns	0.23	ns	ns	ns	-0.13
chr18	67728892	67743160	14269	-0.298	6.24E-03	0.429	4.88E-09	1	***Ptpn2***	-4297	Distal Intergenic	ns	ns	0.05	ns	ns	ns	-0.09	ns
chr18	80565842	80617505	51664	-0.571	4.41E-08	0.205	9.87E-03	1	***Nfatc1***	0	Promoter (<=1kb)	0.14	0.16	0.24	0.16	ns	ns	-0.19	ns
chr19	40613098	40622385	9288	-0.533	6.95E-04	0.300	7.28E-03	1	***Entpd1***	701	Promoter (<=1kb)	0.04	0.08	0.15	0.14	ns	ns	-0.06	ns
chr7	112209481	112216024	6544	-0.364	4.54E-02	0.776	5.71E-09	1	***Mical2***	-9832	Distal Intergenic	0.12	0.11	0.21	0.20	ns	ns	-0.10	ns
chr19	53530126	53532992	2867	-0.703	1.50E-03	0.476	1.42E-03	1	***Dusp5***	1017	Promoter (1-2kb)	0.11	0.07	0.11	0.09	0.08	ns	-0.11	ns
chr2	10148639	10151773	3135	-0.899	6.41E-05	0.394	8.70E-03	1	***Itih5***	-1798	Promoter (1-2kb)	0.22	0.21	0.25	ns	-0.16	ns	-0.09	0.10
chr2	102513465	102551990	38526	-0.258	7.86E-02	0.683	8.33E-11	1	***Pamr1***	0	Promoter (<=1kb)	0.06	0.07	0.17	0.21	ns	0.05	0.08	-0.05
chr2	110348205	110400011	51807	-0.562	6.41E-09	0.483	1.96E-13	1	***Fibin***	0	Promoter (<=1kb)	0.19	ns	ns	ns	0.03	0.09	0.07	ns
chr2	12308830	12316025	7196	-0.503	1.94E-03	0.703	2.45E-11	1	***Itga8***	-6908	Exon (ENSMUST0	0.10	0.06	0.08	0.07	0.13	ns	ns	ns
chr2	133526215	133556637	30423	-0.171	7.02E-02	0.220	4.40E-04	1	***Bmp2***	0	Promoter (<=1kb)	0.14	0.55	0.57	0.48	-0.11	-0.31	-0.30	ns
chr7	96486138	96539432	53295	-0.728	3.37E-10	0.256	3.51E-03	1	***Tenm4***	0	Promoter (<=1kb)	0.14	0.05	0.05	0.05	ns	0.06	ns	ns
chr2	148415852	148423835	7984	-0.920	3.29E-08	0.924	3.17E-17	1	***Thbd***	-7664	Exon (ENSMUST0	0.19	0.03	0.14	0.29	ns	ns	0.08	-0.08
chr2	164444763	164449890	5128	-0.400	2.38E-02	0.300	2.92E-02	1	***Sdc4***	-876	Promoter (<=1kb)	0.47	0.56	0.65	0.66	ns	ns	-0.18	ns
chr8	25470458	25520277	49820	-0.328	3.35E-03	0.250	2.18E-03	1	***Fgfr1***	0	Promoter (<=1kb)	0.22	0.19	0.25	0.18	0.06	ns	ns	0.09
chr2	173276693	173350390	73698	-0.630	1.07E-06	0.465	1.27E-07	1	***Pmepa1***	-160	Promoter (<=1kb)	0.76	0.56	0.86	1.02	ns	0.11	-0.12	-0.16
chr2	59654485	59663549	9065	-0.345	4.69E-02	0.770	1.03E-09	1	***Tanc1***	7674	Intron (ENSMUST	0.03	ns	0.02	ns	0.08	ns	ns	ns
chr2	68856952	68870036	13085	-0.636	1.14E-06	0.422	2.66E-06	1	***Cers6***	0	Promoter (<=1kb)	0.13	0.04	ns	ns	0.04	0.09	0.05	ns
chr3	103717037	103730750	13714	-0.377	3.85E-02	0.571	2.18E-05	1	***Olfml3***	7218	Exon (ENSMUST0	0.56	0.72	0.68	0.55	ns	-0.06	-0.07	0.07
chr3	37333622	37341978	8357	-0.276	4.50E-02	0.387	1.35E-04	1	***Fgf2***	-6368	Exon (ENSMUST0	0.10	0.08	0.11	0.07	0.07	0.06	ns	ns
chr3	53842116	53854363	12248	-0.224	6.70E-02	0.181	5.96E-02	1	***Ufm1***	9326	3' UTR	0.39	0.19	0.28	0.25	ns	0.10	ns	ns
chr3	54390461	54398614	8154	-0.541	4.22E-03	0.960	7.14E-15	1	***Postn***	1572	Promoter (1-2kb)	1.10	0.88	1.23	1.19	-0.17	ns	-0.20	-0.18
chr3	55532667	55556518	23852	-0.547	1.30E-04	0.544	7.61E-09	1	***Dclk1***	4788	3' UTR	0.12	ns	0.04	ns	0.06	ns	ns	0.17
chr3	81022882	81031128	8247	-0.778	2.59E-06	0.919	1.31E-17	1	***Pdgfc***	-5288	Distal Intergenic	0.02	ns	0.03	ns	0.09	0.06	ns	0.08
chr3	81962980	81988507	25528	-0.556	9.61E-09	0.241	7.02E-04	1	***Tdo2***	0	Promoter (<=1kb)	0.10	0.16	0.13	ns	0.09	0.26	0.21	0.09
chr4	102544410	102584941	40532	-0.591	9.98E-12	0.376	5.03E-10	1	***Pde4b***	0	Promoter (<=1kb)	0.08	0.13	0.19	0.07	ns	ns	-0.10	ns

				H3K27me3 peak dynamics*								RNA expression†							
				Aggregate time (GD5.5 to 18.5)		Aggregate genotype (*Kdm6b cKO* vs. ctrl)						Ctrl IS/IIS fibroblasts vs. ctrl GD5.5/8.5 IIS fibroblasts (log_2FC)				*Kdm6b cKO* vs. ctrl IS/IIS fibroblasts (log_2FC)			
Chr	Peak start	Peak end	Peak width	log_2FC	*FDR*	log_2FC	*FDR*	HC	Gene	Peak distance to TSS	Annotation	GD12.5	GD14.5	GD16.5	GD18.5	GD12.5	GD14.5	GD16.5	GD18.5
chr4	119663380	119666396	3017	-0.394	4.88E-02	0.288	8.74E-02	1	***Guca2b***	-4426	Distal Intergenic	0.58	0.97	0.94	0.84	0.10	ns	ns	0.16
chr4	124965948	124994406	28459	-0.487	7.19E-06	0.201	1.43E-02	1	***Rspo1***	0	Promoter (<=1kb)	0.06	0.10	0.07	0.03	0.06	ns	ns	ns
chr4	129039169	129057305	18137	-0.551	5.90E-05	0.214	3.87E-02	1	***Rnf19b***	-966	Promoter (<=1kb)	0.07	ns	0.06	0.04	ns	ns	-0.11	ns
chr4	135274135	135277081	2947	-0.839	1.85E-03	0.719	3.10E-05	1	***Clic4***	-1321	Promoter (1-2kb)	0.20	0.20	0.21	0.12	-0.07	ns	-0.11	0.10
chr4	137862562	137865453	2892	-0.576	1.64E-02	0.624	2.26E-04	1	***Ece1***	265	Promoter (<=1kb)	0.07	0.06	0.08	0.09	0.04	ns	ns	ns
chr4	149952207	149974982	22776	-0.750	4.87E-05	0.668	2.85E-08	1	***Spsb1***	0	Promoter (<=1kb)	0.41	0.40	0.55	0.55	ns	ns	-0.17	ns
chr4	58204058	58213085	9028	-0.652	5.11E-06	0.268	9.99E-03	1	***Svep1***	0	Promoter (<=1kb)	0.65	0.41	0.41	0.43	ns	ns	0.19	0.11
chr4	86047377	86054580	7204	-0.734	1.44E-05	0.856	1.06E-14	1	***Adamtsl1***	0	Promoter (<=1kb)	0.14	ns	ns	ns	0.08	0.08	0.09	ns
chr5	113657478	113666968	9491	-0.278	6.79E-02	0.379	1.15E-03	1	***Cmklr1***	-7052	Distal Intergenic	0.16	0.17	0.19	0.21	ns	ns	ns	-0.04
chr5	135883521	135886290	2770	-0.826	3.16E-04	0.576	8.58E-05	1	***Hspb1***	-1629	Promoter (1-2kb)	0.27	0.51	0.49	0.40	ns	-0.20	-0.21	ns
chr5	143619625	143625445	5821	-0.813	3.56E-04	0.837	1.75E-08	1	***Cyth3***	0	Promoter (<=1kb)	0.13	0.08	0.14	0.10	ns	ns	-0.08	ns
chr5	35689221	35699359	10139	-0.579	1.52E-04	0.303	5.48E-03	1	***Htra3***	-9439	3' UTR	0.73	0.67	0.81	0.97	-0.07	ns	ns	-0.12
chr5	98034356	98039676	5321	-0.391	1.91E-02	0.372	2.15E-03	1	***Antxr2***	-3313	Distal Intergenic	ns	0.09	ns	ns	-0.09	-0.09	ns	ns
chr6	12398325	12416990	18666	-0.694	3.30E-04	0.255	7.22E-02	1	***Thsd7a***	2371	Promoter (2-3kb)	0.06	0.12	0.07	ns	0.07	ns	ns	ns
chr6	144790394	144799324	8931	-0.410	4.79E-03	0.737	6.30E-15	1	***Sox5***	-8417	Distal Intergenic	0.17	0.26	0.22	0.15	ns	ns	ns	0.09
chr6	145734273	145744349	10077	-0.653	2.24E-04	0.700	1.31E-09	1	***Rassf8***	-2399	Promoter (2-3kb)	0.13	0.13	0.22	0.12	ns	ns	-0.13	0.07
chr6	36801108	36824266	23159	-0.291	4.67E-03	0.563	1.40E-16	1	***Ptn***	0	Promoter (<=1kb)	0.25	0.43	ns	-0.37	-0.20	-0.21	-0.16	ns
chr6	53242368	53285951	43584	-0.310	4.98E-04	0.366	1.42E-09	1	***Creb5***	-1319	Promoter (1-2kb)	0.12	0.32	0.33	0.30	-0.14	-0.16	-0.13	0.09
chr6	5497849	5506465	8617	-0.613	1.15E-05	0.222	3.46E-02	1	***Pdk4***	-1540	Promoter (1-2kb)	0.06	0.14	0.16	0.20	ns	ns	ns	-0.09
chr6	7800771	7840871	40101	-0.306	5.25E-04	0.291	2.25E-06	1	***C1galt1***	-3971	Exon (ENSMUST0	0.14	0.12	0.19	0.25	ns	0.06	0.08	-0.05
chr6	90323144	90331024	7881	-0.734	9.26E-06	0.346	3.07E-03	1	***Chst13***	0	Promoter (<=1kb)	0.10	0.14	0.23	0.22	-0.05	ns	-0.11	-0.06
chr7	114126155	114148714	22560	-0.890	6.24E-20	0.483	1.24E-12	1	***Rras2***	-8374	Distal Intergenic	0.36	0.19	0.24	0.22	ns	0.08	ns	ns
chr7	114285307	114289344	4038	-0.466	1.21E-02	0.261	6.44E-02	1	***Psma1***	-9189	Distal Intergenic	0.10	0.06	0.10	0.12	ns	ns	ns	-0.04
chr7	89519288	89532355	13068	-0.561	1.18E-04	0.632	2.18E-11	1	***Prss23***	0	Promoter (<=1kb)	0.66	0.44	0.70	1.07	ns	0.10	0.12	-0.23
chr8	115711500	115735226	23727	-0.398	7.58E-04	0.588	2.84E-14	1	***Maf***	-3706	Distal Intergenic	-0.08	0.14	0.25	0.20	ns	-0.09	-0.08	-0.07
chr8	117224217	117253290	29074	-0.301	7.92E-03	0.170	5.54E-02	1	***Cmip***	-3774	Distal Intergenic	0.07	0.14	0.19	0.12	0.04	ns	ns	ns
chr8	8643622	8656095	12474	-0.354	1.43E-02	0.601	7.91E-10	1	***Efnb2***	-4259	Exon (ENSMUST0	ns	0.05	0.15	0.04	ns	ns	-0.10	0.07
chr9	118904836	118923771	18936	-0.361	7.56E-03	0.374	8.79E-05	1	***Ctdspl***	-2682	Promoter (2-3kb)	0.05	0.06	0.05	ns	0.04	ns	ns	ns
chr9	48836774	48857315	20542	-0.612	1.53E-04	0.464	2.11E-05	1	***Zbtb16***	-552	Promoter (<=1kb)	ns	0.14	0.03	ns	ns	-0.12	ns	0.16
chr9	58473333	58490426	17094	-0.388	2.01E-03	0.199	3.72E-02	1	***Insyn1***	0	Promoter (<=1kb)	0.07	0.11	0.20	0.12	ns	ns	-0.10	ns
chr1	10991450	11029620	38171	-0.127	1.80E-01	0.238	1.39E-05	2	***Prex2***	0	Promoter (<=1kb)	ns	ns	ns	0.05	ns	ns	ns	-0.03
chr1	121340531	121358577	18047	-0.133	3.12E-01	0.374	1.98E-05	2	***Insig2***	-7942	Exon (ENSMUST0	0.07	0.08	0.12	0.16	ns	ns	ns	-0.07
chr1	133801959	133832939	30981	-0.028	8.87E-01	0.476	1.66E-05	2	***Atp2b4***	-918	Promoter (<=1kb)	0.17	0.22	0.31	0.27	ns	ns	-0.17	ns
chr1	133923234	133933000	9767	-0.191	1.77E-01	0.514	1.56E-06	2	***Prelp***	-1820	Promoter (1-2kb)	0.74	0.44	0.47	0.48	-0.17	0.12	0.11	ns
chr1	134002901	134032871	29971	-0.010	9.63E-01	0.387	4.91E-07	2	***Fmod***	-4383	Exon (ENSMUST0	0.19	0.09	0.05	0.02	ns	0.14	0.09	ns
chr1	134066258	134069845	3588	-0.061	7.12E-01	0.357	4.25E-02	2	***Btg2***	9275	Distal Intergenic	0.26	0.32	0.33	0.29	0.09	ns	ns	0.10
chr1	149965591	149968023	2433	-0.186	2.49E-01	0.528	3.90E-04	2	***Pla2g4a***	-4301	Distal Intergenic	0.11	0.06	0.06	0.09	0.05	ns	ns	ns
chr1	152360333	152364973	4641	-0.151	3.18E-01	0.480	1.33E-04	2	***Tsen15***	7109	Distal Intergenic	ns	ns	0.03	0.03	ns	ns	ns	-0.04
chr1	153339394	153348185	8792	-0.126	3.59E-01	0.533	4.30E-09	2	***Lamc1***	-6608	Distal Intergenic	0.52	0.35	0.43	0.30	-0.11	-0.13	-0.08	0.08
chr1	164779056	164791331	12276	-0.150	3.00E-01	0.784	3.07E-13	2	***Dpt***	-5313	Distal Intergenic	0.24	0.26	0.33	0.30	-0.14	-0.08	-0.07	ns
chr1	170127921	170134289	6369	0.067	6.70E-01	0.304	2.73E-03	2	***Uap1***	9424	Distal Intergenic	0.14	0.13	0.21	0.14	-0.07	ns	-0.11	ns
chr1	193231951	193241439	9489	-0.027	8.90E-01	0.620	5.75E-10	2	***Hsd11b1***	0	Promoter (<=1kb)	0.08	0.13	0.13	0.11	0.10	ns	ns	0.06
chr1	45508269	45513318	5050	-0.051	7.69E-01	0.413	9.23E-04	2	***Col5a2***	-4987	Distal Intergenic	0.51	0.35	0.48	0.35	-0.03	0.06	ns	ns
chr1	72876097	72879377	3281	0.011	9.57E-01	0.661	3.36E-04	2	***Igfbp5***	-1213	Promoter (1-2kb)	ns	0.14	ns	-0.12	0.21	0.14	ns	0.15
chr1	88705739	88733845	28107	0.131	3.29E-01	0.250	1.09E-02	2	***Arl4c***	-3518	Exon (ENSMUST0	ns	0.13	0.30	0.30	0.08	ns	-0.19	ns
chr1	90851899	90863734	11836	0.005	9.81E-01	0.653	9.73E-06	2	***Col6a3***	-7928	Distal Intergenic	0.76	0.53	0.67	0.51	-0.12	ns	-0.15	ns
chr10	117848431	117895813	47383	-0.096	4.15E-01	0.312	3.59E-07	2	***Rap1b***	-2396	Promoter (2-3kb)	0.17	0.23	0.29	0.22	ns	ns	-0.12	0.04
chr10	12970695	12981379	10685	0.192	1.10E-01	0.188	4.02E-02	2	***Stx11***	-6397	Distal Intergenic	0.13	0.17	0.21	0.18	ns	ns	-0.10	ns
chr10	13115387	13119351	3965	0.024	9.06E-01	0.466	7.56E-05	2	***Plagl1***	0	Promoter (<=1kb)	ns	ns	0.05	ns	ns	ns	-0.12	0.08
chr10	13925063	13960817	35755	-0.107	4.41E-01	0.738	3.67E-18	2	***Hivep2***	-5258	Exon (ENSMUST0	ns	ns	0.05	ns	ns	ns	-0.11	0.08
chr10	19016426	19049753	33328	-0.103	3.63E-01	0.150	2.85E-02	2	***Tnfaip3***	-769	Promoter (<=1kb)	0.35	0.39	0.43	0.40	0.05	ns	ns	ns
chr10	25346297	25354291	7995	0.124	3.53E-01	0.572	1.38E-11	2	***Epb41l2***	-5507	Distal Intergenic	ns	0.07	0.10	ns	ns	ns	-0.09	0.08
chr10	59683839	59699698	15860	-0.022	9.09E-01	0.219	7.50E-03	2	***Micu1***	-2779	Promoter (2-3kb)	0.15	0.07	0.12	0.15	0.05	0.06	ns	ns
chr10	9631873	9645940	14068	0.087	5.16E-01	0.216	5.85E-03	2	***Samd5***	-932	Promoter (<=1kb)	0.10	ns	ns	ns	0.03	0.08	ns	ns
chr11	108904416	108910896	6481	0.086	5.80E-01	0.515	4.24E-06	2	***Axin2***	-9453	Distal Intergenic	ns	ns	0.04	0.12	ns	ns	ns	-0.07
chr11	16515593	16519688	4096	-0.048	7.83E-01	0.298	2.19E-02	2	***Sec61g***	-7109	Exon (ENSMUST0	0.22	ns	0.06	0.08	-0.03	0.06	ns	-0.11
chr11	16736910	16744823	7914	0.025	9.02E-01	0.552	9.77E-08	2	***Egfr***	-7380	Distal Intergenic	ns	ns	0.13	ns	ns	ns	-0.11	0.13
chr11	43473685	43476951	3267	-0.182	2.69E-01	0.390	2.13E-02	2	***C1qtnf2***	0	Promoter (<=1kb)	0.17	0.06	0.07	0.06	ns	0.10	0.07	ns
chr11	5513751	5518255	4505	-0.076	6.31E-01	0.254	4.91E-02	2	***Xbp1***	-2404	Promoter (2-3kb)	0.16	0.09	0.18	0.11	ns	0.10	-0.09	0.07
chr11	59642366	59651331	8966	0.217	1.07E-01	0.212	4.93E-02	2	***Mprip***	-9974	Distal Intergenic	ns	ns	0.08	ns	ns	ns	-0.07	ns
chr11	61471510	61479402	7893	-0.041	8.22E-01	0.217	8.41E-02	2	***Mfap4***	-6029	Distal Intergenic	0.73	0.36	0.46	0.50	0.14	0.38	0.42	0.11
chr11	82022046	82029912	7867	-0.103	4.85E-01	0.471	5.69E-06	2	***Ccl2***	-5659	Exon (ENSMUST0	0.78	0.86	1.01	0.90	ns	ns	-0.28	ns
chr11	82039198	82045844	6647	-0.118	4.53E-01	0.417	9.03E-03	2	***Ccl7***	0	Promoter (<=1kb)	0.45	0.47	0.60	0.52	ns	ns	-0.16	ns
chr11	90195290	90210441	15152	0.167	1.84E-01	0.448	1.09E-07	2	***Mmd***	7115	3' UTR	ns	ns	0.06	0.20	0.06	ns	ns	-0.19
chr12	101819222	101828632	9411	0.034	8.51E-01	0.256	6.31E-03	2	***Fbln5***	-167	Promoter (<=1kb)	0.09	-0.13	ns	ns	0.16	0.09	ns	ns
chr12	102447843	102451031	3189	-0.062	7.09E-01	0.250	9.94E-02	2	***Lgmn***	-8030	Intron (ENSMUST	0.17	0.04	0.06	0.04	0.05	0.07	ns	ns
chr12	103445167	103451369	6203	-0.056	7.39E-01	0.212	6.59E-02	2	***Ifi27l2a***	-1487	Promoter (1-2kb)	0.88	0.62	0.60	0.51	-0.12	ns	ns	0.11
chr12	105553341	105557119	3779	-0.053	7.58E-01	0.535	7.43E-05	2	***Bdkrb2***	-6107	Distal Intergenic	ns	ns	0.08	0.04	0.05	ns	-0.08	ns
chr12	29918866	29929261	10396	-0.139	3.31E-01	0.260	2.29E-02	2	***Pxdn***	-8347	3' UTR	0.23	0.15	0.28	0.31	ns	ns	ns	-0.08
chr12	72670081	72677596	7516	-0.091	5.47E-01	0.268	2.00E-02	2	***Dhrs7***	-5172	Distal Intergenic	0.15	0.13	0.15	0.04	-0.08	ns	ns	ns
chr12	81843955	81851953	7999	-0.165	2.29E-01	0.349	6.86E-04	2	***Pcnx***	-8070	Intron (ENSMUST	0.11	0.13	0.15	0.14	ns	ns	ns	0.07
chr13	110406822	110444517	37696	0.036	7.97E-01	0.237	3.25E-06	2	***Plk2***	9025	Distal Intergenic	-0.11	ns	0.09	ns	0.13	ns	-0.18	ns
chr13	115095759	115147592	51834	0.109	3.09E-01	0.203	7.30E-04	2	***Itga1***	0	Promoter (<=1kb)	0.10	ns	ns	ns	0.06	0.06	0.07	ns
chr13	49328975	49337707	8733	-0.071	6.52E-01	0.294	6.33E-03	2	***Bicd2***	-3878	Distal Intergenic	0.17	0.23	0.37	0.40	ns	ns	-0.14	-0.05
chr13	53290992	53296199	5208	-0.133	3.90E-01	0.734	1.07E-07	2	***Ror2***	-4868	Distal Intergenic	0.08	0.06	0.22	0.40	0.06	0.12	ns	-0.15
chr13	58864561	58869533	4973	0.020	9.23E-01	0.252	6.45E-02	2	***Ntrk2***	-2202	Promoter (2-3kb)	0.31	0.13	0.04	ns	ns	0.11	0.08	0.09
chr14	123643486	123660056	16571	0.014	9.46E-01	0.192	2.89E-02	2	***Itgbl1***	0	Promoter (<=1kb)	0.38	0.15	0.17	0.17	ns	0.20	0.31	0.14
chr14	41019671	41032658	12988	-0.070	6.30E-01	0.296	1.47E-04	2	***Prxl2a***	-5883	Distal Intergenic	0.16	0.13	0.08	0.07	0.18	0.22	0.27	0.15
chr14	67075870	67094323	18454	-0.026	8.97E-01	0.504	2.78E-05	2	***Ppp2r2a***	-3426	Distal Intergenic	ns	ns	0.06	ns	ns	ns	-0.09	ns
chr14	79283641	79321552	37912	-0.064	6.37E-01	0.224	8.16E-04	2	***Rgcc***	0	Promoter (<=1kb)	ns	ns	0.06	ns	ns	ns	-0.09	ns
chr15	31213297	31219271	5975	-0.107	4.72E-01	0.404	2.49E-04	2	***Dap***	-5043	Distal Intergenic	0.29	0.22	0.31	0.28	ns	0.08	ns	-0.09
chr15	32912823	32919203	6381	0.056	7.41E-01	0.254	3.10E-02	2	***Sdc2***	-1520	Promoter (1-2kb)	0.09	0.10	0.10	0.17	ns	ns	ns	-0.06
chr15	3583653	3601992	18340	-0.151	1.52E-01	0.173	1.64E-02	2	***Ghr***	-161	Promoter (<=1kb)	0.02	ns	ns	ns	0.03	ns	ns	ns
chr15	54282105	54291849	9745	-0.004	9.87E-01	0.475	1.58E-07	2	***Tnfrsf11b***	-3621	Distal Intergenic	0.23	0.09	0.13	0.19	ns	ns	ns	-0.04

				H3K27me3 peak dynamics*								RNA expression†							
				Aggregate time (GD5.5 to 18.5)		Aggregate genotype (*Kdm6b cKO* vs. ctrl)						Ctrl IS/IIS fibroblasts vs. ctrl GD5.5/8.5 IIS fibroblasts (log_2FC)				*Kdm6b cKO* vs. ctrl IS/IIS fibroblasts (log_2FC)			
Chr	Peak start	Peak end	Peak width	log_2FC	*FDR*	log_2FC	*FDR*	HC	Gene	Peak distance to TSS	Annotation	GD12.5	GD14.5	GD16.5	GD18.5	GD12.5	GD14.5	GD16.5	GD18.5
chr15	6301089	6317729	16641	0.059	7.07E-01	0.429	1.91E-07	2	***Dab2***	1221	Promoter (1-2kb)	0.08	0.08	0.17	0.13	0.04	ns	ns	ns
chr15	66852901	66887965	35065	-0.091	5.13E-01	0.638	1.15E-16	2	***Ccn4***	-3355	Distal Intergenic	0.12	0.05	0.11	0.09	ns	0.07	ns	ns
chr15	85196579	85200128	3550	0.002	9.94E-01	0.449	1.25E-03	2	***Fbln1***	-5821	Distal Intergenic	0.33	0.25	0.10	0.05	ns	ns	0.11	0.08
chr16	30075774	30077478	1705	-0.264	1.32E-01	0.598	9.34E-05	2	***Hes1***	9436	Distal Intergenic	0.51	0.45	0.40	0.39	ns	0.09	ns	0.09
chr16	37754713	37776540	21828	-0.044	7.84E-01	0.394	1.19E-08	2	***Fstl1***	-333	Promoter (<=1kb)	0.40	0.21	0.34	0.24	-0.05	ns	ns	ns
chr16	45081758	45086610	4853	-0.266	1.17E-01	0.721	1.09E-07	2	***Ccdc80***	-6844	Distal Intergenic	0.60	0.52	0.59	0.57	-0.15	ns	ns	ns
chr16	76376694	76387521	10828	0.092	5.27E-01	0.493	2.75E-08	2	***Nrip1***	-2867	Promoter (2-3kb)	ns	ns	0.12	ns	ns	ns	-0.16	ns
chr16	85174753	85179859	5107	-0.077	6.27E-01	0.567	3.84E-07	2	***App***	-987	Promoter (<=1kb)	0.20	0.12	0.15	0.12	ns	ns	ns	0.06
chr16	87642784	87698967	56184	0.120	1.60E-01	0.161	1.15E-03	2	***Bach1***	0	Promoter (<=1kb)	0.13	0.21	0.29	0.21	ns	ns	-0.13	0.09
chr16	95677925	95696496	18572	0.093	5.30E-01	0.358	3.98E-04	2	***Ets2***	-5579	Distal Intergenic	ns	0.12	0.13	0.10	ns	ns	-0.11	ns
chr17	14696228	14709199	12972	-0.191	1.74E-01	0.723	6.34E-13	2	***Thbs2***	-1993	Promoter (1-2kb)	0.28	0.07	0.08	0.11	-0.08	ns	ns	ns
chr17	26548704	26558813	10110	-0.136	3.31E-01	0.460	2.75E-06	2	***Ergic1***	-2676	Promoter (2-3kb)	0.18	0.07	0.06	0.07	-0.06	ns	ns	ns
chr17	29103683	29105863	2181	0.005	9.82E-01	0.413	2.81E-03	2	***Cdkn1a***	5783	Distal Intergenic	0.05	0.14	0.11	0.03	-0.10	-0.19	-0.24	ns
chr17	33787649	33796312	8664	-0.020	9.26E-01	0.289	9.65E-03	2	***Angptl4***	-5819	Distal Intergenic	0.05	0.08	0.30	0.22	ns	0.08	ns	-0.18
chr17	73954372	73959233	4862	-0.186	2.10E-01	0.287	2.29E-02	2	***Xdh***	-4176	Distal Intergenic	0.09	0.07	0.07	0.05	ns	ns	0.10	0.11
chr17	86719746	86758389	38644	-0.179	1.26E-01	0.355	7.65E-06	2	***Epas1***	0	Promoter (<=1kb)	0.15	0.11	0.12	0.06	ns	ns	ns	0.08
chr17	88425277	88435967	10691	0.091	5.31E-01	0.413	3.68E-06	2	***Foxn2***	-4744	Distal Intergenic	ns	ns	0.04	ns	ns	ns	-0.07	ns
chr18	11616178	11623900	7723	0.095	5.22E-01	0.292	8.23E-03	2	***Rbbp8***	-9376	Distal Intergenic	ns	0.08	0.16	0.12	ns	ns	-0.17	ns
chr18	38387815	38400512	12698	-0.068	6.50E-01	0.380	4.83E-06	2	***Ndfip1***	-9884	Distal Intergenic	ns	ns	ns	0.08	ns	ns	ns	-0.08
chr18	44710692	44735739	25048	0.083	5.12E-01	0.182	9.49E-03	2	***Mcc***	0	Promoter (<=1kb)	ns	0.14	0.17	0.08	ns	ns	ns	0.09
chr18	58632435	58658927	26493	-0.197	1.16E-01	0.427	1.15E-06	2	***Isoc1***	-539	Promoter (<=1kb)	0.24	0.28	0.33	0.18	0.14	ns	ns	0.10
chr18	60636584	60643337	6754	-0.159	2.79E-01	0.419	4.86E-04	2	***Synpo***	4982	Intron (ENSMUST	0.10	0.08	0.17	0.17	ns	ns	-0.06	ns
chr18	67382301	67385642	3342	-0.219	1.94E-01	0.388	1.44E-02	2	***Tubb6***	-5075	Distal Intergenic	0.18	0.20	0.32	0.28	ns	ns	-0.19	-0.06
chr19	10004076	10009618	5543	-0.140	3.36E-01	0.269	2.96E-02	2	***Rab3il1***	2407	Promoter (2-3kb)	0.08	0.05	0.04	0.02	ns	0.06	0.05	ns
chr19	17837806	17864516	26711	-0.003	9.91E-01	0.640	6.72E-14	2	***Pcsk5***	-174	Promoter (<=1kb)	0.11	ns	ns	ns	0.20	0.11	0.11	0.13
chr19	24031468	24036343	4876	-0.036	8.40E-01	0.383	4.02E-02	2	***Fam189a2***	-449	Promoter (<=1kb)	ns	0.23	0.40	0.45	ns	ns	-0.11	-0.10
chr19	47715628	47729011	13384	-0.151	2.66E-01	0.189	8.75E-02	2	***Sfr1***	-2671	Promoter (2-3kb)	0.16	0.18	0.23	0.14	ns	ns	-0.10	ns
chr2	102902353	102933875	31523	0.010	9.64E-01	0.781	1.14E-19	2	***Cd44***	-688	Promoter (<=1kb)	ns	ns	0.31	0.17	ns	ns	-0.30	ns
chr2	105401436	105445802	44367	-0.048	7.42E-01	0.160	1.95E-02	2	***Rcn1***	-2117	Promoter (2-3kb)	0.34	0.21	0.26	0.14	ns	0.13	ns	ns
chr2	11678735	11697877	19143	0.087	4.68E-01	0.148	2.80E-02	2	***Il15ra***	-7413	3' UTR	ns	0.06	0.07	ns	ns	ns	-0.09	ns
chr2	16350075	16353488	3414	-0.086	5.85E-01	0.339	1.72E-02	2	***Plxdc2***	-2816	Promoter (2-3kb)	0.11	ns	0.09	0.18	-0.07	ns	ns	ns
chr2	168525583	168568804	43222	-0.066	6.66E-01	0.196	4.35E-02	2	***Nfatc2***	0	Promoter (<=1kb)	ns	0.07	0.13	0.07	ns	ns	-0.12	ns
chr2	35236206	35253742	17537	-0.012	9.56E-01	0.333	5.49E-04	2	***Gsn***	-2638	Promoter (2-3kb)	0.46	0.53	0.49	0.56	-0.21	-0.20	ns	-0.05
chr2	3650698	3698877	48180	-0.092	4.59E-01	0.479	2.28E-14	2	***Fam107b***	-5136	Exon (ENSMUST(	0.11	0.19	0.22	0.14	ns	ns	-0.11	ns
chr2	51149448	51222819	73372	0.097	4.26E-01	0.423	3.48E-11	2	***Rnd3***	-337	Promoter (<=1kb)	ns	ns	0.07	ns	ns	ns	-0.16	0.14
chr2	80442302	80491269	48968	-0.078	4.49E-01	0.167	9.29E-04	2	***Frzb***	0	Promoter (<=1kb)	0.32	ns	ns	0.04	0.12	ns	ns	ns
chr2	84779951	84782706	2756	-0.014	9.50E-01	0.289	6.84E-02	2	***Serping1***	-4507	Distal Intergenic	0.51	0.51	0.45	0.54	ns	ns	0.19	ns
chr3	100687223	100693206	5984	0.025	9.00E-01	0.228	4.05E-02	2	***Man1a2***	-1720	Promoter (1-2kb)	0.23	0.13	0.14	0.09	0.06	ns	ns	ns
chr3	129329054	129357012	27959	0.004	9.85E-01	0.420	1.16E-11	2	***Enpep***	0	Promoter (<=1kb)	0.08	0.06	0.12	0.12	ns	ns	ns	-0.03
chr3	132060456	132107986	47531	-0.085	4.40E-01	0.133	2.55E-02	2	***Dkk2***	0	Promoter (<=1kb)	ns	ns	ns	0.13	ns	ns	ns	-0.07
chr3	145905350	145921953	16604	-0.050	7.54E-01	0.237	2.95E-03	2	***Bcl10***	-2309	Promoter (2-3kb)	ns	0.07	0.16	0.10	0.06	ns	-0.15	ns
chr3	37627031	37639573	12543	0.119	3.80E-01	0.742	3.57E-18	2	***Spry1***	-374	Promoter (<=1kb)	0.09	ns	ns	ns	0.05	ns	ns	ns
chr3	51213140	51224092	10953	0.003	9.89E-01	0.196	6.50E-02	2	***Noct***	-355	Promoter (<=1kb)	0.04	ns	0.12	0.05	ns	ns	-0.11	ns
chr3	65399765	65403279	3515	-0.038	8.35E-01	0.464	1.22E-03	2	***Ssr3***	-7142	Distal Intergenic	0.28	0.28	0.27	0.22	-0.04	-0.10	-0.08	ns
chr3	89914942	89926892	11951	-0.211	1.12E-01	0.344	5.69E-04	2	***Il6ra***	-1746	Promoter (1-2kb)	0.07	0.16	0.22	0.22	ns	ns	-0.11	ns
chr4	114389797	114405817	16021	-0.044	8.00E-01	0.345	1.04E-04	2	***Trabd2b***	-907	Promoter (<=1kb)	ns	ns	0.07	0.05	0.03	ns	-0.07	ns
chr4	129746991	129817341	70351	-0.078	6.01E-01	0.179	7.19E-02	2	***Ptp4a2***	0	Promoter (<=1kb)	0.19	0.09	0.16	0.13	-0.05	ns	-0.07	ns
chr4	149782484	149786531	4048	0.102	5.17E-01	0.755	1.18E-07	2	***Slc25a33***	-8207	Exon (ENSMUST(	ns	ns	0.03	0.04	ns	ns	-0.06	ns
chr4	57958181	57977285	19105	-0.090	5.09E-01	0.285	3.49E-04	2	***Txn1***	-1770	Promoter (1-2kb)	ns	ns	0.09	ns	ns	ns	-0.10	-0.12
chr4	63530853	63538601	7749	-0.241	1.19E-01	0.392	1.61E-03	2	***Atp6v1g1***	-6171	Distal Intergenic	0.14	0.10	0.10	0.19	ns	ns	ns	-0.12
chr5	122151165	122153686	2522	-0.069	6.70E-01	0.707	5.48E-06	2	***Ppp1cc***	-4592	Distal Intergenic	0.05	ns	0.12	0.11	ns	ns	ns	-0.07
chr5	125397901	125400277	2377	-0.014	9.45E-01	0.762	1.42E-06	2	***Ubc***	-7699	Distal Intergenic	0.10	0.18	0.18	0.20	ns	-0.09	-0.09	ns
chr5	13113381	13116424	3044	-0.008	9.72E-01	0.546	6.77E-05	2	***Sema3a***	-9169	Distal Intergenic	ns	0.07	0.08	0.07	ns	ns	-0.07	ns
chr5	134751208	134755060	3853	-0.088	5.77E-01	0.522	7.64E-04	2	***Eln***	-3885	Intron (ENSMUST	1.06	0.64	0.87	0.67	-0.30	ns	-0.14	ns
chr5	138987290	139011735	24446	-0.077	6.03E-01	0.321	4.79E-04	2	***Pdgfa***	0	Promoter (<=1kb)	0.04	ns	0.12	0.12	ns	ns	-0.07	-0.05
chr5	149361371	149366095	4725	-0.108	4.86E-01	0.788	3.03E-09	2	***Medag***	-2381	Promoter (2-3kb)	0.19	0.25	0.28	0.23	ns	ns	-0.08	ns
chr5	43498012	43522075	24064	-0.064	6.84E-01	0.801	2.23E-21	2	***C1qtnf7***	0	Promoter (<=1kb)	0.16	0.06	0.06	0.07	0.06	0.04	0.06	ns
chr5	92336762	92347106	10345	-0.197	1.70E-01	0.328	4.47E-03	2	***Cxcl10***	1776	Promoter (1-2kb)	0.32	0.43	0.41	0.24	ns	ns	-0.11	0.09
chr5	92499631	92504926	5296	-0.259	1.21E-01	0.661	7.07E-07	2	***Scarb2***	711	Promoter (<=1kb)	0.11	0.03	0.05	0.02	0.03	ns	ns	ns
chr6	108636875	108656975	20101	-0.057	7.08E-01	0.324	1.37E-05	2	***Bhlhe40***	-3654	Exon (ENSMUST(	0.48	0.33	0.41	0.43	ns	ns	-0.10	ns
chr6	135349791	135360193	10403	-0.034	8.55E-01	0.677	6.02E-11	2	***Emp1***	-2352	Promoter (2-3kb)	0.17	0.21	0.34	0.31	ns	ns	-0.16	ns
chr6	137650023	137663480	13458	0.083	5.28E-01	0.242	8.68E-04	2	***Eps8***	0	Promoter (<=1kb)	0.03	ns	ns	-0.11	0.06	0.04	ns	0.05
chr6	17291004	17306120	15117	-0.132	2.93E-01	0.381	1.93E-06	2	***Cav1***	-215	Promoter (<=1kb)	0.33	0.37	0.49	0.36	-0.10	ns	-0.19	-0.07
chr6	55325485	55340359	14875	-0.004	9.87E-01	0.380	6.27E-03	2	***Aqp1***	0	Promoter (<=1kb)	ns	ns	ns	0.06	ns	ns	ns	-0.08
chr6	97798574	97802803	4230	-0.152	3.29E-01	0.790	4.15E-09	2	***Mitf***	-4249	Distal Intergenic	0.13	0.15	0.12	0.22	0.10	ns	0.11	ns
chr7	112410631	112424129	13499	-0.141	2.82E-01	0.307	8.92E-04	2	***Parva***	-3376	3' UTR	0.11	0.06	0.08	0.05	0.07	ns	ns	ns
chr7	113745020	113766753	21734	-0.104	4.51E-01	0.363	4.60E-05	2	***Spon1***	0	Promoter (<=1kb)	0.40	0.53	0.49	0.43	-0.11	-0.15	-0.12	0.06
chr7	128395801	128403026	7226	-0.256	1.05E-01	0.540	1.25E-05	2	***Rgs10***	1452	Promoter (1-2kb)	0.12	0.13	0.16	0.14	ns	ns	ns	-0.05
chr7	130926134	130934685	8552	0.009	9.69E-01	0.310	4.81E-02	2	***Htra1***	-1426	Promoter (1-2kb)	0.37	0.56	0.60	0.62	0.08	0.11	ns	ns
chr7	132277991	132419691	141701	-0.155	1.63E-01	0.139	9.00E-02	2	***Chst15***	0	Promoter (<=1kb)	ns	0.14	0.09	ns	ns	-0.08	ns	ns
chr7	67376428	67382299	5872	-0.086	5.81E-01	0.717	4.80E-10	2	***Mef2a***	-3570	Distal Intergenic	-0.13	ns	0.12	ns	ns	-0.12	-0.24	ns
chr7	80830418	80834136	3719	-0.006	9.79E-01	0.634	1.77E-05	2	***Iqgap1***	-4444	Distal Intergenic	0.26	0.26	0.35	0.29	ns	ns	-0.08	0.09
chr8	25241392	25255734	14343	-0.145	2.24E-01	0.358	2.94E-06	2	***Tacc1***	0	Promoter (<=1kb)	0.17	0.20	0.21	0.19	0.08	ns	ns	ns
chr8	27079221	27081923	2703	0.094	5.53E-01	0.416	7.81E-03	2	***Adgra2***	-3660	Distal Intergenic	0.05	ns	0.10	0.07	ns	ns	-0.10	ns
chr8	47996183	47999927	3745	-0.025	9.00E-01	0.469	3.25E-04	2	***Wwc2***	-5632	Distal Intergenic	0.17	0.15	0.20	0.19	0.05	0.09	ns	ns
chr8	56289807	56294947	5141	-0.138	3.60E-01	0.935	3.34E-14	2	***Hpgd***	0	Promoter (<=1kb)	0.19	ns	0.03	0.08	-0.09	ns	ns	-0.08
chr8	72127162	72129518	2357	-0.201	2.28E-01	0.404	1.24E-02	2	***Tpm4***	-656	Promoter (<=1kb)	0.41	0.36	0.45	0.45	0.05	ns	-0.06	ns
chr8	77725005	77729106	4102	-0.121	4.38E-01	0.779	4.43E-08	2	***Ednra***	-541	Promoter (<=1kb)	0.05	ns	ns	ns	0.21	0.10	ns	-0.05
chr8	85564191	85568278	4088	-0.019	9.27E-01	0.237	8.97E-02	2	***Dnaja2***	-8847	Distal Intergenic	ns	ns	0.10	0.06	ns	ns	-0.07	ns
chr9	106409294	106425602	16309	0.058	7.20E-01	0.294	2.63E-03	2	***Rpl29***	-3852	Distal Intergenic	ns	0.04	ns	ns	0.04	-0.04	-0.05	-0.10
chr9	119988176	119996551	8376	-0.125	3.76E-01	0.324	2.35E-03	2	***Csrnp1***	-3518	Intron (ENSMUST	0.12	0.13	0.09	0.07	ns	-0.09	-0.08	ns
chr9	79993656	80003684	10029	-0.064	6.73E-01	0.396	1.95E-06	2	***Filip1***	9167	Intron (ENSMUST	0.03	0.16	0.13	0.05	ns	-0.08	-0.11	0.06
chr9	83151392	83161264	9873	-0.027	8.88E-01	0.188	6.40E-02	2	***Hmgn3***	-4707	Distal Intergenic	0.22	0.10	0.25	0.17	ns	0.11	ns	ns
chr1	43703134	43728242	25109	0.184	2.73E-02	0.376	8.60E-13	3	***Ecrg4***	-2360	Promoter (2-3kb)	0.13	0.19	0.27	0.20	0.24	0.43	0.22	ns

				H3K27me3 peak dynamics*								RNA expression†							
				Aggregate time (GD5.5 to 18.5)		Aggregate genotype (*Kdm6b cKO* vs. ctrl)						Ctrl IS/IIS fibroblasts vs. ctrl GD5.5/8.5 IIS fibroblasts (log_2FC)				*Kdm6b cKO* vs. ctrl IS/IIS fibroblasts (log_2FC)			
Chr	Peak start	Peak end	Peak width	log_2FC	*FDR*	log_2FC	*FDR*	HC	Gene	Peak distance to TSS	Annotation	GD12.5	GD14.5	GD16.5	GD18.5	GD12.5	GD14.5	GD16.5	GD18.5
chr10	128892158	128906756	14599	0.265	1.28E-02	0.207	9.40E-03	3	***Cd63***	0	Promoter (<=1kb)	0.21	0.14	0.20	0.20	ns	0.04	-0.03	-0.06
chr14	73393914	73439856	45943	0.935	2.29E-13	0.292	2.25E-03	3	***Itm2b***	-8625	Distal Intergenic	0.19	0.20	0.18	0.17	-0.02	ns	ns	ns
chr17	72901951	72911333	9383	0.766	1.43E-06	0.488	3.80E-06	3	***Lbh***	-6972	Distal Intergenic	0.05	ns	ns	ns	0.05	ns	ns	ns
chr19	24205075	24254080	49006	0.213	6.85E-02	0.315	1.52E-04	3	***Tjp2***	0	Promoter (<=1kb)	ns	0.14	0.26	0.21	0.06	ns	-0.18	ns
chr4	62561956	62565265	3310	0.405	3.30E-02	0.530	1.38E-04	3	***Rgs3***	2109	Promoter (2-3kb)	0.21	0.23	0.33	0.42	ns	ns	-0.09	-0.16
chr1	12986931	12989302	2372	-0.555	2.16E-02	-0.124	5.56E-01	4	***Slco5a1***	1612	Promoter (1-2kb)	0.19	0.25	0.29	0.32	0.11	ns	ns	ns
chr1	14722935	14771881	48947	-0.162	2.41E-02	0.076	1.55E-01	4	***Msc***	0	Promoter (<=1kb)	ns	ns	ns	0.09	ns	ns	ns	-0.05
chr1	80343487	80350887	7401	-0.325	2.86E-02	0.034	8.18E-01	4	***Cul3***	-3007	Distal Intergenic	ns	ns	0.06	ns	ns	ns	-0.11	ns
chr10	56355027	56382924	27898	-0.598	1.90E-11	0.049	5.62E-01	4	***Gja1***	0	Promoter (<=1kb)	0.07	0.20	0.40	0.45	ns	ns	-0.18	-0.19
chr10	81567676	81570378	2703	-0.554	9.38E-03	0.157	3.64E-01	4	***Tle5***	2414	Promoter (2-3kb)	0.11	ns	0.11	0.14	ns	ns	ns	-0.06
chr11	101239998	101244105	4108	-0.859	1.72E-05	0.003	9.88E-01	4	***Ramp2***	-1923	Promoter (1-2kb)	ns	0.08	0.18	0.27	ns	ns	ns	-0.12
chr11	53342518	53346607	4090	-0.372	3.50E-02	0.012	9.51E-01	4	***Aff4***	-4226	Exon (ENSMUST0	ns	0.12	0.19	0.16	0.06	ns	-0.09	0.07
chr11	54402225	54437001	34777	-0.651	2.11E-08	0.062	5.59E-01	4	***Fnip1***	-1198	Promoter (1-2kb)	ns	ns	0.14	0.06	ns	ns	-0.13	0.10
chr11	76402895	76406246	3352	-0.478	9.55E-03	-0.121	4.25E-01	4	***Timm22***	-706	Promoter (<=1kb)	0.06	ns	0.05	0.06	ns	0.04	ns	-0.04
chr11	94413086	94418576	5491	-0.453	1.14E-02	0.125	4.13E-01	4	***Cacna1g***	0	Promoter (<=1kb)	ns	ns	0.10	0.06	ns	ns	-0.06	ns
chr11	95577355	95618926	41572	-0.617	5.18E-04	0.168	2.26E-01	4	***Ngfr***	0	Promoter (<=1kb)	0.08	0.22	0.43	0.38	ns	0.07	-0.24	-0.12
chr12	16752522	16756509	3988	-0.464	3.24E-02	0.200	2.84E-01	4	***Greb1***	686	Promoter (<=1kb)	0.15	0.21	0.28	0.36	0.06	ns	ns	ns
chr12	21104351	21115978	11628	-0.398	6.53E-03	0.077	5.51E-01	4	***Asap2***	0	Promoter (<=1kb)	0.05	0.03	0.05	0.02	0.03	ns	ns	ns
chr12	36037839	36048330	10492	-0.669	7.84E-06	-0.105	4.00E-01	4	***Tspan13***	0	Promoter (<=1kb)	0.08	0.04	0.09	0.13	0.07	0.06	ns	ns
chr13	89741593	89744595	3003	-0.983	2.58E-05	0.038	8.55E-01	4	***Vcan***	0	Promoter (<=1kb)	0.35	0.16	0.24	0.18	0.07	ns	ns	0.11
chr14	31435843	31446116	10274	-0.534	2.13E-03	0.175	2.01E-01	4	***Sh3bp5***	0	Promoter (<=1kb)	0.09	0.04	0.07	0.03	0.06	0.07	ns	ns
chr14	50936030	50941774	5745	-0.346	1.83E-02	0.125	3.07E-01	4	***Pnp***	-2528	Promoter (2-3kb)	0.22	0.27	0.27	0.22	ns	ns	ns	0.08
chr14	66325877	66349301	23425	-0.385	4.12E-03	0.095	4.05E-01	4	***Stmn4***	0	Promoter (<=1kb)	ns	0.14	0.24	0.22	ns	-0.06	-0.13	ns
chr15	6865428	6868560	3133	-0.523	1.23E-02	0.045	8.21E-01	4	***Osmr***	5697	Intron (ENSMUST	0.10	0.02	0.04	0.01	0.06	0.07	ns	ns
chr15	74940283	74947032	6750	-0.254	2.23E-02	0.142	1.08E-01	4	***Ly6e***	-8019	Distal Intergenic	0.45	0.26	0.19	0.13	ns	ns	0.09	0.13
chr15	81477672	81492352	14681	-0.275	3.26E-02	-0.011	9.38E-01	4	***Rbx1***	4050	Exon (ENSMUST0	0.15	ns	0.08	0.12	ns	0.07	ns	-0.12
chr16	14692981	14705712	12732	-0.230	1.84E-02	-0.112	1.52E-01	4	***Snai2***	-140	Promoter (<=1kb)	0.10	0.06	0.13	0.02	ns	0.11	ns	ns
chr16	87442860	87454518	11659	-0.252	3.51E-02	0.002	9.85E-01	4	***Usp16***	-185	Promoter (<=1kb)	0.07	ns	0.13	0.07	ns	ns	-0.10	ns
chr17	29320694	29323516	2823	-0.474	2.56E-02	0.234	1.80E-01	4	***Pi16***	1454	Promoter (1-2kb)	0.53	0.36	0.26	0.20	ns	ns	0.27	0.09
chr17	29501935	29504444	2510	-0.429	3.26E-02	0.182	2.96E-01	4	***Pim1***	8528	Distal Intergenic	ns	0.15	0.13	0.12	ns	-0.07	-0.10	0.05
chr17	50691885	50698745	6861	-0.262	2.63E-02	-0.122	2.09E-01	4	***Btg3***	0	Promoter (<=1kb)	0.08	ns	0.08	0.07	ns	ns	-0.09	ns
chr17	72829035	72836017	6983	-0.322	1.95E-02	0.136	2.37E-01	4	***Ypel5***	-436	Promoter (<=1kb)	0.08	0.07	0.13	0.14	0.03	ns	ns	ns
chr17	79049683	79060198	10516	-0.607	1.73E-04	0.134	3.04E-01	4	***Qpct***	0	Promoter (<=1kb)	0.14	0.20	0.32	0.39	ns	0.06	ns	ns
chr17	8784571	8811226	26656	-0.774	5.07E-20	-0.083	2.71E-01	4	***Pde10a***	0	Promoter (<=1kb)	0.14	0.12	0.17	0.17	0.12	0.06	ns	ns
chr18	52768028	52773165	5138	-0.355	2.60E-02	0.088	5.44E-01	4	***Sncaip***	0	Promoter (<=1kb)	ns	ns	0.06	0.13	ns	ns	ns	-0.08
chr2	125509844	125512568	2725	-0.642	4.85E-03	0.209	2.28E-01	4	***Fbn1***	-1851	Promoter (1-2kb)	0.52	0.34	0.45	0.44	-0.03	ns	ns	ns
chr2	154408892	154413409	4518	-0.306	7.78E-02	0.070	6.94E-01	4	***Snta1***	-793	Promoter (<=1kb)	0.18	0.14	0.17	0.16	-0.05	ns	ns	ns
chr2	18664394	18672118	7725	-0.317	9.42E-03	-0.095	3.63E-01	4	***Commd3***	-266	Promoter (<=1kb)	0.11	0.09	0.12	0.12	ns	ns	ns	-0.05
chr3	100489690	100493276	3587	-0.800	6.29E-04	0.251	1.31E-01	4	***Tent5c***	-366	Promoter (<=1kb)	0.12	0.08	0.04	ns	0.05	0.11	0.10	0.08
chr1	45923244	45944550	21307	-0.448	2.08E-07	0.101	1.58E-01	4	***Slc40a1***	0	Promoter (<=1kb)	0.08	0.07	0.11	0.12	0.05	ns	ns	ns
chr3	63284000	63297827	13828	-0.291	3.08E-02	0.174	1.10E-01	4	***Mme***	0	Promoter (<=1kb)	0.25	0.23	0.15	0.12	ns	ns	0.15	0.13
chr3	96206514	96219079	12566	-0.179	8.80E-02	-0.069	4.28E-01	4	***Bola1***	630	Promoter (<=1kb)	0.09	ns	0.05	0.04	ns	0.06	ns	-0.03
chr4	122961509	122964245	2737	-0.550	2.99E-03	0.190	1.84E-01	4	***Mfsd2a***	-321	Promoter (<=1kb)	0.05	0.06	0.09	0.07	ns	ns	-0.07	ns
chr4	143212732	143269049	56318	-0.295	1.67E-04	-0.039	5.97E-01	4	***Prdm2***	0	Promoter (<=1kb)	ns	ns	0.04	ns	ns	ns	-0.07	0.09
chr4	143297186	143358161	60976	-0.200	1.46E-02	-0.098	1.28E-01	4	***Pdpn***	0	Promoter (<=1kb)	0.48	0.27	0.34	0.37	0.06	0.17	0.17	0.07
chr4	4124168	4145600	21433	-0.841	8.60E-16	-0.011	9.27E-01	4	***Penk***	0	Promoter (<=1kb)	0.68	0.44	0.40	0.30	0.13	0.33	0.34	0.24
chr17	27133838	27188687	54850	-0.622	3.49E-07	0.128	2.04E-01	4	***Uqcc2***	0	Promoter (<=1kb)	0.35	0.12	0.26	0.28	-0.10	0.10	ns	-0.09
chr4	88428354	88476335	47982	-0.338	5.42E-03	0.133	1.78E-01	4	***Hacd4***	0	Promoter (<=1kb)	0.33	0.13	0.20	0.16	ns	0.08	ns	ns
chr5	113801959	113804759	2801	-1.054	2.28E-05	0.111	5.66E-01	4	***Tmem119***	-1443	Promoter (1-2kb)	0.44	0.41	0.60	0.69	0.06	0.17	ns	-0.15
chr2	11548740	11574610	25871	-0.203	7.23E-02	0.053	6.10E-01	4	***Pfkfb3***	0	Promoter (<=1kb)	ns	ns	0.06	ns	ns	ns	-0.06	ns
chr5	137046662	137052680	6019	-0.421	6.07E-03	-0.083	5.33E-01	4	***Ap1s1***	-527	Promoter (<=1kb)	0.12	0.06	0.09	0.09	ns	ns	ns	-0.04
chr2	131044354	131089475	45122	-0.449	8.66E-06	0.004	9.71E-01	4	***Adam33***	0	Promoter (<=1kb)	0.15	ns	ns	ns	-0.04	ns	ns	ns
chr5	17572946	17576534	3589	-0.862	3.23E-05	-0.072	6.86E-01	4	***Sema3c***	0	Promoter (<=1kb)	-0.16	ns	0.07	ns	-0.15	-0.23	-0.15	-0.08
chr2	167226990	167245483	18494	-1.023	1.05E-09	0.045	7.78E-01	4	***Ptgis***	0	Promoter (<=1kb)	0.55	0.27	0.29	0.45	ns	ns	ns	-0.14
chr5	90886018	90910841	24824	-0.234	2.79E-02	-0.003	9.79E-01	4	***Cxcl1***	0	Promoter (<=1kb)	0.72	0.63	0.82	0.67	ns	-0.14	-0.29	ns
chr3	152752357	152758761	6405	-0.726	2.66E-05	0.210	1.08E-01	4	***Pigk***	-4620	Intron (ENSMUST	0.17	0.10	0.09	0.12	ns	ns	0.07	ns
chr6	13061852	13068044	6193	-0.709	4.75E-07	0.118	2.99E-01	4	***Tmem106b***	-1715	Promoter (1-2kb)	0.16	0.13	0.16	0.15	0.06	0.06	0.13	ns
chr6	29322307	29347251	24945	-0.199	1.06E-02	-0.042	5.38E-01	4	***Calu***	-818	Promoter (<=1kb)	0.35	0.25	0.29	0.25	-0.03	ns	-0.06	ns
chr6	82770455	82772764	2310	-0.440	3.75E-02	0.234	1.86E-01	4	***Hk2***	224	Promoter (<=1kb)	0.59	0.60	0.71	0.71	0.06	ns	-0.10	0.12
chr6	91202835	91216519	13685	-0.870	9.35E-09	0.014	9.27E-01	4	***Fbln2***	0	Promoter (<=1kb)	0.92	0.87	1.01	1.22	-0.07	ns	0.08	-0.06
chr7	100281388	100301918	20531	-1.115	7.77E-09	0.151	3.27E-01	4	***P4ha3***	0	Promoter (<=1kb)	0.25	0.11	0.19	0.19	ns	0.07	ns	ns
chr7	130573818	130577401	3584	-0.854	1.02E-05	-0.049	7.81E-01	4	***Tacc2***	-37	Promoter (<=1kb)	ns	ns	0.07	ns	ns	ns	-0.10	ns
chr7	81206984	81212775	5792	-0.754	1.56E-05	0.172	2.06E-01	4	***Pde8a***	-821	Promoter (<=1kb)	0.14	0.16	0.25	0.23	ns	ns	-0.09	ns
chr8	68714702	68754578	39877	-0.230	3.24E-03	0.070	2.90E-01	4	***Csgalnact1***	0	Promoter (<=1kb)	0.12	ns	ns	ns	0.05	ns	ns	ns
chr8	11479261	11483984	4724	-0.424	3.24E-02	0.230	1.60E-01	4	***Rab20***	-551	Promoter (<=1kb)	0.04	0.05	0.04	0.05	0.03	ns	ns	ns
chr8	117111076	117152375	41300	-0.630	3.22E-08	0.045	6.81E-01	4	***Gan***	-5760	3' UTR	ns	ns	0.12	0.05	ns	ns	-0.07	0.08
chr8	17525138	17549340	24203	-0.438	7.22E-07	0.054	4.94E-01	4	***Csmd1***	0	Promoter (<=1kb)	0.07	ns	0.07	0.09	0.04	ns	0.07	0.08
chr8	23257734	23266446	8713	-0.621	1.64E-08	0.104	2.62E-01	4	***Golga7***	-660	Promoter (<=1kb)	0.04	ns	ns	0.02	0.08	0.06	ns	ns
chr8	23372749	23432233	59485	-0.225	1.23E-02	-0.068	3.74E-01	4	***Sfrp1***	0	Promoter (<=1kb)	0.18	ns	ns	ns	0.34	0.23	0.17	0.07
chr8	32262763	32334265	71503	-0.146	5.51E-02	0.035	5.57E-01	4	***Nrg1***	0	Promoter (<=1kb)	0.23	0.44	0.66	0.85	ns	ns	-0.15	-0.17
chr9	49787709	49812522	24814	-0.357	2.95E-05	0.041	6.08E-01	4	***Ncam1***	0	Promoter (<=1kb)	0.13	0.06	0.06	0.04	0.08	ns	ns	ns
chr9	22117136	22155942	38807	-0.185	4.50E-02	-0.102	1.51E-01	4	***Elof1***	0	Promoter (<=1kb)	0.13	0.10	0.12	0.12	ns	ns	ns	-0.07
chr9	45365142	45372092	6951	-0.537	4.39E-03	0.216	1.35E-01	4	***Fxyd6***	0	Promoter (<=1kb)	0.51	0.19	0.15	0.25	ns	0.08	0.12	ns
chr9	48609133	48646042	36910	-0.450	6.52E-07	-0.039	6.52E-01	4	***Nnmt***	-3980	Distal Intergenic	0.29	0.09	0.10	0.11	ns	0.08	0.08	ns
chr9	58322030	58325693	3664	-0.862	3.08E-05	0.169	2.92E-01	4	***Loxl1***	-8844	Distal Intergenic	0.72	0.50	0.66	0.71	-0.11	ns	ns	-0.10
chr9	78590459	78624626	34168	-0.367	2.85E-09	-0.017	7.85E-01	4	***Cd109***	0	Promoter (<=1kb)	ns	0.10	0.19	0.14	ns	-0.05	-0.12	-0.06
chr9	79710430	79739627	29198	-0.154	9.85E-02	0.101	1.39E-01	4	***Col12a1***	0	Promoter (<=1kb)	0.55	0.29	0.31	0.13	0.08	ns	ns	0.12
chrX	41489504	41624706	135203	-0.209	6.32E-02	-0.118	1.99E-01	4	***Gria3***	0	Promoter (<=1kb)	0.24	0.08	0.07	ns	ns	ns	0.07	0.08
chrX	56727623	56731306	3684	-0.395	1.39E-02	-0.120	3.80E-01	4	***Fhl1***	-481	Promoter (<=1kb)	0.21	0.10	0.14	0.11	ns	0.06	ns	0.07
chr1	156526582	156556197	29616	0.126	2.42E-01	-0.034	6.88E-01	5	***Abl2***	-2589	Promoter (2-3kb)	0.06	0.04	0.14	0.06	ns	ns	-0.10	0.12
chr1	161877279	161932918	55640	0.097	4.07E-01	0.015	8.69E-01	5	***Suco***	-597	Promoter (<=1kb)	ns	0.12	0.16	0.08	ns	ns	-0.13	0.11
chr1	165725527	165763442	37916	-0.032	8.45E-01	0.017	8.53E-01	5	***Creg1***	-304	Promoter (<=1kb)	0.20	0.06	0.09	0.09	ns	0.09	ns	ns
chr1	182106117	182124834	18718	-0.099	4.23E-01	0.007	9.48E-01	5	***Srp9***	0	Promoter (<=1kb)	0.15	ns	0.11	0.08	ns	0.10	ns	-0.06
chr1	183976669	184025989	49321	0.029	8.76E-01	0.112	2.41E-01	5	***Dusp10***	0	Promoter (<=1kb)	ns	ns	0.04	0.04	ns	ns	-0.04	ns

				H3K27me3 peak dynamics*								RNA expression†							
				Aggregate time (GD5.5 to 18.5)		Aggregate genotype (*Kdm6b cKO* vs. ctrl)						Ctrl IS/IIS fibroblasts vs. ctrl (log$_2$FC)				*Kdm6b cKO* vs. ctrl IS/IIS fibroblasts (log$_2$FC)			
Chr	Peak start	Peak end	Peak width	log$_2$FC	*FDR*	log$_2$FC	*FDR*	HC	Gene	Peak distance to TSS	Annotation	GD12.5	GD14.5	GD16.5	GD18.5	GD12.5	GD14.5	GD16.5	GD18.5
chr1	60172746	60177445	4700	-0.045	7.99E-01	0.000	9.99E-01	5	***Nbeal1***	-3154	Distal Intergenic	0.03	ns	ns	ns	0.07	ns	ns	0.07
chr1	79765072	79772923	7852	-0.057	7.31E-01	0.155	1.82E-01	5	***Wdfy1***	-3025	Intron (ENSMUST	0.05	ns	0.06	0.12	0.04	ns	ns	0.06
chr1	82833935	82838509	4575	-0.055	7.45E-01	0.089	5.47E-01	5	***Agfg1***	-974	Promoter (<=1kb)	0.06	0.07	0.13	0.12	0.04	ns	ns	ns
chr10	117194972	117207375	12404	-0.093	5.28E-01	0.164	1.49E-01	5	***Yeats4***	9983	Distal Intergenic	0.06	0.06	0.08	0.08	ns	ns	ns	-0.05
chr10	120900947	120906357	5411	-0.065	6.94E-01	0.118	4.23E-01	5	***Msrb3***	-1846	Promoter (1-2kb)	0.11	0.05	0.08	0.08	0.04	0.06	ns	ns
chr10	13003322	13008106	4785	-0.014	9.49E-01	-0.065	6.13E-01	5	***Sf3b5***	0	Promoter (<=1kb)	0.20	ns	0.10	0.09	ns	0.07	ns	-0.07
chr10	50580366	50589446	9081	-0.113	4.03E-01	-0.135	1.88E-01	5	***Ascc3***	-3223	Distal Intergenic	ns	ns	0.09	0.03	ns	ns	-0.09	0.10
chr10	60270950	60273710	2761	-0.248	1.57E-01	0.215	2.24E-01	5	***Psap***	-3917	Distal Intergenic	0.22	0.14	0.16	0.14	-0.04	ns	ns	ns
chr10	77273185	77290297	17113	-0.133	2.08E-01	-0.039	6.50E-01	5	***Pofut2***	6268	Distal Intergenic	0.30	0.18	0.21	0.21	ns	ns	ns	-0.05
chr10	77563744	77579816	16073	-0.151	1.23E-01	-0.043	5.90E-01	5	***Pttg1ip***	-1904	Promoter (1-2kb)	0.19	0.32	0.32	0.21	-0.09	-0.11	-0.11	ns
chr10	78009773	78013301	3529	0.020	9.22E-01	0.169	2.73E-01	5	***Pfkl***	0	Promoter (<=1kb)	ns	ns	ns	0.03	ns	ns	ns	-0.04
chr10	79694829	79704028	9200	0.200	1.30E-01	-0.159	1.57E-01	5	***Bsg***	-463	Promoter (<=1kb)	0.38	0.26	0.30	0.35	ns	0.09	ns	-0.07
chr10	84538466	84544426	5961	-0.083	6.03E-01	0.099	5.46E-01	5	***Ckap4***	-4404	Distal Intergenic	0.51	0.31	0.38	0.34	ns	0.10	ns	ns
chr10	95924209	95938051	13843	0.035	8.38E-01	0.054	5.87E-01	5	***Eea1***	-2599	Promoter (2-3kb)	0.06	0.07	0.16	0.12	ns	ns	-0.09	ns
chr11	100291130	100315412	24283	0.026	8.94E-01	-0.076	4.89E-01	5	***Eif1***	-4473	Exon (ENSMUST	0.04	ns	0.05	0.08	-0.02	ns	-0.06	-0.08
chr11	101279215	101284230	5016	-0.017	9.36E-01	-0.133	3.15E-01	5	***Coa3***	-101	Promoter (<=1kb)	0.11	0.05	0.10	0.10	ns	0.07	ns	-0.07
chr11	102412518	102425637	13120	-0.054	7.33E-01	-0.044	6.75E-01	5	***Slc25a39***	-4572	Distal Intergenic	0.17	0.13	0.26	0.28	ns	ns	ns	-0.08
chr11	119902875	119910800	7926	0.107	4.37E-01	-0.067	5.54E-01	5	***Chmp6***	-2641	Promoter (2-3kb)	0.05	0.04	0.07	0.06	ns	ns	ns	-0.03
chr11	120642279	120673128	30850	-0.090	4.88E-01	-0.029	7.76E-01	5	***Pycr1***	0	Promoter (<=1kb)	0.19	0.08	0.09	0.05	ns	0.07	ns	ns
chr11	17244320	17256518	12199	-0.043	7.98E-01	0.066	5.10E-01	5	***C1d***	-1061	Promoter (1-2kb)	0.10	ns	0.02	0.04	ns	ns	ns	-0.04
chr11	31844171	31870495	26325	0.082	4.65E-01	0.085	1.81E-01	5	***Cpeb4***	-1716	Promoter (1-2kb)	ns	ns	0.04	ns	ns	ns	-0.09	ns
chr11	3271812	3278451	6640	0.079	6.16E-01	-0.159	2.21E-01	5	***Drg1***	-5397	Distal Intergenic	ns	ns	ns	0.01	ns	0.05	ns	-0.04
chr11	45830103	45851760	21658	-0.056	6.74E-01	-0.070	3.35E-01	5	***Clint1***	-204	Promoter (<=1kb)	0.09	ns	0.13	0.08	ns	ns	-0.09	ns
chr11	46417817	46436362	18546	-0.085	5.62E-01	0.092	4.11E-01	5	***Med7***	-563	Promoter (<=1kb)	0.04	0.04	0.08	0.06	0.03	0.04	ns	ns
chr11	52090943	52097059	6117	-0.075	6.35E-01	-0.028	8.59E-01	5	***Ppp2ca***	-1622	Promoter (1-2kb)	ns	ns	0.08	0.08	0.05	ns	-0.11	ns
chr11	68853329	68901166	47838	-0.164	1.29E-01	-0.130	1.09E-01	5	***Ndel1***	0	Promoter (<=1kb)	0.05	0.07	0.14	0.06	ns	ns	-0.14	ns
chr11	74727107	74748089	20983	0.038	8.13E-01	-0.073	3.89E-01	5	***Pafah1b1***	-2437	Promoter (2-3kb)	ns	0.10	0.15	0.12	ns	ns	-0.10	ns
chr11	75427156	75430125	2970	0.024	9.06E-01	0.050	8.02E-01	5	***Serpinf1***	-4455	Exon (ENSMUST	0.40	0.30	0.37	0.38	-0.05	0.10	0.04	-0.08
chr11	80423223	80427281	4059	-0.042	8.19E-01	-0.106	5.01E-01	5	***Psmd11***	-1334	Promoter (1-2kb)	ns	ns	0.11	0.11	ns	ns	-0.09	ns
chr11	82107112	82111570	4459	-0.065	6.94E-01	0.199	2.17E-01	5	***Ccl8***	-3615	Distal Intergenic	0.10	0.15	0.16	0.16	0.04	ns	ns	ns
chr11	93971327	93992360	21034	-0.011	9.56E-01	-0.027	7.62E-01	5	***Nme1***	-2806	Promoter (2-3kb)	0.28	0.10	0.13	0.23	ns	ns	ns	-0.11
chr11	96844805	96848722	3918	-0.071	6.60E-01	0.109	5.28E-01	5	***Copz2***	-1148	Promoter (1-2kb)	0.43	0.22	0.27	0.22	-0.05	0.13	ns	ns
chr12	111459968	111534066	74099	-0.076	4.99E-01	0.057	3.91E-01	5	***Gm266***	0	Promoter (<=1kb)	0.08	ns	ns	ns	-0.04	ns	ns	ns
chr12	17248324	17266243	17920	-0.003	9.88E-01	-0.133	1.02E-01	5	***Pdia6***	-302	Promoter (<=1kb)	0.37	0.29	0.27	0.33	0.07	ns	ns	-0.07
chr12	70926405	70932971	6567	-0.056	7.33E-01	0.083	5.06E-01	5	***Actr10***	-4886	Distal Intergenic	0.08	0.07	0.11	0.11	0.04	ns	ns	ns
chr13	55514591	55522724	8134	-0.005	9.84E-01	-0.102	4.48E-01	5	***Pdlim7***	-915	Promoter (<=1kb)	0.09	ns	0.05	0.06	ns	ns	ns	-0.06
chr13	55582004	55592924	10921	-0.060	7.13E-01	-0.093	4.30E-01	5	***Tmed9***	-245	Promoter (<=1kb)	0.44	0.37	0.40	0.40	ns	ns	ns	-0.06
chr13	56292351	56310204	17854	0.018	9.27E-01	0.087	3.64E-01	5	***Cxcl14***	0	Promoter (<=1kb)	0.13	ns	ns	ns	0.36	0.44	0.36	ns
chr13	81653115	81655815	2701	0.042	8.18E-01	-0.179	2.85E-01	5	***Lysmd3***	-1848	Promoter (1-2kb)	0.09	0.10	0.14	0.05	ns	ns	-0.10	0.12
chr13	92758260	92779408	21149	-0.047	7.45E-01	0.081	2.83E-01	5	***Thbs4***	0	Promoter (<=1kb)	0.19	ns	ns	ns	0.06	0.12	0.10	ns
chr13	96673389	96676853	3465	-0.033	8.62E-01	0.151	3.61E-01	5	***Hmgcr***	-2453	Promoter (2-3kb)	0.03	ns	0.04	0.04	0.04	0.04	ns	ns
chr14	18897292	18908861	11570	-0.104	4.52E-01	0.094	3.78E-01	5	***Ube2e2***	-3025	Distal Intergenic	0.06	0.09	0.09	0.10	ns	ns	ns	-0.05
chr14	20395699	20407191	11493	0.137	2.92E-01	-0.049	6.75E-01	5	***Mrps16***	-2065	Promoter (2-3kb)	0.16	ns	0.11	0.09	ns	0.09	ns	-0.05
chr14	45405570	45422970	17401	0.187	1.23E-01	0.138	1.57E-01	5	***Gnpnat1***	-657	Promoter (<=1kb)	0.04	ns	0.03	0.04	0.03	0.04	ns	ns
chr14	46822345	46829109	6765	-0.004	9.85E-01	0.002	9.93E-01	5	***Gmfb***	-103	Promoter (<=1kb)	0.03	ns	0.03	0.02	0.03	ns	ns	ns
chr14	61440242	61467597	27356	0.089	4.33E-01	-0.088	1.97E-01	5	***Kpna3***	-368	Promoter (<=1kb)	0.06	0.12	0.19	0.12	ns	ns	-0.09	ns
chr14	65652728	65659076	6349	0.011	9.58E-01	0.136	3.52E-01	5	***Scara5***	-7327	Distal Intergenic	ns	0.13	0.16	0.10	ns	-0.10	ns	ns
chr14	74717400	74730628	13229	0.145	2.43E-01	0.070	4.99E-01	5	***Esd***	-1669	Promoter (1-2kb)	ns	ns	0.10	0.09	ns	ns	ns	-0.09
chr15	12283122	12320597	37476	0.043	7.64E-01	0.052	4.73E-01	5	***Golph3***	-853	Promoter (<=1kb)	0.15	0.07	0.14	0.12	ns	ns	-0.08	ns
chr15	39074496	39084027	9532	-0.124	3.54E-01	-0.046	6.95E-01	5	***Cthrc1***	0	Promoter (<=1kb)	0.24	ns	ns	ns	0.08	0.12	0.08	ns
chr15	57895359	57899356	3998	-0.057	7.34E-01	0.132	3.87E-01	5	***Derl1***	-2911	Promoter (2-3kb)	0.23	0.13	0.17	0.20	ns	ns	ns	-0.06
chr15	73072773	73081344	8572	0.113	4.05E-01	-0.027	8.26E-01	5	***Chrac1***	-9048	Distal Intergenic	0.11	0.13	0.17	0.15	ns	ns	ns	-0.05
chr15	75005985	75014098	8114	-0.055	7.40E-01	0.176	1.29E-01	5	***Ly6a***	-7954	Exon (ENSMUST	0.98	0.83	0.85	0.78	ns	0.13	0.10	ns
chr15	75055105	75057473	2369	-0.046	7.94E-01	0.153	3.37E-01	5	***Ly6c1***	-6275	Distal Intergenic	0.77	0.57	0.63	0.65	ns	0.18	0.17	ns
chr15	79774706	79789637	14932	0.062	6.93E-01	-0.127	2.32E-01	5	***Dnal4***	0	Promoter (<=1kb)	ns	ns	0.03	0.02	ns	ns	ns	-0.02
chr15	84996383	84999335	2953	-0.030	8.71E-01	0.107	5.89E-01	5	***031439G07Rik***	-7832	Distal Intergenic	ns	0.06	0.16	0.13	ns	ns	-0.11	ns
chr15	85300554	85335544	34991	-0.050	7.50E-01	0.030	7.79E-01	5	***Atxn10***	-701	Promoter (<=1kb)	0.13	0.12	0.12	0.13	0.05	ns	ns	ns
chr15	93341498	93358951	17454	-0.047	7.64E-01	0.009	9.31E-01	5	***Yaf2***	-4563	Exon (ENSMUST	0.05	ns	0.05	0.03	0.03	ns	ns	ns
chr15	98725725	98731506	5782	-0.176	2.77E-01	0.043	8.35E-01	5	***Fkbp11***	0	Promoter (<=1kb)	0.43	0.14	0.17	0.10	ns	0.16	ns	ns
chr15	99022505	99025543	3039	-0.061	7.17E-01	0.139	4.05E-01	5	***Tuba1c***	-4348	Distal Intergenic	0.04	0.05	0.13	0.11	0.05	ns	-0.11	ns
chr16	11143717	11144582	866	0.205	1.31E-01	-0.155	1.82E-01	5	***Zc3h7a***	-1810	Promoter (1-2kb)	0.08	0.07	0.13	0.07	ns	0.08	ns	0.09
chr16	17132716	17137291	4576	-0.069	6.70E-01	0.173	1.97E-01	5	***Sdf2l1***	-333	Promoter (<=1kb)	0.08	0.06	0.05	0.12	ns	ns	ns	-0.06
chr16	30391580	30460605	69026	0.017	9.34E-01	0.059	5.35E-01	5	***Atp13a3***	0	Promoter (<=1kb)	0.09	0.14	0.22	0.16	ns	ns	-0.12	0.09
chr16	35981375	35982094	720	-0.019	9.28E-01	0.022	9.14E-01	5	***Kpna1***	-1221	Promoter (1-2kb)	ns	ns	0.06	0.02	ns	ns	-0.09	ns
chr16	49788518	49826017	37500	-0.017	9.12E-01	0.085	1.25E-01	5	***Cd47***	0	Promoter (<=1kb)	0.15	0.18	0.19	0.15	ns	-0.08	ns	ns
chr16	8672591	8677193	4603	-0.150	3.23E-01	0.018	9.23E-01	5	***Carhsp1***	-436	Promoter (<=1kb)	0.24	0.17	0.23	0.21	ns	0.09	ns	ns
chr16	91368582	91371592	3011	0.021	9.18E-01	0.137	4.03E-01	5	***Ifnar2***	-1191	Promoter (1-2kb)	0.26	0.22	0.24	0.29	0.06	ns	ns	ns
chr16	91933838	91959331	25494	0.021	9.03E-01	-0.033	6.76E-01	5	***Atp5o***	-2151	Promoter (2-3kb)	0.17	0.10	0.12	0.14	ns	ns	ns	-0.11
chr17	34736777	34739133	2357	-0.173	2.83E-01	0.119	5.13E-01	5	***C4b***	-678	Promoter (<=1kb)	0.19	0.14	0.04	0.04	0.03	0.05	0.31	0.11
chr17	35427980	35441827	13848	-0.025	8.91E-01	-0.009	9.35E-01	5	***H2-Q7***	0	Promoter (<=1kb)	0.10	0.16	0.04	0.04	ns	-0.10	ns	ns
chr17	46103634	46111175	7542	-0.035	8.49E-01	0.039	7.47E-01	5	***Mrps18a***	0	Promoter (<=1kb)	ns	ns	0.05	0.03	ns	ns	ns	-0.05
chr17	47361605	47369074	7470	-0.155	2.19E-01	-0.139	1.61E-01	5	***Mrps10***	0	Promoter (<=1kb)	0.03	ns	ns	0.02	0.03	ns	ns	ns
chr18	34374290	34391455	17166	-0.087	5.56E-01	-0.035	7.96E-01	5	***Reep5***	-220	Promoter (<=1kb)	0.40	0.22	0.29	0.32	ns	ns	ns	-0.08
chr18	53418144	53435956	17813	0.117	3.39E-01	0.131	1.22E-01	5	***Ppic***	-29	Promoter (<=1kb)	0.35	0.12	0.22	0.13	ns	0.09	ns	-0.07
chr19	10450825	10493694	42870	-0.078	5.68E-01	-0.060	5.12E-01	5	***Lrrc10b***	0	Promoter (<=1kb)	ns	ns	0.13	0.16	ns	ns	-0.06	-0.05
chr19	34244243	34264559	20317	-0.151	3.01E-01	0.064	6.70E-01	5	***Acta2***	0	Promoter (<=1kb)	0.17	0.11	0.04	0.07	ns	ns	ns	-0.05
chr19	4013324	4019737	6414	-0.033	8.63E-01	-0.133	3.14E-01	5	***Ndufv1***	-518	Promoter (<=1kb)	0.06	0.06	0.06	0.08	ns	ns	ns	-0.04
chr19	41899135	41908977	9843	0.086	5.68E-01	-0.068	6.05E-01	5	***Pgam1***	-2946	Promoter (2-3kb)	0.11	ns	0.13	0.19	0.06	ns	ns	-0.12
chr19	42133484	42138710	5227	-0.033	8.63E-01	-0.056	7.11E-01	5	***Avpi1***	-4425	Distal Intergenic	0.04	ns	ns	0.04	0.02	ns	ns	ns
chr19	42138803	42141900	3098	0.006	9.80E-01	0.175	3.02E-01	5	***Marveld1***	-5500	Distal Intergenic	0.13	0.05	0.06	0.02	ns	0.04	ns	ns
chr19	5434222	5452384	18163	-0.133	2.65E-01	-0.054	5.80E-01	5	***Fosl1***	0	Promoter (<=1kb)	0.13	0.17	0.27	0.19	ns	ns	-0.16	ns
chr2	13587923	13595395	7473	-0.219	1.08E-01	0.131	2.65E-01	5	***Vim***	8554	Distal Intergenic	0.17	0.20	0.28	0.18	ns	-0.05	-0.12	ns
chr2	152111988	152126708	14721	-0.043	7.81E-01	-0.075	3.69E-01	5	***Srxn1***	6464	Distal Intergenic	0.09	0.10	0.20	0.15	ns	ns	-0.10	ns
chr2	152128505	152155721	27217	-0.139	2.01E-01	0.000	9.98E-01	5	***Tcf15***	0	Promoter (<=1kb)	ns	0.20	0.21	0.32	ns	ns	ns	-0.08

				H3K27me3 peak dynamics*								RNA expression†							
				Aggregate time (GD5.5 to 18.5)		Aggregate genotype (*Kdm6b cKO* vs. ctrl)						Ctrl IS/IIS fibroblasts vs. ctrl GD5.5/8.5 IIS fibroblasts (log_2FC)				*Kdm6b cKO* vs. ctrl IS/IIS fibroblasts (log_2FC)			
Chr	Peak start	Peak end	Peak width	log_2FC	*FDR*	log_2FC	*FDR*	HC	Gene	Peak distance to TSS	Annotation	GD12.5	GD14.5	GD16.5	GD18.5	GD12.5	GD14.5	GD16.5	GD18.5
chr2	155370502	155381242	10741	0.076	6.17E-01	0.162	1.38E-01	5	*Trp53inp2*	0	Promoter (<=1kb)	0.07	0.07	0.11	0.16	0.03	ns	ns	-0.04
chr2	158292725	158300554	7830	-0.020	9.22E-01	0.127	3.52E-01	5	*Lbp*	-5939	Distal Intergenic	0.30	0.16	0.08	0.10	0.08	ns	0.15	ns
chr2	163815507	163819826	4320	0.057	7.37E-01	0.137	3.28E-01	5	*Ccn5*	-1035	Promoter (1-2kb)	0.16	ns	ns	ns	-0.05	ns	ns	ns
chr2	173728471	173734797	6327	-0.135	3.42E-01	0.159	1.89E-01	5	*Vapb*	-2714	Promoter (2-3kb)	0.11	0.05	0.11	0.10	ns	0.05	ns	ns
chr2	174474492	174519608	45117	-0.024	8.93E-01	-0.036	6.80E-01	5	*Prelid3b*	-1411	Promoter (1-2kb)	0.05	0.03	0.07	0.07	0.04	ns	ns	ns
chr2	29851842	29867389	15548	-0.068	6.47E-01	-0.089	3.77E-01	5	*Cercam*	-1775	Promoter (1-2kb)	0.30	0.16	0.18	0.15	-0.09	ns	ns	ns
chr2	30836845	30848566	11722	-0.174	2.79E-01	0.165	3.48E-01	5	*Prrx2*	0	Promoter (<=1kb)	0.05	ns	0.09	0.05	ns	0.06	ns	-0.04
chr2	32382429	32391427	8999	-0.016	9.39E-01	0.042	7.79E-01	5	*Lcn2*	0	Promoter (<=1kb)	0.14	0.27	0.24	0.22	0.05	ns	ns	ns
chr2	32405414	32409577	4164	-0.031	8.72E-01	-0.133	3.80E-01	5	*Slc25a25*	6994	3' UTR	0.10	0.05	0.06	0.03	ns	ns	ns	0.06
chr2	92024840	92034156	9317	-0.010	9.64E-01	0.147	3.69E-01	5	*Creb3l1*	-338	Promoter (<=1kb)	0.40	0.20	0.29	0.26	-0.07	0.12	ns	ns
chr3	130717395	130719480	2086	-0.034	8.55E-01	-0.199	2.36E-01	5	*Ostc*	-7951	Distal Intergenic	0.53	0.24	0.30	0.32	ns	0.14	ns	-0.07
chr3	135693254	135708002	14749	-0.122	2.95E-01	-0.055	5.37E-01	5	*Nfkb1*	-1707	Promoter (1-2kb)	0.25	0.31	0.37	0.26	ns	-0.10	-0.25	0.12
chr3	144725613	144730226	4614	0.139	3.44E-01	0.064	6.67E-01	5	*Sh3glb1*	-5278	3' UTR	0.33	0.31	0.41	0.42	ns	ns	-0.06	-0.07
chr3	31070646	31087909	17264	-0.003	9.90E-01	-0.019	8.37E-01	5	*Skil*	-7149	Distal Intergenic	0.21	0.25	0.34	0.29	ns	ns	-0.12	0.11
chr3	36430393	36442472	12080	-0.160	2.33E-01	0.013	9.28E-01	5	*Anxa5*	9856	Distal Intergenic	0.41	0.37	0.46	0.45	-0.03	ns	-0.09	ns
chr3	88571810	88579637	7828	-0.010	9.64E-01	-0.138	2.03E-01	5	*Ssr2*	0	Promoter (<=1kb)	0.49	0.32	0.34	0.29	0.10	0.16	ns	ns
chr3	93539026	93547477	8452	-0.212	1.26E-01	-0.001	9.93E-01	5	*S100a10*	-7603	Distal Intergenic	0.17	0.15	0.23	0.12	-0.07	ns	-0.09	ns
chr4	108411106	108415312	4207	0.070	6.66E-01	0.123	3.91E-01	5	*Gpx7*	-4145	Distal Intergenic	0.45	0.24	0.30	0.24	ns	0.13	ns	ns
chr4	116654938	116680684	25747	-0.065	6.65E-01	-0.041	7.04E-01	5	*Akr1a1*	-3258	Exon (ENSMUST0	0.16	ns	0.09	0.07	ns	ns	ns	-0.05
chr4	119296046	119301690	5645	-0.029	8.82E-01	-0.065	6.20E-01	5	*Ybx1*	-1442	Promoter (1-2kb)	ns	ns	0.08	0.07	ns	ns	-0.09	-0.07
chr4	150015212	150050448	35237	-0.058	6.98E-01	0.085	3.38E-01	5	*H6pd*	-6189	Exon (ENSMUST0	0.17	0.12	0.09	0.11	ns	ns	0.08	ns
chr4	152280789	152297428	16640	-0.035	8.36E-01	-0.111	1.99E-01	5	*Gpr153*	0	Promoter (<=1kb)	0.20	0.06	0.10	0.08	ns	0.06	ns	ns
chr4	41723065	41737832	14768	-0.140	3.49E-01	-0.218	1.09E-01	5	*Dctn3*	0	Promoter (<=1kb)	0.15	0.12	0.14	0.17	ns	ns	ns	-0.09
chr4	43984665	44007700	23036	-0.007	9.71E-01	-0.107	1.81E-01	5	*Clta*	0	Promoter (<=1kb)	ns	0.11	0.16	0.13	ns	ns	-0.07	-0.09
chr4	8525798	8532904	7107	-0.092	5.44E-01	-0.061	6.68E-01	5	*Rab2a*	-2740	Promoter (2-3kb)	0.28	0.22	0.28	0.27	ns	ns	ns	-0.06
chr5	107989939	107993315	3377	0.003	9.90E-01	0.236	1.24E-01	5	*Dipk1a*	-2854	Promoter (2-3kb)	0.09	0.08	0.15	0.21	ns	ns	ns	-0.09
chr5	113495729	113499678	3950	-0.210	2.01E-01	0.218	1.79E-01	5	*Wscd2*	5282	Intron (ENSMUST	ns	ns	0.08	ns	ns	ns	-0.05	ns
chr5	136941814	136947157	5344	0.090	5.62E-01	-0.144	4.96E-01	5	*Fis1*	-6118	Distal Intergenic	0.20	0.15	0.17	0.22	ns	ns	ns	-0.09
chr5	145224497	145230150	5654	0.030	8.77E-01	-0.122	3.06E-01	5	*Zfp655*	-1565	Promoter (1-2kb)	ns	ns	0.08	0.04	0.04	ns	ns	0.07
chr5	147820169	147855916	35748	0.106	3.62E-01	0.075	3.51E-01	5	*Pomp*	-4545	Exon (ENSMUST0	0.09	ns	0.07	0.09	ns	ns	ns	-0.09
chr5	148399721	148441146	41426	-0.017	9.30E-01	0.015	8.76E-01	5	*Slc7a1*	0	Promoter (<=1kb)	0.06	0.08	0.12	0.08	ns	ns	-0.10	ns
chr5	23714916	23720128	5213	0.054	7.55E-01	-0.047	7.84E-01	5	*Al506816*	-2249	Promoter (2-3kb)	0.30	0.16	0.28	0.24	-0.07	ns	ns	-0.06
chr5	24845977	24856028	10052	-0.117	4.11E-01	0.147	2.10E-01	5	*Rheb*	-3353	Distal Intergenic	0.11	0.11	0.17	0.15	ns	ns	-0.09	ns
chr5	35518759	35535599	16841	-0.039	8.34E-01	0.134	3.51E-01	5	*Cpz*	0	Promoter (<=1kb)	0.56	0.28	0.33	0.37	ns	0.26	0.25	ns
chr5	36796651	36806654	10004	-0.039	8.08E-01	-0.129	1.06E-01	5	*Mrfap1*	0	Promoter (<=1kb)	0.16	0.13	0.16	0.16	ns	ns	ns	-0.08
chr5	67844431	67872829	28399	-0.157	1.64E-01	0.089	3.17E-01	5	*Atp8a1*	0	Promoter (<=1kb)	ns	0.43	0.51	0.51	ns	ns	-0.12	ns
chr5	77257375	77262002	4628	0.037	8.41E-01	0.013	9.40E-01	5	*Rest*	-3489	Distal Intergenic	ns	ns	0.10	ns	0.04	ns	-0.10	ns
chr5	90428154	90472923	44770	-0.010	9.54E-01	0.093	1.02E-01	5	*Alb*	0	Promoter (<=1kb)	0.15	ns	ns	ns	-0.08	ns	ns	ns
chr6	121612375	121641582	29208	-0.146	1.44E-01	0.048	5.48E-01	5	*A2m*	0	Promoter (<=1kb)	0.32	0.44	0.37	0.33	0.16	0.12	0.20	0.11
chr6	125161881	125163389	1509	-0.048	7.79E-01	0.129	2.51E-01	5	*Gapdh*	0	Promoter (<=1kb)	0.40	0.45	0.48	0.55	0.08	-0.05	-0.09	-0.15
chr6	125499780	125504641	4862	-0.008	9.70E-01	0.212	1.10E-01	5	*Cd9*	-4989	Intron (ENSMUST	0.41	0.19	0.37	0.38	ns	ns	ns	-0.15
chr6	17630974	17636362	5389	-0.131	3.56E-01	0.055	6.93E-01	5	*Capza2*	0	Promoter (<=1kb)	0.08	0.09	0.18	0.15	ns	ns	-0.07	ns
chr6	34409510	34425972	16463	0.110	4.31E-01	0.101	3.73E-01	5	*Akr1b7*	0	Promoter (<=1kb)	ns	0.23	0.20	0.15	ns	ns	ns	0.10
chr6	37448245	37463589	15345	0.077	5.56E-01	0.044	6.17E-01	5	*Creb3l2*	-6099	Distal Intergenic	0.07	ns	0.07	0.04	0.05	ns	ns	ns
chr6	4087324	4092840	5517	-0.162	2.60E-01	0.044	7.68E-01	5	*Bet1*	-352	Promoter (<=1kb)	0.16	0.04	0.09	0.10	ns	0.09	ns	-0.04
chr6	50534755	50557654	22900	0.026	8.90E-01	0.015	8.89E-01	5	*Cycs*	8295	Exon (ENSMUST0	ns	ns	ns	0.04	ns	0.09	ns	-0.08
chr6	56824212	56829899	5688	-0.087	5.41E-01	-0.106	3.10E-01	5	*Fkbp9*	-2160	Promoter (2-3kb)	0.45	0.21	0.26	0.20	-0.06	0.11	ns	ns
chr6	73231745	73247047	15303	-0.077	5.71E-01	-0.018	8.63E-01	5	*Suclg1*	-1335	Promoter (1-2kb)	0.03	ns	0.04	0.04	0.05	0.06	ns	ns
chr7	100483816	100494041	10226	0.053	7.57E-01	0.204	2.29E-01	5	*Ucp2*	0	Promoter (<=1kb)	0.07	0.22	0.39	0.23	ns	ns	-0.28	-0.14
chr7	105488706	105495238	6533	-0.118	4.22E-01	0.030	8.47E-01	5	*Cavin3*	-6406	Distal Intergenic	0.37	0.28	0.38	0.29	ns	0.12	ns	ns
chr7	121022431	121034436	12006	-0.146	3.18E-01	-0.208	1.02E-01	5	*Mettl9*	-9	Promoter (<=1kb)	0.18	0.14	0.16	0.15	0.04	ns	ns	ns
chr7	126632502	126641431	8930	-0.164	2.67E-01	0.046	7.75E-01	5	*Nupr1*	-1641	Promoter (1-2kb)	0.94	0.89	1.04	1.12	ns	ns	ns	-0.12
chr7	13039970	13046820	6851	-0.085	5.62E-01	-0.001	9.94E-01	5	*Ube2m*	-1695	Promoter (1-2kb)	0.27	0.21	0.25	0.33	ns	ns	ns	-0.14
chr7	134223234	134228226	4993	-0.140	3.53E-01	0.154	2.89E-01	5	*Adam12*	0	Promoter (<=1kb)	ns	ns	0.10	0.08	ns	ns	-0.10	-0.07
chr7	137420184	137435992	15809	-0.035	8.42E-01	-0.049	6.47E-01	5	*Glrx3*	-1622	Promoter (1-2kb)	0.13	0.10	0.14	0.11	ns	ns	ns	-0.08
chr7	141175959	141183905	7947	0.001	9.96E-01	-0.148	1.76E-01	5	*Rnh1*	-3102	Exon (ENSMUST0	0.28	0.29	0.37	0.38	ns	ns	ns	-0.11
chr7	16733370	16736757	3388	0.050	7.72E-01	-0.124	4.32E-01	5	*Ap2s1*	-1653	Promoter (1-2kb)	0.19	0.13	0.18	0.17	ns	ns	ns	-0.08
chr7	24520191	24527803	7613	0.125	3.72E-01	-0.157	1.67E-01	5	*Irgq*	-2886	Promoter (2-3kb)	0.02	0.05	0.04	0.01	0.04	ns	ns	0.05
chr7	3279485	3283853	4369	0.212	1.81E-01	0.152	3.27E-01	5	*Myadm*	-5227	Distal Intergenic	0.18	ns	0.10	0.08	ns	ns	ns	0.06
chr7	55835783	55839845	4063	-0.037	8.43E-01	-0.072	6.60E-01	5	*Cyfip1*	-1900	Promoter (1-2kb)	0.06	0.08	0.12	0.08	0.05	ns	ns	ns
chr7	80948022	80961126	13105	-0.118	3.32E-01	-0.112	1.93E-01	5	*Sec11a*	-242	Promoter (<=1kb)	0.30	0.24	0.27	0.26	ns	ns	ns	-0.07
chr7	89941623	89946289	4667	-0.092	5.50E-01	-0.030	8.51E-01	5	*Hikeshi*	-419	Promoter (<=1kb)	0.07	ns	0.04	0.07	ns	0.06	ns	-0.09
chr7	90458409	90466067	7659	-0.146	2.39E-01	-0.087	3.95E-01	5	*Tmem126a*	-1180	Promoter (1-2kb)	0.15	0.05	0.09	0.07	ns	0.07	ns	ns
chr7	99860207	99921338	61132	0.019	9.24E-01	-0.070	4.66E-01	5	*Spcs2*	0	Promoter (<=1kb)	0.16	0.08	0.13	0.16	ns	ns	ns	-0.06
chr8	11486149	11497492	11344	-0.163	2.24E-01	-0.105	3.72E-01	5	*Naxd*	-14	Promoter (<=1kb)	0.15	0.10	0.12	0.14	ns	ns	0.06	ns
chr8	123638742	123650621	11880	-0.125	4.07E-01	0.118	4.35E-01	5	*Rhou*	-3308	Intron (ENSMUST	ns	0.12	0.15	0.08	ns	ns	-0.10	ns
chr8	3368833	3372936	4104	-0.097	5.31E-01	-0.088	5.79E-01	5	*Arhgef18*	7981	Intron (ENSMUST	0.04	ns	ns	ns	0.02	ns	ns	ns
chr8	40923124	40931847	8724	0.013	9.53E-01	0.152	2.02E-01	5	*Pdgfrl*	0	Promoter (<=1kb)	0.28	0.04	0.04	0.03	ns	0.16	0.10	ns
chr8	72707447	72716080	8634	0.078	6.20E-01	-0.063	6.76E-01	5	*Sin3b*	-7205	3' UTR	0.14	0.14	0.16	0.16	0.05	ns	ns	ns
chr8	94379930	94384082	4153	-0.195	2.14E-01	0.133	4.03E-01	5	*Herpud1*	-2356	Promoter (2-3kb)	0.18	0.10	0.15	0.13	ns	ns	-0.12	ns
chr9	109907450	109924366	16917	0.061	6.98E-01	0.079	4.60E-01	5	*Map4*	-7094	Exon (ENSMUST0	ns	ns	0.16	0.10	ns	ns	-0.08	ns
chr9	111074513	111109861	35349	-0.056	6.93E-01	0.104	1.74E-01	5	*Lrrfip2*	-7731	Exon (ENSMUST0	0.10	0.20	0.30	0.25	ns	ns	-0.15	ns
chr9	114392401	114400745	8345	0.030	8.72E-01	-0.095	3.80E-01	5	*Glb1*	-331	Promoter (<=1kb)	0.16	0.08	0.12	0.12	0.04	0.07	ns	ns
chr9	50756323	50762242	5920	0.015	9.46E-01	0.062	6.48E-01	5	*Cryab*	1928	Promoter (1-2kb)	0.48	0.45	0.53	0.59	ns	ns	ns	-0.08
chr9	57555462	57559676	4215	-0.174	2.50E-01	-0.043	8.00E-01	5	*Scamp2*	-1267	Promoter (1-2kb)	0.06	ns	0.05	0.05	0.04	ns	ns	ns
chr9	61326033	61369816	43784	-0.007	9.72E-01	0.128	1.49E-01	5	*Tle3*	-2550	Promoter (2-3kb)	0.06	ns	0.11	0.09	0.05	ns	ns	ns
chr9	66922193	66939542	17350	0.032	8.67E-01	0.075	5.26E-01	5	*Rab8b*	-2506	Promoter (2-3kb)	0.03	0.05	0.08	0.02	ns	ns	-0.07	0.06
chr9	67051348	67070805	19458	-0.014	9.48E-01	0.180	1.16E-01	5	*Tpm1*	-1942	Promoter (1-2kb)	0.22	0.12	0.21	0.20	0.13	0.09	-0.10	ns
chr9	71196884	71267818	70935	-0.075	6.01E-01	-0.084	4.00E-01	5	*Aldh1a2*	0	Promoter (<=1kb)	0.14	0.33	0.41	0.71	0.08	ns	-0.13	-0.32
chr9	90043190	90056645	13456	-0.120	3.79E-01	0.062	6.06E-01	5	*Ctsh*	0	Promoter (<=1kb)	0.71	0.60	0.74	0.72	-0.11	ns	-0.07	-0.10
chr9	96479594	96491400	11807	-0.149	1.93E-01	0.023	8.23E-01	5	*Rnf7*	-919	Promoter (<=1kb)	0.13	0.08	0.14	0.14	ns	0.12	ns	-0.08
chr9	96631672	96664853	33182	-0.057	6.93E-01	0.089	2.91E-01	5	*Rasa2*	-55	Promoter (<=1kb)	ns	ns	0.07	0.03	ns	ns	-0.11	ns
chrX	7901878	7904795	2918	-0.002	9.93E-01	-0.026	8.93E-01	5	*Timm17b*	-1319	Promoter (1-2kb)	0.17	0.06	0.09	0.09	ns	0.05	ns	ns
chr11	117974904	117980450	5547	0.522	7.22E-03	0.239	1.11E-01	6	*Socs3*	-5718	Distal Intergenic	0.11	ns	ns	ns	0.06	0.12	ns	ns

				H3K27me3 peak dynamics*								RNA expression†							
				Aggregate time (GD5.5 to 18.5)		Aggregate genotype (*Kdm6b cKO* vs. ctrl)						Ctrl IS/IS fibroblasts vs. ctrl GD5.5/8.5 IIS fibroblasts (log_2FC)				*Kdm6b cKO* vs. ctrl IS/IS fibroblasts (log_2FC)			
Chr	Peak start	Peak end	Peak width	log_2FC	*FDR*	log_2FC	*FDR*	HC	Gene	Peak distance to TSS	Annotation	GD12.5	GD14.5	GD16.5	GD18.5	GD12.5	GD14.5	GD16.5	GD18.5
chr11	60955848	60991634	35787	0.243	9.33E-02	0.108	4.15E-01	6	***Map2k3***	5186	Distal Intergenic	0.10	0.05	0.11	0.05	ns	ns	-0.08	ns
chr15	25408694	25485676	76983	0.264	4.78E-03	0.109	1.53E-01	6	***Basp1***	0	Promoter (<=1kb)	0.27	0.14	0.25	0.23	0.13	0.11	ns	ns
chr4	137259263	137285421	26159	0.294	4.98E-02	0.129	3.28E-01	6	***Wnt4***	0	Promoter (<=1kb)	ns	ns	ns	0.06	ns	ns	ns	-0.04
chr5	124033048	124051604	18557	0.241	8.26E-02	0.019	8.98E-01	6	***Vps37b***	-778	Promoter (<=1kb)	0.09	0.13	0.13	0.13	0.07	ns	ns	ns
chr9	106099492	106103074	3583	0.304	9.66E-02	0.184	2.78E-01	6	***Col6a4***	-2709	Promoter (2-3kb)	-0.25	ns	0.17	0.22	0.06	ns	-0.16	ns
chr9	114787148	114813237	26090	0.254	3.13E-02	-0.011	9.33E-01	6	***Cmtm7***	-5292	3' UTR	0.07	0.08	0.15	0.12	0.09	ns	ns	ns
chr1	33908002	33912524	4523	-0.373	4.14E-02	-0.338	1.88E-02	7	***Dst***	0	Promoter (<=1kb)	0.11	0.12	0.17	0.12	ns	ns	ns	0.15
chr19	17125843	17144060	18218	-0.202	5.83E-02	-0.144	8.38E-02	7	***Prune2***	0	Promoter (<=1kb)	0.10	0.11	0.11	0.11	0.09	ns	ns	ns
chr19	38043901	38052779	8879	-0.305	5.31E-03	-0.242	2.15E-03	7	***Myof***	-324	Promoter (<=1kb)	0.28	0.31	0.38	0.32	ns	ns	ns	0.09
chr2	113369978	113440098	70121	-0.204	3.56E-03	-0.166	9.67E-04	7	***Fmn1***	0	Promoter (<=1kb)	0.07	0.07	0.10	0.08	ns	ns	ns	0.05
chr2	122750458	122765289	14832	-0.163	7.66E-02	-0.182	3.28E-03	7	***Sqor***	0	Promoter (<=1kb)	0.05	0.05	0.05	ns	ns	0.08	0.07	ns
chr2	78813705	78867354	53650	-0.184	8.06E-03	-0.142	3.78E-03	7	***Ube2e3***	-770	Promoter (<=1kb)	0.08	0.06	0.12	0.10	0.04	ns	ns	ns
chr3	114021162	114034812	13651	-0.319	2.64E-03	-0.142	8.98E-02	7	***Col11a1***	0	Promoter (<=1kb)	0.84	0.33	0.30	0.16	0.11	0.27	0.22	0.16
chr3	94887627	94899806	12180	-0.254	4.08E-02	-0.209	3.05E-02	7	***Psmb4***	-666	Promoter (<=1kb)	0.16	0.08	0.10	0.14	ns	ns	ns	-0.10
chr5	8770749	8804192	33444	-0.250	1.72E-03	-0.176	2.59E-03	7	***Abcb1b***	0	Promoter (<=1kb)	0.10	0.25	0.25	0.18	ns	ns	ns	0.15
chr6	145070400	145099898	29499	-0.402	6.49E-10	-0.090	9.84E-02	7	***Bcat1***	0	Promoter (<=1kb)	0.19	0.05	0.09	0.05	ns	0.06	ns	ns
chr7	105816279	105829047	12769	-0.178	5.94E-02	-0.320	1.07E-07	7	***Mrpl17***	-5180	Exon (ENSMUST0	0.17	0.08	0.13	0.12	ns	0.10	ns	-0.07
chr8	118240863	118292728	51866	-0.151	5.69E-02	-0.124	2.12E-02	7	***Cdh13***	0	Promoter (<=1kb)	0.20	0.39	0.42	0.42	-0.11	ns	-0.12	ns
chr9	22091244	22106131	14888	-0.202	8.48E-02	-0.186	3.94E-02	7	***Cnn1***	0	Promoter (<=1kb)	0.04	0.06	0.04	0.06	ns	ns	ns	-0.04
chr9	95675396	95703555	28160	-0.151	6.63E-02	-0.206	5.67E-05	7	***Pcolce2***	0	Promoter (<=1kb)	0.08	0.06	0.05	0.05	-0.07	ns	ns	ns
chrX	36267432	36328544	61113	-0.173	5.01E-02	-0.248	1.84E-05	7	***Lonrf3***	0	Promoter (<=1kb)	ns	ns	0.13	0.06	ns	ns	-0.12	ns
chr1	13590135	13605543	15409	-0.111	3.03E-01	-0.136	3.82E-02	8	***Tram1***	-225	Promoter (<=1kb)	0.29	0.12	0.19	0.19	ns	0.07	ns	ns
chr1	173365149	173406667	41519	-0.081	5.17E-01	-0.218	9.69E-04	8	***Cadm3***	0	Promoter (<=1kb)	0.27	0.33	0.30	0.25	-0.15	-0.10	ns	ns
chr1	52053459	52111505	58047	-0.061	5.51E-01	-0.117	1.30E-02	8	***Stat1***	0	Promoter (<=1kb)	0.04	0.04	0.02	ns	ns	0.05	0.06	0.06
chr10	117275065	117338152	63088	0.027	8.55E-01	-0.160	1.87E-03	8	***Lyz2***	0	Promoter (<=1kb)	0.24	0.37	0.34	0.35	0.04	ns	ns	ns
chr10	5358211	5373495	15285	-0.040	8.04E-01	-0.177	1.84E-02	8	***Syne1***	0	Promoter (<=1kb)	0.05	0.11	0.16	0.09	0.07	ns	ns	0.10
chr11	23772388	23823508	51121	0.032	8.34E-01	-0.275	8.57E-07	8	***Rel***	-1418	Promoter (1-2kb)	ns	0.10	0.10	0.03	ns	ns	-0.17	0.10
chr11	3932029	3949253	17225	-0.110	3.47E-01	-0.253	2.13E-04	8	***Tcn2***	0	Promoter (<=1kb)	0.16	0.12	0.15	0.17	ns	ns	0.08	ns
chr11	5652647	5700866	48220	-0.021	9.03E-01	-0.170	5.16E-03	8	***Mrps24***	6776	Exon (ENSMUST0	0.14	0.08	0.13	0.11	ns	ns	ns	-0.08
chr12	40038820	40066578	27759	-0.031	8.51E-01	-0.146	3.95E-02	8	***Arl4a***	-795	Promoter (<=1kb)	ns	0.18	0.21	0.16	ns	ns	-0.12	ns
chr12	55498777	55549778	51002	-0.031	8.30E-01	-0.245	2.12E-06	8	***Nfkbia***	-6130	Exon (ENSMUST0	0.33	0.43	0.45	0.48	ns	-0.13	-0.15	-0.04
chr12	84742346	84755661	13316	-0.076	5.74E-01	-0.171	2.45E-02	8	***Npc2***	6879	3' UTR	0.36	0.31	0.32	0.35	0.10	0.09	0.16	ns
chr13	117186908	117229128	42221	-0.040	7.49E-01	-0.128	1.29E-02	8	***Emb***	0	Promoter (<=1kb)	ns	ns	0.03	0.03	ns	ns	ns	0.04
chr13	3917112	3972925	55814	0.031	7.99E-01	-0.206	3.38E-07	8	***Net1***	0	Promoter (<=1kb)	0.12	0.23	0.30	0.23	0.10	ns	-0.10	ns
chr13	66877087	66895632	18546	0.033	8.45E-01	-0.330	2.10E-06	8	***Uqcrb***	7154	Distal Intergenic	0.11	ns	ns	0.10	ns	ns	ns	-0.15
chr13	69820826	69875327	54502	-0.010	9.55E-01	-0.197	1.19E-04	8	***Med10***	9241	Distal Intergenic	0.06	0.06	0.12	0.10	0.03	ns	ns	ns
chr14	105217929	105258900	40972	-0.037	7.91E-01	-0.211	6.47E-05	8	***Ndfip2***	0	Promoter (<=1kb)	0.08	0.07	0.15	0.13	ns	ns	-0.11	ns
chr14	14121605	14143375	21771	-0.019	9.12E-01	-0.294	3.01E-08	8	***Psmd6***	-621	Promoter (<=1kb)	0.08	ns	0.10	0.12	ns	ns	ns	-0.07
chr14	20084642	20116965	32324	-0.020	9.05E-01	-0.118	6.09E-02	8	***Saysd1***	-1459	Promoter (1-2kb)	0.08	0.03	0.08	0.07	ns	0.05	ns	ns
chr14	29929976	29967265	37290	-0.073	5.50E-01	-0.147	2.14E-02	8	***Selenok***	-1043	Promoter (1-2kb)	0.16	ns	0.12	0.14	ns	ns	ns	-0.09
chr14	47439853	47472279	32427	0.004	9.81E-01	-0.143	7.80E-03	8	***Fbxo34***	0	Promoter (<=1kb)	0.04	0.12	0.11	0.09	ns	ns	-0.07	ns
chr14	55448915	55476126	27212	-0.023	8.93E-01	-0.219	3.40E-04	8	***Dhrs4***	-2632	Promoter (2-3kb)	0.07	0.06	0.07	0.08	0.03	ns	ns	-0.04
chr15	94590371	94609386	19016	-0.127	2.31E-01	-0.244	1.25E-04	8	***Twf1***	-482	Promoter (<=1kb)	0.07	ns	0.04	0.05	0.04	ns	ns	ns
chr16	10406128	10412130	6003	-0.040	8.21E-01	-0.256	7.44E-03	8	***Nubp1***	0	Promoter (<=1kb)	0.05	0.03	0.06	0.09	0.03	ns	ns	-0.03
chr16	35489501	35554726	65226	-0.023	9.00E-01	-0.135	8.07E-02	8	***Pdia5***	0	Promoter (<=1kb)	0.24	0.11	0.14	0.10	ns	0.10	ns	ns
chr17	33985453	33993376	7924	-0.148	2.15E-01	-0.153	8.42E-02	8	***H2-K1***	3298	Distal Intergenic	0.26	0.24	0.11	0.17	-0.09	-0.12	ns	ns
chr18	40219554	40250300	30747	-0.079	4.95E-01	-0.224	9.75E-05	8	***Yipf5***	-125	Promoter (<=1kb)	0.27	0.16	0.20	0.19	ns	0.08	ns	ns
chr18	76860533	76927810	67278	-0.088	5.28E-01	-0.284	6.40E-04	8	***Ier3ip1***	-2207	Promoter (2-3kb)	0.23	ns	0.15	0.16	ns	0.11	ns	-0.08
chr2	112422997	112454593	31597	-0.118	3.37E-01	-0.307	4.61E-05	8	***Emc7***	-404	Promoter (<=1kb)	0.10	ns	0.07	0.10	ns	ns	ns	-0.05
chr2	120152244	120214710	62467	-0.014	9.44E-01	-0.139	9.60E-02	8	***Ehd4***	0	Promoter (<=1kb)	0.13	0.11	0.25	0.14	ns	ns	-0.19	0.08
chr2	122120314	122146029	25716	-0.030	8.35E-01	-0.130	1.77E-02	8	***B2m***	-1657	Promoter (1-2kb)	0.08	ns	-0.07	-0.09	-0.06	-0.07	ns	0.07
chr2	148878558	148914890	36333	0.008	9.63E-01	-0.281	2.78E-08	8	***Cst3***	-2866	Promoter (2-3kb)	0.42	0.30	0.32	0.41	0.07	0.14	0.17	ns
chr2	38644091	38681916	37826	-0.021	9.10E-01	-0.201	3.68E-03	8	***Psmb7***	-4	Promoter (<=1kb)	0.08	ns	0.08	0.08	ns	ns	ns	-0.04
chr2	90822636	90845956	23321	0.091	4.21E-01	-0.165	7.66E-03	8	***Mtch2***	-1199	Promoter (1-2kb)	0.08	ns	0.07	0.12	ns	ns	ns	-0.06
chr3	95044541	95052421	7881	-0.031	8.62E-01	-0.159	7.20E-02	8	***Psmd4***	-1927	Promoter (1-2kb)	0.12	0.13	0.19	0.22	ns	ns	ns	-0.10
chr4	126617827	126677320	59494	-0.055	7.05E-01	-0.256	1.38E-04	8	***Psmb2***	-310	Promoter (<=1kb)	0.12	ns	0.08	0.11	ns	ns	ns	-0.10
chr4	127209858	127243576	33719	-0.026	8.81E-01	-0.206	1.68E-03	8	***Smim12***	-208	Promoter (<=1kb)	0.05	0.05	0.06	0.07	ns	ns	ns	-0.03
chr4	33290093	33307631	17539	-0.043	7.66E-01	-0.225	1.79E-04	8	***Pnrc1***	0	Promoter (<=1kb)	ns	0.14	0.09	0.11	ns	-0.11	-0.08	ns
chr4	46196475	46239106	42632	-0.050	7.03E-01	-0.267	1.06E-06	8	***Xpa***	-164	Promoter (<=1kb)	0.05	0.07	0.06	0.06	ns	ns	ns	-0.04
chr5	104411659	104455187	43529	-0.106	2.40E-01	-0.115	3.10E-02	8	***Spp1***	0	Promoter (<=1kb)	0.29	0.52	0.50	0.43	0.03	ns	ns	0.17
chr5	109560797	109603124	42328	-0.038	8.14E-01	-0.345	9.53E-08	8	***Crlf2***	-1804	Promoter (1-2kb)	0.12	0.12	0.13	0.18	0.05	ns	ns	-0.05
chr5	3315471	3352785	37315	0.013	9.49E-01	-0.166	8.80E-02	8	***Cdk6***	0	Promoter (<=1kb)	0.06	ns	ns	ns	0.04	ns	ns	ns
chr5	35105846	35165938	60093	0.023	8.97E-01	-0.128	8.21E-02	8	***Lrpap1***	-80	Promoter (<=1kb)	0.28	0.26	0.27	0.28	ns	0.08	ns	ns
chr5	8029509	8053413	23905	0.024	8.86E-01	-0.203	9.55E-04	8	***Sri***	0	Promoter (<=1kb)	0.14	0.13	0.16	0.17	ns	ns	ns	-0.08
chr6	113741187	113850797	109611	0.056	7.09E-01	-0.216	4.90E-03	8	***Sec13***	-444	Promoter (<=1kb)	0.24	0.09	0.17	0.18	ns	0.11	ns	-0.06
chr6	3399413	3424755	25343	-0.034	8.33E-01	-0.288	3.10E-06	8	***Samd9l***	0	Promoter (<=1kb)	0.06	0.07	0.06	0.02	ns	ns	ns	0.06
chr6	71823509	71830627	7119	-0.032	8.64E-01	-0.221	1.60E-02	8	***Mrpl35***	0	Promoter (<=1kb)	ns	ns	ns	0.02	ns	ns	ns	-0.05
chr6	83508304	83539291	30988	0.007	9.75E-01	-0.278	8.38E-04	8	***Actg2***	0	Promoter (<=1kb)	0.11	0.17	0.13	0.18	0.04	ns	ns	-0.05
chr7	103806426	103812872	6447	0.078	6.20E-01	-0.252	4.70E-02	8	***Hbb-bt***	1124	Promoter (1-2kb)	0.12	0.18	0.18	0.18	0.03	ns	ns	ns
chr7	116448574	116504106	55533	-0.015	9.32E-01	-0.118	8.03E-02	8	***Nucb2***	-263	Promoter (<=1kb)	0.42	0.34	0.33	0.31	ns	0.08	0.07	ns
chr7	118995106	119049798	54693	0.110	2.72E-01	-0.273	3.34E-07	8	***Gprc5b***	0	Promoter (<=1kb)	ns	ns	ns	0.03	ns	ns	ns	-0.03
chr7	127896488	127903119	6632	0.016	9.38E-01	-0.285	3.03E-03	8	***Vkorc1***	-871	Promoter (<=1kb)	0.58	0.33	0.42	0.36	-0.04	0.18	ns	ns
chr7	28028069	28039442	11374	-0.090	5.04E-01	-0.374	6.92E-07	8	***Psmc4***	7580	Distal Intergenic	0.09	0.05	0.12	0.17	0.04	0.06	ns	-0.06
chr7	30321994	30353323	31330	0.045	7.79E-01	-0.234	2.62E-03	8	***Sdhaf1***	0	Promoter (<=1kb)	0.09	0.04	0.06	0.06	ns	0.04	ns	ns
chr7	44496049	44531115	35067	-0.094	4.77E-01	-0.221	6.36E-03	8	***Emc10***	0	Promoter (<=1kb)	0.25	0.19	0.21	0.22	ns	ns	ns	-0.07
chr7	44554299	44593901	39603	-0.072	6.13E-01	-0.223	6.39E-03	8	***Napsa***	0	Promoter (<=1kb)	0.11	0.25	0.22	0.18	0.03	ns	ns	0.09
chr7	44781167	44808644	27478	-0.065	6.17E-01	-0.262	1.30E-05	8	***Atf5***	7014	Exon (ENSMUST0	0.25	0.11	0.16	0.22	ns	0.10	ns	-0.10
chr7	47117832	47176237	58406	-0.031	8.39E-01	-0.210	2.84E-04	8	***Ptpn5***	0	Promoter (<=1kb)	ns	ns	ns	0.11	ns	ns	ns	-0.06
chr7	49716849	49760246	43398	-0.133	1.51E-01	-0.238	1.18E-05	8	***Htatip2***	0	Promoter (<=1kb)	0.13	0.09	0.10	0.11	ns	ns	0.05	ns
chr7	7121303	7127197	5895	0.012	9.55E-01	-0.304	1.16E-03	8	***Zfp954***	0	Promoter (<=1kb)	ns	ns	0.02	ns	ns	ns	-0.04	ns
chr8	104648068	104664663	16596	-0.079	5.60E-01	-0.196	1.18E-02	8	***Ciao2b***	-6103	Exon (ENSMUST0	0.08	ns	0.08	0.10	ns	ns	ns	-0.08
chr8	107588624	107614683	26060	-0.092	5.04E-01	-0.207	1.87E-02	8	***Psmd7***	-160	Promoter (<=1kb)	0.14	0.10	0.16	0.18	ns	ns	ns	-0.07
chr8	119337991	119344281	6291	-0.045	7.96E-01	-0.177	7.77E-02	8	***Hsbp1***	-207	Promoter (<=1kb)	0.11	ns	0.10	0.11	ns	0.07	ns	-0.09
chr8	46214500	46266738	52239	0.008	9.66E-01	-0.150	8.26E-03	8	***Slc25a4***	-3216	Exon (ENSMUST0	0.23	0.21	0.23	0.19	0.05	ns	ns	-0.07

				H3K27me3 peak dynamics*								RNA expression†							
				Aggregate time (GD5.5 to 18.5)		Aggregate genotype (*Kdm6b cKO* vs. ctrl)				Peak distance		Ctrl IS/IIS fibroblasts vs. ctrl GD5.5/8.5 IIS fibroblasts (log_2FC)				*Kdm6b cKO* vs. ctrl IS/IIS fibroblasts (log_2FC)			
Chr	Peak start	Peak end	Peak width	log_2FC	*FDR*	log_2FC	*FDR*	HC	Gene	to TSS	Annotation	GD12.5	GD14.5	GD16.5	GD18.5	GD12.5	GD14.5	GD16.5	GD18.5
chr8	83618970	83652138	33169	-0.053	6.91E-01	-0.120	6.40E-02	8	***Gipc1***	-539	Promoter (<=1kb)	0.11	0.06	0.08	0.09	ns	0.06	ns	-0.03
chr9	48495678	48518605	22928	-0.097	4.25E-01	-0.223	1.09E-03	8	***Gm5617***	236	Promoter (<=1kb)	0.06	ns	0.04	0.04	0.02	0.03	ns	ns
chr9	64256478	64274230	17753	-0.023	9.02E-01	-0.204	8.64E-03	8	***Map2k1***	-2847	Promoter (2-3kb)	0.09	0.08	0.12	0.13	0.04	ns	ns	ns
chr9	64741791	64776700	34910	0.013	9.51E-01	-0.190	2.49E-02	8	***Rab11a***	-4033	Distal Intergenic	0.09	ns	0.10	0.12	ns	ns	ns	-0.05
chrX	10041448	10278388	236941	-0.091	4.57E-01	-0.157	2.94E-02	8	***Srpx***	0	Promoter (<=1kb)	0.24	0.07	0.08	ns	ns	0.09	ns	ns
chrX	100627135	100630885	3751	0.026	8.99E-01	-0.235	6.25E-02	8	***Pdzd11***	-567	Promoter (<=1kb)	0.10	0.06	0.07	0.10	0.03	ns	ns	-0.04
chrX	106162772	106189420	26649	-0.019	9.18E-01	-0.168	1.37E-02	8	***Pgk1***	0	Promoter (<=1kb)	0.13	0.07	0.11	0.20	0.05	ns	ns	-0.09
chrX	10720413	10729396	8984	-0.105	4.50E-01	-0.229	2.04E-02	8	***Mid1ip1***	2945	Promoter (2-3kb)	0.06	0.06	0.07	0.07	0.03	ns	ns	ns
chrX	107351042	107501185	150144	-0.095	4.22E-01	-0.163	1.70E-02	8	***Itm2a***	0	Promoter (<=1kb)	0.09	ns	ns	ns	0.06	0.14	0.10	ns
chrX	112285819	112323804	37986	-0.074	5.98E-01	-0.238	2.88E-03	8	***Apool***	0	Promoter (<=1kb)	0.02	ns	0.04	0.04	0.03	ns	ns	ns
chrX	150802668	150809918	7251	-0.050	7.65E-01	-0.237	2.11E-02	8	***Maged2***	2543	Promoter (2-3kb)	0.24	0.12	0.15	0.08	ns	0.07	ns	ns
chrX	159376489	159398209	21721	-0.056	7.03E-01	-0.192	9.26E-03	8	***Eif1ax***	4311	3' UTR	ns	ns	0.06	ns	ns	ns	-0.07	-0.06
chrX	162888981	162978282	89302	0.000	9.98E-01	-0.204	7.22E-03	8	***Ctps2***	0	Promoter (<=1kb)	0.03	0.04	0.05	0.05	0.03	ns	ns	ns
chrX	164357717	164401547	43831	-0.078	5.51E-01	-0.191	7.96E-03	8	***Vegfd***	0	Promoter (<=1kb)	0.59	0.34	0.37	0.36	0.06	ns	0.11	ns
chrX	166266957	166416690	149734	-0.084	5.40E-01	-0.224	5.50E-03	8	***Gpm6b***	0	Promoter (<=1kb)	ns	ns	0.07	ns	ns	-0.11	-0.16	ns
chrX	36876016	36945517	69502	-0.096	4.38E-01	-0.265	1.22E-04	8	***Ube2a***	0	Promoter (<=1kb)	0.04	ns	0.06	0.06	ns	ns	ns	-0.04
chrX	37184642	37191074	6433	-0.057	7.27E-01	-0.239	2.32E-02	8	***Ndufa1***	89	Promoter (<=1kb)	0.27	0.09	0.17	0.20	ns	0.09	ns	-0.06
chrX	48449232	48452581	3350	0.031	8.75E-01	-0.277	5.06E-02	8	***Elf4***	1588	Promoter (1-2kb)	0.14	0.17	0.22	0.16	ns	ns	-0.09	0.06
chrX	52057787	52163172	105386	-0.127	2.47E-01	-0.243	3.17E-04	8	***Gpc4***	2080	Promoter (2-3kb)	0.15	0.04	0.07	0.07	ns	0.05	ns	ns
chrX	7307023	7369277	62255	-0.080	4.55E-01	-0.202	1.16E-04	8	***Clcn5***	0	Promoter (<=1kb)	0.02	ns	0.05	0.03	0.05	0.04	ns	ns
chrX	73464975	73546303	81329	-0.051	7.07E-01	-0.233	1.02E-04	8	***Bgn***	0	Promoter (<=1kb)	0.74	0.62	0.67	0.69	ns	ns	0.04	-0.07
chrX	73787441	73799390	11950	-0.121	3.58E-01	-0.213	2.29E-02	8	***Ssr4***	0	Promoter (<=1kb)	0.57	0.44	0.49	0.51	ns	0.14	0.03	-0.09
chrX	74353845	74371953	18109	-0.043	7.82E-01	-0.254	3.21E-04	8	***Ubl4a***	0	Promoter (<=1kb)	0.16	0.05	0.10	0.12	ns	0.09	ns	-0.05
chrX	8136496	8142389	5894	-0.122	3.99E-01	-0.267	2.34E-02	8	***Rbm3***	529	Promoter (<=1kb)	0.30	0.29	0.32	0.35	ns	ns	-0.07	-0.11
chrX	8193615	8200471	6857	0.114	4.21E-01	-0.244	2.47E-02	8	***Ebp***	-103	Promoter (<=1kb)	0.14	0.13	0.14	0.16	ns	ns	ns	-0.04
chrX	96092243	96191645	99403	-0.104	4.26E-01	-0.227	6.38E-03	8	***Msn***	0	Promoter (<=1kb)	0.17	0.22	0.33	0.31	-0.05	ns	-0.14	ns
chrX	9646865	9689053	42189	-0.014	9.41E-01	-0.161	2.41E-02	8	***Dynlt3***	0	Promoter (<=1kb)	0.16	0.12	0.19	0.18	ns	ns	ns	-0.04

Table 2.3 Genes with triple characteristics (peri-implantation H3K27me3 winding, post-implantation H3K27me3 erosion, and increased RNA expression).

Genes with the triple characteristics of 1) a nearby H3K27me3 peak (+/- 10 kb from the TSS) that increases in the peri-implantation period; 2) subsequent erosion of this peak from GD5.5 to GD18.5; and 3) increased RNA expression in ctrl fibroblasts in mid-to-late gestation, related to Figure 2.6.

				H3K27me3 peak dynamics*									RNA expression‡							
						Aggregate time (GD5.5 to 18.5)		Aggregate genotype (Kdm6b cKO vs. ctrl)					Ctrl IS/IS fibroblasts vs. ctrl GD5.5/8.5 IIS fibroblasts (log_2FC)				*Kdm6b cKO* vs. ctrl IS/IS fibroblasts (log_2FC)			
Chr	Peak start	Peak end	Peak width	GD5.5 vs. GD5.0 log_2FC	FDR	log2FC	*FDR*	log_2FC	*FDR*	HC	Gene†	Peak distance to TSS	Annotation	GD12.5	GD14.5	GD16.5	GD18.5	GD12.5	GD14.5	GD16.5	GD18.5
chr1	119416777	119431478	14702	0.977	4.38E-10	-1.297	1.78E-20	0.212	5.58E-02	1	***Inhbb***	0	Promoter (<=1kb)	0.35	0.49	0.77	1.02	0.19	0.11	ns	-0.25
chr1	153103882	153121565	17684	0.309	4.67E-03	-1.088	7.04E-12	1.130	1.17E-26	1	***Lamc2***	5669	3' UTR	0.07	ns	0.06	ns	ns	ns	ns	ns
chr1	21081429	21095180	13752	0.248	2.62E-02	-0.373	1.91E-03	0.396	1.41E-06	1	***Tram2***	-2200	Promoter (2-3kb)	0.10	0.04	0.06	0.07	ns	ns	ns	ns
chr10	95388854	95405991	17138	0.970	9.18E-10	-1.487	2.37E-12	0.448	2.54E-03	1	***Socs2***	8836	3' UTR	0.48	0.42	0.49	0.41	ns	0.08	ns	ns
chr11	35179428	35185579	6152	0.189	9.15E-02	-1.346	3.23E-16	0.340	5.18E-03	1	***Slit3***	1645	Promoter (1-2kb)	0.35	0.21	0.10	0.10	ns	ns	0.11	ns
chr12	102238230	102275940	37711	0.340	1.08E-04	-0.461	3.36E-06	0.159	3.99E-02	1	***Rin3***	-7108	3' UTR	0.08	ns	0.11	0.07	ns	ns	ns	ns
chr12	102280465	102296091	15627	0.219	5.10E-02	-1.454	5.59E-13	0.610	8.10E-06	1	***Rin3***	0	Promoter (<=1kb)	0.08	ns	0.11	0.07	ns	ns	ns	ns
chr12	80508949	80527103	18155	0.427	9.97E-05	-0.832	2.58E-09	0.321	1.69E-03	1	***Galnt16***	0	Promoter (<=1kb)	0.18	0.10	0.16	0.14	-0.06	ns	ns	ns
chr12	85535691	85595718	60028	0.284	2.83E-03	-0.259	7.12E-03	0.276	5.42E-05	1	***Jdp2***	-3309	Exon (ENSMUST0	0.15	0.10	0.16	0.16	ns	ns	ns	ns
chr13	41359134	41372348	13215	0.239	3.31E-02	-0.298	1.37E-02	0.688	8.35E-18	1	***Nedd9***	0	Promoter (<=1kb)	0.11	0.22	0.25	0.22	ns	ns	-0.11	ns
chr14	23801422	23835575	34154	0.268	1.03E-02	-0.994	8.34E-09	0.378	2.01E-03	1	***Kcnma1***	0	Promoter (<=1kb)	0.30	0.26	0.20	0.14	0.05	ns	ns	ns
chr15	36288612	36308461	19850	0.177	9.89E-02	-0.253	9.83E-02	0.512	1.11E-05	1	***Rnf19a***	-5465	Exon (ENSMUST0	0.10	0.20	0.24	0.22	ns	ns	ns	0.11
chr18	31925591	31940279	14689	0.217	5.43E-02	-0.751	2.67E-07	0.470	2.18E-06	1	***Lims2***	0	Promoter (<=1kb)	0.15	0.18	0.20	0.15	ns	ns	ns	ns
chr3	101079406	101086004	6599	0.523	2.09E-04	-0.545	3.25E-03	0.360	6.16E-03	1	***Ptgfrn***	-5957	Exon (ENSMUST0	0.26	0.03	0.05	0.06	ns	ns	ns	ns
chr3	101087302	101118605	31304	0.658	4.47E-09	-0.580	7.07E-06	0.314	6.46E-04	1	***Ptgfrn***	0	Promoter (<=1kb)	0.26	0.03	0.05	0.06	ns	ns	ns	ns
chr3	107760378	107787841	27464	0.322	7.47E-04	-0.743	1.11E-09	0.618	7.35E-14	1	***Csf1***	0	Promoter (<=1kb)	0.42	0.50	0.60	0.54	ns	ns	-0.16	ns
chr3	116091023	116159822	68800	0.169	8.38E-02	-0.179	3.68E-02	0.351	7.61E-11	1	***Vcam1***	0	Promoter (<=1kb)	0.10	ns	ns	ns	ns	ns	ns	ns
chr3	52232980	52261367	28388	0.231	2.61E-02	-0.315	3.68E-03	0.207	1.12E-02	1	***Foxo1***	-6969	Exon (ENSMUST0	0.19	0.16	0.27	0.38	0.07	0.12	0.08	-0.09
chr4	137771273	137787174	15902	0.216	4.67E-02	-0.810	8.21E-06	0.240	7.81E-02	1	***Alpl***	0	Promoter (<=1kb)	0.14	ns	ns	ns	0.06	0.05	0.05	ns
chr4	137851994	137860508	8515	0.220	4.91E-02	-0.389	1.84E-02	0.359	2.87E-03	1	***Ece1***	-1729	Promoter (1-2kb)	0.07	0.06	0.08	0.09	0.04	ns	ns	ns
chr5	102754349	102764638	10290	0.237	3.36E-02	-0.321	4.59E-02	0.523	8.68E-06	1	***Arhgap24***	-4133	Intron (ENSMUST	0.07	ns	ns	ns	ns	ns	ns	ns
chr5	96782134	96795453	13320	0.304	5.67E-03	-0.502	3.97E-03	0.291	2.27E-02	1	***Anxa3***	0	Promoter (<=1kb)	0.68	0.67	0.84	0.94	ns	ns	ns	-0.08
chr6	112480706	112494706	14001	0.229	4.07E-02	-0.643	3.49E-06	0.263	1.02E-02	1	***Oxtr***	0	Promoter (<=1kb)	ns	ns	ns	0.23	ns	ns	ns	-0.13
chr7	112209481	112216024	6544	0.228	3.25E-02	-0.364	4.54E-02	0.776	5.71E-09	1	***Mical2***	-9832	Distal Intergenic	0.12	0.11	0.21	0.20	ns	ns	-0.10	ns
chr7	112218421	112236211	17791	0.507	2.95E-05	-0.735	4.90E-04	0.591	1.72E-05	1	***Mical2***	0	Promoter (<=1kb)	0.12	0.11	0.21	0.20	ns	ns	-0.10	ns
chr7	112278041	112294560	16520	0.211	3.13E-02	-0.591	4.86E-03	0.556	8.95E-05	1	***Mical2***	6742	Intron (ENSMUST	0.12	0.11	0.21	0.20	ns	ns	-0.10	ns
chr7	112300036	112307241	7206	0.266	1.38E-02	-0.913	1.32E-05	0.672	5.22E-07	1	***Mical2***	-8788	Exon (ENSMUST0	0.12	0.11	0.21	0.20	ns	ns	-0.10	ns
chr7	112323786	112372861	49076	0.171	4.90E-02	-1.055	5.56E-09	0.458	2.40E-04	1	***Mical2***	0	Promoter (<=1kb)	0.12	0.11	0.21	0.20	ns	ns	-0.10	ns
chr7	96198476	96224987	26512	0.250	1.48E-02	-0.609	1.20E-07	0.164	7.41E-02	1	***Tenm4***	0	Promoter (<=1kb)	0.14	0.05	0.05	0.05	ns	0.06	ns	ns
chr7	96486138	96539432	53295	0.217	4.43E-02	-0.728	3.37E-10	0.256	3.51E-03	1	***Tenm4***	0	Promoter (<=1kb)	0.14	0.05	0.05	0.05	ns	0.06	ns	ns
chr7	96637320	96701440	64121	0.222	4.39E-02	-0.861	3.08E-08	0.203	9.64E-02	1	***Tenm4***	0	Promoter (<=1kb)	0.14	0.05	0.05	0.05	ns	0.06	ns	ns
chr7	96703395	96774811	71417	0.238	2.54E-02	-1.019	2.32E-15	0.268	6.41E-03	1	***Tenm4***	-3123	Exon (ENSMUST0	0.14	0.05	0.05	0.05	ns	0.06	ns	ns
chr8	125695173	125734656	39484	0.325	7.38E-04	-0.312	9.45E-04	0.253	1.87E-04	1	***Ntpcr***	0	Promoter (<=1kb)	0.03	ns	0.03	ns	ns	ns	ns	ns
chr8	25470458	25520277	49820	0.281	4.31E-03	-0.328	3.35E-03	0.250	2.18E-03	1	***Fgfr1***	0	Promoter (<=1kb)	0.22	0.19	0.25	0.18	0.06	ns	ns	0.09
chr1	134975961	135020165	44205	0.970	2.17E-17	-1.162	1.31E-08	0.200	2.01E-01	4	***Lgr6***	0	Promoter (<=1kb)	ns	ns	0.14	0.19	0.03	ns	ns	ns
chr1	135078582	135145923	67342	0.226	4.41E-02	-0.277	1.67E-02	-0.043	6.94E-01	4	***Lgr6***	0	Promoter (<=1kb)	ns	ns	0.14	0.19	0.03	ns	ns	ns
chr1	45923244	45944550	21307	0.265	5.03E-03	-0.448	2.08E-07	0.101	1.58E-01	4	***Slc40a1***	0	Promoter (<=1kb)	0.08	0.07	0.11	0.12	0.05	ns	ns	ns
chr11	102447603	102455702	8100	0.221	4.86E-02	-0.231	7.95E-02	0.089	4.57E-01	4	***Fam171a2***	0	Promoter (<=1kb)	0.03	ns	ns	ns	ns	ns	ns	ns
chr12	16734026	16750161	16136	0.738	5.84E-08	-1.181	4.50E-13	0.138	3.10E-01	4	***Greb1***	0	Promoter (<=1kb)	0.15	0.21	0.28	0.36	0.06	ns	ns	ns
chr14	121689590	121714550	24961	0.706	9.83E-11	-0.808	1.24E-12	0.101	3.09E-01	4	***Dock9***	0	Promoter (<=1kb)	0.04	ns	0.02	ns	ns	ns	ns	ns
chr14	121727504	121730468	2965	0.177	8.06E-02	-1.098	4.17E-07	0.212	1.85E-01	4	***Dock9***	8393	Intron (ENSMUST	0.04	ns	0.02	ns	ns	ns	ns	ns
chr14	121731124	121752820	21697	0.696	1.94E-09	-1.115	8.06E-27	0.139	1.15E-01	4	***Dock9***	0	Promoter (<=1kb)	0.04	ns	0.02	ns	ns	ns	ns	ns
chr17	27133838	27188687	54850	0.181	7.45E-02	-0.622	3.49E-07	0.128	2.04E-01	4	***Uqcc2***	0	Promoter (<=1kb)	0.35	0.12	0.26	0.28	-0.10	0.10	ns	-0.09
chr17	75174576	75187418	12843	0.171	6.07E-02	-0.570	1.42E-04	0.171	1.44E-01	4	***Ltbp1***	0	Promoter (<=1kb)	0.17	0.07	0.09	0.08	ns	ns	ns	ns
chr2	11548740	11574610	25871	0.194	7.83E-02	-0.203	7.23E-02	0.053	6.10E-01	4	***Pfkfb3***	0	Promoter (<=1kb)	ns	ns	0.06	ns	ns	ns	-0.06	ns
chr2	116067331	116109206	41876	0.363	1.22E-04	-0.329	5.68E-04	0.046	6.05E-01	4	***Meis2***	0	Promoter (<=1kb)	0.14	ns	ns	ns	ns	ns	ns	ns
chr2	131044354	131089475	45122	0.185	7.97E-02	-0.449	8.66E-06	0.004	9.71E-01	4	***Adam33***	0	Promoter (<=1kb)	0.15	ns	ns	ns	-0.04	ns	ns	ns
chr2	167196226	167211534	15309	0.358	1.01E-03	-0.386	3.72E-02	-0.001	9.95E-01	4	***Ptgis***	0	Promoter (<=1kb)	0.55	0.27	0.29	0.45	ns	ns	ns	-0.14
chr2	167226990	167245483	18494	0.442	1.96E-05	-1.023	1.05E-09	0.045	7.78E-01	4	***Ptgis***	0	Promoter (<=1kb)	0.55	0.27	0.29	0.45	ns	ns	ns	-0.14
chr3	142280046	142326960	46915	0.253	1.89E-02	-0.580	2.46E-03	-0.100	5.36E-01	4	***Pdlim5***	0	Promoter (<=1kb)	0.14	0.06	0.08	0.07	ns	ns	ns	ns
chr3	152752357	152758761	6405	0.218	3.90E-02	-0.726	2.66E-05	0.210	1.08E-01	4	***Pigk***	-4620	Intron (ENSMUST	0.17	0.10	0.09	0.12	ns	ns	0.07	ns
chr3	90459123	90470388	11266	0.203	7.51E-02	-0.796	2.06E-08	0.057	6.64E-01	4	***Npr1***	0	Promoter (<=1kb)	0.04	ns	ns	ns	ns	ns	ns	ns
chr5	111392799	111438216	45418	0.229	3.79E-02	-0.876	4.11E-12	0.068	5.59E-01	4	***Mn1***	0	Promoter (<=1kb)	0.06	ns	0.02	ns	ns	ns	ns	ns
chr5	123287452	123326694	39243	0.267	5.23E-03	-0.326	4.57E-03	-0.005	9.68E-01	4	***Wdr66***	0	Promoter (<=1kb)	0.04	ns	ns	ns	ns	ns	ns	ns
chr5	38058542	38069216	10675	0.465	9.97E-05	-0.304	3.03E-02	0.094	4.51E-01	4	***Stx18***	-7341	Intron (ENSMUST	0.05	ns	0.04	0.03	ns	ns	ns	ns
chr5	41593034	41621391	28358	0.300	2.59E-03	-0.291	3.60E-03	-0.058	5.22E-01	4	***Rab28***	6111	Distal Intergenic	0.02	ns	0.01	0.02	ns	ns	ns	ns
chr7	118480338	118489426	9089	0.199	8.24E-02	-1.143	2.18E-07	0.189	2.60E-01	4	***Itpripl2***	2549	Promoter (2-3kb)	0.20	0.09	0.11	0.09	ns	ns	ns	ns
chr8	68714702	68754578	39877	0.172	7.77E-02	-0.230	3.24E-03	0.070	2.90E-01	4	***Csgalnact1***	0	Promoter (<=1kb)	0.12	ns	ns	ns	0.05	ns	ns	ns
chr9	49569394	49574210	4817	0.307	5.28E-03	-0.351	3.24E-02	-0.046	7.82E-01	4	***Ncam1***	-845	Promoter (<=1kb)	0.13	0.06	0.06	0.04	0.08	ns	ns	ns
chr9	49787709	49812522	24814	0.222	2.21E-02	-0.357	2.95E-05	0.041	6.08E-01	4	***Ncam1***	0	Promoter (<=1kb)	0.13	0.06	0.06	0.04	0.08	ns	ns	ns
chr9	22091244	22106131	14888	0.263	1.16E-02	-0.202	8.48E-02	-0.186	3.94E-02	7	***Cnn1***	0	Promoter (<=1kb)	0.04	0.06	0.04	0.06	ns	ns	ns	-0.04

Table 2.4 Details of scRNA-Seq.

scRNA-Seq sample descriptions, quality control metrics, and samples used for each correlation analysis, related to Figures 2.2, 2.5, 2.12, and 2.13.

										Samples used in CUT&RUN/scRNA-Seq correlation analyses							
Batch	Genotype	Location	GD	Viability	# of cells	Total genes detected	Median genes per cell	Median UMI count per cell	Fig. 2D	Fig. 5B, 5D, S6 time analysis	Fig. 5B, 5D, S6 genotype analysis	Fig. 5C time analysis	Fig. 5C genotype analysis	Fig. S5A time analysis	Fig. S5A genotype analysis	Fig. S5B time analysis	Fig. S5B genotype analysis
1	*Kdm6b*$^{f/f}$	IS myo/endo	12.5	79	2758	18377	1879	4935	✓	✓	✓	✓	✓	✓	✓		
1	*Kdm6b*$^{f/f}$	IS myo/endo	14.5	77	4662	18455	1128	2796	✓	✓	✓	✓	✓	✓	✓		
1	*Kdm6b*$^{f/f}$	IS myo/endo	16.5	77	5720	18579	1298	3280	✓	✓	✓	✓	✓	✓	✓		
1	*Kdm6b*$^{f/f}$	IS myo/endo	18.5	76	3733	18240	1778	4597	✓	✓	✓	✓	✓	✓	✓		
1	*Kdm6b cKO*	IS myo/endo	12.5	77	5367	18761	1552	3809	✓		✓		✓		✓		
1	*Kdm6b cKO*	IS myo/endo	14.5	74	3898	18967	1526	3699	✓		✓		✓		✓		
1	*Kdm6b cKO*	IS myo/endo	16.5	71	2494	18479	1607	4106	✓		✓		✓		✓		
1	*Kdm6b cKO*	IS myo/endo	18.5	72	5153	17883	1238	2982	✓		✓		✓		✓		
2	*Kdm6b*$^{f/f}$	IS myo/endo	12.5	78	2758	18664	2255	7656	✓	✓	✓	✓	✓	✓	✓		
2	*Kdm6b cKO*	IS myo/endo	12.5	79	2735	18387	2560	10061	✓		✓		✓		✓		
2	*Kdm6b*$^{f/f}$	IS myo/endo	18.5	73	2473	18069	2308	8911	✓	✓	✓	✓	✓	✓	✓		
2	*Kdm6b cKO*	IS myo/endo	18.5	70	1687	17229	1979	6806	✓		✓		✓		✓		
2	*Kdm6b*$^{f/f}$	IIS	12.5	79	1169	17136	1656	4761	✓	✓	✓	✓	✓			✓	✓
2	*Kdm6b*$^{f/f}$	IIS	14.5	81	2733	18169	1947	6535	✓	✓	✓	✓	✓			✓	✓
2	*Kdm6b*$^{f/f}$	IIS	16.5	76	3007	18179	2372	9289	✓	✓	✓	✓	✓			✓	✓
2	*Kdm6b*$^{f/f}$	IIS	18.5	78	3255	18322	2310	9137	✓	✓	✓	✓	✓			✓	✓
2	*Kdm6b cKO*	IIS	12.5	71	2545	18696	2573	9755	✓		✓		✓				✓
2	*Kdm6b cKO*	IIS	14.5	71	3108	18288	2171	7607	✓		✓		✓				✓
2	*Kdm6b cKO*	IIS	16.5	70	2690	18329	2090	7097	✓		✓		✓				✓
2	*Kdm6b cKO*	IIS	18.5	71	1209	17470	1864	6030	✓		✓		✓				✓
3	*Kdm6b*$^{f/f}$	IS myo/endo	12.5	84	3868	19240	2418	8080	✓	✓	✓	✓	✓	✓	✓		
3	*Kdm6b cKO*	IS myo/endo	12.5	78	3714	19180	2383	8025	✓		✓		✓		✓		
3	*Kdm6b*$^{f/f}$	IIS	5.5	83	3440	19009	1561	3907	✓	✓				✓		✓	
3	*Kdm6b*$^{f/f}$	IIS	8.5	77	3726	19038	1883	5467	✓	✓				✓		✓	
3	*Kdm6b cKO*	IIS	5.5	80	3310	19107	1939	5590	✓								
3	*Kdm6b cKO*	IIS	8.5	82	4157	19268	2217	6983	✓								

Methods and Materials

Mice

C57BL/6J (B6), *Pdgfra-cre* (C57BL/6-Tg(*Pdgfra-cre*)1Clc/J)[108], *Ltf-iCre* (*Ltf*$^{tm1(icre)Tdku}$/J)[107], *Kdm6b*$^{f/f}$ (B6.Cg-*Kdm6b*$^{tm1.1Rbo}$/J)[131], and B6CBAF1/J mice were purchased from The Jackson Laboratory. *Pgr-cre* mice (*Pgr*$^{cre/+}$)[104] were the gift of Francesco DeMayo and John Lydon. *Kdm6b*$^{f/f}$ mice were intercrossed with *Pgr-cre* mice to generate *Pgr-cre* (*Pgr*$^{cre/+}$) *Kdm6b*$^{f/f}$ mice, with *Pdgfra-cre* to generate *Pdgfra-cre* Kdm6b$^{f/f}$ mice, or with *Ltf-iCre* to generate *Ltf-iCre (Ltf* $^{icre/+}$) *Kdm6b*$^{f/f}$ mice. Vasectomized ICR males were purchased from Taconic Farms. Mice were housed in a specific pathogen-free animal barrier facility at UCSF. To maintain a consistent microbiota, all females were born in the Erlebacher lab holding room except for the B6CBAF1/J mice used for Figure 2.6, which were purchased from The Jackson Laboratory. All experiments were performed using female mice because only females become pregnant. Virgin females, 6-10 weeks old, were used for all experiments and were mated to B6 males unless otherwise indicated. All experiments were approved by the UCSF IACUC (Protocols #AN194381, AN193713, AN179716, and AN178689).

Matings and parturition timing experiments

Virgin females, 6-10 weeks old, were used for all experiments and were mated to B6 males unless otherwise indicated. Vaginal plugs were checked in the mornings, and noon of that day was counted as GD0.5. To determine labor onset timing, pregnant mice were checked twice daily (9 am and 6 pm) for evidence of delivery, uterine bleeding, or maternal distress. If apparent at 9 am, labor onset timing was scored as GDX.5, with X being the number of days after mating (i.e., GD0.5). If apparent at 6 pm, it was scored as GD(X+1) (i.e., midnight of the next gestation day).

For parturition rescue experiments, mice were given a single intraperitoneal injection of 60 µg 16,16-dimethyl $PGF_{2\alpha}$ (Cayman Chemical, cat. #16750), a metabolically stable $PGF_{2\alpha}$ analog, on GD18.5. For CUT&RUN experiments, nonpregnant uteri were obtained from B6CBAF1/J mice that were given daily subcutaneous injections of 2 mg P4 (Sigma-Aldrich, cat. #P0130) dissolved in 100 µl sesame seed oil (Sigma-Aldrich, cat. #S3547) for the 3 days prior to sacrifice. For vasectomized matings, B6CBAF1/J mice were mated to vasectomized ICR males and sacrificed five days later (the equivalent of GD5.5).

P4 and $PGF_{2\alpha}$ measurements

Serum P4 concentrations were measured using a commercial ELISA kit (Cayman Chemical, cat. #582601) according to the manufacturer's instructions. Prostaglandin concentration measurements were performed on dissected uterine tissues initially snap frozen and stored at -80°C prior to batch processing. This initially entailed weighing and pulverizing the tissue in liquid nitrogen. The lipids were then extracted with 500 µl ice-cold methanol-chloroform (1:2) containing 10 µM indomethacin (Sigma-Aldrich, cat. #I7378). A volume corresponding to 10 mg of tissue was taken and methanol was added to a final volume of 1 ml. The samples were then sonicated for 3 cycles of 7 seconds on and 30 seconds off at 4°C in a Diagenode Bioruptor sonicator. Samples were vortexed and then centrifuged for 15 minutes at 10,000x*g* at 4°C to pellet precipitated proteins. The supernatants were kept at -80°C overnight to precipitate additional proteins, and following an additional centrifugation the supernatants were evaporated in a speed vac. The samples were then resuspended in ELISA buffer and subjected to a commercial $PGF_{2\alpha}$ ELISA kit (Cayman Chemical, cat. #516011) according to the manufacturer's instructions.

Immunohistochemistry and immunofluorescence

Uterine tissues were fixed overnight at 4°C in 4% paraformaldehyde/PBS and embedded in paraffin. Sections were cut at 10 μm, baked for 30 minutes at 65°C. H&E staining was performed using routine methods. For immunofluorescence, deparaffinized slides were first placed in a solution of 90% methanol and 3% H_2O_2 at room temperature for 20 minutes, then washed twice in PBS. The sections were then subjected to antigen retrieval using a Biocare Decloaking Chamber NxGen (110°C for 5 minutes, then allowed to cool for 10 minutes in the chamber). After equilibrating to room temperature for 10 minutes, the slides were washed twice in PBS and then blocked in 1% BSA/3% donkey serum/0.4% Triton X-100 for 1 hour at room temperature, followed by application of primary antibodies, diluted in 1% BSA, 0.4% Triton X-100, and incubation at 4°C overnight. Antibody sources, dilutions and antigen retrieval methods for mouse specimens were COX-1 (Abcam, cat. #ab109025, RRID: AB_10865291, 1:4000; decloaking in 10 mM Tris-EDTA pH 9.0) and α-SMA (Invitrogen, cat. #53-9760-82, RRID: AB_2574461, 1:300; decloaking in 10 mM Tris-EDTA pH 9.0). The slides were washed twice in PBS between all subsequent steps. The COX-1 immunostaining employed biotin tyramide amplification, and so the sections were next incubated for 30 minutes at room temperature with horseradish peroxidase- (HRP-) conjugated donkey anti-rabbit IgG-secondary antibodies (Jackson ImmunoResearch) diluted 1:200 in TNB blocking buffer (PerkinElmer). They were then incubated in 1.8 μg/ml biotin-tyramide/0.0015% H_2O_2/PBS for 5 minutes at room temperature, then in 5 μg/ml streptavidin-Alexa Fluor 594 for 30 minutes at room temperature. The sections were then incubated with TrueBlack Lipofuscin Autofluorescence Quencher (Biotium, cat. #23007) and then mounted using DAPI mounting media (Electron Microscopy Sciences, cat. #

17989). All immunofluorescence images were captured using an Axio Imager M2 microscope running on Zen software (Zeiss). Adobe Photoshop was used to increase image brightness using the brightness/contrast function; in these cases, the alteration was applied over the entire image and was equally applied to all images within an experiment.

qRT-PCR

qRT-PCR was performed on RNA isolated from whole ovaries using TRIzol (Thermo Fisher Scientific, cat. #15596026), and from uterine epithelial sheets and uterine fibroblasts using the RNeasy Plus Mini Kit (Qiagen, cat. #74034). Whole ovaries were homogenized in TRIzol prior to RNA extraction. Uterine fibroblasts were isolated by first digesting uterine tissues in Liberase TM (Roche, cat. #5401127001; 0.28 WU/ml), DNase I (Roche, cat. #1010415901; 30 μg/ml), and trypsin (ThermoFisher, cat. #15090046; 0.05%) in Ca^{++}/Mg^{++}-containing HBSS for 60 minutes at 37°C with trituration every 10 minutes. 5 mM EDTA (Life Technologies, cat. #15575020) was added for the final 15 minutes of the incubation. The cell suspensions were passed through 100 μm filters and then negatively selected as previously described (Nancy et al., 2018) using LD magnetic bead columns (Miltenyi, cat. #130-042-901) and antibodies toward red blood cells (Ter-119, Miltenyi, cat. #130-049-901, RRID: AB_2936424), leukocytes (CD45, Miltenyi, cat. #130-052-301, RRID: AB_2877061), epithelial cells (CD326, Invitrogen, cat. #14-5791-85, RRID: AB_953626), and endothelial cells (CD102, Biolegend, cat. #105602, RRID: AB_10599101). Microbead-coupled goat anti-rat IgG antibodies (Miltenyi Biotec, cat. #130-048-502, RRID: AB_244364) were used as secondary reagents for the CD326 and CD102 antibodies, which were not directly bead coupled. Epithelial sheets were isolated from dissected IS myo/endo or from non-pregnant uteri filleted lengthwise. The tissues were cut into 3 mm

pieces and incubated in HBSS with 125 μg/ml thermolysin (Sigma-Aldrich, cat. #T7902), first at 4°C for 15 minutes, then at 37°C for 1 hour. After gently rinsing the tissues in 1 ml PBS, the epithelial sheets were lightly scraped away from the associated connective tissue using curved forceps, then washed twice in PBS. cDNA was synthesized from 1 μg RNA using an iScript cDNA Synthesis Kit (Bio-Rad, cat. #1708891). PCR reactions were performed with Evagreen dye (Biotium, cat. #31000) using a CFX Connect Real-Time PCR Detection System (Bio-Rad). Primers were designed with NCBI Primer-Blast software and a test qRT-PCR reaction was performed on every primer pair to ensure no self-amplification, to verify melting curves, and to confirm the correct product length. The cycle threshold (Ct) value of the housekeeping gene *Actb* was subtracted from the Ct of the experimental gene to determine the ΔCt. Statistical analyses were performed using ΔCt values. Expression of a given gene relative to *Actb* was determined using the formula $2^{-\Delta Ct}$. Primers sequences were as follows: *Actb*-Forward: 5'-GCTCTGGCTCCTAGCACCAT-3', *Actb*-Reverse: 5'-GCCACCGATCCACACAGAGT-3'; *Kdm6b*-Forward: 5'-GGTTCCTGGTGGCCAATCTT-3', *Kdm6b*-Reverse: 5'-AGCTGGTACTGATAGGCGGT-3'; *Ptgs1*-Forward: 5'-TACTCACAGTGCGGTCCAAC-3', *Ptgs1*-Reverse: 5'-TTGGGCCAGAAGCTGAACAT-3'; *Akr1c18*-Forward: 5'-GCTGATATGTTTAAGGCTCACCCTAA-3', *Akr1c18*-Reverse: 5'-AGAGTCCAGCATCACACAAAAGATC-3'.

Ovary transplants

Bilateral mouse ovary transplantation was performed as previously described (Mason, Parkinson, & Habermehl, 2018) and in accord with institutional best practice for anesthesia, analgesia, and

post-operative monitoring. Animals were mated to B6 males for parturition timing experiments no earlier than 14 days after surgery.

scRNA-Seq sample processing

Dissected uterine tissues were thoroughly minced and stored in 90% fetal bovine serum (FBS) (R&D Systems, cat. #S11150) and 10% DMSO (Sigma-Aldrich, cat. #D8418) in liquid nitrogen prior to processing of multiple samples at the same time. scRNA-Seq data was collected over 3 separate experimental batches, details of which are further outlined in Table 2.4. For non-pregnant and GD5.5 IIS samples, each replicate consisted of uteri from 2 mice pooled together. At the time of processing, tissues were thawed, washed twice in PBS, and enzymatically disaggregated with Liberase TM (Roche, cat. #5401127001; 0.28 WU/ml), DNase I (Roche, cat. #1010415901; 30 μg/ml) and trypsin (ThermoFisher, cat. #15090046; 0.05%) in Ca^{++}/Mg^{++}-containing HBSS for 60 minutes at 37°C with trituration every 10 minutes. 5 mM EDTA (Life Technologies, cat. #15575020) was added for the final 15 minutes of the incubation. The cell suspensions were filtered through 100 μm filters and checked for viability. All sequencing experiments were performed on samples with a minimum of 70% viable cells, as determined by a Nexcelom Cellaca MX cell counter. Cells were washed in PBS with 0.04% BSA and then incubated with lipid-conjugated oligonucleotides for cell hashing (10X Genomics) for 5 minutes at room temperature. Cells were then washed twice with PBS with 1% BSA. 125,000 cells per sample were multiplexed and, from these pools, 340,000 cells were loaded onto the Chromium Controller (10X Genomics). Samples were processed for single-cell encapsulation and cDNA library generation using the Chromium Single Cell 3' v3.1 Reagent Kits (10X Genomics).

Libraries were subsequently sequenced on an Illumina NovaSeq 6000 (Illumina). All samples were sequenced at a sequencing depth of 30,000 reads per cell.

scRNA-Seq data pre-processing and analysis

10X sequencing data was demultiplexed, aligned and quantified using the Cell Ranger Single-Cell Software Suite (10X Genomics) against the mm10 mouse reference genome provided by Cell Ranger to generate feature-barcode matrices. Raw feature-barcode matrices were loaded into Seurat [132] and genes with fewer than 3 UMIs were dropped from the analyses. Matrices were further filtered to remove events with greater than 20% mitochondrial content, events with greater than 50% ribosomal content, or events with fewer than 100 total genes. The individual processed objects per library were normalized and variance stabilized using negative binomial regression via the scTransform method offered by Seurat. Count matrices were merged into a single Seurat object and the batch (or library) of origin was stored in the metadata of the object. The log-normalized counts for highly variable genes (3,000) were reduced to a lower dimension using PCA and the individual libraries were aligned in the shared PCA space in a batch-aware manner (each individual library being considered a batch) using the Harmony algorithm [133]. The resulting Harmony components were used to generate a batch corrected UMAP, and to identify clusters of transcriptionally similar cells across each of the 26 samples. We removed several clusters composed mostly of cells containing high contents of mitochondrial gene transcripts or low nUMI (transcripts per cell), as well as one immune/non-immune doublet cluster. All differential expression analysis was performed using the FindMarkers function in Seurat, using a two-sided Wilcoxon's rank sum test and $P_{adj}<0.05$ for significance. The specific samples

included in the UMAP analyses in Figure 2.2D and the correlation analyses in Figures 2.5, S2.5, and S2.6 are listed in Table 2.4.

Cell purification for H3K27me3 CUT&RUN

Uterine fibroblasts were isolated from total non-pregnant uteri (P4-tx) or from IIS or IS myo/endo at various time points in pregnancy or pseudopregnancy. For GD0.5, P4-tx, xVASX (on the equivalent of GD5.5), GD5.5 IIS, and GD8.5 IIS samples, each replicate consisted of tissues from 2 mice pooled together. Deciduomas were removed from GD14.5 *Kdm6b cKO* IIS samples. Dissected tissues were thoroughly minced and stored in 90% FBS (R&D Systems, cat. #S11150) and 10% DMSO (Sigma-Aldrich, cat. #D8418) in liquid nitrogen prior to processing of multiple samples at the same time. Tissues were thawed, washed twice in PBS and then enzymatically disaggregated with Liberase TM (Roche, cat. #5401127001; 0.28 WU/ml), DNase I (Roche, cat. #1010415901; 30 μg/ml) and trypsin (ThermoFisher, cat. #15090046; 0.05%) in $Ca^{++}Mg^{++}$-containing HBSS for 60 minutes at 37°C with intermittent trituration. 5 mM EDTA (Life Technologies, cat. #15575020) was added for the final 15 minutes of the incubation. Fibroblasts were then negatively selected through the use of M-280 sheep anti-rat IgG Dynabeads (ThermoFisher, cat. #11035) and antibodies toward leukocytes (rat anti-CD45; clone 30-F11, Biolegend, cat. #103102, RRID: AB_312967), epithelial cells (rat anti-EpCAM; clone G8.8, eBioscience, cat. #14-5791-85, RRID: AB_953626), and endothelial cells (rat anti-CD102, clone 3C4, Biolegend, cat. #105602, RRID: AB_10599101). Viability was assessed using trypan blue exclusion and only samples with a viability above 65% were used. To assess purity, the post-Dynabead selected cells were stained with eBioscience Fixable Viability Dye eFluor506 (Invitrogen, cat. #65-0866-14) for 15 minutes, followed by a PBS wash and then 30 minutes of

surface staining with antibodies against CD45 (Invitrogen, clone 30-F11, cat. #12-0451-83, RRID: AB_465669), CD326 PE-Cy7 (Biolegend, cat. #118216, RRID: AB_1236471) and CD102 FITC (Biolegend, cat. #105606, RRID: AB_313199). The protocol routinely achieved a purity of ~95%, as assessed by flow cytometry for these same markers (Figure 2.11). From our scRNA-Seq analysis, we expect the purified cells to contain 3-17% and 5-17% pericytes and smooth muscle cells, respectively, since the negative selection antibody cocktail would not be expected to remove these cells.

H3K27me3 CUT&RUN

H3K27me3 distributions were determined by the CUT&RUN assay [134,135]. The assay was performed using the CUT&RUN Assay Kit (Cell Signaling Technology, cat. #86652) following the manufacturer's instructions with minor modifications. Briefly, one input control was prepared per sample group by taking an aliquot of 1.5 x 10^5 purified fibroblasts and adding 200 µl DNA extraction buffer with RNase A (10 mg/ml) and Proteinase K (20 mg/ml) and incubating the suspension at 55°C for 1 hour with shaking. The tubes were then placed on ice for 5 minutes and then sonicated for 8 cycles of 8 seconds on and 90 seconds off at 4°C in a Diagenode Bioruptor sonicator. The lysates were then clarified by centrifugation at 18,500x*g* for 10 minutes at 4°C. The supernatants were transferred to a new microcentrifuge tube and stored at -20°C. To perform the H3K27me3 CUT&RUN assay, 1.5 x 10^5 purified fibroblasts from every sample were resuspended in wash buffer (20 mM HEPES-NaOH pH 7.5, 150 mM NaCl, 0.5 mM spermidine, and protease inhibitor cocktail), followed by addition of activated concanavalin A-magnetic beads and incubation for 10 minutes at room temperature. Tubes were placed on a magnetic rack and the supernatant was discarded. The cell-bead conjugates were then resuspended in 100 µl

digitonin buffer (wash buffer with 2.5% digitonin solution) containing 2 µl of anti-H3K27me3 antibodies (Cell Signaling Technology, cat. #9733, RRID: AB_2616029) and then incubated overnight at 4°C with constant rotation. The samples were then placed on a magnetic rack so that the cell-bead conjugates could be washed with 250 µl of digitonin buffer, and then resuspended in 50 µl pAG-Mnase pre-mix buffer (Cell Signaling Technology, cat. #57813) followed by rotation at 4°C for 1 hour. The samples were then placed on a magnetic rack again, washed with digitonin buffer, and resuspended in ice-cold 150 µl digitonin buffer with 3 µl of 100 mM $CaCl_2$, then incubated for 1 hour at 4°C. 150 µl of stop buffer was then added and the tubes were incubated in a 37°C heat block for 30 minutes without shaking to release DNA fragments into solution. The samples were centrifuged at 16,000x*g* for 2 minutes at 4°C. The tubes were placed on a magnetic rack and supernatants containing the enriched chromatin were collected. DNA from the H3K27me3 and input samples was purified using spin columns (Cell Signaling Technology, cat. #14209) according to the manufacturer's instructions. CUT&RUN libraries were prepared using the Nextera Flex Library Prep Kit (Illumina). Size selection was performed using SPRIselect beads (Beckman Coulter) and fragment sizes were determined with an Agilent 2100 Bioanalyzer using the High Sensitivity DNA kit (Agilent). Samples were sequenced on the Illumina NovaSeq 6000 (Illumina) with paired-end reads.

CUT&RUN data processing and analysis

Raw reads were mapped to the mouse mm10 genome assembly using STAR[136] alignment (--outFilterMismatchNoverLmax 0.04 --outFilterMismatchNmax 999 --alignSJDBoverhangMin 1 --outFilterMultimapNmax 1 --alignIntronMin 20 --alignIntronMax 1000000 --alignMatesGapMax 1000000). BAM files were also generated by STAR. PCR duplicates were removed by Picard[137],

and peak calling was performed using MACS2[138] (--keep-dup 1 --bw 500 --nomodel --extsize 400 --slocal 5000 --llocal 100000 -p 0.01 --broad --broad-cutoff 0.5).

Differential peak analysis was performed in Diffbind (Stark R., 2011). A count matrix was created using replicate BAM and MACS2 broadPeak files (*n*=3 per condition) with bUseSummarizeOverlaps=TRUE and summits=FALSE. For the CUT&RUN experiment in Figure 2.3, a multi-factor design with contrasts, i.e., design="~Condition+Tissue" with condition specifying gestation day and tissue specifying genotype, was established in order to incorporate all of the data into a single model with time and genotype as independent covariates. Normalization and differential peak calling was performed using DESeq2. Peaks with low concentrations (<5) were removed, resulting in a total of 64,923 peaks present for at least one time point in either *Kdm6b cKO* or control fibroblasts. For the CUT&RUN experiment shown in in Figure 2.6, the consensus peak set from Figure 2.3 was used to generate the count matrix and DESeq2 was used for differential peak calling. For the differential peak calling between B6 and B6CBAF1/J GD5.5 samples (Figure 2.14A), EdgeR was used because these samples were subjected to CUT&RUN at different times. Volcano plots in Figures 2.3 and 2.6 were plotted with $\log_2$FC values from DiffBind's dba.report and frequency distribution histograms were made using Prism and designating bin width to be tabulated to the exact frequency. For line plots, H3K27me3 peak concentrations from the dba.report were normalized to GD5.5 control levels and graphed in Prism. K-means clustering and heat-map visualization (Figure 2.11C-D) was performed using the R package ComplexHeatmap[139].

CUT&RUN BigWig visualization

To generate bigwig files for CUT&RUN datasets, all aligned BAM files were converted to the BED format with the BEDTools[140] (version 2.29.1) bamtobed and slopped using bedtools slopBed. The BED files were converted to bedgraph format using the bedtools coverageBed command. The bedgraphs were then normalized and each replicate of a given experimental condition was pooled and merged by sample group using bedtools merge. Finally, bedGraphToBigWig[141] (version 2.8) was used to generate the bigwig files displayed on browser tracks throughout the manuscript using the IGV browser (Broad Institute). For all samples processed and sequenced in the same experiment, IGV tracks were set at a fixed data range. For tracks shown in Figure 2.6, which include samples from two separate experiments, the data range was set after autoscaling to the chromosome relevant to the gene shown.

Detections of correlations between histone peak dynamics and gene expression profiles

To generate a meaningful and relevant set of peaks for the correlation analysis, we first assigned every gene to a single nearby H3K27me3 peak, if such a peak existed. Specifically, we used the annotatePeak function in ChIPSeeker[142] to identify each peak's nearest gene and annotate its genomic features, and then excluded peaks that were located more than 10 kb away from the assigned gene's TSS. If multiple peaks were assigned to a gene, we then chose the peak to be considered for further analysis according to an algorithm whereby we first prioritized peaks that changed over time (i.e., $FDR<0.1$ for ~time as determined by the aggregate analysis), choosing the one with the lowest *FDR*, and then peaks that differed by genotype (i.e., $FDR<0.1$ for ~genotype as determined by the aggregate analysis), again choosing the one with the lowest *FDR*. This resulted in a final list of 12,401 peaks, each assigned to 1 gene.

The RNA expression data for the correlation analysis came from our scRNA-Seq experiments described in Fig 2. All differential expression analysis was performed using the FindMarkers function in Seurat, considering only the *Pdgfra*$^{+}$ fibroblast population, and using a two-sided Wilcoxon's rank sum test and P_{adj}<0.05 for significance. The samples used for each of these comparisons are listed in Table 2.4. Briefly, for time-based comparisons to GD5.5/8.5, GD5.5 and GD8.5 IIS samples were combined to generate the GD5.5/8.5 baseline. This baseline was compared to GD12.5-GD18.5 samples (both IS myo/endo and IIS samples combined in Figure 2.5B or separately in Figure 2.12A-B). For the time-based comparisons to GD12.5 (Figure 2.5C), data from GD12.5 IS myo/endo and IIS were combined to generate the baseline and then compared to GD14.5-18.5, again combining respective data for IS myo/endo and IIS. For genotype-based comparisons, data from *Kdm6b cKO* fibroblasts on GD12.5-18.5 were compared to gestation day-matched controls, combining IS myo/endo and IIS samples for Figure 2.5B, or considering them separately for Figure 2.12A-B. For the analyses of pericytes and SMCs (Figure 2.13A-B), the same differential analysis was performed but using data from the *Pdgfrb*$^{+}$ and *Myh11*$^{+}$ clusters, respectively (both IS myo/endo and IIS combined).

We then performed an enrichment analysis to determine whether a gene with a given expression characteristic was over- (or under-) represented within a given histone category. That is, for each RNA expression category (upregulated with time in control fibroblasts, downregulated with time in control fibroblasts, higher in *Kdm6b cKO* fibroblasts, and/or lower in *Kdm6b cKO* fibroblasts) and histone category (HC1-9), we determined fold-enrichment by tallying the number of genes that simultaneously fell into both the RNA expression category and histone category, and then

dividing this number by the number of genes expected by chance to simultaneously fall within both the RNA expression category and histone category. This latter number was calculated by multiplying the total number genes within the given RNA expression category (including those that were not necessarily peak-associated) with the total number of genes within the given histone category, and then dividing this product by the total number of genes detectable by scRNA-Seq (19,562). We based analyses involving dual RNA characteristics (e.g., increased expression with time in control fibroblasts *and* lower expression in *Kdm6b cKO* fibroblasts compared to control fibroblasts) upon the actual total number of genes with both characteristics in order to ensure that we would not detect correlations if time- and genotype-dependent changes in gene expression were somehow linked independently of the behavior of the nearby H3K27me3 peak. This same approach was used for the analyses of pericytes and SMCs (Figure 2.13A-B), but using these cells' respective gene expression data.

For the reciprocal analyses shown in Figures 2.5D and S2.6C-D, we compiled a list of every peak-associated gene that showed both upregulated expression in control fibroblasts at any point from GD12.5-18.5 compared to GD5.5/8.5 as well as gestation-day matched differential expression between *Kdm6b cKO* and control fibroblasts. For each of the 9 histone categories, we then calculated fold-enrichment by tallying the number of genes on this list that fell into that histone category and then dividing this number by the number of genes expected by chance to fall within that histone category. This latter number was calculated by multiplying the total number genes (i.e., including those that were not necessarily peak-associated) that showed the expression characteristics described above with the total number of genes within the given

histone category, and then dividing this product by the total number of genes detectable by scRNA-Seq (19,562).

For both forms of analyses, the resulting heat-maps (Figures 2.5, S2.5, and S2.6) were colored by the values for fold-enrichment scores, using a two-tailed Fisher's exact test (fisher.test, R) to determine whether a gene subset was significantly over- or under-represented. The *P*-value threshold for this assessment was based upon a 0.05 cutoff, but included a Bonferroni correction for the 9 different histone categories, giving a corrected threshold *P*-value for significance of $5.6x10^{-3}$.

Associations between different features of H3K27me3 dynamics

To detect possible associations between the three different features of H3K27me3 dynamics studied here (time-dependent changes from GD5.5 to GD18.5, effects of KDM6B deficiency, peak tuning from GD0.5 to GD5.5), we determined the fold-enrichment for any two given features by tallying the number of peaks that satisfied these two features, and then dividing this number by the number of peaks expected if the two features varied independently. The resulting heat-maps (Figure 2.14B, D-E) are colored by the fold-enrichment values, using a two-tailed Fisher's exact test (fisher.test, R) and a Bonferroni correction for the 9 sets of categories that existed for each comparison, which as above gave a corrected threshold *P*-value for significance of $5.6x10^{-3}$.

Quantification and statistical analysis

The number of independent biological replicates and specific tests employed for each experiment are shown in the figure or stated in the figure legend. All analyses aside from those based upon CUT&RUN and scRNA-Seq data were performed using GraphPad Prism software, for which $P<0.05$ was considered significant. qRT-PCR analyses employed raw ΔCt values. All *t*-tests were two-tailed. Parturition timing experiments were analyzed using a two-sided log-rank (Mantel-Cox) test. $FDR<0.1$ was considered significant for CUT&RUN differential peak analyses. As described in further detail above, we used a two-tailed Fisher's exact test (fisher.test, R) to identify associations between gene expression characteristics and nearby histone dynamics, or between different features of histone dynamics. These tests included a Bonferroni correction for the 9 different comparisons per analysis, giving a corrected threshold *P*-value for significance of $5.6x10^{-3}$.

Chapter 3: Circumvention of luteolysis reveals parturition pathways in mice dependent upon innate type 2 immunity

Chapter 3 was adapted from the following article, written primarily by Johan Siewiera and Adrian Erlebacher, and published in *Immunity*:

Siewiera J, McIntyre TI, Cautivo KM, Mahiddine K, Rideaux D, Molofsky AB, Erlebacher A. Circumvention of luteolysis reveals parturition pathways in mice dependent upon innate type 2 immunity. Immunity. 2023 Mar 14;56(3):606-619.e7. doi: 10.1016/j.immuni.2023.01.005. Epub 2023 Feb 6. PMID: 36750100; PMCID: PMC10023352.

Additional author contributions for Chapter 3 are described in the Author Contributions section at the end of the chapter. I performed the experiments shown in Figures 3.7A-E and 3.14A-F.

Summary

Although mice normally enter labor when their ovaries stop producing progesterone (luteolysis), parturition can also be triggered in this species through uterus-intrinsic pathways potentially analogous to the ones that trigger parturition in humans. Such pathways, however, remain largely undefined in both species. Here, we report that mice deficient in innate type 2 immunity experienced profound parturition delays when manipulated endocrinologically to circumvent luteolysis, thus obliging them to enter labor through uterus-intrinsic pathways. We found that these pathways were in part driven by the alarmin IL-33 produced uterine interstitial fibroblasts. We also implicated important roles for uterine group 2 innate lymphoid cells, which demonstrated IL-33-dependent activation prior to labor onset, and eosinophils, which displayed evidence of elevated turnover in the prepartum uterus. These findings reveal a role for innate

type 2 immunity in controlling the timing of labor onset through a cascade potentially relevant to human parturition.

Introduction

Parturition, i.e., the act of giving birth, is the end result of a process that transforms the late gestation gravid uterus into the highly contractile tissue that expels the conceptus (for reviews, see refs.[91,92]). In humans, this process is thought to be mediated through a core set of uterus-intrinsic pathways that operate under the influence of endocrine, mechanical, and fetus-derived signals. The nature of these pathways is poorly understood, however, a knowledge gap that exemplifies the lack of insight into parturition mechanisms across species[91]. In turn, this deficit has hindered the development of rational therapies for preterm labor, a highly prevalent obstetrical complication and major cause of neonatal morbidity and mortality[47].

A major difficulty in elucidating parturition mechanisms with human relevance is the high degree of divergence across species in the endocrine control of labor onset[91]. Pregnancy requires the maintenance of high plasma progesterone (P4) concentrations, and primates enter labor while these concentrations remain elevated, highlighting these species' reliance on uterus-intrinsic parturition pathways. In contrast, parturition onset in mice, the species of choice for mechanistic dissection, is triggered when the ovary starts expressing the P4-metabolizing enzyme 20α-hydroxysteroid dehydrogenase (20α-HSD). This process, known as luteolysis, leads to a systemic drop in P4 concentrations and consequent rapid maturation of the myometrium, the smooth muscle layer of the uterus. However, sidelining the effects of luteolysis through exogenous P4 administration extends gestation length only ~2 days[98,143], suggesting that mice also bear uterus-intrinsic parturition pathways. Indeed, the peri-partum uterus of both mice and

humans show evidence of low-grade, sterile inflammation, which has led to the suggestion that immune activation contributes to parturition in both species [95,144]. To date, work on mouse parturition has not addressed these P4-independent, uterus-intrinsic parturition pathways but rather the pathways that induce luteolysis[145].

Previously, we identified *Il33*, which encodes the cytokine interleukin-33 (IL-33), as one of ~800 genes in mice subject to active, transcriptional silencing in the stromal cells of the early gestation decidua, the specialized endometrial tissue that surrounds the conceptus and that separates it from the myometrium[98]. IL-33 is an IL-1 superfamily member that functions as a pro-inflammatory alarmin and potent driver of type 2 immunity when released by tissue damage from its nucleus-sequestered state, with many of its effects mediated through group 2 innate lymphoid cells (ILC2s) and eosinophils[146]. Thus, given that placental growth and development disrupts the integrity of neighboring decidual tissue, *Il33* silencing appeared as a feature of the maternal-fetal interface that could limit maladaptive inflammatory reactions. However, we also found that *Il33* expression is maintained in the myometrium, suggesting a potential requirement for IL-33 activity in this tissue layer. Indeed, IL-33 has been implicated in the sensitization of smooth muscle cells (SMCs) to pro-contractile signals and is thought to contribute to a diverse set of pathologic and infectious processes that involve SMC contraction[147].

Here, we present evidence that IL-33, ILC2s, and eosinophils play key roles in the control of on time labor onset in mice. These roles are not apparent when parturition is governed by luteolysis, but instead when we artificially maintain high circulating P4 concentrations to create an experimental model that obliges labor to be initiated by uterus-intrinsic pathways, as it does in humans. We also map the source of IL-33 to platelet-derived growth factor receptor α- (PDGFRα-) expressing interstitial uterine fibroblasts and reveal activation of the type 2 immune

axis in the uterus immediately prior to labor onset. These observations provide a foundation for dissecting further upstream and downstream components of a labor-inducing cascade potentially relevant to human parturition.

Results

IL-33 is required for on-time parturition when only uterus-intrinsic pathways are available to drive labor onset.

To evaluate the role of IL-33 in mouse parturition, we first assessed whether IL-33 deficiency affected P4 metabolism systemically given that changes in plasma P4 concentrations alone can influence parturition timing. In addition, injection of supplemental P4 or its more potent analog medroxyprogesterone acetate[148] (MPA) was the means by which we sidelined ovarian control over labor onset and obliged it instead to commence through uterus-intrinsic pathways. When left untreated, control C57BL/6 (B6) and *Il33*$^{-/-}$ mice showed similar plasma P4 concentrations on gestation day (GD) 16.5 and GD17.5 and the same luteolysis-induced decline in plasma P4 evident on GD18.5 (Figure 3.1A). Plasma P4 concentrations were also similar when the mice were injected daily with 2 mg P4; these concentrations, when measured 24 h post-injection, were ~2-3-fold higher than endogenous P4 concentrations prior to luteolysis (Figure 3.1A). When given a single injection of 250 μg depot medroxyprogesterone acetate (DMPA; also known as Depo-Provera) on GD12.5, both strains also showed similar plasma MPA concentrations on GD18.5-20.5 (Figure 3.1B). As expected[149], this depot formulation achieved constant plasma MPA concentrations (Figure 3.1B), which thus allowed us to create an experimental model that exposed the uterus to an extended period of constant P4 agonist activity, as is normally the case up until the time of luteolysis. Indeed, the injected DMPA was required

for the mice to remain pregnant past GD19.5 since they still underwent luteolysis as evidenced by their low plasma P4 concentration on GD18.5 onwards (Figure 3.1A).

Having thus established that IL-33 deficiency does not affect systemic P4 metabolism, we determined labor onset timing in pregnant B6 and *Il33*$^{-/-}$ mice that were either left untreated, thus allowing parturition to occur secondary to luteolysis, or injected with DMPA on GD12.5, thus obliging it to occur through uterus-intrinsic pathways (Figure 3.1C). Importantly, since P4 inhibits cervical ripening/dilation in mice[150], we scored labor onset in an inverse fashion, i.e. based upon whether the mice were still pregnant without evidence of dystocia or distress, which would, in addition to delivery itself, indicate the onset of strong uterine contraction (e.g., Figure 3.8A).

Following mating with B6 males, untreated B6 and *Il33*$^{-/-}$ females both delivered on ~GD19.5 (Figure 3.1D), in accord with luteolysis occurring 24 h earlier in both strains (Figure 3.1A). Also as expected, DMPA injection extended gestation length in B6 mice, by ~2-3 days. Accordingly, ~GD22.0 defined the day of labor onset that we consider to be "normal" for mice delivering through uterus-intrinsic pathways. By contrast, labor entry for DMPA-injected *Il33*$^{-/-}$ mice was delayed by yet another ~2 days (Figure 3.1D). This extended delay was unlikely due to altered P4 sensitivity or metabolism in the uterus, since uterine expression of genes encoding the progesterone receptor (PR; encoded by *Pgr*), 20α-HSD (*Akr1c18*) and the additional P4-metabolizing enzyme steroid 5α-reductase 1 (*Srd5a1*) was unaltered in *Il33*$^{-/-}$ mice (Figure 3.8B), nor could it be attributed to a difference in fetal or placental growth or the *Il33* heterozygosity of the pups, since fetal and placental weights were similar between the two groups (Figure 3.8C) and DMPA-injected B6 females mated to *Il33*$^{-/-}$ males entered labor at the same time as DMPA-injected B6 females mated to B6 males (Figure 3.1D). Litter size was moreover slightly

increased in *Il33*$^{-/-}$ mice, a situation that would be expected to predispose towards premature rather than delayed labor onset[92] (Figure 3.8C). Lastly, the identical parturition timing of untreated B6 and *Il33*$^{-/-}$ mice (Figure 3.1D) meant that the extended delay of DMPA-injected *Il33*$^{-/-}$ mice could not be explained by intrinsic defects in myometrial contractility. As exemplified by mice with defects in connexin 43 expression by SMCs[7], which prevents these cells from achieving the electrical coupling necessary for synchronous contraction, such defects would be expected to delay luteolysis-driven parturition onset. Together, these results suggest that maternal IL-33 plays a critical role in labor onset timing in mice when parturition occurs through uterus-intrinsic pathways.

PDGFRα^{+} *interstitial fibroblasts in the myometrium, undecidualized endometrium and mesometrial triangle are the main sources of IL-33 in the pregnant uterus.*

In order to identify potential cellular sources of IL-33 within the uterus, we performed a flow cytometric analysis of *Il33*$^{mCherry/+}$ mice bearing a nuclear localized *Il33* reporter construct[151]. For non-pregnant (NP) mice and pregnant mice on GD3.5 (i.e., one day prior to implantation), we analyzed the whole uterus as a unit. For pregnant mice on GD7.5, we dissected the decidua of each implantation site away from its overlying myometrium, and for GD11.5 onwards we additionally separated out the mesometrial triangle, the histologically distinct segment of the myometrium that abuts the decidua basalis (i.e., the portion of the decidua that in turn abuts the placenta; Figure 3.2A). Importantly, the non-mesometrial triangle portion of the myometrium at these later stages lacks an associated decidua and instead bears an undersurface of undecidualized endometrium replete with luminal epithelial cells (and so hereafter will be referred to as “myo/endo”; see Figure 3.2C). Accordingly, the decidua basalis constituted the

decidual tissue for these later time points. GD20.5 uteri came from mice injected daily with 2 mg P4 for four days starting on GD16.5. As with DMPA injection, this injection regimen, when continued, extended gestation length in B6 mice to ~GD22.5 (data not shown). To assess whether such injections might by themselves affect IL-33mCherry expression, a subset of mice analyzed on GD17.5 were injected daily with P4 for four days starting on GD13.5.

In line with *Il33* being transcriptionally silenced in decidual stromal cells[98], IL-33mCherry expression was not detected in these cells (Figure 3.2B, 3.9A and 3.10A). In contrast, IL-33mCherry was expressed by 10-30% of the stromal cells in the myometrium, myo/endo, and mesometrial triangle (Figure 3.2B and 3.10A). Importantly, percentages obtained on GD17.5 were the same whether or not the mice were P4-injected (Figure 3.2B), demonstrating that *Il33* expression in the prepartum uterus was not itself regulated by P4. Leukocytes were almost completely IL-33mCherry$^-$, and while endothelial and epithelial cells expressed low but appreciable IL-33mCherry in the myo/endo and mesometrial triangle on GD17.5 and GD20.5, they were outnumbered >10-fold by the stromal cells in these tissues (Figure 3.9B-D).

Importantly, IL-33mCherry expression within the stromal compartment was largely confined to cells expressing PDGFRα, a mesenchymal marker that also identifies IL-33-producing fibroblastic stromal cells in other organs[152] (Figure 3.2B, 3.10A). The PDGFRα$^+$ cells also expressed Sca-1 (Ly6A) and gp38 (podoplanin), two other stromal markers, but their expression of the contractile markers *Acta2* and *Myh11* was low. These latter markers were instead expressed by the PDGFRα$^-$ stromal cells, identifying them as SMCs and/or pericytes (Figure 3.10B-C). By immunofluorescence, PDGFRα$^+$ cells in the late gestation uterus were interspersed between muscle fibers in the myometrium and mesometrial triangle, where they were particularly abundant, and constituted a large fraction of endometrial stromal cells (Figure

3.2C). SMCs were PDGFRα$^-$, as were decidual stromal cells. Together, these observations indicate that the IL-33-expressing cells of the pregnant uterus were predominantly PDGFRα$^+$ interstitial fibroblasts, a population that comprises the stroma of the myo/endo and that densely populates the mesometrial triangle.

Il33 deletion in uterine interstitial fibroblasts delays labor onset.

To evaluate the labor induction requirements for IL-33 specifically produced by uterine PDGFRα$^+$ stromal cells, we measured parturition timing in mice bearing floxed *Il33* alleles and either a *Pdgfra-cre* driver to target inactivation to all PDGFRα-expressing cells, or a *Pgr-cre* driver to target inactivation to PR-expressing cells, which reside in reproductive tissues[104] (Figure 3.3A). In the late gestation uterus, *Pgr-cre*-targeted cells included ~90% of the PDGFRα$^+$ stromal cells in the myo/endo and mesometrial triangle (Figure 3.11). Importantly, DMPA-treated *Il33$^{fl/fl}$* mice entered labor at the same time as DMPA-treated B6 mice, confirming that homozygosity for a floxed *Il33* allele by itself had no effect on parturition timing (Figure 3.3B). By contrast, labor onset in DMPA-treated *Pdgfra-cre Il33$^{fl/fl}$* mice was delayed 2-3 days compared to DMPA-treated *Pdgfra-cre* mice (Figure 3.3C), and labor onset in DMPA-treated *Pgr-cre Il33$^{fl/fl}$* mice was delayed 2-3 days compared to DMPA-treated *Pgr-cre* mice (Figure 3.3D). Parturition onset in these two latter strains was somewhat earlier than expected considering the labor onset timing of DMPA-treated B6 and *Il33$^{fl/fl}$* mice, a shift that presumably reflects the fact that the *Pgr-cre* driver is a *Pgr* gene-disrupting allele, and so its presence likely reduces uterine responsiveness to MPA. All strains showed similar delivery times as B6 mice when not treated with DMPA (Figure 3.3B-D; the lack of an effect of the *Pgr-cre* driver in this case likely reflects the fact that luteolysis is an abrupt event associated with an abrupt decline in

plasma P4 concentrations). Together with the IL-33 and PDGFRα expression studies above, these results suggest that PDGFRα$^+$ interstitial fibroblasts of the myo/endo and mesometrial triangle with a history of PR expression are critical local sources of IL-33 when parturition proceeds via uterus-intrinsic pathways.

Prior to labor onset, ILC2s expand in the mesometrial triangle and become highly activated in an IL-33-dependent fashion.

IL-33 binds a dimeric cell surface receptor comprised of the IL-1 receptor accessory protein and an IL-33-specific subunit called ST2 (encoded by *Il1rl1*). Thus, we next performed flow cytometry to identify ST2-expressing cells in the uterus. We expected these cells would potentially mediate the parturition-promoting effects of IL-33, and that their respective activation states, to the extent that they were IL-33-dependent, would indicate presence of intrauterine IL-33 bioactivity. Cells with distinct ST2 staining were ILC2s, fractions of T helper 2 (Th2) and regulatory T (Treg) cells, and eosinophils (Figure 3.12A-E). Macrophages also stained positive for ST2, albeit dimly (Figure 3.12C-D). Focusing on the lymphoid compartment, we found that ST2$^+$ ILC2s, Th2 and Treg cells were rare in the NP uterus and the decidua, and that ST2$^+$ Th2 and Treg cell densities were similarly rare in the myometrium, myo/endo, and mesometrial triangle of pregnant mice (Figures 4A and 3.12F). By contrast, and consistent with prior work[153], ILC2s were present at moderate densities in these latter three tissues, where they constituted ~90% of all ST2$^+$ lymphoid cells. Moreover, ILC2 densities increased ~2-fold in the mesometrial triangle from GD15.5-20.5 (Figure 3.4A). This increase occurred earlier in B6 mice than in *Il33*$^{-/-}$ mice, revealing not only that IL-33 promoted uterine ILC2 proliferation/accumulation in the prepartum uterus, but also that its impact in the mesometrial triangle started becoming apparent

around GD17.5.

Next, we assessed the activation state of uterine ILC2 by measuring production of their signature type 2 cytokines IL-5 and IL-13 (Figure 3.4B, C). Consistent with prior work[153], all uterine ILC2s in B6 and *Il33*$^{-/-}$ mice expressed at least some amount of IL-5 judged in comparison to isotype-stained controls. In addition, ~30% of ILC2s in the GD7.5 myometrium expressed high amounts of IL-5 as well as IL-13. This level of expression was equivalent between B6 and *Il33*$^{-/-}$ mice, indicating that it was not driven by IL-33. IL-5 and IL-13 expression perhaps mildly subsided through mid-gestation but then clearly increased in late gestation in B6 mice starting on ~GD18.5. Particularly high expression was observed in the mesometrial triangle, where ~80% of ILC2s were IL-5^{hi} IL-13^{+} by GD20.5. This late gestational phase of IL-5 and IL-13 expression was not a consequence of the exogenous P4 given to extend gestation length past GD19.5 since uterine ILC2s in B6 mice given the same P4 regimen prior to sacrifice on GD18.5 showed the same percentage of IL-5^{hi} IL-13^{+} cells as their untreated counterparts. On the other hand, IL-5 and IL-13 induction was not observed in *Il33*$^{-/-}$ mice, demonstrating that it required IL-33. These results thus support the idea that IL-33 bioactivity increases within the mesometrial triangle over the few days before labor onset, and suggested a parallel but less intense increase in IL-33 bioactivity in the myo/endo.

We further defined the location of ILC2s in the late gestation uterus by performing thick section immunofluorescence microscopy in conjunction with *Il5-cre*R26RFP mice, which mark as RFP^{+} all cells with a history of IL-5 expression, i.e., ILC2s and rare T cells[152]. In confirmation of our flow cytometric analysis, the marked cells were absent from the decidua on GD17.5 but were present in the myo/endo and mesometrial triangle (Figure 3.5). In the myo/endo, they were located between muscle fibers and were especially concentrated in the endometrium. In the

mesometrial triangle, they showed an association with larger blood vessels and smooth muscle fibers but were otherwise relatively uniformly distributed.

ILC2 depletion or loss of ILC2 responsiveness to IL-33 delays labor onset.

To functionally assess whether IL-33 acts through ILC2s to promote labor onset, we first employed a model of diphtheria toxin- (DT-) inducible ILC2 depletion (*Il5-cre* iDTR mice) in which the constitutively active *Rosa26* locus expresses a Cre-inducible DT receptor (iDTR), and one *Il5* locus bears a knocked-in Cre driver to target iDTR expression to cells with a history of IL-5 expression (i.e., ILC2s and rare T cells, as above). Accordingly, DT injection every other day from GD12.5 achieved a ~50% decrease in ILC2 density in the myo/endo and mesometrial triangle by GD18.5 compared to control, DT-treated *Il5-cre* mice (Figure 3.6A). When given DMPA, these DT-treated mice showed a ~1-2 day extended delay in labor onset compared to control DMPA- DT-treated *Il5-cre* mice, which themselves showed no difference in labor onset timing compared to DMPA-treated *Il5-cre* mice (Figure 3.6B). We also evaluated parturition timing in *Il5-cre Il1rl1*$^{fl/fl}$ mice in which *Il1rl1* deletion is similarly targeted to ILC2s and rare T cells. These mice demonstrated a loss of surface ST2 on ~75% of uterine ILC2s (Figure 3.6C), and, with DMPA-treatment, a ~2-day extended delay in labor onset compared to control DMPA-treated *Il5-cre* and DMPA-treated *Il1rl1*$^{fl/fl}$ mice (Figure 3.6D). By contrast, DMPA-treated *Rag2*$^{-/-}$ mice deficient in T and B cells but not ILC2s delivered at the same time as DMPA-treated B6 mice (Figure 3.6E). All these strains delivered at the same time as B6 mice when not given DMPA (Figure 3.6B, 6D and 6E). Together, these data indicated that IL-33 promotes labor onset through effects on ILC2s, potentially including those residing in the uterus.

Decidual Ptgs2 induction is downstream of IL-33 in the prepartum uterus, but is non-essential for on time labor onset.

We next sought additional insight into IL-33-induced parturition mechanisms by performing RNA-sequencing (RNA-Seq) on dissected uterine tissue layers of pregnant B6 and *Il33*$^{-/-}$ mice. The tissues were collected on GD18.5 and the mice were not treated with DMPA nor P4. Notably, the gene expression differences across the two genotypes were relatively minor, with almost no difference reaching an *FDR* of less that 0.05 (Figure 3.13A, Table 3.1, and GSE181904). This lack of a difference was consistent with the lack of a parturition delay in *Il33*$^{-/-}$ mice when luteolysis was available to induce labor onset (Figure 3.1D), and reinforced the notion that the parturition delay in DMPA-treated *Il33*$^{-/-}$ mice was not due to a cell-intrinsic defect in myometrial SMC maturation or function. The expression of genes encoding ILC2-derived factors such as IL-5 and IL-13 were not detectable in mice of either genotype, likely reflecting the relative scarcity of uterine ILC2s.

Despite so few expression differences, *Ptgs2*, encoding the prostaglandin synthesis enzyme COX-2, emerged as the most down-regulated protein-coding gene in the *Il33*$^{-/-}$ decidua on GD18.5 (~2.5-fold, p_{raw}=0.007; Figure 3.13A). This observation was notable since COX-2 induction is the signature hallmark of "decidual activation," a poorly understood process that has nonetheless been considered a key event in human parturition given the contractile effects of the prostaglandin species consequently produced[95]. Indeed, *Ptgs2* mRNA and COX-2 protein expression were also lower on GD20.5 in the *Il33*$^{-/-}$ decidua (Figure 3.13B-C), as were PGE_2 concentrations, a finding attributable to reduced production rather than increased metabolism since decidual concentrations of PGE metabolites were reduced in parallel on GD20.5 and were almost undetectable in the *Il33*$^{-/-}$ decidua (Figure 3.13D). In contrast to the decidua, *Ptgs2*

expression was unaltered in the myo/endo and mesometrial triangle, where absolute expression was much less to begin with (Figure 3.13B). In addition, the expression of *Ptgs1*, encoding the second prostaglandin synthesis enzyme COX-1, as well as the concentrations of $PGF_{2\alpha}$ and PGD_2, prostaglandin species produced at high amounts in the prepartum mouse uterus in a COX-1-dependent fashion[1,154,155], were unaltered in all tissue layers (Figure 3.13D).

Notwithstanding these indications that IL-33 might promote parturition onset by inducing decidual COX-2 expression, the injection of DMPA-treated B6 mice with SC-236, a long-acting and selective COX-2 inhibitor, did not further extend gestation length (Figure 3.13E). As expected [59], the same dosing nonetheless inhibited inflammation-induced PTL (data not shown). Thus, decidual COX-2 induction was not a key component of the IL-33-regulated parturition cascade. These observations are in line with the thought that COX-2-derived prostaglandins foster the progression of non-inflammation-associated labor rather than trigger its onset [65]. Moreover, they raise the possibly that decidual activation, rather than being a determinant of labor onset timing in humans as has been suggested[95], is instead a byproduct of labor-inducing events taking place in the myometrium.

Eosinophil turnover increases in the prepartum uterus and IL-5 is required for on time labor onset via uterus-intrinsic parturition pathways.

Given their function as IL-33- and IL-5-regulated effectors of type 2 immunity, we next evaluated the possibility that eosinophils instead served as effectors of the labor cascade. On GD16.5, uterine eosinophils were rare and their densities were respectively similar in B6 and *Il33*$^{-/-}$ mice across all three tissue layers, with P4 treatment causing mild, genotype-independent and largely statistically insignificant density reductions (Figure 3.7A). After this point, however,

eosinophil densities diverged between the two genotypes, with *Il33*$^{-/-}$ mice showing marked reductions on GD18.5 (in P4-untreated mice) and GD20.5 (in P4-treated mice) in all tissue layers (Figure 3.7A). Indeed, eosinophils were barely detectable in the GD18.5 and GD20.5 myo/endo and mesometrial triangle of *Il33*$^{-/-}$ mice. A parallel decline was also apparent in B6 mice, but it was more modest. Uterine eosinophil tissue densities were consequently much lower in *Il33*$^{-/-}$ mice than in B6 mice on GD18.5 and GD20.5 (Figure 3.7A). Importantly, blood eosinophil frequencies were also greatly reduced in *Il33*$^{-/-}$ mice (Figure 3.7B, left). This observation is consistent with prior work establishing that IL-33 is required for optimal eosinophilopoiesis[156] and suggested that the pronounced loss of eosinophils from the prepartum uteri of *Il33*$^{-/-}$ mice was at least partly due to their paucity of blood eosinophils. Consistent with this possibility, *Pgr-cre Il33*$^{f/f}$ mice with reproductive tissue-targeted *Il33* deletion showed similar uterine eosinophil densities on GD20.5 compared to both *Pgr-cre* and B6 controls, and a less severe and statistically insignificant reduction in blood eosinophil frequencies compared to B6 mice (Figure 3.7B, 7C; of note, within the interpretive limits imposed by the wide variance of these data, blood eosinophil frequencies in *Pgr-cre Il33*$^{f/f}$ and *Pgr-cre* mice were similar to each other yet somewhat reduced compared to B6 mice suggesting that the loss of one *Pgr* allele affects eosinophilopoiesis). Our findings with respect to gestation day- and genotype-dependent differences in uterine eosinophil tissue densities were corroborated when we calculated eosinophils as percentages of the total leukocytes that respectively reside within each uterine tissue layer (Figure 3.14A, 14B). Together, these observations thus suggest that uterine eosinophil turnover increases over the days leading up to labor onset, potentially through uterine IL-33-independent pathways, with increased recruitment from the blood necessary to offset increased intrauterine eosinophil death. Such death could be the result of the eosinophils

performing death-inducing effector functions such as cytolysis[157].

To gain further support for the idea that eosinophil turnover increases in the prepartum uterus, we took advantage of the prior observation that eosinophils with longer tissue-residence times upregulate expression of the integrin subunit CD11c in certain contexts[158]. Accordingly, we assessed CD11c expression by uterine eosinophils in P4-injected B6 mice while also employing the intravenous injection of PerCP-Cy5.5-conjugated anti-CD45 antibodies to discriminate extravascular (PerCP-Cy5.5^{lo}) from intravascular (PerCP-Cy5.5^{hi}) cells[159] (Figure 3.7D, 7E). As expected, uterine eosinophils in the intravascular compartment did not express CD11c. By contrast, ~25-35% of the extravascular eosinophils in the myo/endo and mesometrial triangle were CD11c^{+} on GD16.5, suggesting that at least these cells were not recent recruits from the blood. On GD20.5, however, CD11c^{+} percentages had substantially declined. These observations were consistent with the idea that eosinophil turnover increases in the uterus prior to labor onset since they implied that the cells with longer tissue residence had died and that the dynamics of the remaining cells were not at steady-state.

Of note, exogenous P4 treatment increased the percentage of CD11c^{+} cells in the GD16.5 myo/endo and mesometrial triangle of both B6 and *Il33*$^{-/-}$ mice (Figure 3.14C). Together with its aforementioned ability to mildly reduce uterine eosinophil tissue densities (Figure 3.7A), exogenous P4 thus appeared to have a suppressive effect on uterine eosinophil turnover in the prepartum uterus. This possibility is consistent with the known effects of ovarian hormones on uterine eosinophil dynamics[160,161]. Locally-produced factors also appeared to control eosinophil phenotypes in the prepartum uterus, as CD11c expression by decidual eosinophils was low on GD16.5 in mice injected with P4 (Figure 3.7D, 7E, and 3.14C).

Lastly, we assessed parturition timing in *Il5*$^{-/-}$ mice to determine whether eosinophils

functionally contributed to uterus-intrinsic parturition pathways. IL-5 is an activator of mature eosinophils as well as a critical eosinophil development and survival factor, as demonstrated by the profound reductions in eosinophil numbers in the blood and tissues of *Il5*$^{-/-}$ mice[157,162,163]. Such reductions were also apparent in the late gestation uterus of *Il5*$^{-/-}$ mice (Figure 3.14D). As expected from prior work[164], *Il5*$^{-/-}$ mice delivered on time when not DMPA-treated. In contrast, DMPA-injected *Il5*$^{-/-}$ mice showed an extended delay in parturition onset compared to DMPA-injected B6 controls (Figure 3.7F). Since an extended parturition delay was not apparent in DMPA-injected *Rag2*$^{-/-}$ mice deficient in B cells (Figure 3.6E), the only other cell type thought to be a direct IL-5 target in mice[162,165], these observations strongly implicated a role for eosinophils in uterus-intrinsic parturition pathways. Of note, the injection of DMPA-treated B6 mice with antibodies towards CCR3, a chemokine receptor expressed by eosinophils, did not appreciably extend gestation length compared to isotype-injected controls (Figure 3.14E). As expected from the ability of these antibodies to deplete eosinophils[166], this injection substantially depleted eosinophils from the blood as well as from the GD20.5 decidua and mesometrial triangle (Figure 3.14D, 3.14F). However, eosinophil depletion was less robust in the myo/endo, and the depletion seen in the decidua did not reach that achieved by IL-5 deficiency (Figure 3.14F). Together with the observation of delayed onset in *Il5*$^{-/-}$ mice, these data suggest that eosinophils in the myo/endo and possibly the decidua are sufficient to trigger on time labor onset. They are also consistent with the idea that IL-5 produced within the uterus helps to locally activate eosinophils to promote labor onset. It is also possible that IL-5 promotes labor onset by acting on a previously unrecognized non-eosinophil, non-B cell target cell within the uterus.

Discussion

Mechanisms of parturition induction, a question with major implications for maternal-fetal health, remain largely undefined. In this study, we dissect these mechanisms in mice under experimental conditions that oblige labor onset to rely upon uterus intrinsic pathways, as they normally do in humans. Under these conditions, we implicate several components of innate type 2 immunity as key contributors of the parturition cascade. These findings contrast with prior ones that ruled out roles for components of type 2 immunity when parturition is driven by luteolysis (e.g., in mast cell- and eosinophil-deficient mice[164,167], thus emphasizing the different physiologies at play and revealing that exogenous progestin administration can be used to uncover previously unrecognized components of the parturition cascade.

Importantly, some of our experiments employed mice with systemic defects in type 2 immunity. In these cases, we cannot directly establish the extent to which parturition delay phenotypes are due to altered immune activity within the uterus itself. For example, reduced eosinophilopoiesis likely contributes to the extended parturition delay of DMPA-treated *Il33*$^{-/-}$ mice given that eosinophils are themselves required for on time parturition onset and their low frequency in the blood likely contributes to their low tissue densities in the prepartum *Il33*$^{-/-}$ uterus. Similarly, reduced eosinophilopoiesis likely contributes to the parturition delays of DMPA-treated *Il5-cre* iDTR mice and *Il5-cre Il1rl1*$^{fl/fl}$ mice, given that *Rag2*$^{-/-}$ *Il2rg*$^{-/-}$ mice lacking ILC2s and *Il1rl1*$^{-/-}$ mice with global ST2 deficiency also bear reduced numbers of blood eosinophils[156,158]. However, our data also reveal increased activity of type 2 immunity in the prepartum uterus and a local requirement for this activity in stimulating labor onset. Specifically, in the days leading up to labor onset we observed increased uterine eosinophil turnover and IL-33-dependent expansion and activation of uterine ILC2s, as well as an extended parturition delay

in DMPA-treated *Pgr-cre Il33*$^{f/f}$ mice. These latter mice target *Il33* deletion to cells of reproductive tissues, including the interstitial fibroblasts of the uterus that express high amounts of IL-33. Moreover, they did not show reductions in uterine eosinophil tissue densities, indicating that their parturition delay is independent of processes that might reduce eosinophil numbers in the uterus.

Considering how type 2 immune circuitry within peripheral tissues is currently conceptualized, these observations suggest a two-pronged general model for how type 2 immunity promotes labor onset in mice. In the first prong, IL-33 activity is generated in the prepartum uterus and acts locally on ILC2s, eosinophils, and other IL-33 responsive cells. These latter cells likely include uterine macrophages, given that they express low amounts of ST2, as well as mast cells given that mast cells are present in the mouse uterus and classically express ST2[146,168], even though we could not detect them by flow cytometry. In response, these cell types produce factors that in turn directly or indirectly promote uterine SMC contraction, perhaps in ways that are akin to those that promote SMC contraction in the lung and gut during classical type 2-associated immune responses (asthma, helminth clearance, etc.). In the second prong, prepartum activation of an as yet unidentified but IL-33-independent pathway promotes uterine eosinophil turnover and perhaps also eosinophil effector function. This pathway appears to be active within all uterine tissue layers and might also contribute to the component of ILC2 expansion in the prepartum mesometrial triangle that is IL-33-independent. It also appears to be suppressed by P4 given that the uterine eosinophils of mice supplemented with exogenous P4 prior to sacrifice on GD16.5 show increased positivity for CD11c and slight reductions in uterine eosinophil tissue densities.

Although many details of this model remain to be clarified, it is worth specifically discussing how IL-33 bioactivity might be generated in the late gestation uterus, since elucidation of this question could help identify more upstream components of the labor cascade. One possibility is that it is generated by the low-grade inflammation characteristic of the late gestation uterus[95,144]. This idea is in line with the classical view of IL-33 being a nucleus-sequestered alarmin released in response to noxious stimuli, as well as with the ability of inflammation-associated proteases to process IL-33 into more active forms[146,169]. Such inflammation might be related to the second prong of type 2 immune activation mentioned above. Uterine stretch might also generate IL-33 bioactivity given that IL-33 can be released from living cells in response to mechanical tension[170]. Lastly, given that ILC2s are regulated by multiple factors, it is possible that their activation in late gestation does not reflect greater IL-33 bioactivity per se, but rather synergy between constant ST2 signaling and increased signaling via other inputs.

Of note, PGD_2, another type 2 immune regulator with activating and chemotactic effects on ILC2s and eosinophils[171], is abundantly produced in the prepartum uterus in a COX-1-dependent fashion[154,155]. Due to its pro-contractile effects on myometrial tissue strips assayed *in vitro*, this prostaglandin species has been suggested to contribute to labor induction by directly promoting myometrial SMC contractility[155,172]. However, our results raise the possibility that it may also promote labor onset in part by stimulating type 2 immunity, potentially as a component of the second prong described above given that its production is not dependent upon IL-33. Additional work will be required to evaluate this possibility. Additional work will also be required to evaluate the roles of factors produced by ILC2s, which in the context of the prepartum uterus may be complex. For example, uterine ILC2-derived IL-5 might promote both

the survival and death of uterine eosinophils through inhibitory and stimulatory effects on eosinophil apoptosis and effector function, respectively[157,163].

Further evaluation of the role of type 2 immunity in mouse parturition will also need to consider the seemingly specialized function of the mesometrial triangle, with its massive population of IL-33-expressing interstitial fibroblasts and its accumulation of ILC2s that become activated in late gestation and localize to larger blood vessels and dispersed muscle fibers. This structure also houses large numbers of NK cells and dendritic cells[159,173], and appears to originate the electrical activity that drives uterine contractions[174]. We therefore speculate that it serves as a hub that integrates information from multiple sources to ensure that labor commences only when all tissue compartments are sufficiently mature. Indeed, the potential importance of the mesometrial triangle is also suggested by the upstream role of IL-33 in promoting decidual activation, even though such activation appears to be non-essential for on time labor onset.

Of note, potential roles for IL-33 in mouse pregnancy prior to labor onset were the subject of a recent paper by Valero-Pacheco et al.[175]. This paper identified the interstitial fibroblasts of the myo/endo as the major producers of IL-33 of the pregnant uterus, in accord with the data presented here. However, we could not confirm certain other aspects of the work, including its suggestion that decidual stromal and endothelial cells are major IL-33 producers, or that maternal IL-33 deficiency mildly reduces fetal weights and litter sizes in late gestation. The study also reported that IL-33 deficiency alters the development and vascularization of GD7.5-9.5 implantation sites. While provocative with respect to mechanisms of early pregnancy success or failure, such alterations are unlikely the cause of the parturition delay seen in *Il33*$^{-/-}$ mice, since this delay was also apparent when we ablated ILC2s starting on GD12.5. Moreover, since our RNA-Seq analysis performed on GD18.5 revealed only minimal gene expression differences

between the respective uterine tissue layers of B6 and *Il33*$^{-/-}$ mice, the alterations observed in early gestation by Valero-Pacheco et al. did not appear to have substantial downstream consequences for late gestation.

Although our use of progestin supplementation creates an endocrine state in mice that models the conditions under which parturition occurs in humans, further work will be needed to determine the extent to which the pathways we thus uncovered are relevant to humans. Notably, increased circulating concentrations of soluble ST2, a secreted, alternative splice form of ST2 that acts as an IL-33 decoy receptor, has recently been reported as being predictive of impending labor onset in pregnant women[176]. These observations were interpreted as reflecting a labor-inhibiting role for IL-33, in line with suggestions stemming from work on PTL pathways in mice[177]. However, this latter study did not directly assess labor onset timing in *Il33*$^{-/-}$ mice, and the increase in circulating soluble ST2 in humans might instead reflect a counter-regulatory response induced by the low-grade inflammation characteristic of the prepartum uterus[95,144] given that inflammation is frequently associated with increased soluble ST2 production[178]. Indeed, our data showing that type 2 immunity is required for on time labor onset in mice is consistent with several lines of evidence suggesting that type 2 immunity promotes parturition in humans. Most recently, ILC2s have been detected in the human decidua basalis at term and have been shown to be the most abundant ILC in the human decidua parietalis, a tissue layer that is anatomically analogous to the undecidualized endometrium on the undersurface of the mouse myometrium where we find ILC2s to be abundant. In both locations, the cells show increased densities in cases of PTL[179,180]. Older data has moreover found associations with PTL and the presence of eosinophils in the amniotic fluid, and case reports exist of type I allergic reactions triggering PTL[181]. Type I allergic reactions can also trigger PTL in guinea pigs, which, like

humans, enter labor without a drop in plasma P4 concentrations[182]. Whether or not ILC2s are present in the human myometrium has not yet been described, and unfortunately their scarcity may preclude their detection by single cell RNA sequencing. Together, however, these results indicate the ability of type 2 immune pathways to foster pathological labor onset in humans, raising the possibility that components of these pathways also contribute to normal parturition.

Limitations of the Study

This study presents evidence that innate type 2 immunity plays an important role in the control of parturition onset in mice when their endocrine state is manipulated experimentally to mimic the context of human parturition. One limitation of our study is our use of genetic models with systemic immunological effects. This limits our ability to interpret certain cases of delayed parturition as being due to altered activity of cells residing within pregnant uterus itself. Although mitigated by the delayed parturition phenotype of *Pgr-cre Il33*$^{f/f}$ mice with reproductive tissue-targeted IL-33 deficiency, this limitation applies to experiments using *Il33*$^{-/-}$, *Il5-cre* iDTR and *Il5-cre Il1rl1*$^{fl/fl}$ mice. Given the systemic loss of eosinophils seen in *Il5*$^{-/-}$ mice, we are similarly unable to determine the extent to which ILC2-derived IL-5 promotes parturition onset by locally activating uterine eosinophils. We moreover cannot rule out the possibility that IL-5 promotes parturition onset through direct effects on a non-eosinophil, non-B cell target cell expressing the IL-5 receptor. Our study does not identify upstream triggers of innate type 2 immune activity within the late gestation uterus, nor how such activity leads to increased myometrial contractility. Lastly, we present progestin supplementation in mice as an experimentally tractable model for dissecting parturition mechanisms potentially relevant to human parturition. Whether activation of innate type 2 immunity, which we thus uncover as an

important mechanism in this context, plays a role in human parturition will need its own direct experimental validation. Additional experiments are also needed to assess the role of innate type 2 immunity in inflammation-induced preterm birth in both mice and humans.

Acknowledgements

We thank Zhi-En Wang for performing cell sorting, Sofía Bustamante Eguiguren for assistance with the histology, Walter Eckalbar for assistance with the RNA-Seq analysis, and Gabrielle Rizzuto for comments on the manuscript. The graphical abstract was created in BioRender.com. Supported by NIH-NIAID R01AI150191 to A.E.

Author Contributions

J.S., T.I.M., K.M.C., K.M., and D.R. performed experiments. J.S., A.B.M, and A.E. designed experiments. J.S. and A.E. analyzed data and wrote and edited the manuscript. A.B.M. and T.I. M. edited the manuscript. A.E. conceived of the project and supervised the research.

Figures

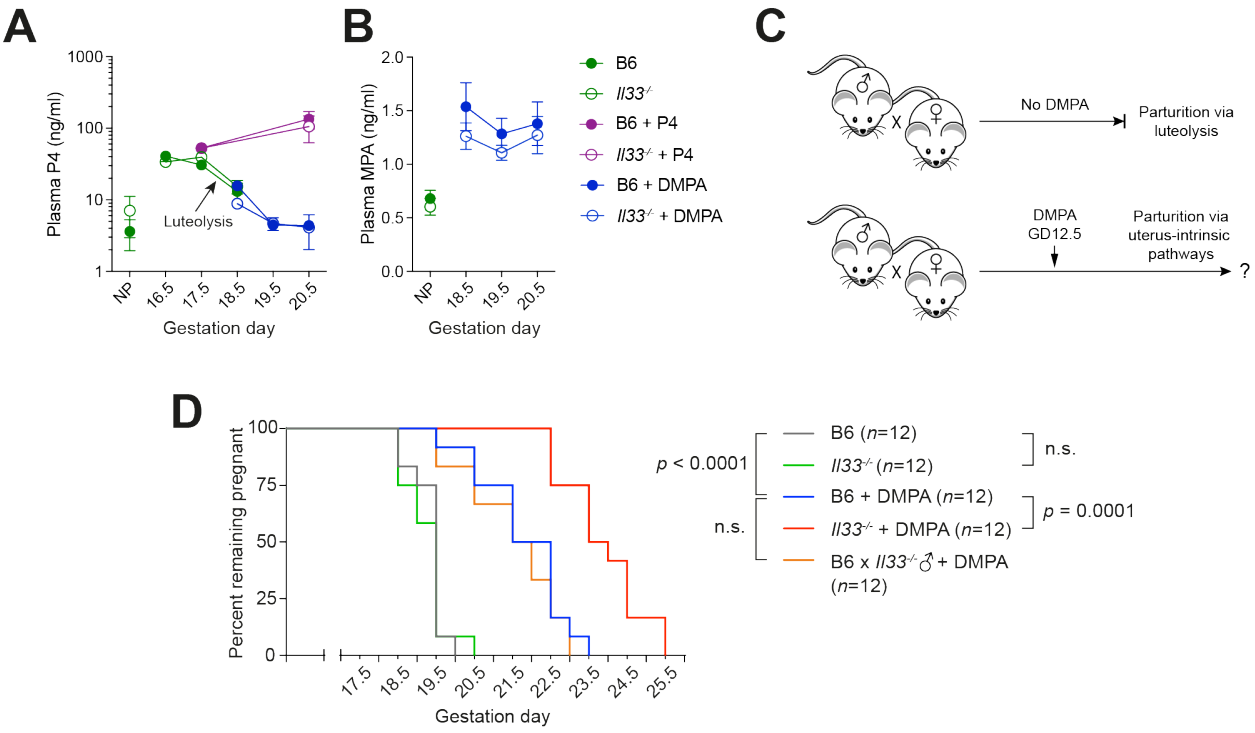

Figure 3.1 IL-33 deficiency delays labor onset in mice when parturition occurs through uterus-intrinsic pathways.

(**A**) Late gestation plasma P4 concentrations, assessed by ELISA, in untreated mice, mice injected daily with 2 mg P4 starting on GD16.5, and mice injected once on GD12.5 with 250 µg DMPA. Untreated, NP mice are also shown. *n*=3-6 mice/group; mean+/-SEM. (**B**) Late gestation plasma MPA concentrations, assessed by ELISA, in mice injected with DMPA on GD12.5 (*n*=6 mice/group; mean+/-SEM). Data for NP mice demonstrate the ELISA background (*n*=3 mice/group). (**C**) Schematic of parturition timing experiments. In the absence of DMPA administration, mice enter labor on ~GD19.5 as the result of luteolysis. DMPA administration, which extends gestation length, allows for the evaluation of uterus-intrinsic parturition pathways. Maintaining pregnancy this way causes 100% fetal demise by GD22.5, presumably due to fetal overgrowth or uterine contraction against a closed cervix (e.g., Figure 3.8A). (**D**) Parturition timing in *Il33*$^{-/-}$ and control B6 mice that were either untreated or injected with DMPA on GD12.5. Groups were compared by the log-rank test. Females were mated with B6 males unless otherwise indicated. See also Figure 3.8.

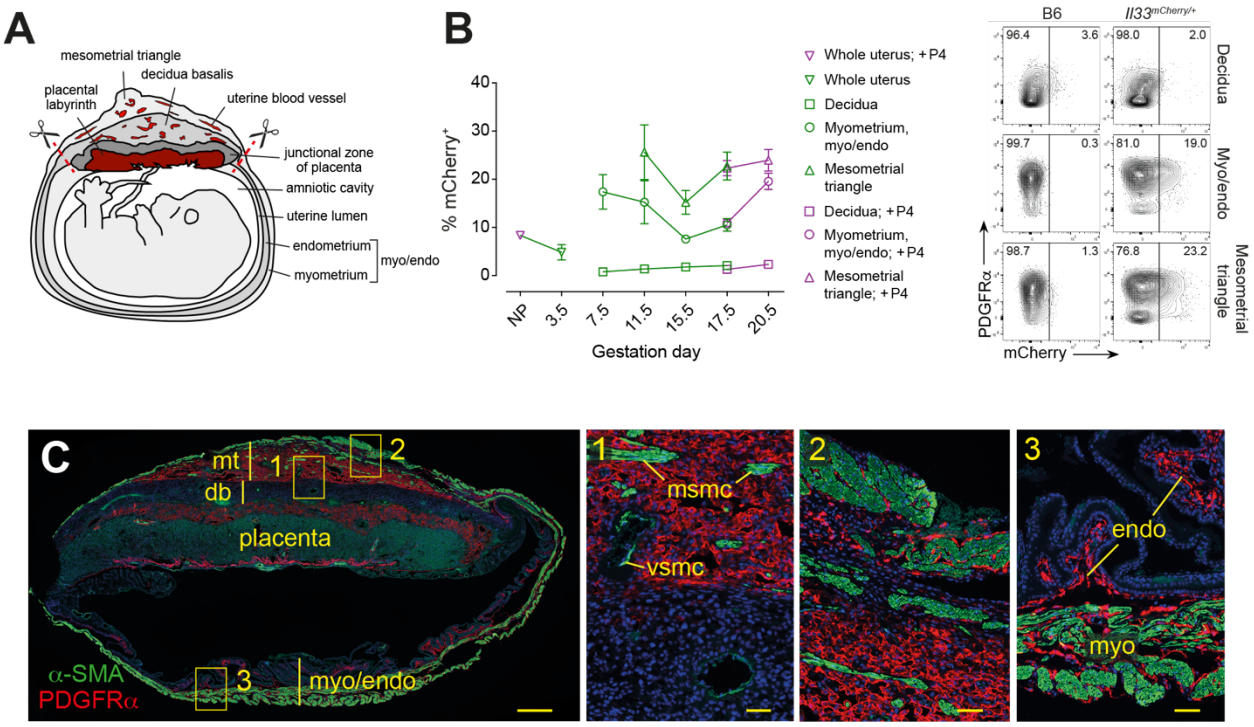

Figure 3.2 Myo/endo and mesometrial triangle PDGFRα$^+$ stromal cells are the main sources of IL-33 in the pregnant uterus.

(**A**) Schematic of an implantation site on ~GD13.5. Red dashed lines show where we separate the mesometrial triangle from the myo/endo. (**B**) Percent IL-33mCherry positivity among stromal (CD45$^-$ ICAM2$^-$ EpCAM$^-$) cells of the NP and pregnant uterus in *Il33$^{mCherry/+}$ mice*, as determined by flow cytometry (*n*=5 mice/group; mean+/-SEM; see Figure 3.9A for gating). Representative contour plots with PDGFRα co-staining (*n*=5 mice/group collected over 2-3 independent experiments per genotype) are shown for *mice* on GD20.5; Figure 3.10A shows plots for all time points. The mCherry gate was placed so that less than 1% of the stromal cells in B6 mice on GD17.5 were mCherry$^+$. P4 was given to non-pregnant mice to establish a pregnancy-like endocrine state. (**C**) PDGFRα immunostaining of an GD18.5 implantation site, with bracketed areas shown in close-up (representative of *n*=4 B6 mice). The embryo was removed before fixation. α-smooth muscle actin (α-SMA) identifies SMCs. db, decidua basalis; mt, mesometrial triangle; myo, myometrium; endo, endometrium. Note that the mesometrial triangle contains both vascular SMCs (vsmc) and myometrial SMC bundles (msmc), which are characteristically dispersed at this anatomic location. Scale bars: 500 μm (left panel); 50 μm (three right panels). See also Figures 3.9 and 3.10.

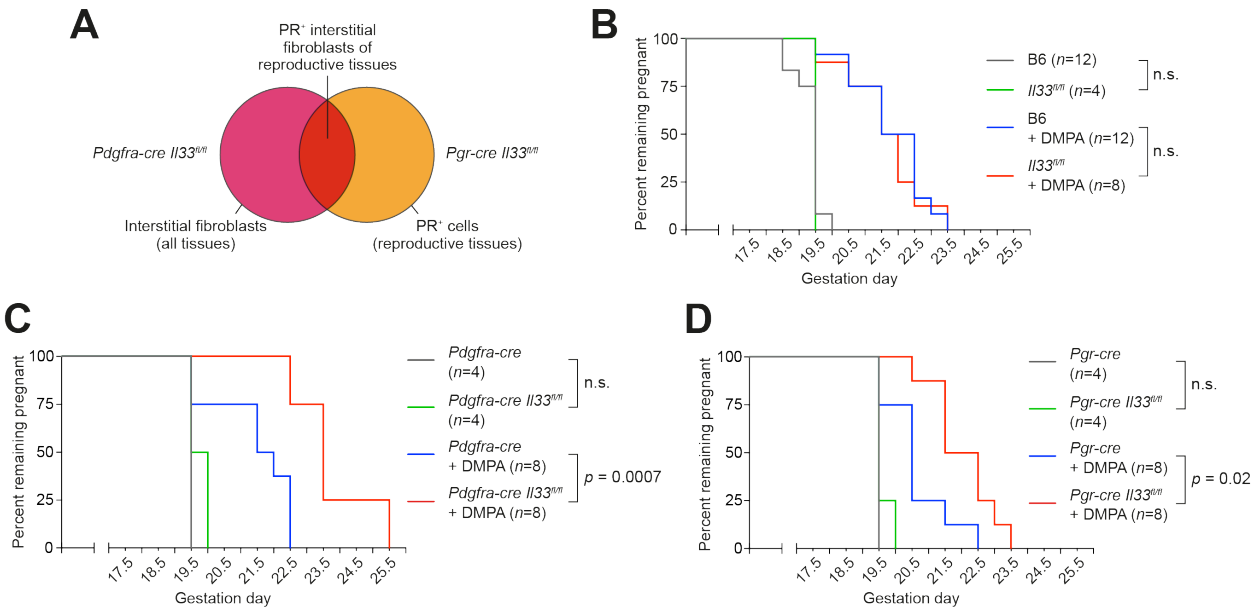

Figure 3.3 Cell type-specific requirements for *Il33* expression in parturition.

(**A**) Schematic of cell types targeted for *Il33* deletion. The *Pdgfra-cre* experiment used mice hemizygous for a *Pdgfra-cre* transgene and the *Pgr-cre* experiment used mice heterozygous for a *Pgr* allele bearing a targeted *cre* construct. Targeted cells common to both experiments are interstitial fibroblasts of reproductive organs, including the uterus. (**B-D**) Parturition timing. Where indicated, mice were injected with DMPA on GD12.5. B6 mice are the same as in Figure 3.1D. Groups were compared by the log-rank test. See also Figure 3.11.

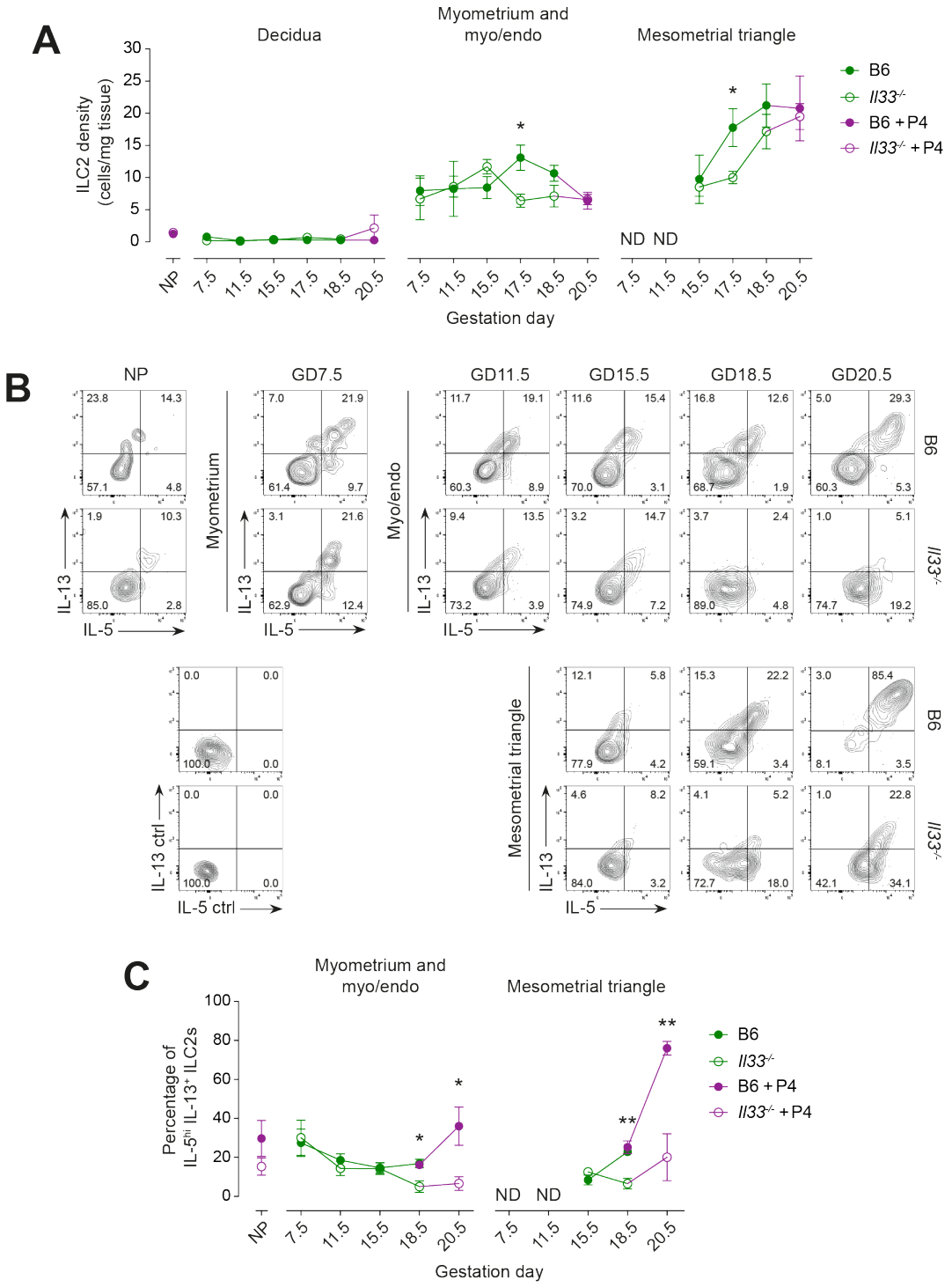

Figure 3.4 IL-33 dependent uterine ILC2 expansion and activation shortly before labor onset.

(Figure caption continued on the next page)

Figure 3.4. (Figure caption continued from the previous page) Where indicated, mice were given daily P4 injections starting on GD16.5 to extend gestation to GD20.5, or starting on GD14.5 prior to sacrifice on GD18.5 to assess the effects of P4 injection per se. (**A**) ILC2 tissue densities in whole NP uteri and dissected uterine tissue layers of B6 and *Il33*$^{-/-}$ mice, as determined by flow cytometry. *, $p<0.05$ by Student's *t*-test ($n=6$ mice/group; mean+/-SEM). ND, not determined. (**B, C**) IL-5 and IL-13 production by uterine ILC2s. Uterine cell suspensions were stimulated ex vivo with PMA/ionomycin, and IL-5/13 expression was assessed by intracellular staining. Panel B shows representative contour plots ($n=4$ mice/group collected over 2-5 independent experiments per time point), including isotype control (ctrl) staining for the GD18.5 mesometrial triangle; panel C shows quantified percentages of IL-5^{hi} IL-13^{+} ILC2s. *, $p<0.05$; **, $p<0.01$ by Student's *t*-test ($n=4$ mice/group; mean+/-SEM). See also Figure 3.12.

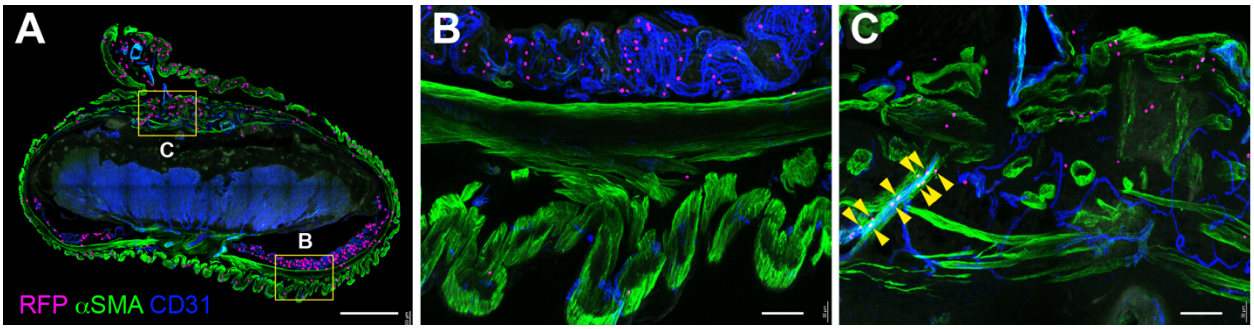

Figure 3.5 Distribution of ILC2s in the late gestation uterus.

Anti-RFP immunofluorescence was performed on 300 μm sections of GD17.5 implantation sites from *Il5-cre*R26RFP mice, in which *Il5-cre*-mediated recombination induces high, permanent, RFP (tdTomato) expression in ILC2s and rare T cells. Embryos were removed before fixation. The sections were co-stained with antibodies to α-SMA and CD31 to visualize SMCs and endothelial cells, respectively. RFP^+ cells were artificially surfaced in (**A**) so that they would be evident in the panoramic view. Note the RFP^+ cells associated with myometrial SMC bundles and vascular structures, including an arteriole coated with vascular SMCs (**C**; arrowheads). Data are representative of *n*=4 mice. Scale bars: 1 μm (**A**); 100 μm (**B**, **C**).

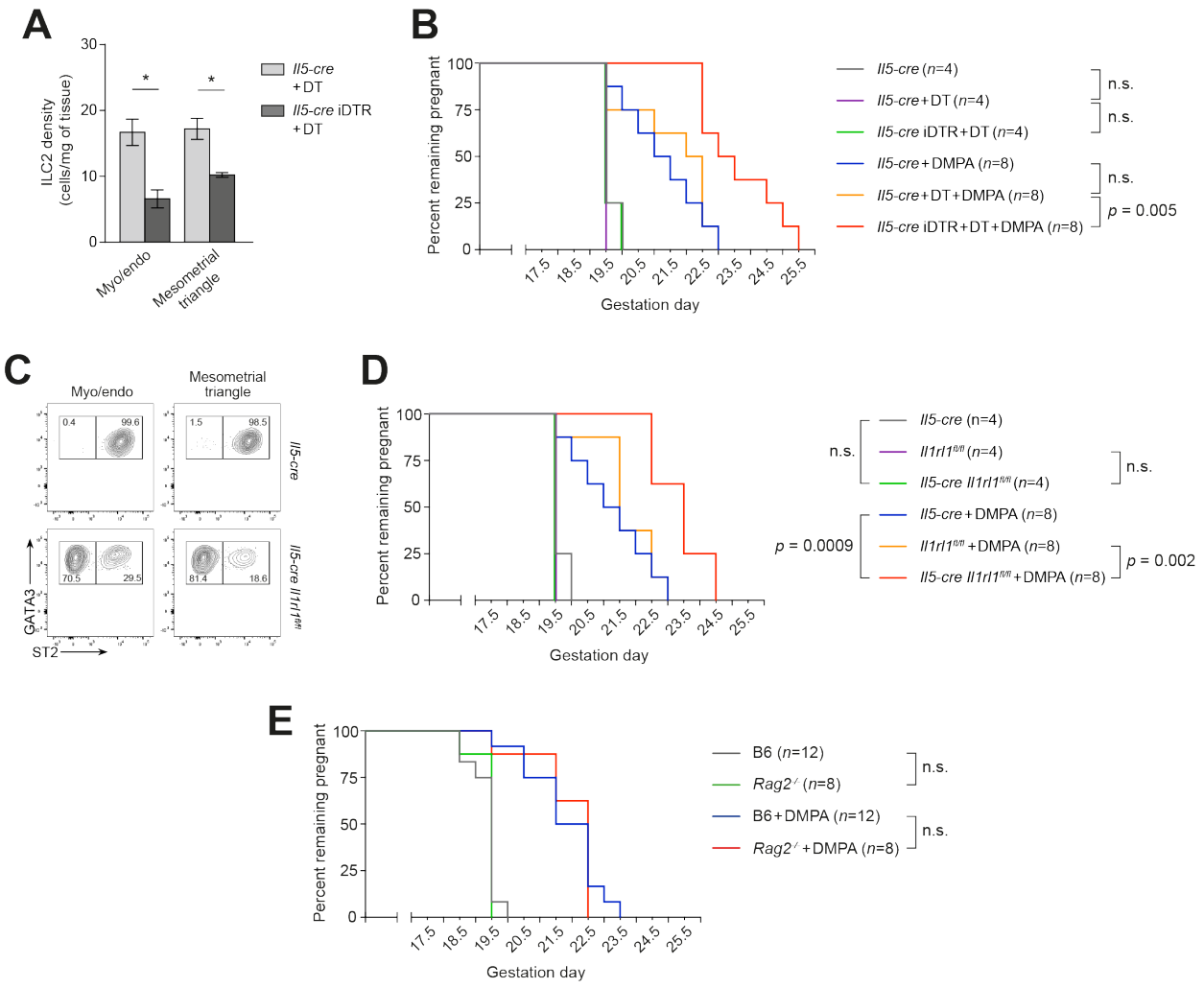

Figure 3.6 Delayed labor onset in mice with depleted or IL-33-unresponsive ILC2s.

For parturition timing experiments, mice were injected as indicated with a single dose of DMPA on GD12.5. Groups were compared by the log-rank test. (**A**) Extent of ILC2 depletion in *Il5-cre* iDTR and control *Il5-cre* mice given DT every other day as indicated starting on GD12.5 and sacrificed on GD18.5. *, $p<0.05$ by Student's *t*-test ($n=4$ mice/group; mean+/-SEM). (**B**) Parturition timing in such ILC2-depleted mice. (**C**) ST2 expression by uterine ILC2s in *Il5-cre Il1rl1*$^{f/f}$ and control *Il5-cre* mice (representative contour plots from GD18.5; $n=3$/group collected over 3 independent experiments). (**D**) Parturition timing in *Il5-cre Il1rl1*$^{f/f}$ mice. (**E**) Parturition timing in *Rag2*$^{-/-}$ mice. B6 mice are the same as in Figure 3.1D.

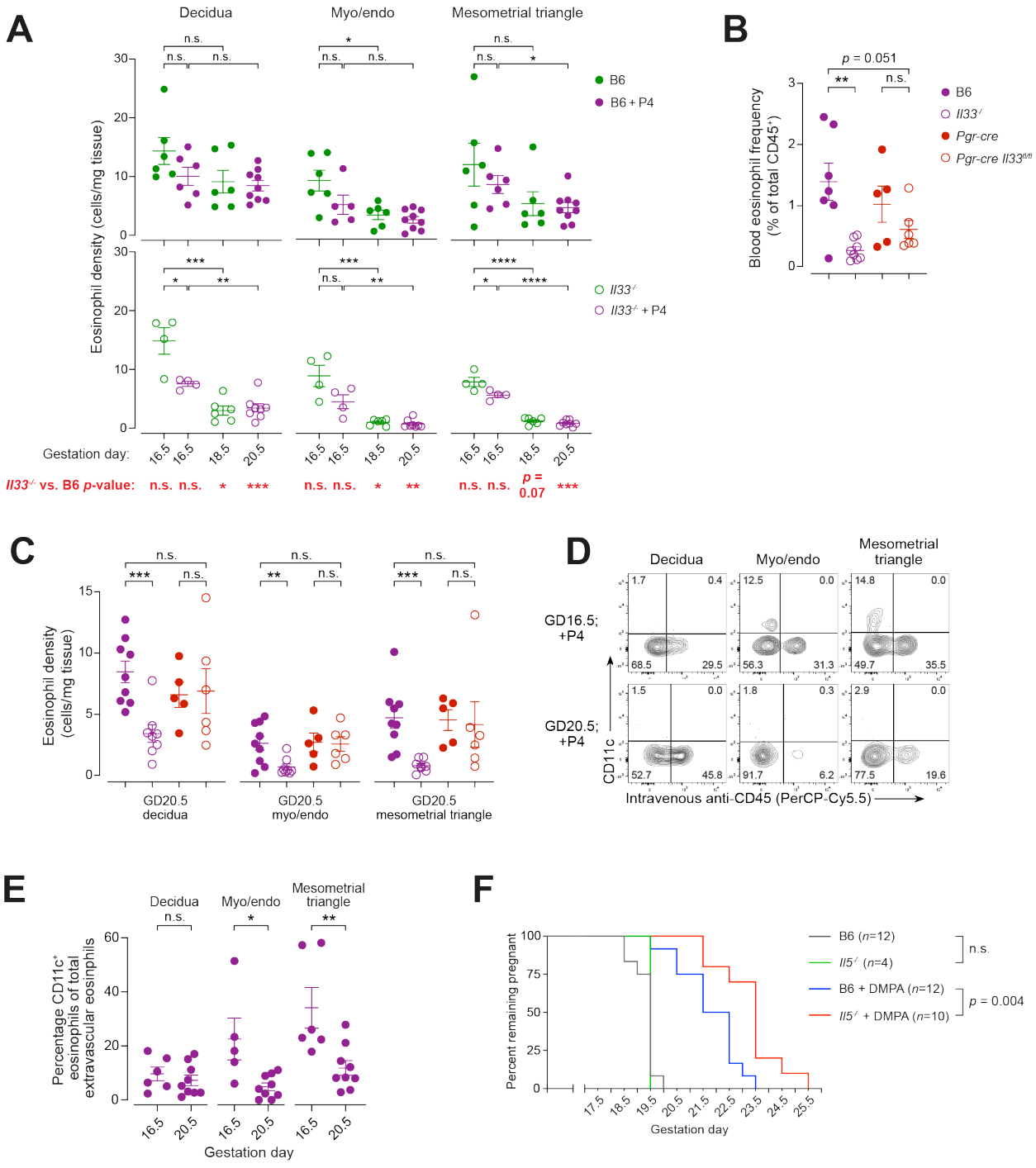

Figure 3.7 Eosinophil dynamics in the prepartum uterus and delayed labor onset in IL-5-deficient mice.

(Figure caption continued on the next page)

Figure 3.7. (Figure caption continued from the previous page) (**A-E**) Analysis of uterine densities, blood frequencies, and CD11c expression by eosinophils in late gestation. See Figure 3.12D for gating. Mice were intravenously injected 5 minutes before sacrifice with PerCP-Cy5.5-conjugated anti-CD45 antibodies. Only extravascular cells were used to calculate tissue densities. Mice sacrificed on GD20.5 were injected daily with P4 starting on GD16.5; where indicated some mice sacrificed on GD16.5 were injected daily with P4 starting on GD12.5. All graphs show data for individual mice and mean+/-SEM. *, $p<0.05$; **, $p<0.01$; ***, $p<0.001$; ****, $p<0.0001$ by Student's *t*-test. (**A**) Eosinophil tissue densities in the prepartum uterus. (**B**) Blood eosinophil frequencies on GD20.5. (**C**) Uterine eosinophil densities on GD20.5. B6 and *Il33*$^{-/-}$ data are the same as in Panel A. (**D**, **E**) CD11c expression by uterine eosinophils in B6 mice (representative contour plots from n=6-9 mice/group collected over 5 independent experiments per time point, and summary data, respectively). (**F**) Parturition timing in *Il5*$^{-/-}$ mice. Groups were compared by the log-rank test. B6 mice are the same as in Figure 3.1D. See also Figures 3.12 and 3.13.

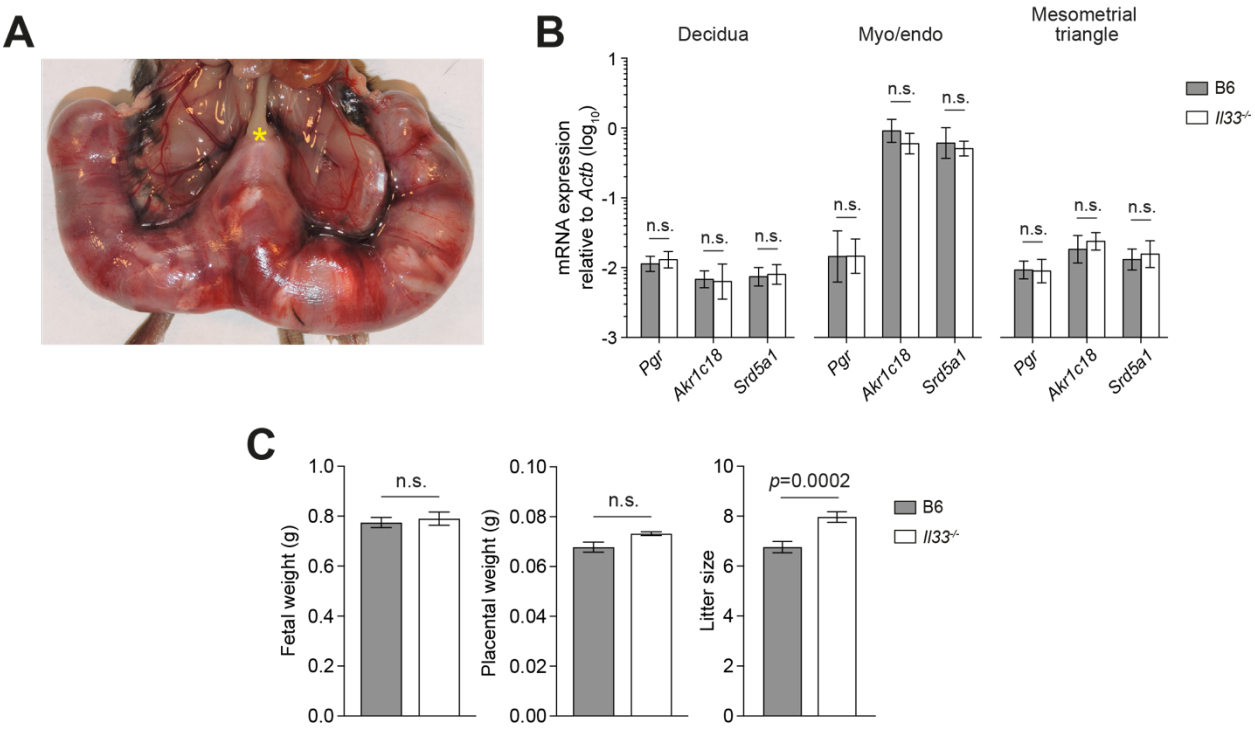

Figure 3.8 Defects in uterus-intrinsic parturition pathways in *Il33*$^{-/-}$ mice.

(**A**) Representative image of a mouse experiencing dystocia, with dead pups backed up against a closed cervix (asterisk). (**B**) qRT-PCR analysis of gene expression on GD20.5 in the dissected uterine tissue layers of mice given DMPA on GD12.5 (*n*=6 mice/group; mean+/-SD). The mesometrial triangle is the portion of the myometrium that overlies the decidua basalis; the myo/endo is the remaining portion of the myometrium, which has an inner surface of undecidualized endometrium. See text and Figure 3.2A for further description of this anatomy. *Pgr* encodes the progesterone receptor; *Akr1c18* encodes 20α-HSD, which, in addition to being upregulated in the ovary during luteolysis, is also expressed relatively highly in the uterus. n.s., not significant. (**C**) Fetal weights, placental weights, and litter sizes measured on GD17.5 (*n*=4-5 mice/group for weights, *n*=31-34 for litter sizes; weights were first averaged over all pups within a litter; graph shows mean+/-SEM of these averages). Data were analyzed by Student's *t*-test.

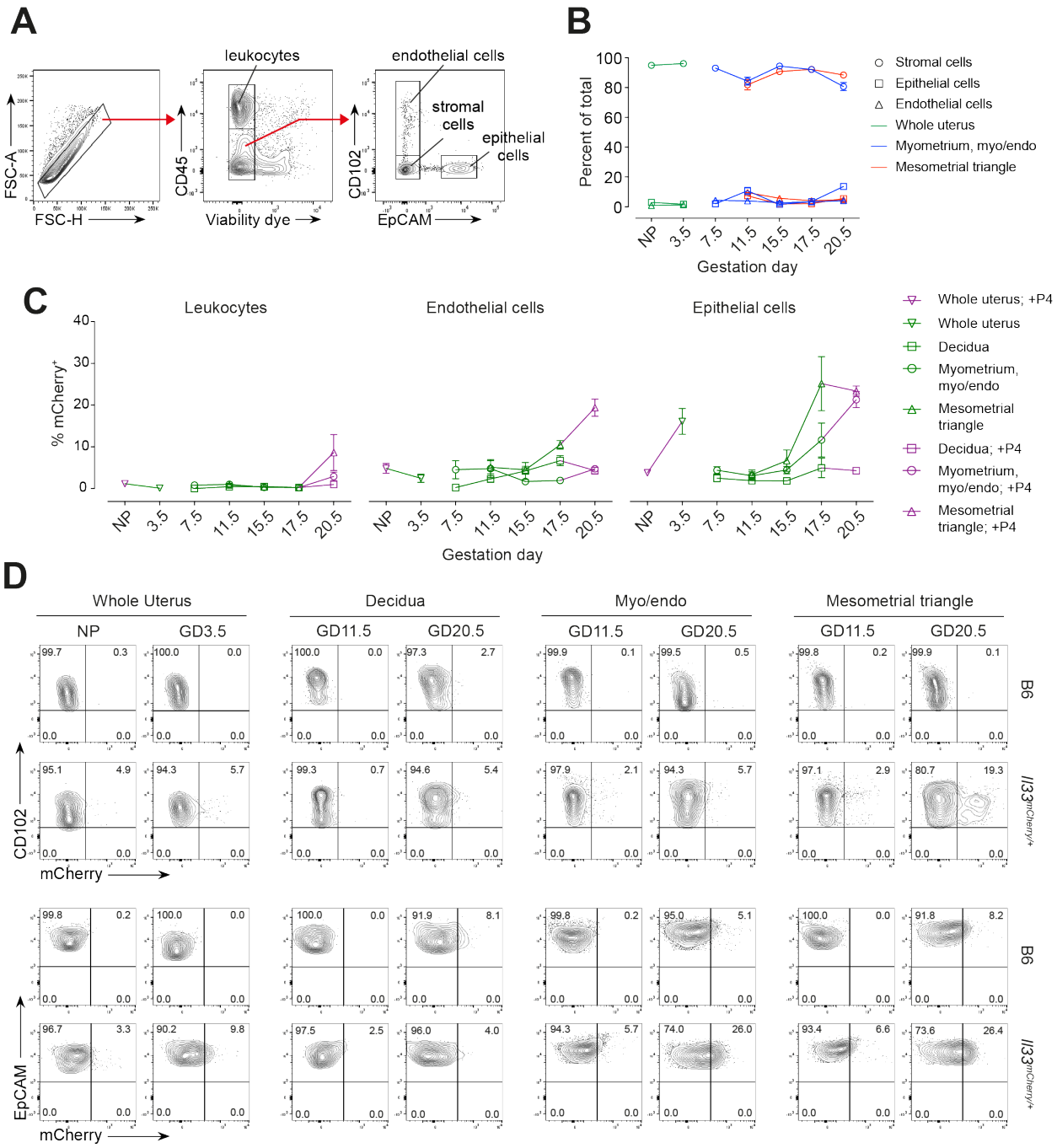

Figure 3.9 Contributions of immune, endothelial and epithelial cells to uterine IL-33 production.

(Figure caption continued on the next page)

Figure 3.9. (Figure caption continued from the previous page) (**A**) Gating scheme to identify uterine stromal cells, endothelial cells, epithelial cells, and leukocytes, using the GD20.5 myo/endo as a representative tissue. (**B**) Relative proportions of stromal, endothelial, and epithelial cells within dissected uterine tissue layers, as determined by flow cytometry after enzymatic disaggregation. (**C, D**) Percentages of IL-33mCherry$^+$ cells within leukocytes, endothelial cells, and epithelial cells (C; *n*=5 mice/group; mean+/-SEM), and representative contour plots of IL-33mCherry expression by endothelial and epithelial cells from *Il33*$^{mCherry/+}$ *and control B6 mice* (D). Whole NP uteri, whole GD3.5 uteri, and dissected uterine tissue layers on the indicated days of gestation were disaggregated and analyzed by flow cytometry. Gates were placed so that less than 1% of the cells' respective counterparts in B6 mice on GD17.5 were mCherry$^+$.

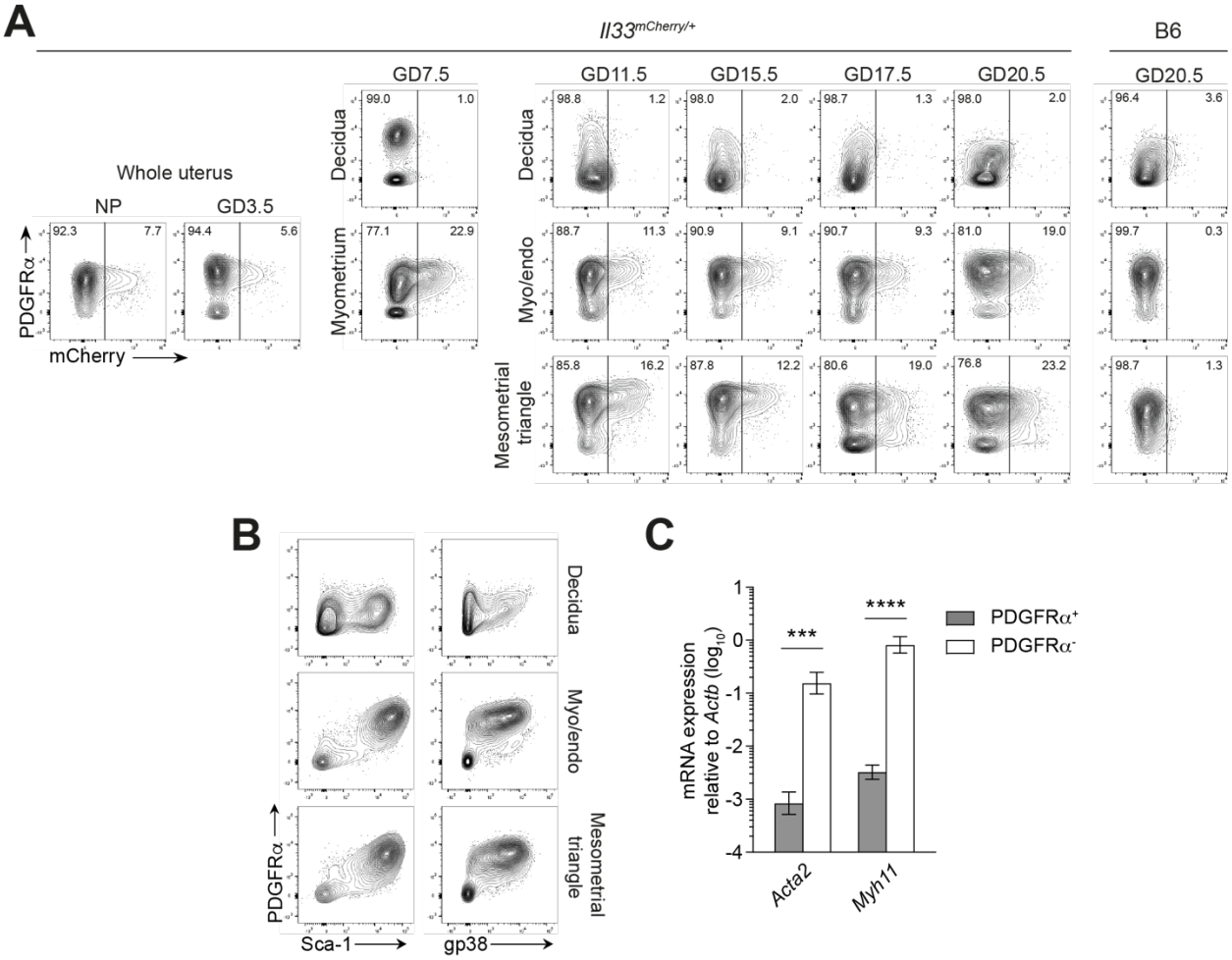

Figure 3.10 Characterization of stromal cells in the prepartum uterus.

(**A**) Representative contour plots (n=5 mice/group), with PDGFRα co-staining, of uterine stromal cells (CD45$^-$ CD102$^-$ EpCAM$^-$; see Figure 3.9A for gating) from non-pregnant *Il33*$^{mCherry/+}$ mice, pregnant *Il33*$^{mCherry/+}$ mice at various points of gestation, and B6 mice on GD20.5. See Figure 3.3.2B for summary data. The mCherry positivity gate was placed so that less than 1% of the stromal cells in B6 mice on GD17.5 were mCherry$^+$. Plots for GD20.5 mice are the same as those in Figure 3.3.2B. GD20.5 mice were given daily P4 injections starting on GD16.5 to extend gestation; non-pregnant mice were given 3 daily P4 injections prior to sacrifice in order to establish a pregnancy-like endocrine state. (**B**) Expression of the mesenchymal markers Sca-1/Ly6A and gp38/podoplanin among uterine stromal cells from B6 mice on GD20.5 (representative data from n=5 mice). *(***C**) qRT-PCR analysis of *Acta2* and *Myh11* mRNA expression in PDGFRα$^+$ and PDGFRα$^-$ stromal cells sorted from the GD15.5 myo/endo (n=3 mice/group; mean+/-SD). ***, p<0.001; ****, p<0.0001 by Student's t-test.

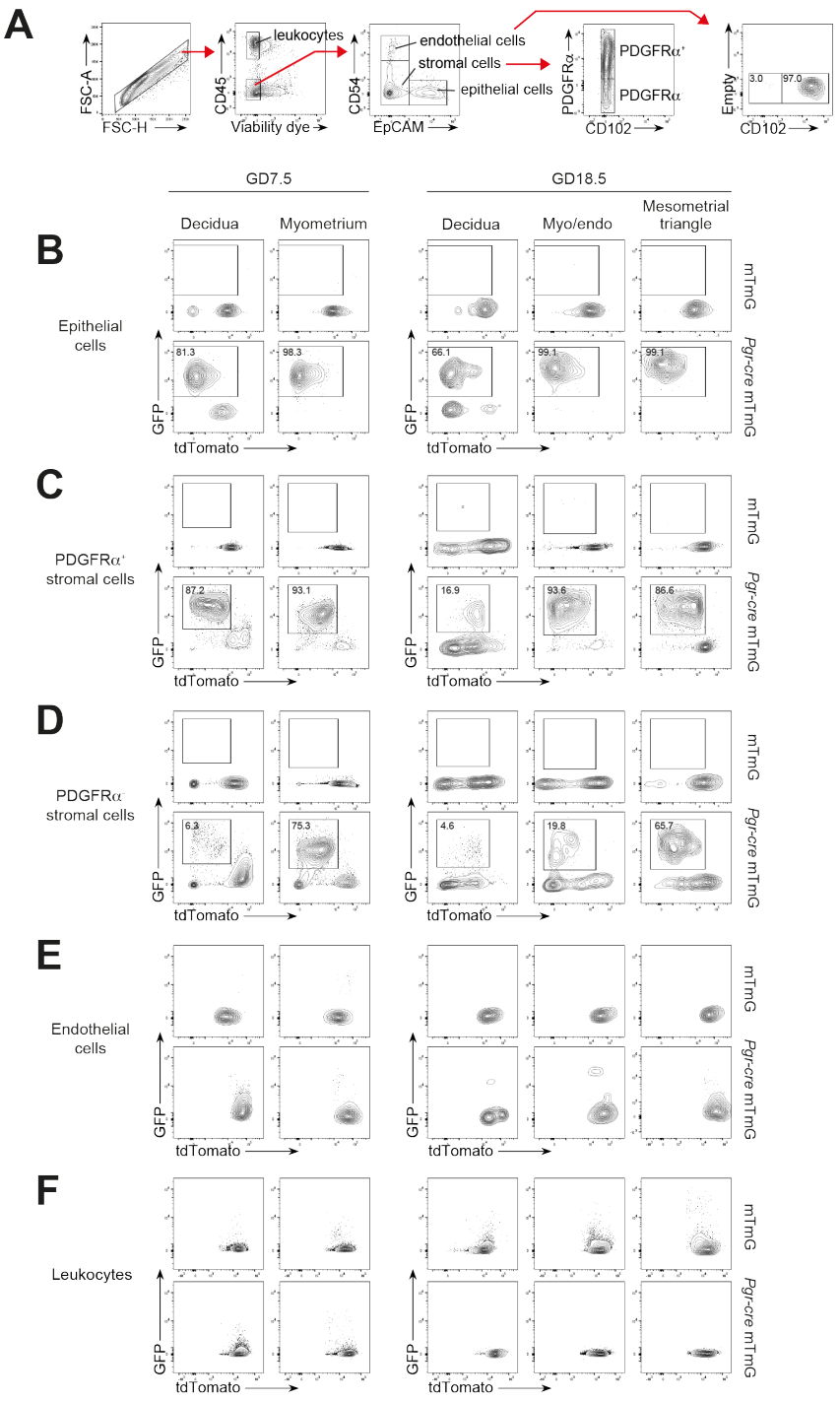

Figure 3.11 Identification of cell types in the GD7.5 and GD18.5 uterus with historical expression of *Pgr*.

(Figure caption continued on the next page)

Figure 3.11. (Figure caption continued from the previous page). To lineage trace *Pgr*-expressing cells in the uterus, we employed mTmG mice [183] in which the constitutively active *Rosa26* locus drives membrane-associated tdTomato expression prior to Cre-mediated recombination, and membrane-associated GFP expression post-recombination. Of note, but with irrelevance to the present study, we modified the *mTmG* allele by incorporating chicken egg ovalbumin-derived peptides into the *mG* portion of the construct. Similarly modified mTmG mice were used as controls (upper set of plots for each gated cell type in panels B-F). (**A**) Gating scheme. Unlike in Figure 3.9A, where CD102 was used to identify endothelial cells, these experiments instead used CD54. Separate experiments performed on non-pregnant uteri from non-transgenic mice (shown here) demonstrated that all of the $CD45^-$ $EpCAM^-$ $CD54^-$ cells gated as stromal cells were $CD102^-$ and >90% of the $CD45^-$ $EpCAM^-$ $CD54^+$ cells gated as endothelial cells were $CD102^+$. (**B**-**F**) tdTomato and GFP expression amongst the major uterine cell types. The percentage of recombined cells is shown in the GFP^+ $tdTomato^{lo}$ gate displayed for the *Pgr-cre* mTmG mice. Note that *Pgr-cre* mTmG mice showed thorough recombination in uterine epithelial cells in all tissue layers on both GD7.5 and GD18.5, in PDGFRα^+ stromal cells in both the decidua and myometrium on GD7.5, and in PDGFRα^+ stromal cells in the myo/endo and mesometrial triangle on GD18.5. PDGFRα^- stromal cells in the GD7.5 myometrium and GD18.5 myo/endo and mesometrial triangle, which include myometrial SMCs (Figure 3.10C), were only partially recombined, presumably reflecting the previously described recombination that takes place in the circular but not longitudinal smooth muscle layer of myometrium[104]. The PDGFRα^+ stromal cells in the GD18.5 decidua were PDGFRα^{lo} (see Figure 3.10A), consistent with our immunofluorescence analysis (Figure 3.2C). Unexpectedly, PDGFRα^- stromal cells in the GD18.5 decidua (representing ~75% of all stromal cells at this location) were almost entirely unrecombined, despite the PDGFRα^+ stromal cells of the GD7.5 decidua showing high recombination. This suggests that most of the stromal cells in the GD18.5 decidua are not derived from PDGFRα^+ stromal cells of the GD7.5 decidua. Endothelial cells and leukocyte showed no recombination in any uterine tissue layer at either time point. Data are representative of n=2-3 mice/group.

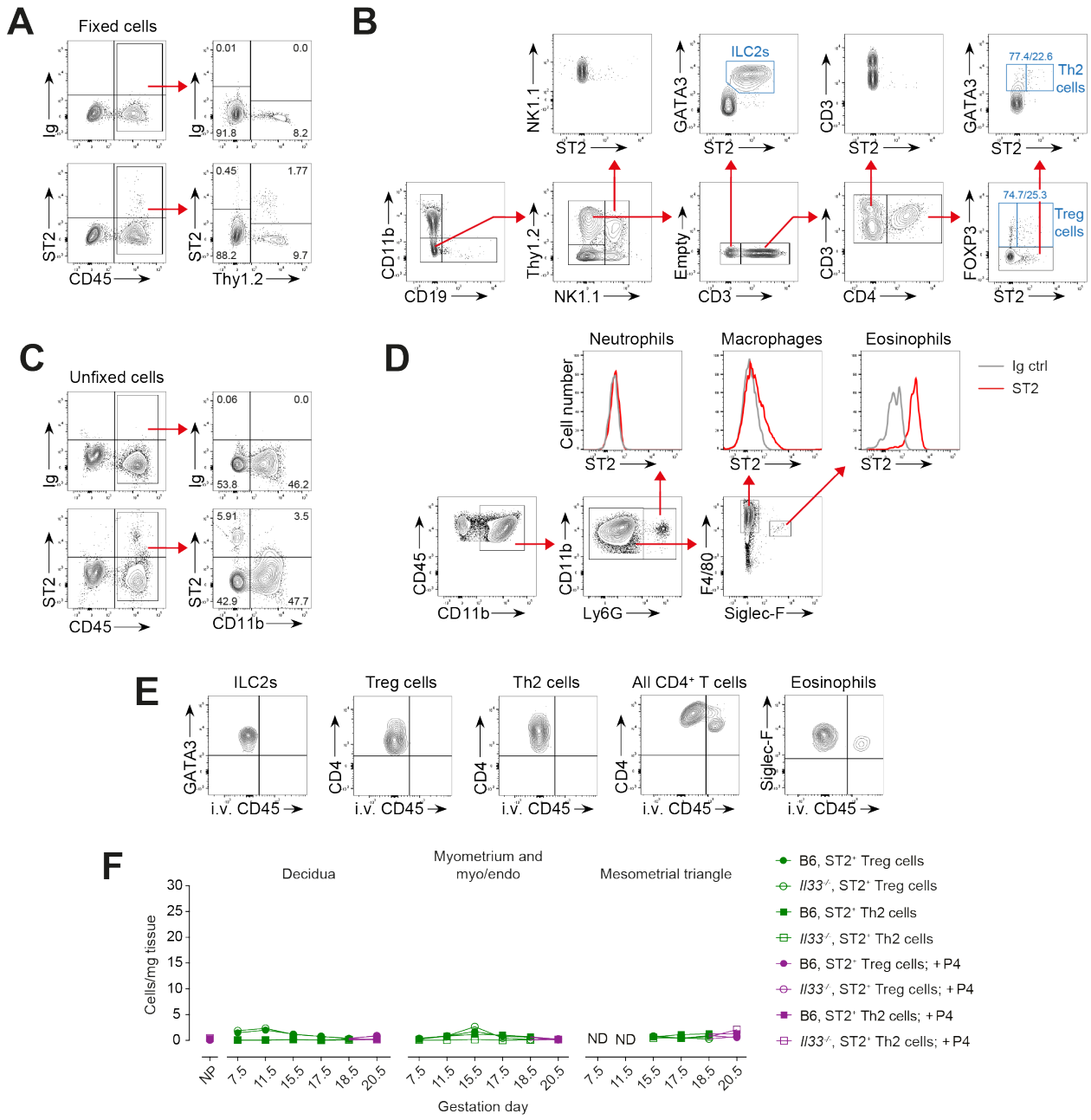

Figure 3.12 Identification of ST2-expressing cells in the uterus; analysis of uterine ST2⁺ T cell densities.

(Figure caption continued on the next page)

Figure 3.12. (Figure caption continued from the previous page) (**A-E**) Identification of ST2-expressing cell types in the late gestation uterus, using the mesometrial triangle as a representative tissue. Data are representative of at least *n*=5 mice/group. (**A**, **B**) Analysis of lymphoid cells on GD17.5. The cells were fixed, a prerequisite for staining for the ILC2/Th2 marker GATA3 and the Treg marker FOXP3. The left plots in (**A**) were gated on viable non-doublets. Note that ST2 expression was confined to the $CD45^+$ compartment. Panel (**B**) shows ST2 expression among lymphoid cell types and the gating scheme to identify ILC2s (Lin^- $Thy1.2^+$ $CD3^-$ $GATA3^+$ $ST2^+$ cells), $ST2^+$ Treg cells ($CD3^+$ $CD4^+$ $FOXP3^+$) and $ST2^+$ Th2 cells ($CD3^+$ $CD4^+$ $FOXP3^-$ $GATA3^+$). The first plot was gated on viable non-doublet $CD45^+$ cells. Since staining the cells for GATA3 and FOXP3 required permeabilization, this approach was not suitable for visualizing eosinophils. Note that all ILC2s were $ST2^+$, whereas only minor fractions of Treg cells and Th2 cells were $ST2^+$. (**C**, **D**) Analysis of myeloid cells on GD16.5. The cells were unfixed, which allowed for the detection of ST2 expression by macrophages and eosinophils. The left plots in (**C**) were gated on viable non-doublets. Again, ST2 expression was confined to the $CD45^+$ compartment. Panel (**D**) shows low ST2 expression by macrophages ($CD11b^+$ $F4/80^+$ $Siglec\text{-}F^-$ cells), high ST2 expression by eosinophils ($CD11b^+$ $F4/80^{int}$ $Siglec\text{-}F^+$ cells), and no ST2 expression by neutrophils ($CD11b^+$ $Ly6G^+$ cells). (**E**) Visualization of blood/tissue partitioning of uterine $CD45^+$ cells with ST2 expression, accomplished by injecting the mice i.v. with PerCP-Cy5.5-conjugated anti-CD45 antibodies 5 min prior to sacrifice (Tagliani 2011). The mesometrial triangle is shown as a representative tissue (GD17.5 for lymphoid cells, GD16.5 for eosinophils). This technique was applied for all determinations of uterine leukocyte tissue densities and frequencies (Figures 4A, 7A, 7C, 7E, S5F, S7A, S7A-D, S7F); such determinations counted only extravascular (i.e., PerCP-$Cy5.5^{lo}$) cells. Note that all ILC2s, Treg cells, and Th2 cells were extravascular, as they were in the myo/endo (not shown); in the decidua, ~20% of Treg cells ~50% and Th2 cells were intravascular (not shown). (**F**) Tissue densities of $ST2^+$ Treg and $ST2^+$ Th2 cells in whole NP uteri and dissected uterine tissue layers of *Il33*$^{-/-}$ and B6 mice on the indicated days of gestation, as determined by flow cytometry (*n*=6 mice/group; mean+/-SEM). Where indicated, mice were given daily P4 injections starting on GD16.5 to extend gestation to GD20.5; non-pregnant mice were given 3 daily P4 injections prior to sacrifice in order to establish a pregnancy-like endocrine state. No differences were detected between *Il33*$^{-/-}$ and B6 mice. ND, not determined.

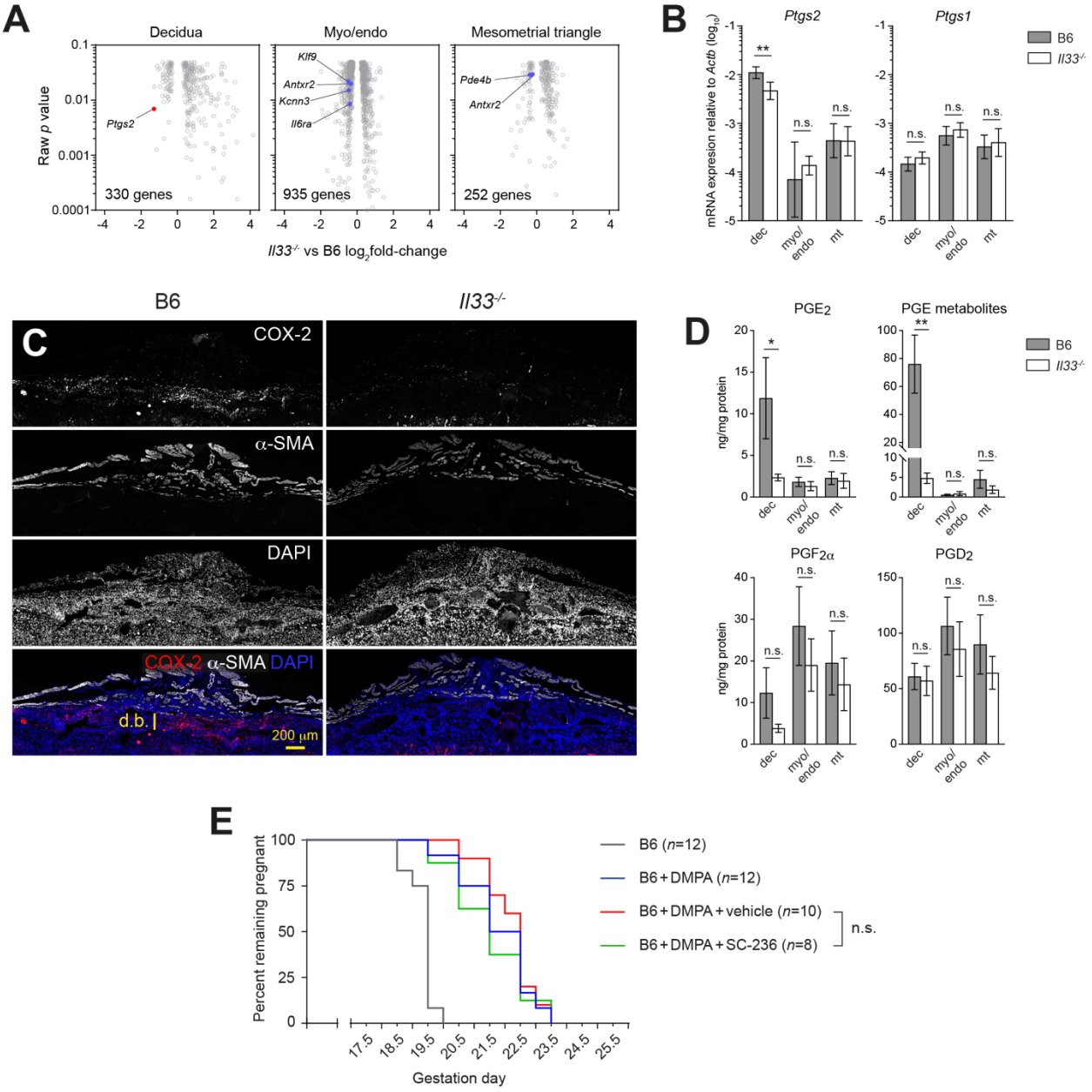

Figure 3.13 IL-33 enhances COX-2 expression in the late gestation decidua, but COX-2 activity is not a critical component of uterus-intrinsic parturition pathways.

(Figure caption continued on the next page)

Figure 3.13. (Figure caption continued from the previous page) (**A**) RNA-Seq analysis of the prepartum uterus. Volcano plot of differentially expressed protein coding genes (p_{raw}<0.05) between *Il33*$^{-/-}$ and B6 uterine tissue layers on GD18.5 (n=4-5 mice/group). Some genes linked to birth defects in mice or altered birth timing[145,184,185] are indicated (blue). Overexpression of *Kcnn3* has been shown to delay labor onset[186]. (**B**) qRT-PCR analysis of uterine *Ptgs2* mRNA expression on GD20.5. Mice were injected with DMPA on GD12.5. **, p<0.01 by Student's t-test (n=6 mice/group; mean+/-SD). mt, mesometrial triangle. (**C**) COX-2 immunostaining of B6 and *Il33*$^{-/-}$ implantation sites on GD20.5 (representative of n=4 mice/group). Mice were injected daily with 2 mg P4 starting on GD15.5. (**D**) Concentrations of PGE_2, PGE metabolites, $PGF_{2\alpha}$, and PGD_2, quantified by ELISA, in uterine tissues on GD20.5. Mice were injected daily with 2 mg P4 starting on GD15.5. *, p<0.05; **, p<0.01 by Mann-Whitney U test (n=6 mice/group; mean+/-SEM). (**E**) Effects of SC-236 on labor onset timing in DMPA-treated B6 mice. Data for B6 and B6+DMPA mice are from Figure 3.3.1D. SC-236 was injected daily starting on GD16.5. Groups were compared by the log-rank test.

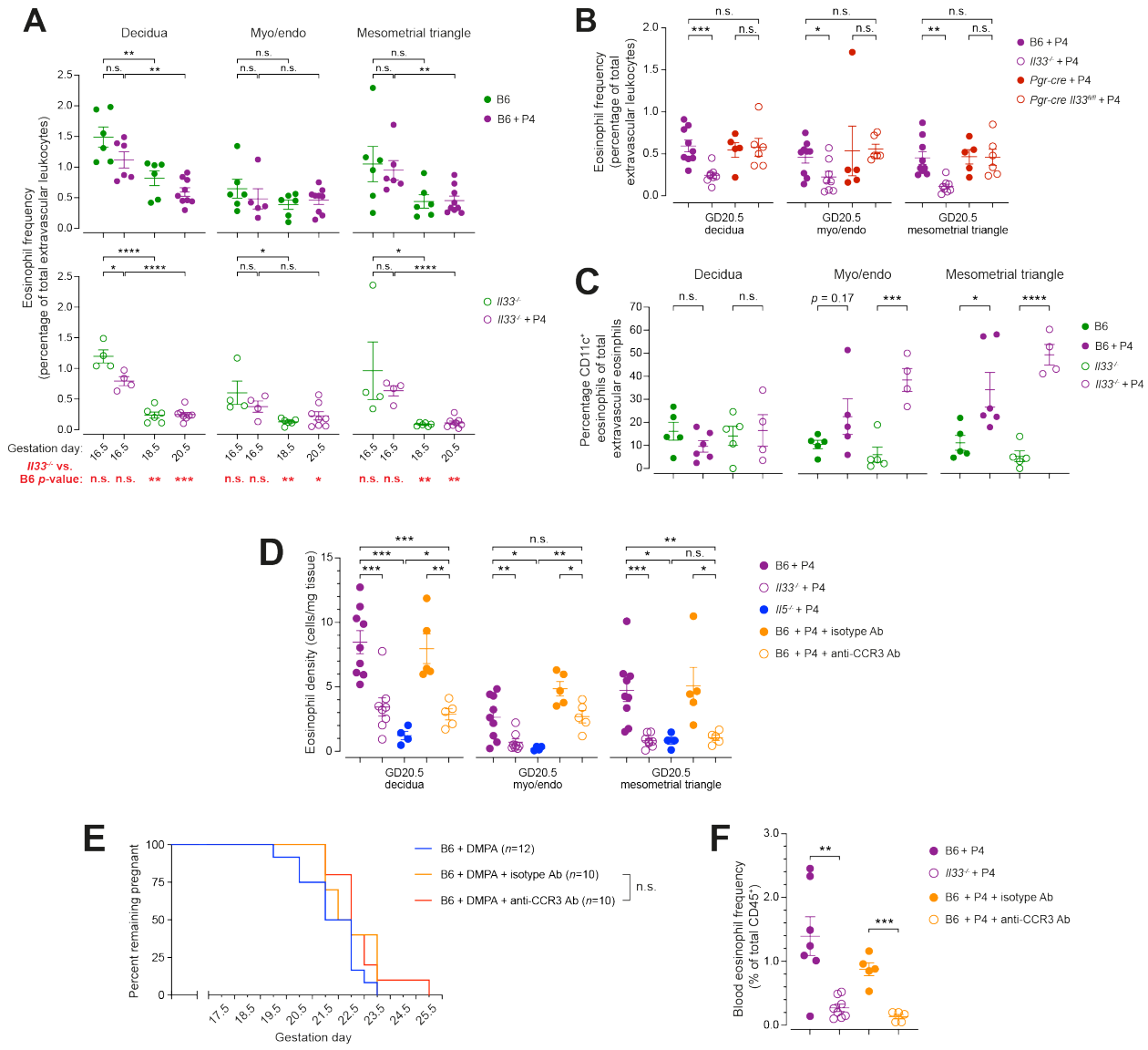

Figure 3.14 Additional analysis of eosinophil dynamics and phenotypes in the late gestation uterus.

(Figure caption continued on the next page)

Figure 3.14. (Figure caption continued from the previous page) All mice analyzed by flow cytometry were intravenously injected 5 minutes before sacrifice with PerCP-Cy5.5-conjugated anti-CD45 antibodies. Only extravascular cells were used in the calculations. Eosinophil gating was performed as shown in Figure 3.12D. (**A**, **B**) Analysis of uterine eosinophil frequencies in late gestation. Mice sacrificed on GD20.5 were injected daily with P4 starting on GD16.5; where indicated some mice sacrificed on GD16.5 were injected daily with P4 starting on GD12.5. Graphs show data for individual mice and mean+/-SEM. *, $p<0.05$; **, $p<0.01$; ***, $p<0.001$; ****, $p<0.0001$ by Student's *t*-test. (**A**) Eosinophil frequencies in the prepartum uterus. (**B**) Uterine eosinophil frequencies on GD20.5. B6 and *Il33*$^{-/-}$ data are the same as in Panel A. (**C**) CD11c expression by extravascular eosinophils in the GD16.5 uteri of B6 and *Il33*$^{-/-}$ mice. Where indicated, mice received daily P4 injections starting on GD12.5. P4-treated B6 mice are the same as in Figure 3.7E. The graph shows data for individual mice and mean+/-SEM. *, $p<0.05$; ***, $p<0.001$; ****, $p<0.0001$ by Student's *t*-test. (**D-F**) Effect of IL-5 deficiency and anti-CCR3 antibody administration on uterine eosinophil tissue densities (**D**), parturition timing (**E**), and blood eosinophil frequencies (**F**). See also Figure 3.7F. Anti-CCR3 and isotype control antibodies (500 μg) were administered once on GD16.5. For assessments of uterine eosinophil densities and blood eosinophil frequencies (**D**, **F**), mice were injected daily with P4 starting on GD16.5 and sacrificed on GD20.5. Graphs show data for individual mice and mean+/-SEM. *, $p<0.05$; **, $p<0.01$; ***, $p<0.001$ by Student's *t*-test. B6 and *Il33*$^{-/-}$ data are the same as in Figure 3.7A and 7B. For parturition timing experiments (**E**), mice were injected with DMPA on GD12.5 and groups were compared by the log-rank test. B6 mice are the same as in Figure 3.1D.

Table 3.1 RNA-seq analysis of the prepartum B6 and *Il33*$^{-/-}$ uterus.

Available for download online under “Supplemental information” at https://www.sciencedirect.com/science/article/pii/S1074761323000158?via%3Dihub.

Table 3.2 qRT-PCR primers

Gene	Forward	Reverse
Actb	5'-GCTCTGGCTCCTAGCACCAT-3'	5'-GCCACCGATCCACACAGAGT-3'
Akr1c18	5'-GCTGATATGTTTAAGGCTCACCCTAA-3'	5'-AGAGTCCAGCATCACACAAAAGATC-3'
Acta2	5'-AGCCATCTTTCATTGGGATGGAG-3'	5'-CATGGTGGTACCCCCTGACA-3'
Il33	5'-TGAGACTCCGTTCTGGCCTC-3'	5'-CCCGTGGATAGGCAGAGAAG-3'
Myh11	5'-TTGAACAGGAGGCCAGAGAG-3'	5'-GCTGCTTGACCTTGTGTTT-3'
Pgr	5'-CATGGTCCTTGGAGGTCGTA-3'	5'-CTCTCGTTAGGAAGGCCCAC-3'
Ptgs1	5'-TACTCACAGTGCGGTCCAAC-3'	5'-TTGGGCCAGAAGCTGAACAT-3'
Ptgs2	5'-GGCCATGGAGTGGACTTAAA-3'	5'-GGTTCTCAGGGATGTGAGGA-3'
Srd5a1	5’-ACAAAATACCCAGGGGAGGC-3’	5’-GAACAGAGCAAACACCACGC-3’

Methods and Materials

Mice

C57BL/6J (B6), *Pdgfra-cre* (C57BL/6-Tg (Pdgfra-cre)1Clc/J), iDTR (C57BL/6-*Gt(ROSA)26Sor*$^{tm1(HBEGF)Awai}$/J), *Rag2*$^{-/-}$ (B6.Cg-*Rag2*$^{tm1.1Cgn}$/J), and mTmG (B6.129(Cg)-*Gt(ROSA)26Sor*$^{tm4(ACTB-tdTomato,-EGFP)Luo}$/J) mice were purchased from The Jackson Laboratory and were all on a B6 background. Il33$^{-/-}$ mice (*Il33*$^{Gt/Gt}$; ref.[187]) were the gift of Jean-Philippe Girard, B6(C)-*Il5*$^{tm1.1(icre)Lky}$/J mice (*Il5-cre*; ref.[188]) were the gift of Richard Locksley, *Il33*$^{fl/fl}$ and *Il1rl1*$^{fl/fl}$ mice[189] were the gifts of Richard Lee, B6.*Il33*$^{mCherry/mCherry}$ (IL-33mCherry) mice[151] were the gift of Marco Colonna, and *Pgr-cre* mice[104] were the gift of Francesco DeMayo and John Lydon. If not already on a B6 background, all mice were backcrossed with B6 mice to reach at least N10. Mice were heterozygous for the *Il5-cre* allele, which causes *Il5* gene disruption, when the allele was used to target gene deletion to IL-5-expressing cell types. It was intercrossed to homozygosity to generate IL-5-deficient (*Il5*$^{-/-}$) mice. *Il5-cre* B6.Cg-*Gt(ROSA)26Sor*$^{tm14(CAG-tdTomato)Hze}$/J (*Il5-cre*R26RFP) mice have been described previously[152]. *Il33*$^{fl/fl}$ mice were intercrossed with *Pgr-cre* mice to generate *Pgr-cre Il33*$^{fl/fl}$ mice or with *Pdgfra-cre* mice to generate *Pdgfra-cre Il33*$^{fl/fl}$ mice. *Il5-cre* mice were intercrossed with iDTR mice to generate *Il5-cre* iDTR mice or with *Il1rl1*$^{fl/f}$ mice to generate *Il5-cre Il1rl1*$^{fl/f}$ mice. *Pgr-cre* mice were intercrossed with mTmG mice, modified to include sequences encoding ovalbumin-derived peptides as described in the Figure 3.11 legend, to generate the mice for the lineage tracing experiment. The mice were maintained in specific pathogen-free animal barrier facility at UCSF. In order to maintain a consistent microbiota, all females used for experiments were born in the Erlebacher lab holding room except for the mice used for Figure 3.5, which were born in the Molofsky lab holding room, and the mice used for the anti-CCR3-mediated eosinophil depletion

experiment, which were purchased from The Jackson Laboratory. All experiments were performed using female mice because only females become pregnant. Virgin females, 6-10 weeks old, were used for all experiments and were mated to B6 males unless otherwise indicated. All experiments were approved by the UCSF IACUC (Protocols #AN178689 and #AN193713).

Pregnancy experiments

Vaginal plugs were checked in the mornings, and noon of that day was counted as GD0.5. To determine labor onset timing, pregnant mice were checked twice daily (9 am and 6 pm) for evidence of delivery, uterine bleeding, or maternal distress. If apparent at 9 am, labor onset timing was scored as GDX.5, with X being the number of days after mating (i.e., GD0.5). If apparent at 6 pm, it was scored as GD(X+1).0 (i.e. midnight of the next gestation day). For parturition timing experiments, pregnant mice were injected subcutaneously with a single dose of 250 μg depot medroxyprogesterone acetate (DMPA; Depo-Provera, Pfizer) in 100 μl PBS on GD12.5. This dose was chosen because it was the minimum needed to consistently extend gestation length in B6 mice past 24 h. To analyze mice on GD20.5, gestation was extended by giving subcutaneous daily injections of 2 mg P4 (Sigma-Aldrich) dissolved in 0.1 ml sesame seed oil (Sigma-Aldrich) starting on GD16.5. To control for the effect of these injections, some mice were analyzed on GD16.5 or GD17.5 after they received subcutaneous daily injections of 2 mg P4 starting on GD12.5 or GD13.5, respectively. Non-pregnant mice were injected with P4 for the 3 days prior to sacrifice in order to mimic the endocrine state of pregnancy. *Il5-cre* iDTR and *Il5-cre* mice received intraperitoneal injections of 300 ng diphtheria toxin (Calbiochem) in 200 μl PBS every other day until the mice delivered or when they reached the end point of the

experiment. The COX-2 specific inhibitor SC-236 (Axon Medchem) was injected intraperitoneally at 6 mg/kg in 200 µl 50:50 PBS:DMSO. Anti-CCR3 antibodies and isotype control antibodies (clones 6S2-19-4 and LTF-2, respectively; Bio-X-Cell), were intravenously injected on GD16.5 at a dose of 500 µg in 100 µl PBS.

Tissue digestion and flow cytometry

Non-pregnant and GD3.5 uteri were digested as whole tissues. For pregnant mice on GD7.5, the decidua was separated from the overlying myometrium. From GD11.5 to GD20.5, the myometrium and mesometrial triangle were further separated. As previously described[190], tissues and tissue layers were enzymatically disaggregated via incubation in Liberase™ TL Research Grade (50 µg/ml; Roche), DNAse I (30 µg/ml; Roche) and trypsin (0.05%; ThermoFisher Scientific) in HBSS buffer for 45 min at 37º C, with trituration every 10 minutes. EDTA was then added to a 5 mM final concentration and the samples were incubated 15 minutes more at 37º C. The cell suspensions were then filtered through 40 µm nylon mesh, and washed in PBS. For surface staining, the cells were first incubated with rat anti–mouse CD16/CD32 (BioXCell, clone 2.4G2; 5 µg/ml for 1×10^6 cells) to block nonspecific antibody binding. Antibodies, purchased from BD Biosciences, BioLegend, Invitrogen, or MD Bioproducts were: FITC-conjugated anti-CD102 (clone 3C4), Bv-711 or PE-Cy7-conjugated anti-CD326 (EpCAM clone G8.8), PE or APC-conjugated anti-CD140a (clone APA5), APC-Cy7-conjugated anti-gp38/podoplanin (clone 8.1.1), BV711-conjugated anti-Ly-6A/E (Sca-1 clone D7), PE-conjugated anti-CD54 (clone YN1/1.7.4), PerCP-Cy5.5- or BUV395-conjugated anti-CD45 (clone 30-F11), BV711-conjugated anti-CD4 (clone RMA4-5), BV605-conjugated anti-CD11b (clone M1/70), APC-Cy7-conjugated anti-NK1.1 (clone PK136), PE/Dazzle594-conjugated anti-

CD19 (clone 6D5), PE-conjugated anti-T1/ST2 (clone DJ8), BV421-conjugated anti-CD90.2 (Thy1.2 clone 53-2.1), AF700-conjugated anti-CD3 (clone 17A2), APC-conjugated anti-Ly-6G (clone 1A8), FITC-conjugated anti-F4/80 (clone BM8), BV421-conjugated anti-Siglec-F (clone E50-2440), BV650-conjugated anti-CD11c (clone N418). Intracellular staining was performed after surface staining using PE-Cy7-conjugated anti-FOXP3 (clone FJK-16s), eFluor-660-conjugated anti GATA3 (clone TWAJ), PE-Cy7-conjugated anti-IL-13 (clone eBio13A), and anti-IL-5 (clone TRFK5) followed by FITC-conjugated anti-rat IgG1 (clone MRG1-58). For the detection of IL-5 and IL-13 expression, 1 ml cell suspensions in RPMI/10% FBS were incubated with 50 ng/ml phorbol 12-myristate 13-acetate (PMA; Adipogen) and 500 ng/ml ionomycin (Adipogen) for a total of 4 h. Brefeldin A (1 µl of GolgiPlug™, BD Biosciences) and 2 µM monensin (Abcam) secretion inhibitors were added to the culture after 1 h. Live/dead discrimination employed Fixable Viability Dye eFluor 506 (Invitrogen).

To visualize IL-33mCherry expression among the major uterine cell lineages, leukocytes were identified as $CD45^+$ cells, stromal cells as $CD45^-$ $EpCAM^-$ $CD102^-$ cells, epithelial cells as $CD45^-$ $CD102^-$ $EpCAM^+$ cells, and endothelial cells as $CD45^-$ $EpCAM^-$ $CD102^+$ cells (see Figure 3.9A). The stromal cells were further subdivided based upon their staining with antibodies to PDGFRα, Sca1 and gp38. The same scheme was used for the lineage tracing experiments (Figure 3.10), except that CD54 instead of CD102 was used to identify endothelial cells (see Figure 3.10A). For leukocyte analyses, the mice were injected intravenously with PerCP-Cy5.5-conjugated anti-CD45 antibodies 5 minutes prior to sacrifice in order to discriminate intravascular from extravascular cells[159]. ILC2s were identified as $CD45^+$ lin^- ($CD11b^-$ $CD3\varepsilon^-$ $CD4^-$ $CD19^-$ $NK1.1^-$) Thy1.2 $(CD90.2)^+$ $GATA3^+$ IL1RL1 $(ST2)^+$ cells (or just as $CD45^+$ lin^- $Thy1.2^+$ $GATA3^+$ cells in the case of *Il5-cre Il1rl1*$^{f/f}$ mice). Treg cells were identified as $CD45^+$

CD11b$^-$ CD3ε$^+$ CD4$^+$ FOXP3$^+$ cells; Th2 cells were identified as CD45$^+$ CD11b$^-$, CD3ε$^+$, CD4$^+$, FOXP3$^-$, GATA3$^+$ cells. Eosinophils were identified as CD45$^+$ CD11b$^+$ Ly-6G$^-$ F4/80^{int} Siglec-F$^+$ cells. Intravascular cells were identified as PerCP-Cy5.5^{hi} and extravascular cells as PerCP-Cy5.5^{lo}. Samples were run on a five-laser LSRFortessa™ X-20 (BD Biosciences) and data were analyzed using FlowJo software (Tree Star, USA) and compiled using Prism (GraphPad). Cell counts were performed using flow cytometry counting beads (CountBright Absolute™; Life Technologies) per the manufacturer's instructions. For Figure 3.10B, stromal cells from the GD18.5 myo/endo of B6 mice were gated as live (DAPI$^-$) CD45$^-$ CD102$^-$ EpCAM$^-$ cells and sorted based upon their relative expression of PDGFRα using a MoFlo XDP (Beckman Coulter).

Thin section immunofluorescence

Uterine tissues were fixed overnight at 4°C in 4% paraformaldehyde/PBS and embedded in paraffin. Sections were cut at 5 μm, baked 30 min at 65˚C, then deparaffinized in xylene and ethanol using standard methods. The slides were incubated in methanol for 5 min, air-dried for 30 min, and then incubated with 3% H_2O_2/0.1% sodium azide in PBS for 30 min. The sections were then subjected to antigen retrieval in 10 mM citrate pH 6.0 using a Biocare Decloaking chamber™ NxGen (110°C for 30 sec, allowed to cool down for 10 min in the chamber, then 5 min at room temperature). The sections were then blocked in 1% BSA/3% donkey serum/0.4% Triton X-100 for 1 h at room temperature, followed by application of primary antibodies, diluted in 1% BSA, 0.4% Triton X-100, and incubation at 4°C overnight. Antibody sources, dilutions and antigen retrieval methods were as follows: AF488-conjugated mouse anti-smooth muscle actin (α-SMA, clone 1A4, eBioscience; 1:100), AF647-conjugated mouse anti-α-SMA (clone

1A4, Novus Biological; 1:1000), rabbit anti-PDGFRα (clone EPR22059-270, Abcam; 1:1000), and rabbit anti-COX-2 (clone D5H5, Cell Signaling Technology; 1:1000).

The slides were washed three times in PBS between all subsequent steps. The PDGFRα and COX-2 immunostaining employed biotin tyramide amplification, and so the sections were next incubated for 30 min at room temperature with horseradish peroxidase- (HRP-) conjugated donkey anti-rabbit IgG-secondary antibodies (Jackson ImmunoResearch) diluted 1:200 in TNB blocking buffer (PerkinElmer). They were then incubated in 1.8 μg/mL biotin-tyramide/0.0015% H_2O_2/PBS for 5 min at room temperature, then in 5 μg/ml streptavidin-Alexa Fluor 594 for 30 min at room temperature, and then mounted using DAPI mounting media (Electron Microscopy Sciences). All immunofluorescence images were captured using an Axio Imager M2 microscope running on Zen software (Zeiss). Panoramic views were generated by tiling images taken with the 10X objective. Adobe Photoshop was sometimes used to increase image brightness using the brightness/contrast function; in these cases, the alteration was applied over the entire image and was equally applied to all images within an experiment.

Thick section immunofluorescence

Implantation sites of GD17.5 *Il5-cre*R26RFP mice were harvested and fixed in fresh 4% paraformaldehyde overnight at 4°C, after embryos were removed. After washing with 1X PBS, 300 μm sections were prepared using a vibrating microtome (Precisionary Compresstome VF-310-0Z). Tissue sections were then dehydrated through a methanol/H_2O series (20%, 40%, 60%, 80%, 100%; 10 min each), bleached in chilled fresh 5% H_2O_2/methanol for 2 h at 4°C, then rehydrated with the above methanol/H_2O series (10 min each). The sections were then washed and incubated in permeabilization buffer (PBS/0.2% Triton X-100/0.3 M glycine) for 24 h at

room temperature, blocked in PBS/0.2% Triton X-100/5% donkey serum overnight at 4°C, washed again in PBS/0.2% Tween-20, then incubated with primary antibodies diluted in PBS/0.2% Tween-20/3% donkey serum overnight at room temperature. The sections were then washed 3-4 times in PBS/0.2% Tween-20 for 30 min each, incubated with secondary antibodies diluted in PBS/0.2% Tween-20/3% donkey serum at room temperature for 6–8 h, washed in PBS/0.2% Tween-20 for 1 day, dehydrated in an ascending ethanol series (20%, 30%, 50%, 70%, 95%, 100%; 10 min each), then cleared in methyl salicylate.

To visualize RFP^+ ($tdTomato^+$) cells, sections were stained with anti-DsRed antibodies (Living Colors anti-DsRed rabbit polyclonal, Takara Bio; 1:500), concurrently with rat anti-CD31 antibodies (MEC13.3, Biolegend; 1:100) to visualize endothelial cells, and AF488-conjugated anti-α-SMA antibodies (clone 1A4, eBioscience; 1:200) to visualize SMCs. AF555-conjugated donkey anti-rabbit IgG (ThermoFisher Scientific) and AF647-conjugated donkey anti-rat IgG (Abcam) were used as secondary antibodies at 1:400 dilution.

Stained slides were scanned using a Nikon A1R laser scanning confocal microscope equipped with 405, 488, 561, and 650 nm lasers and a 16X/0.8 Plan Apo long working distance water immersion objective. Z steps were acquired every 6 μm, and Z-stacks were rendered in 3D dimensions and quantitatively analyzed using Bitplane Imaris v9.7 software package (Andor Technology PLC). RFP^+ cells were identified and surfaced using the Imaris spots function based on the anti-RFP fluorescence signal together with the Ortho slicer function to filter for size and morphology.

RNA-Seq and qRT-PCR

Whole tissue layers were homogenized in TRIzol (Thermo Fisher Scientific), and RNA was isolated according to the manufacturer's instructions. For RNA-Seq, the samples were then given to the UCSF Functional Genomics Core for quality control testing, single-end 50-bp RNA-Seq library preparation (Universal Plus mRNA kit, Nugen), and sequencing on an Illumina HiSeq 4000 system. Sequencing provided 1.034 billion total reads for the 28 samples, with an average of 853 millions of these reads aligning uniquely to the mouse genome (mm10/GRCm38.96). Alignment was performed using the Splice-aware STAR aligner STAR_2.7.2b. Reads uniquely mapped to known mRNAs were used to identify genes with differential expression between B6 and *Il33*$^{-/-}$ samples using the DESeq2 R package v1.24.0. Each tissue layer was analyzed independently, and Cooke's cutoff was applied to exclude outliers. We only analyzed protein coding genes for which at least two samples of the nine total per tissue layer had RPKMs greater than 30 (average RPKM for *Actb* was ~90,000, 198,000, and 179,000 in the decidua, myo/endo and mesometrial triangle, respectively).

For qRT-PCR analyses, cDNA was synthesized from 1 μg RNA using an iScript cDNA Synthesis Kit (Bio-Rad). The PCR reaction was performed with Evagreen dye (Biotium) using a CFX Connect Real-Time PCR Detection System (Bio-Rad). Primers are listed in Table 3.2.

Prostaglandin measurements

Dissected uterine tissues were snap frozen and stored at -80°C before further processing. They were then weighed and pulverized in liquid nitrogen. The lipids were extracted with 500 μl ice-cold methanol-chloroform mixture (1:2) containing 10 μM indomethacin. A volume corresponding to 10 mg of tissue was taken and methanol was added to a final volume of 1 ml.

These samples were sonicated 3 times (7 seconds each) and then vortexed. 100 µl was then dried in a speed vac and resuspend in PBS to quantify protein amounts using the Bradford assay (Abcam). The remaining 900 µl was centrifuged for 15 min at 10,000x*g* at 4°C to pellet precipitated proteins. The supernatants were kept at -80°C overnight to precipitate any additional proteins, and then evaporated in a speed vac. The samples were than resuspended in ELISA buffer, and concentrations of PGE_2, PGE metabolites, $PGF_{2\alpha}$, and PGD_2 were determined using commercial ELISA kits (Cayman Chemical) following the manufacturer's instructions.

Statistics and reproducibility

The number of independent biological replicates and specific test employed for each experiment is shown in the figure or stated in the figure legend. Except for the RNA-Seq, statistical analyses were performed using Prism 9 (GraphPad). $p<0.05$ was considered to be statistically significant. Student's *t*-tests and Mann-Whitney *U* tests were unpaired and two-tailed. For the analysis of labor onset timing, a log-rank test was applied to all groups within an experiment to determine the overall *p* value shown in the figure; comparisons between pairs of groups were then calculated and considered to be significant if their *p* value was less than the Bonferroni-adjusted threshold *p* value calculated using the total number of meaningful comparisons within the experiment. The analysis of qRT-PCR data was performed on delta C_T values.

Chapter 4: H3K27me3 demethylases are required for inflammation-induced PTL

Introduction

Preterm birth (PTB) is the global leading cause of death among children under the age of five[191]. PTB results from preterm labor (PTL), a complex syndrome with multiple etiologies. Aside from its immediate consequences, PTB can have long-lasting developmental effects that persist into adulthood[192-196]. Thus, a critical challenge to modern obstetrics today is prevention of PTL, but progress on this issue is hindered by our profound lack of understanding regarding the fundamental mechanisms contributing to normal labor.

Although many pathological processes can likely trigger PTL, only acute pathological inflammation (i.e., intraamniotic infection/inflammation and chorioamnionitis) has been well characterized and causally linked to PTL[54,197-200]. Other etiologies remain poorly understood and, as a result, the majority of preterm births (~60%) are classified as idiopathic[201,202]. Regardless, both preterm and term parturition share common downstream phenotypic changes, known as the "common pathway of labor." These include remodeling and dilation of the cervix, rupture of the fetal membranes, and uterine contractions, all of which collectively facilitate the expulsion of the fetus[203]. Upstream components of the cascades that drive normal labor, and whether they are shared with idiopathic PTL, have remained less clear.

During the pre-partum period, both mouse and human uteri show evidence of low-level, sterile inflammation, suggesting potential shared mechanisms of activation that might act as upstream contributors to both PTL and term labor. Proinflammatory cytokines like TNF-α, IL-1β and IL-8 trigger activation of NF-κB which results in heightened levels of COX-2, $PGF_{2\alpha}$, the gap junction protein connexin 43 (CX43) and upregulation of the oxytocin receptor (OXTR)[204,205]. COX-derived prostaglandin production is thought to be one of the converging

pathways between normal labor and inflammation-induced PTL, but the exact intersection points are unknown.

COX-1 and COX-2 are the two known cyclooxygenase isoforms, catalyzing the first step in PG synthesis from arachidonic acid to PGH_2. Although structurally similar, COX-1 and COX-2 differ in their functions and pattern of regulation[206,207]. COX-1 is constitutively expressed in almost all tissue types and is commonly labeled as a "housekeeping" gene due to its involvement in general tissue homeostasis. In contrast, COX-2 is typically absent in most tissues but can be rapidly induced in response to cytokines, mitogens and growth factors. During pregnancy, concentrations of the COX products, PGE_2 and $PGF_{2\alpha}$, increase in maternal and fetal tissues prior to labor onset[208,209]. These inflammatory mediators can stimulate uterine contractions *in vitro* and *in vivo* as well as induce cervical remodeling and dilation[210]. As previously discussed in Chapter 2, COX-1-derived PGs in mice are essential for normal labor onset and likely contribute to PTL [59,97]. In humans, studies have shown induction of both COX-1 and COX-2 in extraembryonic membranes from PTL patients[211,212].

Blocking PG production with nonsteroidal anti-inflammatory drugs (NSAIDs) have proven effective in attenuating the progression of term labor and PTL in both mice[12,213] and humans[214,215]. Despite their efficacy, however, fetal and maternal side effects have limited their use[216,217]. Identifying the upstream pathways that induce COX expression prior to PTL may provide more efficacious therapy without causing significant morbidity.

To further dissect the pathways required for PTL, researchers have developed various mouse models of PTB. The most common of these is lipopolysaccharide (LPS)-induced PTB, a well-established model of inflammation-induced labor that is thought to mimic the key aspects of chorioamnionitis-induced PTB in humans[218]. In mice, LPS injection (like intrauterine infection)

causes PTB within 24 hours by premature induction of luteolysis[59,205,219]. LPS stimulates the Toll-like receptor (TLR)-4 in the uterus and activates an inflammatory cascade that induces expression of cyclooxygenase (COX-2) and a significant increase in uterine and ovarian PG concentrations. Administration of a COX-2-selective inhibitor (SC-236) prevents preterm delivery and reduces PG production[59]. Administration of a COX-1-selective inhibitor (SC-560) attenuates uterine and ovarian PG production but does not inhibit PTL as effectively as SC-236, suggesting a more prominent role for COX-2 over COX-1 in driving PTL in mice[59]. This is moreover confirmed by studies showing that COX-1-deficient mice exhibit no delay in their onset of PTL after LPS[59]. These findings suggest that the mechanisms required for inflammation-mediated PTL depend on COX-2 while normal term labor depends on COX-1. How these different parturition pathways induce the activities of different COX isoforms remains an open question.

Additional observations in mice suggest that uterus-intrinsic parturition pathways are also active in LPS-induced PTL. That is, supplementing mice with exogenous progesterone delays PTL but only by 24 hours[59]. How parturition still occurs in spite of high P4 levels remains poorly characterized despite its potential greater relevance towards inflammation-induced PTB in humans. Together, identifying the upstream components of the cascades that drive normal labor and PTL, including those that trigger uterine prostaglandin production, is critical to understanding all forms of labor onset.

In addition to LPS, a recently published model uses all-trans retinoic acid (ATRA), administered twice daily from GD16.5-17.5, to induce PTB[74]. This model stems from observations that alcohol dehydrogenase 1 (*Adh1*) and aldehyde dehydrogenase family 1, subfamily A2 (*Aldh1a2*), critical enzymes for retinoic acid metabolism, is overtly upregulated in

almost all stromal cells in the late gestation uterus. The mechanism behind RA-induced PTB remains unclear, but ATRA treatment was shown to downregulate extracellular matrix genes such as *Col1a1, Penk, Eln, Fn1,* and *Postn,* suggesting that stromal cell-derived RA may play a vital role in the degradation of the extracellular matrix required for parturition onset. Whether RA-induced PTB also involves COX induction remains unknown.

Using two different models, our laboratory previously implicated demethylation of H3K27me3 as contributing to the labor cascade in mice[98]. In one model, late gestation administration of GSK-J4, an inhibitor of the two known H3K27 demethylases KDM6A and KDM6B[99-101], delayed delivery when the mice were supplemented with exogenous P4, to mimic the systemic hormonal environment that prevails during parturition in humans. In another model, GSK-J4 delayed parturition when the mice were allowed to deliver normally (i.e., via luteolysis). My results presented in Chapter 2 suggest that the relevant GSK-J4 target cell type for this delay are the undecidualized PDGFRα$^+$ fibroblasts that exist throughout the entire uterus, including in the segments of undecidualized uterus positioned between each implantation site (inter-implantation sites) as well as in each implantation site's anti-mesometrial pole. However, whether KDM6A, KDM6B, and/or H3K27me3 demethylation is a component of PTL pathways remained unknown.

Here, we reveal that KDM6B is required within PDGFRα$^+$ fibroblasts for the initiation of mouse preterm labor using both the LPS and ATRA models of PTB. These results provide novel insight into PTL parturition pathways, and provide a foothold, centered on epigenetics, for further dissection of upstream and downstream parturition pathway components. These results dovetail with our findings from Chapter 2, suggesting that KDM6B may be a critical

convergence point for natural and inflammation-induced labor onset pathways, thus providing potential insight into pathogenic mechanisms in PTL.

Results

A potential role for KDM6A and KDM6B in LPS-induced uterus-intrinsic PTB pathways

To study the role of KDM6A and KDM6B in pre-term labor pathways, we generated *Pgr-cre Kdm6a*$^{f/f}$ and *Pgr-cre Kdm6b*$^{f/f}$ mice (hereafter referred to as *Kdm6a cKO* and *Kdm6b cKO* mice) to target gene deletion within progesterone receptor (PR)-expressing cells of reproductive tissues[104]. *Kdm6a cKO* mice showed early pregnancy failure soon after implantation (see Chapter 5), forcing us to evaluate the role of *Kdm6a* in late gestation by studying *Pgr-cre Kdm6a*$^{f/+}$ mice, in which *Kdm6a* gene dosage is reduced in half ("*Kdm6a cHet* mice").

We then evaluated whether *Kdm6a* and/or *Kdm6b* contribute to inflammation-induced PTL. These experiments took advantage of the well-established LPS injection model of PTL but incorporated the additional feature of progesterone (P4) administration, which, by sidelining the potential luteolytic effects of LPS[59], allowed us to assess the uterus-intrinsic components of the response. Accordingly, mice were injected intravenously with 5 μg ultrapure LPS on GD16.5 at the same time as injecting them subcutaneously with P4 to functionally rescue any loss in ovarian function (Figure 4.1A). Then, since the cervix does not dilate in this situation, we did not score for actual delivery but rather for intrauterine pup death 24 hours after LPS injection, which was interpreted as being the consequence of uterine contractions.

Using this model, we found that both *Kdm6a cHet* and *Kdm6b cHet* mice were resistant to LPS-induced preterm birth, with pup viability significantly higher in both strains 24 hours after LPS injection, when compared to floxed controls (Figure 4.1A-B). However, *Pgr-cre*$^{+}$ mice

bearing completely wild-type *Kdm6a* and *Kdm6b* alleles also showed significantly less intrauterine pup death when compared to floxed controls, implying that the *Pgr-cre* allele may itself may be contributing to the uterus's insensitivity to LPS (Figure 4.1C). Therefore, while it remains possible that loss of even one *Kdm6a* or *Kdm6b* allele within PR^+ cells is sufficient to protect against the parturition-inducing effects of LPS, we can't rule out the possibility that this phenotype is entirely driven by the *Pgr-cre* allele.

A role for KDM6B in LPS-induced luteolysis PTB pathways

Given our aforementioned results on the role of KDM6B in luteolysis-induced term labor (see Chapter 2), we then assessed whether *Kdm6b* plays a role in the luteolysis pathways that trigger preterm birth in mice (i.e., without P4 supplementation; Figure 4.2A). These experiments employed *Kdm6b cKO* mice generated with a *Pdgfra-cre* driver to target *Kdm6b* gene deletion to all uterine fibroblasts. As discussed in Chapter 2 and shown again in Figure 4.2B, these mice naturally deliver 1-3 days later than $Kdm6b^{f/f}$ and $Pdgfra\text{-}cre\ Kdm6b^{wt/wt}$ controls, which both consistently deliver on GD19.5 as is typical for mice on a C57BL/6 (B6) background.

Without P4 administration, intravenous injection of a low dose of LPS (0.25 μg) on GD16.5 induced delivery within 24-48 hours in wildtype (wt) B6 mice, whereas *Kdm6b cKO* mice were completely resistant to the effects of LPS (Figure 4.2B). That is, even when challenged with a low dose of LPS on GD16.5, *Kdm6b cKO* sustained their pregnancies until GD20.5-22.5, i.e., normal delayed delivery timing for these mice. Of note, the low dose of LPS used was not sufficient to trigger classic signs of systemic inflammation such as lethargy, piloerection or poor grooming.

In wt B6 controls, low dose LPS administration led to rapid ovarian induction of *Akr1c18*, which encodes the P4-catabolizing enzyme 20α-hydroxysteroid dehydrogenase (20α-HSD) (Figure 4.2C) as well as a precipitous decline in serum P4 concentrations (Figure 4.2D), indicating that even a low dose of LPS induces luteolysis in wt mice. In contrast, *Kdm6b cKO* mice maintained high serum P4 levels after LPS administration (Fig. 4.2D), implicating a critical role for KDM6B in fibroblasts in triggering LPS-induced luteolysis and preterm labor.

Early administration of LPS delays parturition in wild-type mice

To assess how the timing of LPS administration affects murine parturition timing, we then injected wt mice with the same low dose (0.25 μg) of LPS at GD12.5 or GD14.5 (mid-gestation) (Figure 4.3A). Surprisingly, and in contrast to the PTL phenotype observed when LPS is injected in late gestation, mid-gestation LPS administration delayed parturition onset by 1-3 days in wt mice (Fig. 4.3B). This delay was in turn associated with a delay in luteolysis since mice treated with LPS at mid-gestation maintained high serum P4 concentrations through GD18.5, in contrast to untreated mice (Fig. 4.3C). This result was unlikely due to LPS-induced intrauterine growth restriction, since similar doses administered at GD12.5 had no effect on fetal weights[220].

Administration of ATRA induces PTL in control, but not Kdm6b cKO mice

We also evaluated whether KDM6B contributes to ATRA-induced PTL. These experiments took advantage of a newly established ATRA injection model of PTL (Figure 4.4A)[74]. Consistent with previously published data, *Aldh1a2* expression increased with advancing gestation in uterine fibroblasts (Figure 4.4B). This expression pattern was not seen in

other cell types known to be involved in parturition such as SMCs (Figure 4.4B). *Kdm6b cKO* fibroblasts showed suppressed induction of *Aldh1a2* levels compared to controls, with significant divergence starting on GD16.5 (Figure 4.4B). These results, in combination with our previous data that *Kdm6b cKO* mice are delayed in normal parturition, raises the possibility that the uterus must reach a retinoic acid threshold for on-time labor onset.

Interestingly, the ATRA dose (32 mg/kg) used in the original study[74] induced fetal death in mice on a B6 background and did not affect parturition timing (data not shown). However, 16 mg/kg of ATRA induced PTB by accelerating the timing of parturition by 24 hours in wt B6 mice, whereas *Kdm6b cKO* mice were completely resistant (Fig. 4.4C). That is, similar to the LPS phenotype, when challenged with ATRA from GD16.5-17.5, *Kdm6b cKO* mice sustained their pregnancies until GD20.5-GD21.5, i.e., normal delivery timing for these mice (Fig. 4.4C).

Surprisingly, ATRA was found to induce PTB independent of alterations in uterine *Ptgs1* or *Ptgs2* levels, since neither cyclooxygenase isoform was found to be transcriptionally induced in any uterine tissue layer in response to ATRA (Figure 4.4D). Moreover, we did not detect a change in *Kdm6a* or *Kdm6b* mRNA levels, suggesting that ATRA-induced PTL does not require upregulation of these enzymes (Figure 4.4D). Instead, it suggests that the *Kdm6b cKO* resistance to ATRA-induced PTL is likely due to a uterine defect that already exists prior to ATRA administration.

Discussion

These data indicate a role for KDM6B in inflammation-induced PTL. KDM6B's role in luteolysis-dependent PTL pathways, in conjunction with the data presented in Chapter 2, raises the possibility that a KDM6B-regulated epigenetic pathway is a common element upstream of

both term labor and preterm labor onset. We also present evidence in support of a role for KDM6B in ATRA-induced PTL, although the mechanism behind this pathway is still unclear.

One shared pathway of term labor and inflammation-induced PTL is COX-derived prostaglandin production, but the COX isoforms required for PTL versus normal labor are different. While COX-2 is dispensable for normal mouse parturition onset, it plays a significant role in both the uterus-intrinsic and luteolysis pathways of LPS-induced PTB. *Ptgs2* mRNA expression increases in the decidua 6 hours after LPS injection, and pup viability is higher in LPS/P4-injected B6 mice given the selective COX-2 inhibitor SC-236, consistent with fetal death in this model being due to the generation of a COX-2-derived prostaglandin that induces uterine contraction against a closed cervix (unpublished data from the Erlebacher lab). COX-2 upregulation has also been shown to be a feature of LPS-induced PTL without P4 supplementation, with selective inhibition of COX-2 via the drug SC-236 preventing preterm delivery and the increase in prostaglandins[59].

The putative role for COX-1 in murine PTL is more complex. Selective inhibition of COX-1 concurrent with LPS administration attenuates PTL, but not to the extent seen with selective inhibition of COX-2[59]. Interestingly, inhibition of either COX-1 or COX-2 yields equivalent reduction in PG production in WT mice, but COX-1 inhibition is not as effective in reducing the actual PTL phenotype[59]. This observation suggests the possibility of distinct downstream effects of COX-1 versus COX-2. One hypothesis is that COX-2-derived PGs contribute to a reduction in the synthesis of luteotrophic factors such as prolactin or gonadotropins to trigger labor onset. Alternatively, COX-2 derived PGs might act differently than COX-1 derived PGs on cell populations within the uterus, leading to varied downstream effects like cytokine production.

Given our previous data on the role of KDM6B within uterine fibroblasts in promoting on-time COX-1 induction during normal pregnancy, in conjunction with published data on LPS-induced PTL in mice, it seems likely that *Kdm6b cKO* mice are resistant to LPS-induced PTL because they start with lower baseline levels of COX-1-derived $PGF_{2\alpha}$. In other words, a threshold must be reached, either via COX-1 or COX-2-derived PGS, to trigger luteolysis. Given that COX-2 seems to be the predominant isoform required for LPS-induced PTB, these results also raise the possibility that KDM6B lies upstream of decidual COX-2 induction. The mechanism by which this would occur remains unclear, but could involve an active process whereby LPS-dependent induction or activation of KDM6B[100] reduces H3K27me3 at key PTL-promoting loci, upstream of decidual COX-2. Alternatively, my data presented in Chapter 2 shows that *Kdm6b cKO* fibroblasts express lower levels of *Ccl2* and *Ccl7*, which encode chemokines important for recruiting leukocytes (mostly macrophages and T cells) in response to LPS[221]. This raises the possibility that LPS resistance in *Kdm6b cKO* mice is due to a deficiency in leukocyte recruitment. This would be in line with prior observations showing that depletion of uterine natural killer cells[222] or macrophages[223] leads to significant reductions in LPS-induced preterm birth.

Lastly, our results raise questions regarding mechanisms of ATRA-induced PTL, including how KDM6B contributes this process. Indeed, while the resistance of *Kdm6b cKO* mice to ATRA-induced PTB implicates a role for KDM6B, the lack of *Ptgs1* or *Ptgs2* induction by ATRA raises important questions. First, epithelial *Ptgs1* may have been undetectable due to the technical aspects of the experiment. Specifically, the qRT-PCR was done on whole uterine tissue layers on GD17.5, thus raising the possibility that epithelial *Ptgs1* signal was diluted by other dominant cell types in the tissue layer (SMCs and fibroblasts) or that 1 day of ATRA

treatment was not enough to detect a significant difference. Future experiments should include qRT-PCR analyses on purified cell types (luminal epithelial cells) as well as the administration of ATRA concurrently with the COX-inhibitor indomethacin to assess whether this rescues PTL. If ATRA does not effectively induce uterine *Ptgs1* or *Ptgs2*, it remains possible that ATRA is acting directly on the ovaries to induce luteolysis. Indeed, retinoic acid receptors (RARs) and the 'retinoid X' receptors (RXRs) are both expressed by murine ovaries[224], and *Pdgfra*$^{+}$ cells are present in the ovarian stroma, theca interna and externa, and ovarian epithelium[73]. In conclusion, the mechanism behind ATRA-induced luteolysis and PTL remains unknown, but the pathway is likely to be completely independent from that of LPS-induced PTL, given that retinoic acid has been shown to inhibit NF-κB activity[225-227].

Figures

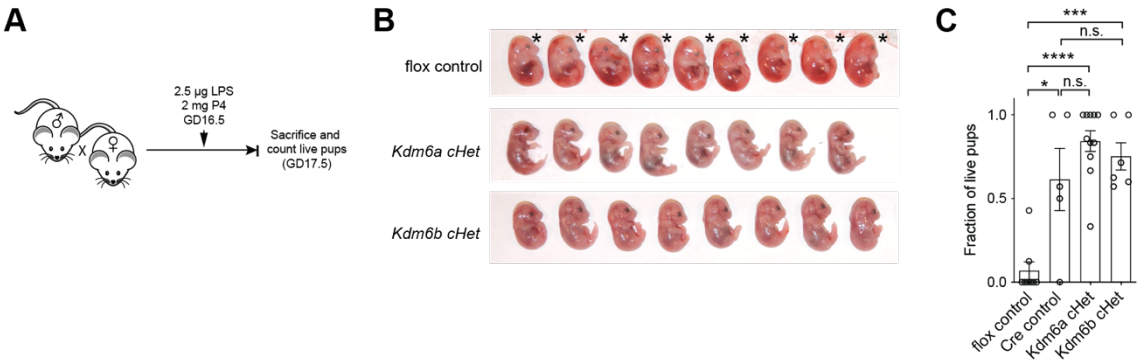

Figure 4.1 KDM6A and KDM6B are required for LPS-induced PTL.

(A) Schematic of LPS-induced PTL experiments. Mice were injected intravenously with 2.5 µg LPS concurrently with 2 mg P4 on GD16.5. Mice were sacrificed 24 hours later on GD17.5. (B, C) Representative litters (B) and quantified pup viability (C; mean+/-SEM) of mice 24 h after injection with 2 mg P4 and 2.5 µg LPS on GD16.5. Non-viable pups (*) frequently appear hyperemic. **, P<0.01; ****, P<0.0001 by Mann-Whitney *U* test. (n=5-12 mice/group).

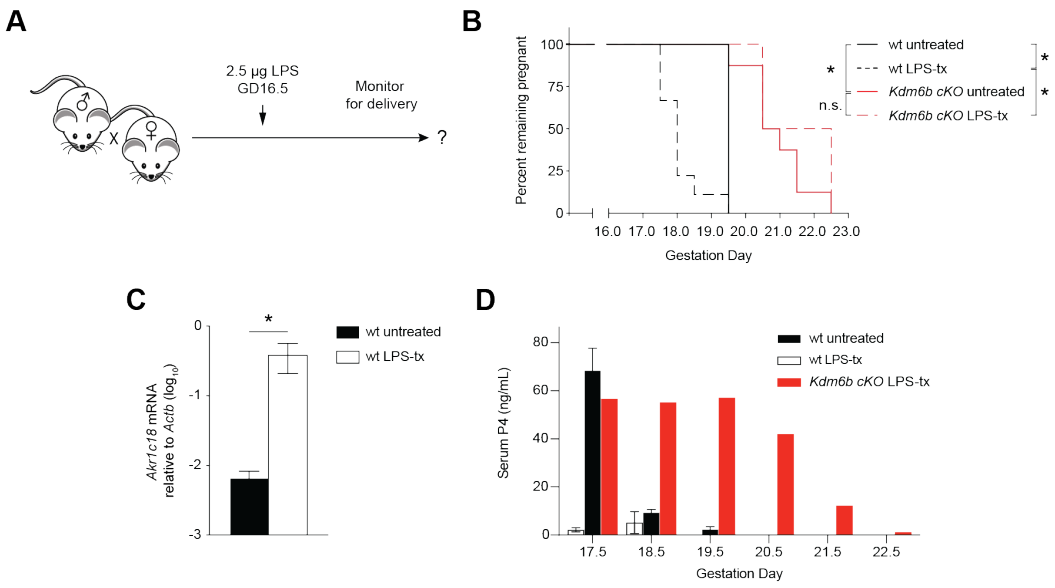

Figure 4.2 KDM6B is required for LPS-induced PTL.

(A) Schematic of LPS-induced PTL experiments. Wildtype (wt) or *Kdm6b cKO* mice were either untreated or injected intravenously with 0.25 µg LPS on GD16.5 and subsequently monitored for delivery. (B) Parturition timing in wt or *Kdm6b cKO* mice that were either untreated or injected with LPS on GD16.5. *, $P<0.05$ by the log-rank test (n=3-9 mice/group). Females were mated with B6 males. (C) *Akr1c18* mRNA expression in the ovaries. *, $P<0.05$ by Student's t-test (n=3 mice/group). (D) Serum P4 concentrations, assessed by ELISA, in mice injected with LPS on GD16.5 or left untreated (n=1-4 mice/group).

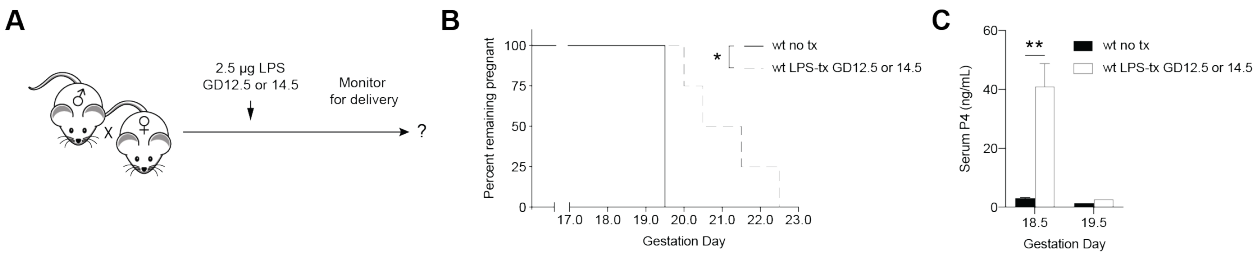

Figure 4.3 LPS injection in mid-gestation delays gestation length.

(A) Schematic of LPS-induced PTL experiment. Wildtype mice were either untreated or injected intravenously with 0.25 µg LPS on GD12.5 or GD14.5 (mid-gestation) and subsequently monitored for delivery. (B) Parturition timing in wt mice that were either untreated or injected with LPS in mid-gestation. *, $P<0.05$ by the log-rank test (n=3-4 mice/group). Females were mated with B6 males. (C) Serum P4 concentrations on GD18.5 and 19.5 in untreated mice or mice injected with LPS in mid-gestation. **, $P<0.01$ by Student's t-test (n=2-4 mice/group).

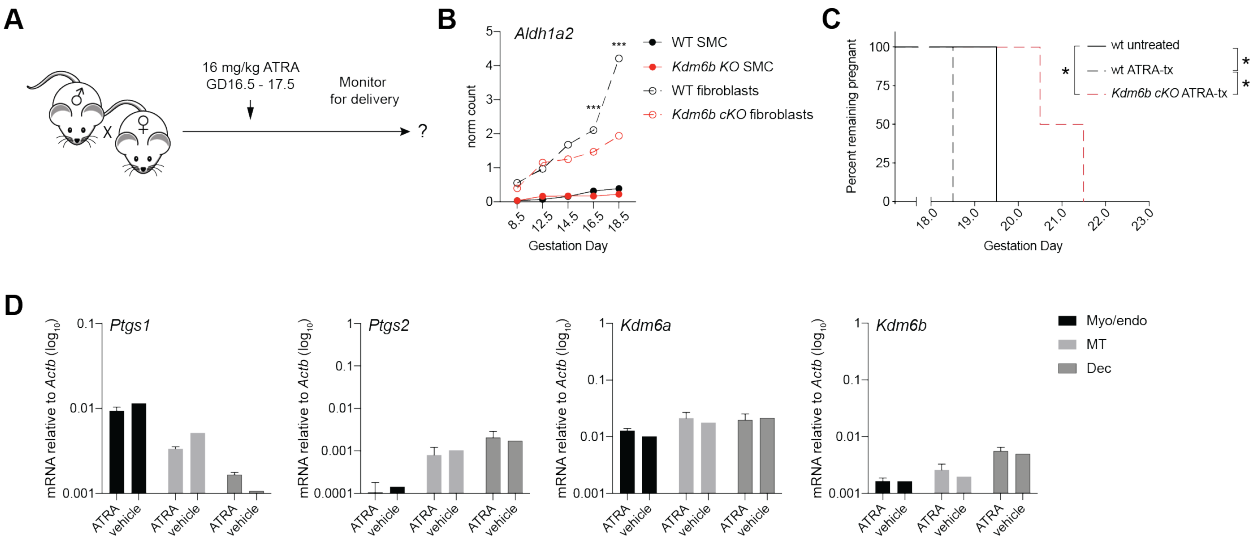

Figure 4.4 ATRA injection induces PTL in WT but not *Kdm6b cKO* mice.

(A) Schematic of ATRA-induced PTL experiment. Wildtype mice were either untreated or injected with 16 mg/kg ATRA intraperitoneally twice daily on GD16.5 and GD17.5 and subsequently monitored for delivery. (B) Normalized mRNA counts for *Aldh1a2* in control and *Kdm6b cKO* smooth muscle cells (SMCs) and fibroblasts from GD8.5, GD12.5, GD14.5, GD16.5, and GD18.5. (from the scRNA-Seq analysis described in Chapter 2 and including data from both IS myo/endo and IIS). Note the strong expression in fibroblasts compared to SMCs, and the divergence between WT and *Kdm6b cKO* mice starting on GD14.5. ***, *FDR*<0.001, ****, *FDR*<0.0001 by a two-sided Wilcoxon rank-sum test. (C) Parturition timing in wt and *Kdm6b cKO* mice that were either untreated or injected with ATRA twice daily GD16.5-17.5. *, *P*<0.05 by the log-rank test (*n*=2-4 mice/group). Females were mated with B6 males. (D) qRT-PCR analysis of gene expression on GD17.5 in the dissected uterine tissue layers of mice injected with vehicle or 16 mg/kg ATRA (*n*=1-2 mice/group; mean+/-SEM). The mesometrial triangle (MT) is the portion of the myometrium that overlies the decidua basalis; the myo/endo is the remaining portion of the myometrium, which has an inner surface of undecidualized endometrium with associated uterine epithelial cells.

Methods and Materials

Mice

C57BL/6J (B6), *Pdgfra-cre* (C57BL/6-Tg(*Pdgfra-cre*)1Clc/J)[108], *Kdm6a*$^{f/f}$ (B6;129S-*Kdm6a*$^{tm1.1Kaig}$/J)[131,228], and *Kdm6b*$^{f/f}$ (B6.Cg-*Kdm6b*$^{tm1.1Rbo}$/J) [131] mice were purchased from The Jackson Laboratory. *Pgr-cre* mice (*Pgr*$^{cre/+}$)[104] were the gift of Francesco DeMayo and John Lydon. *Pgr*-cre mice were intercrossed with *Kdm6a*$^{f/f}$ mice to generate *Pgr-cre* (*Pgr*$^{cre/+}$) *Kdm6a*$^{f/f}$ mice or with *Kdm6b*$^{f/f}$ mice to generate *Pgr-cre* (*Pgr*$^{cre/+}$) *Kdm6b*$^{f/f}$ mice. *Kdm6b*$^{f/f}$ mice were intercrossed with *Pdgfra-cre* to generate *Pdgfra-cre* Kdm6b$^{f/f}$ mice. Mice were housed in a specific pathogen-free animal barrier facility at UCSF. To maintain a consistent microbiota, all females were born in the Erlebacher lab holding room. All experiments were performed using female mice because only females become pregnant. Virgin females, 6-10 weeks old, were used for all experiments and were mated to B6 males unless otherwise indicated. All experiments were approved by the UCSF IACUC (Protocols #AN194381, AN193713, AN179716, and AN178689).

Matings and parturition timing experiments

Virgin females, 6-10 weeks old, were used for all experiments and were mated to B6 males unless otherwise indicated. Vaginal plugs were checked in the mornings, and noon of that day was counted as GD0.5. To determine labor onset timing, pregnant mice were checked twice daily (9 am and 6 pm) for evidence of delivery, uterine bleeding, or maternal distress. If apparent at 9 am, labor onset timing was scored as GDX.5, with X being the number of days after mating (i.e., GD0.5). If apparent at 6 pm, it was scored as GD(X+1) (i.e., midnight of the next gestation day).

LPS experiments

For uterus-intrinsic LPS-induced preterm labor experiments, mice were intravenously injected with 2.5 μg of ultrapure LPS (InvivoGen) in 100 μl of PBS on GD16.5, concomitantly with 2 mg P4 (Sigma-Aldrich) dissolved in 0.1 ml sesame seed oil (Sigma-Aldrich) injected subcutaneously. Mice were sacrificed 24 hours later and pup viability was assessed. For luteolysis preterm labor experiments, mice were intravenously injected with 0.25 ug of ultrapure LPS (InvivoGen) in 100 μl of PBS on GD12.5, GD14.5, or GD16.5. Mice were subsequently monitored for delivery.

All-trans retinoic acid experiments

Mice were injected intraperitoneally with 16 mg/kg all-trans retinoic acid (Sigma, cat# R2625) dissolved in 20% DMSO/80% sesame seed oil twice daily from GD16.5 to GD17.5. Mice injected intraperitoneally with 20% DMSO/80% sesame seed oil twice daily from GD16.5 to GD17.5 for vehicle-treated controls. Mice were subsequently monitored for delivery.

Serum P4 measurements

For serum P4 measurements, blood was collected retro-orbitally using microhematocrit capillary tubes (Fisher Scientific) and allowed to clot for 45 min at room temperature, then centrifuged at 1500*g* for 10 min to collect the serum supernatant. P4 concentrations were measured using a commercial ELISA kit (Cayman Chemical, cat. #582601) according to the manufacturer's instructions.

qRT-PCR

Whole tissue layers were homogenized in TRIzol (Thermo Fisher Scientific), and RNA was isolated according to the manufacturer's instructions. cDNA was synthesized from 1 μg RNA using an iScript cDNA Synthesis Kit (Bio-Rad). The PCR reaction was performed with Evagreen dye (Biotium) using a CFX Connect Real-Time PCR Detection System (Bio-Rad). Primers were designed with NCBI Primer-Blast software and a test qRT-PCR reaction was performed on every primer pair to ensure no self-amplification, to verify melting curves, and to confirm the correct product length. The cycle threshold (Ct) value of the housekeeping gene *Actb* was subtracted from the Ct of the experimental gene to determine the ΔCt. Statistical analyses were performed using ΔCt values. Expression of a given gene relative to *Actb* was determined using the formula $2^{-\Delta Ct}$. Primers sequences were as follows: *Actb*-Forward: 5'-GCTCTGGCTCCTAGCACCAT-3', *Actb*-Reverse: 5'-GCCACCGATCCACACAGAGT-3'; *Akr1c18*-Forward: 5'-GCTGATATGTTTAAGGCTCACCCTAA-3', *Akr1c18*-Reverse: 5'-AGAGTCCAGCATCACACAAAAGATC-3'.

Chapter 5: Histone demethylase KDM6A is critical for murine decidualization and pregnancy

Introduction

Dynamic deposition and erasure of the repressive histone mark, histone 3 lysine 27 trimethyl (H3K27me3), has been demonstrated to be essential for cell differentiation and cell identity. These marks are deposited by the polycomb repressive complex 2 (PRC2) to induce transcriptional silencing and can be subsequently removed via the histone demethylases KDM6A or KDM6B to facilitate gene expression. Although much of what is known about H3K27me3 dynamics is in the context of embryonic development, research from our laboratory and others has also revealed the importance of these epigenetic mechanisms within the pregnant uterus[98,190,229].

One reproductive process that requires a delicate balance of H3K27me3 dynamics is decidualization, the process by which the endometrium transforms into the decidua during early pregnancy[98,190]. In mice, decidualization is triggered upon embryo attachment to the epithelium, prompting the proliferation and differentiation of endometrial stromal cells (ESCs) into decidual stromal cells (DSCs)[230,231]. DSCs are characterized by their large size, multinuclear polyploidy, and abundance of glycogen and lipids. In humans, they also express various functional markers including prolactin and insulin-like growth factor binding proteins (IGFBPs). DSCs make up the majority of cells within the decidua and are important for immune modulation and structural support of the placenta (for reviews see refs.[37,38,232]). In short, a proper decidualization response in early pregnancy is vital for pregnancy success[233].

Decidualization of ESCs requires coordinated interactions between morphogens, transcription factors, cytokines, and signaling pathways. Many members of the transforming

growth factor-β (TGF-β) superfamily have been shown to be vital for this process, revealed through the use of conditional gene deletion strategies in mice[234]. These models have uncovered essential roles for bone morphogenetic proteins (BMPs) and their receptors. Conditional deletion of *Bmp2* using a *Pgr-cre* driver results in female sterility due to decidualization defects, associated with dysregulation of multiple decidualization-related genes including *Msx1/Msx2, Wnt4/6,* FK-506 binding proteins (*Fkbp5*), and prostaglandin synthase2 (*Ptgs2*)[235]. Although numerous BMPs are expressed in the uterus throughout pregnancy, only *Bmp2* is tightly linked with implantation[236,237]. That is, it is completely absent during the pre-implantation period but is induced in the subepithelial stroma surrounding the site of the blastocyst after implantation. Post-implantation, expression of *Bmp2* wanes in the primary decidua but increases in the proliferating secondary decidua. Studies on conditional inactivation of BMP receptors have confirmed the importance of BMPs in decidualization[238,239].

Previous work from our laboratory showed that decidualization was associated with a dramatic induction of enhancer of zeste homolog 2 (EZH2), the catalytic subunit of the PRC2 complex. This EZH2 upregulation was also associated with *de novo* accumulation of H3K27me3 on ~800 protein-coding genes[98,229]. Conditional ablation of *Ezh2* within the uterine stroma and epithelium leads to ectopic myofibroblast formation, peri-embryonic collagen deposition, and amplified TGF-β-driven fibroblast activation and ECM remodeling in the decidua, ultimately leading to pregnancy failure in mid-gestation[229]. This data, combined with prior research indicating the necessity of TGF-β receptor signaling for decidualization, suggests that PRC2-mediated gene silencing in DSCs selectively suppresses pregnancy-averse features of the TGF-β response[234,240,241].

In addition to the set of ~800 genes accruing H3K27me3 at their promoters during decidualization, a distinct set of 1,967 protein-coding loci lost H3K27me3 during decidualization[83], raising the possibility that dynamic accumulation and erasure of H3K27me3 is required to coordinate decidualization gene expression programs. How the KDM6A/B enzymes are involved in the removal of H3K27me3 during decidualization, and whether this is critical for pregnancy success remained unknown.

To address these questions, we used a *Pgr-cre* driver to conditionally ablate *Kdm6a* and *Kdm6b* in the uterine stroma and epithelium to study critical events in early pregnancy. While *Kdm6b cKO* mice demonstrated normal implantation and decidualization, *Kdm6a cKO* mice exhibited compromised decidualization and, consequently, were completely infertile. RNA-seq analysis demonstrated that ablation of *Kdm6a* led to dysregulation of genes previously shown to be required for decidualization. These data implicate *Kdm6a* as a pivotal regulator of gene expression in murine decidualization required for pregnancy success.

Results

Kdm6a cKO mice exhibit early pregnancy loss

To assess how KDM6A and/or KDM6B activity regulates decidualization in early mouse gestation, we generated *Kdm6a* and *Kdm6b cKO* mice by intercrossing $Kdm6a^{f/f}$ or $Kdm6b^{f/f}$ mice with mice bearing a *Pgr-cre* driver, which targets gene deletion to progesterone receptor (PR)-expressing reproductive tissues[104]. KDM6A was undetectable in DSCs of *Kdm6a cKO* uteri (Figure 5.1A), as expected since *Pgr-cre* is expressed postnatally at high levels in the epithelial and stromal compartments of the uterus[104]. Age-matched $Pgr^{wt/wt}Kdm6a^{f/f}$ or $Pgr^{wt/wt}Kdm6b^{f/f}$ mice were used as controls.

Notably, *Kdm6b cKO* mice sustained their pregnancies to term and exhibited normal implantation site weights at GD5.5, suggesting a non-essential role for *Kdm6b* in murine reproduction (see Figure 2.8A). Strikingly however, *Kdm6a cKO* mice were unable to carry pregnancies to term, as evidenced by the complete absence of litters during a 6-month breeding period with wildtype B6 males. Together, these findings suggest a function for KDM6A in the early gestation decidua.

Ablation of Kdm6a in the uterus leads to a defect in decidualization

To identify possible causes of pregnancy failure in *Kdm6a cKO* mice, we first performed a thorough examination of the decidua using H&E staining, allowing us to visualize and assess the structure and overall morphology of the decidual bed. This analysis revealed that the pregnancy failure evident in *Kdm6a cKO* mice occurs around GD8.5 and is associated with partial liquefaction of the decidua (Figure 5.1B).

Given these observations, we next considered that pregnancy failure might be due to an inability of ESCs to fully decidualize. Indeed, we found using immunofluorescence that KDM6A expression is transiently elevated in early gestation DSCs in parallel to the elevated expression of EZH2 that we previously described and that which we believe is the reason DSCs accumulate H3K27me3 in early gestation (Figure 5.2)[98]. Moreover, there was no detectable KDM6A staining in the inter-implantation sites at this timepoint, further suggesting a DSC-specific role for KDM6A (Figure 5.2). These observations together raise the possibility that H3K27me3 status in early gestation DSCs is highly dynamic, with the generation of the marks occurring simultaneously with their erasure by KDM6A to determine the final setpoint that lasts throughout the lifetime of the decidua.

Stromal proliferation is intact, but differentiation is compromised in Kdm6a cKO DSCs

To more comprehensively determine how KDM6A deficiency in DSCs affects decidual physiology, we performed RNA-sequencing on DSCs and MSCs from control and *Kdm6a cKO* mice on GD6.5. Strikingly, 1,700 protein-coding genes were upregulated and 2,100 were downregulated in *Kdm6a cKO* DSCs (*FDR*<0.05) (Figure 5.3B), suggesting major transcriptional alterations in the absence of KDM6A.

Since decidualization requires coordinated progression of stromal cell proliferation and differentiation at the site of implantation, we first looked at proliferation genes in the RNA-Seq. None of the differentially expressed genes in DSCs were related to proliferation (i.e., *Mki67, Ccnb1, Cenpf, Birc5, Ccne1, Ube2c, Cdc20,* or *Cep55*), suggesting that KDM6A is dispensable for the proliferation phase of decidualization. We next analyzed markers of differentiation for stromal cell decidualization and found that many critical decidualization genes were downregulated in *Kdm6a cKO* DSCs including: *Bmp2, Fst, Il15, Fkbp5, Dact1, Cdh1, Msx1, Msx2, Notch1, Nr5a2, Prlr, and Sphk1*[242] (*FDR*<0.05) (Figure 5.3C). Of these, *Dact1* and *Nr5a2* were upregulated in *Ezh2 cKO* DSCs[229], consistent with the idea that KDM6A is specifically required to remove H3K27me3 to allow for de-repression of genes required for decidualization. Indeed, the promoters of *Bmp2*, *Cdh1, Msx1, Msx2,* and *Nr5a2* all harbor significantly less H3K27me3 in wild-type decidua compared to wild-type inter-implantation sites[98], suggesting possible KDM6A activity at these loci (Figure 5.3C). Of note, a number of classical decidualization markers were expressed normally in *Kdm6a cKO* DSCs (e.g., *Hoxa10*, *Bmpr2, E2f8, Prl8a2, Ptgs2, Wnt6, Hand2*), suggesting that KDM6A is not required for the entire decidualization gene program.

Interestingly, while *Cldn3* downregulation in *Kdm6a cKO* DSCs was suggestive of potential defective vascularization and angiogenesis, CD31 staining by immunofluorescence was comparable in uterine sections of WT and *Kdm6a cKO* mice on GD6.5 (Figure 5.4).

The number of downregulated decidualization genes in *Kdm6a cKO* DSCs suggested that the loss of demethylase activity had widespread effects on decidual homeostasis. Indeed, our analysis of upregulated genes in *Kdm6a cKO* DSCs revealed massive superinduction of *Inhbb* and *Inhba*, which encode components of the TGF-β superfamily member activin. Interestingly, activin and TGF-β are already expressed at high levels in the wild-type decidua and TGF-β signaling is required for normal decidualization [240,241], suggesting that KDM6A is critical for balancing normal activin/TGF-β signaling in early pregnancy.

Discussion

Here, we identify a critical role for KDM6A in decidualization and pregnancy success in mice. While embryo attachment, early fibroblast proliferation, and decidual vascularization appear normal, *Kdm6a cKO* DSCs fail terminally differentiate into DSCs, ultimately leading to subfertility. To our knowledge, this is the first study implicating a role for KDM6A in early mouse decidualization and pregnancy.

Given the canonical role of KDM6A as a histone demethylase, the decidualization failure in *Kdm6a cKO* mice seems likely to be caused by an inability to remove H3K27me3 at loci required for this process, including *Bmp2, Fst, Il15, Fkbp5,* and *Dact1, Cdh1, Msx1, Msx2, Notch1, Nr5a2, Prlr, and Sphk1*. Indeed, *Fst cKO* mice, who fail to decidualize and are severely subfertile, show increased activin B expression and impaired BMP signaling, similar to *Kdm6a cKO* DSCs[243]. This aberrant activin signaling in *Fst* and *Kdm6a cKO* mice is likely responsible

for the reduced BMP signaling, since antagonism between TGF-β/activin and BMPs has been reported in many developmental processes[244-246] and tissues[247-252]. The mechanism behind the activin superinduction remains unclear, but could be a result of dampened antagonism by *Fst*[253]. Collectively, our results suggest that KDM6A is required to upregulate *Fst* to repress activin signaling and preserve BMP signaling.

Whether the decidualization failure itself is caused by the superinduction of activin or the inability to express decidualization genes remains an open question. The similarity of *Kdm6a cKO* mice to the phenotype of *Bmp2 cKO* mice suggests that it may be the latter, and that the superinduction of TGF-β is a downstream consequence of impaired decidualization. *Bmp2 cKO* mice show normal embryo attachment, fibroblast proliferation, and vascularization of the endometrium, but compromised differentiation into DSCs[235]. BMPs signal through cell-surface heterodimeric receptor complexes comprising of type 1 receptors (ALK2, ALK3, or ALK6) and type 2 receptors (ACVR2A, ACVR2B, or BMPR2). Conditional deletion of the BMP type 1 receptor, ALK2, results in impaired stromal cell decidualization and infertility, but the *Alk2 cKO* females do not phenocopy *Bmp2 cKO* mice, suggesting that additional ligand-receptor pairs are likely involved in decidualization[238]. Conditional deletion of the BMP type 2 receptor, *Bmpr2*, results in mid-gestation pregnancy failure because of defective spiral artery remodeling, which also differs from the *Alk2 cKO* or *Kdm6a cKO* phenotypes[239]. Therefore, uterine BMP signaling is critical at various gestational stages and seemingly uses context-dependent receptors.

Notably, *Msx* homeobox genes (*Msx1* and *Msx2*) act downstream of BMP2 to regulate endometrial decidualization[254] and are also downregulated in *Kdm6a cKO* mice. While single knockouts of *Msx1* or *Msx2* develop normally presumably due to functional compensation of one for the other, ablation of both *Msx1* and *Msx2* causes a dramatically impaired decidual response.

Again, similar to both *Kdm6a cKO* and *Bmp2 cKO* mice, *Msx1*$^{-/-}$*Msx2*$^{-/-}$ uterine fibroblasts proliferate normally but fail to terminally differentiate into DSCs, raising the possibility that KDM6A-mediated regulation of *Bmp2* drives stromal cell differentiation via *Msx1/2* expression. Interestingly, *Wnt4* is markedly suppressed in *Msx1*$^{-/-}$*Msx2*$^{-/-}$ uteri, but not in *Kdm6a cKO* uteri, suggesting multiple nonredundant pathways required for decidualization.

The canonical role of KDM6A suggests that its role in early pregnancy is de-repression of decidualization genes via removal of H3K27me3. This seems likely given that many of the decidualization genes downregulated in *Kdm6b cKO* mice also lose H3K27me3 at their loci with decidualization (Figure 5.3C). Whether or not our phenotype is directly dependent upon KDM6A demethylase activity, however, remains an open question given that KDM6A been shown to have demethylase-independent functions as well[228,255-259]. For example, while several groups have found that KDM6A is required for embryonic development[228,258,260,261], a demethylase-dead version of KDM6A rescues embryonic lethality in *Kdm6a*$^{-/-}$ embryos[256]. This was not due to functional compensation by KDM6B, since embryos deficient for both enzymes survived to term. Therefore, KDM6A has functions beyond simply H3K27me3 demethylation. In the event that future experiments show that decidualization loci like *Bmp2* or *Fst* do not lose H3K27me3 in a KDM6A-dependent fashion, one alternative scenario is that these loci lose H3K27me3 through replicational dilution, a possibility given that the process of decidualization entails significant cellular proliferation. In this scenario, KDM6A may be coordinating with KMT2B to regulate deposition of a different mark required for transcriptional upregulation, such as the activating mark H3K4me3[262].

Finally, this study raises the question of what regulates KDM6A. One possibility is that both PRC2[229] and KDM6A are themselves contextually programmed by TGF-β signaling,

especially since TGF-β1 and activin are expressed at high levels in the early decidua[234,263,264]. KDM6A has been previously linked to TGF-β, but its effects appear to be context-specific. For instance, while TGF-β suppresses KDM6A translation and protein expression in a variety of cancer cell lines[265], TGF-β can also induce KDM6A activity in renal mesangial cells[266]. Given the dysregulation of TGF-β signaling in *Kdm6a cKO* mice, in addition to our findings in *Ezh2 cKO* mice[229], it seems plausible that a delicate balance of TGF-β/KDM6A/EZH2 activity is required to establish a pro-decidualization environment that selectively allows for TGF-β target and decidualization genes to either be transcriptionally induced or silenced.

Figures

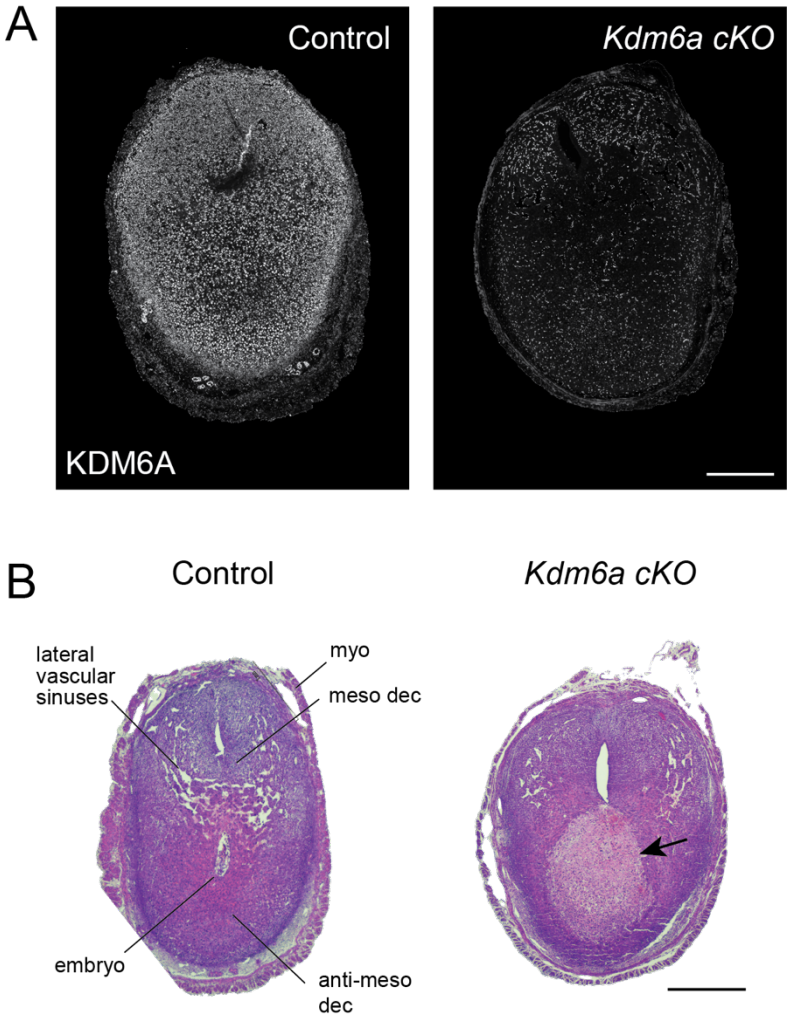

Figure 5.1 Post-implantation failure in *Kdm6a cKO* mice.

(A) Immunofluorescence detection of KDM6A expression in control and *Kdm6a cKO* GD6.5 implantation sites. Although DSCs no longer express KDM6A in *Kdm6a cKO* mice, endothelial cells and immune cells continue to stain positive for KDM6A. Representative images from $n = 3$ mice/group. Scale bar, 500 μm. **(B)** H&E stains of representative implantation sites on GD7.5 from control and *Kdm6a cKO* mice. Implantation site architecture is labeled in control implantation site. Arrow denotes necrosing decidua in *Kdm6a cKO* implantation site. Scale bar, 500 μm.

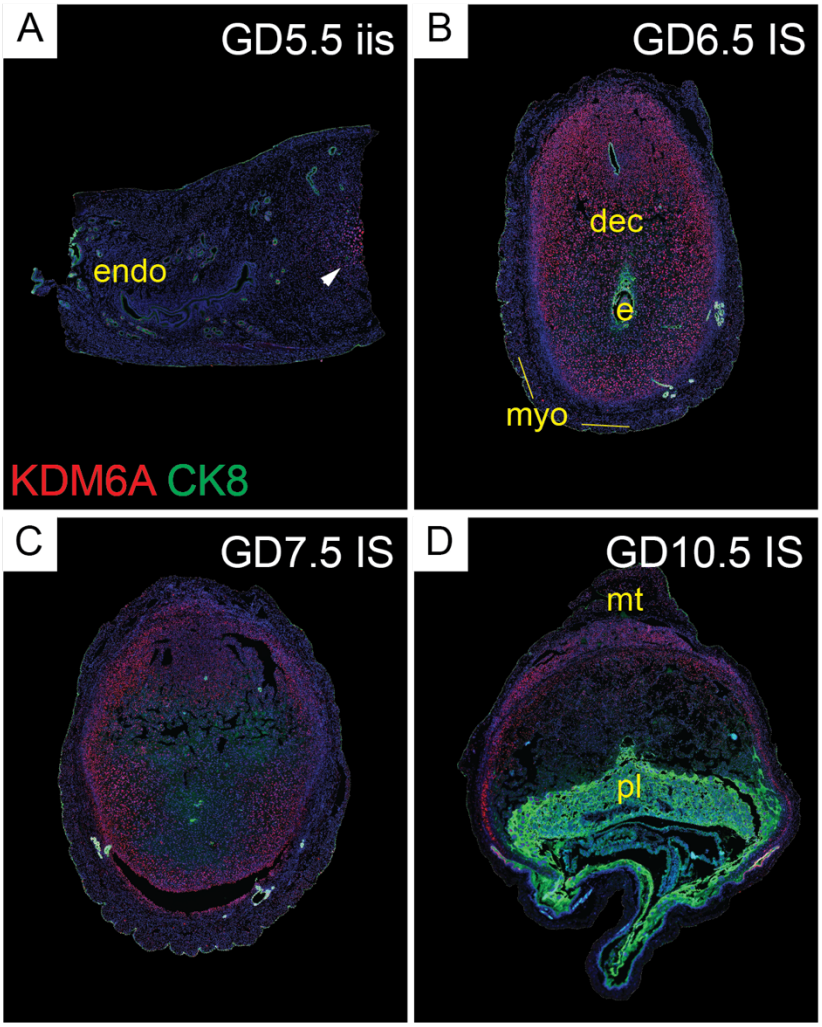

Figure 5.2 KDM6A immunostaining of post-implantation uteri.

On GD5.5, KDM6A was expressed at undetectable levels by ESCs in inter-implantation sites, but stronger expression was detectable at GD5.5 at the implantation site (A; arrowheads). On GD6.5, KDM6A was strongly expressed in most DSCs (B). On GD7.5, low or undetectable KDM6A staining was found in the primary decidual zone, but strong staining was still detectable in the secondary decidual zone (C). By GD10.5, KDM6A was expressed at low or undetectable levels in the decidua, but strongly expressed in the anti-mesometrial myo/endo (D). Cytokeratin 8 (CK8) identifies uterine epithelial cells and trophoblasts. DAPI counterstain. Endo, endometrium; myo; myometrium; dec, decidua; e, embryo; pl, placenta.

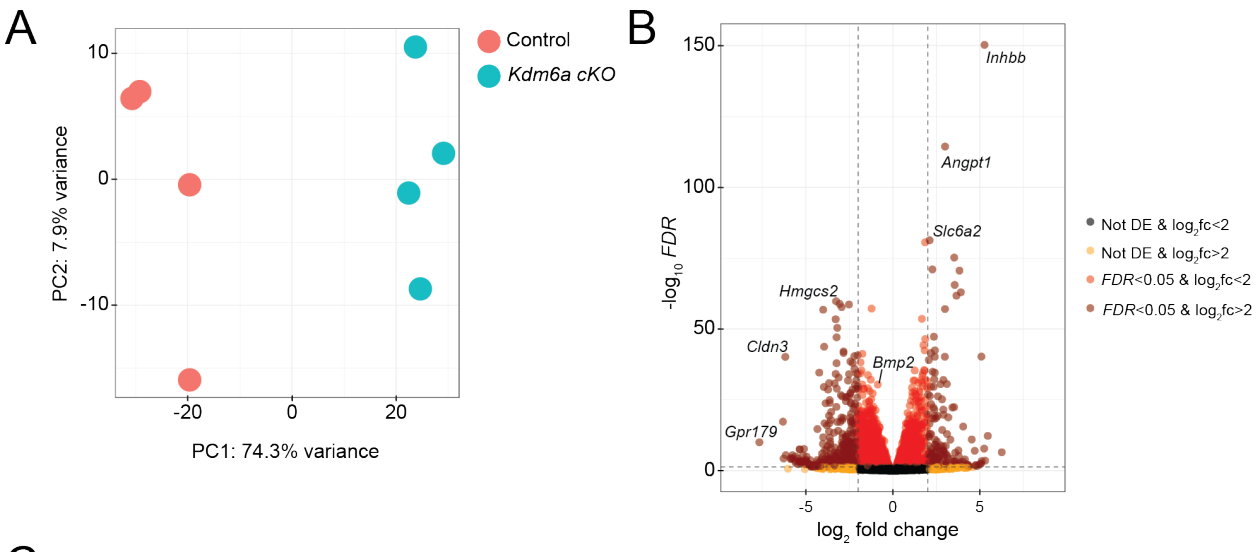

C

Gene	*Kdm6a cKO* vs. Control DSC RNA		Decidua vs. IIS [H3K27me3]		Decidua vs. Myo [H3K27me3]		Reference
	log_2fc	*FDR*	log_2fc	*FDR*	log_2fc	*FDR*	
Bmp2	-1.20	0.00	-1.30	0.00	-1.27	0.00	Lee 2007
Fst	-0.50	0.01	-2.11	0.00	-1.92	0.03	Fullerton 2017
Msx1	-2.03	0.01	-0.48	0.00	-0.39	0.00	Daikoku 2011, Nallasamy 2012
Msx2	-1.32	0.00	-0.70	0.00	-0.63	0.00	Daikoku 2011, Nallasamy 2012
Nr5a2	-2.06	0.02	-0.53	0.00	-0.36	0.01	Zhang 2013
Cdh1	-1.58	0.00	-0.56	0.01	-	-	Reardon 2012
Il15	-1.11	0.00	-	-	-	-	Shindoh 2014
Fkbp5	-1.76	0.00	-	-	-	-	Guzeloglu-Kayisli 2021
Dact1	-0.35	0.03	-	-	-	-	Lee 2007
Notch1	-0.70	0.00	-	-	-	-	Afshar 2012
Prlr	-1.06	0.00	-	-	-	-	Reese 2000
Sphk1	-1.19	0.00	-	-	-	-	Mizugishi 2007

Figure 5.3 Impaired expression of decidualization genes in *Kdm6a cKO* DSCs.

RNA-seq was performed on purified decidual stromal cells from *n*=4 *Kdm6a cKO* mice and *n*=4 control mice sacrificed on GD6.5. (A) PCA plot of *Kdm6a cKO* and control DSCs. PC1 explains most of the variance between the three replicates in each group (74.3%). (B) Volcano plot of expression all genes differentially expressed (*FDR*<0.05) between the *Kdm6a cKO* and control DSCs. Note the superinduction of *Inhbb* and downregulation of *Bmp2*. (C) Table of key decidualization genes significantly downregulated in *Kdm6a cKO* DSCs compared to controls. Data from Nancy et al, 2018 is included to show differences in H3K27me3 between decidua (where DSCs reside) and IIS (where undecidualized endometrial stromal cells reside) as well as between decidua and the myometrium (where undecidualized fibroblasts reside)[98]. The final column lists key references defining the role of each gene in murine decidualization[235,243,254,267-274].

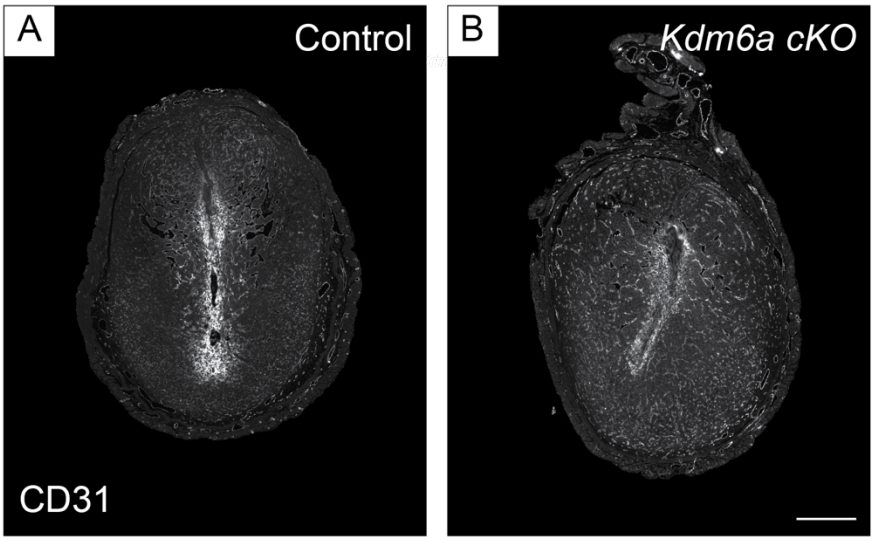

Figure 5.4 Immunofluorescence detection of CD31 expression in control and *Kdm6a cKO* GD6.5 implantation sites.

Representative images from *n*=2 mice/group. Scale bar, 500 μm.

Methods and Materials

Mice

C57BL/6J (B6) and *Kdm6a*$^{f/f}$ (B6;129S-*Kdm6a*$^{tm1.1Kaig}$/J)[131,228] mice were purchased from The Jackson Laboratory. *Pgr-cre* mice (*Pgr*$^{cre/+}$)[104] were the gift of Francesco DeMayo and John Lydon. *Pgr-cre* mice were intercrossed with *Kdm6a*$^{f/f}$ mice to generate *Pgr-cre* (*Pgr*$^{cre/+}$) *Kdm6a*$^{f/f}$ mice. Mice were housed in a specific pathogen-free animal barrier facility at UCSF. To maintain a consistent microbiota, all females were born in the Erlebacher lab holding room. All experiments were performed using female mice because only females become pregnant. Virgin females, 6-10 weeks old, were used for all experiments and were mated to B6 males unless otherwise indicated. All experiments were approved by the UCSF IACUC (Protocols #AN194381, AN193713, AN179716, and AN178689).

Matings

Virgin females, 6-10 weeks old, were used for all experiments and were mated to B6 males unless otherwise indicated. Vaginal plugs were checked in the mornings, and noon of that day was counted as GD0.5.

Immunohistochemistry and immunofluorescence

Uterine tissues were fixed overnight at 4°C in 4% paraformaldehyde/PBS and embedded in paraffin. Sections were cut at 10 μm, baked for 30 minutes at 65°C. H&E staining was performed using routine methods. For immunofluorescence, deparaffinized slides were first placed in a solution of 90% methanol and 3% H_2O_2 at room temperature for 20 minutes, then washed twice in PBS. Sections then underwent antigen retrieval either by incubation with 1 mg/ml trypsin in

PBS for 13 min at 37°C, or by boiling in 0.01M citric acid (pH 6.0) or TE (0.01M Tris Base, 0.01M EDTA, 0.05% Tween 20, pH 9.0) in a Biocare Decloaking Chamber NxGen (110°C for 5 minutes, then allowed to cool for 10 minutes in the chamber). After equilibrating to room temperature for 10 minutes, the slides were washed twice in PBS and then blocked in 1% BSA/3% donkey serum/0.4% Triton X-100 for 1 hour at room temperature, followed by application of primary antibodies, diluted in 1% BSA, 0.4% Triton X-100, and incubation at 4°C overnight. Antibody sources, dilutions and antigen retrieval methods for mouse specimens were KDM6A (Cell Signaling, cat. #33510, RRID: AB_2721244, 1:1000, decloaking in 10 mM Tris-EDTA pH 9.0) and CD31 (Becton Dickinson, cat. #557355, RRID: AB_396660, 1:300, trypsin). The slides were washed twice in PBS between all subsequent steps. The KDM6A and CD31 immunostaining employed biotin tyramide amplification, and so the sections were next incubated for 30 minutes at room temperature with horseradish peroxidase- (HRP-) conjugated donkey anti-rabbit IgG-secondary antibodies (Jackson ImmunoResearch) diluted 1:200 in TNB blocking buffer (PerkinElmer). They were then incubated in 1.8 μg/ml biotin-tyramide/0.0015% H_2O_2/PBS for 5 minutes at room temperature, then in 5 μg/ml streptavidin-Alexa Fluor 594 for 30 minutes at room temperature. The sections were then incubated with TrueBlack Lipofuscin Autofluorescence Quencher (Biotium, cat. #23007) and then mounted using DAPI mounting media (Electron Microscopy Sciences, cat. # 17989). All immunofluorescence images were captured using an Axio Imager M2 microscope running on Zen software (Zeiss). Adobe Photoshop was used to increase image brightness using the brightness/contrast function; in these cases, the alteration was applied over the entire image and was equally applied to all images within an experiment.

RNA-Seq

Decidual stromal cells were isolated by first digesting uterine tissues in Liberase TM (Roche, cat. #5401127001; 0.28 WU/ml), DNase I (Roche, cat. #1010415901; 30 μg/ml), and trypsin (ThermoFisher, cat. #15090046; 0.05%) in Ca^{++}/Mg^{++}-containing HBSS for 60 minutes at 37°C with trituration every 10 minutes. 5 mM EDTA (Life Technologies, cat. #15575020) was added for the final 15 minutes of the incubation. The cell suspensions were passed through 100 μm filters and then negatively selected as previously described[98] using LD magnetic bead columns (Miltenyi, cat. #130-042-901) and antibodies toward red blood cells (Ter-119, Miltenyi, cat. #130-049-901, RRID: AB_2936424), leukocytes (CD45, Miltenyi, cat. #130-052-301, RRID: AB_2877061), epithelial cells (CD326, Invitrogen, cat. #14-5791-85, RRID: AB_953626), and endothelial cells (CD102, Biolegend, cat. #105602, RRID: AB_10599101). Microbead-coupled goat anti-rat IgG antibodies (Miltenyi Biotec, cat. #130-048-502, RRID: AB_244364) were used as secondary reagents for the CD326 and CD102 antibodies, which were not directly bead coupled. RNA was isolated from purified stromal cells using the RNeasy Plus Mini Kit (Qiagen, cat. #74034). For RNA-Seq, the samples were then given to the UCSF Functional Genomics Core for quality control testing, single-end 50-bp RNA-Seq library preparation (Universal Plus mRNA kit, Nugen), and sequencing on an Illumina HiSeq 4000 system. Alignment was performed using the Splice-aware STAR aligner STAR_2.7.2b. Reads uniquely mapped to known mRNAs were used to identify genes with differential expression between B6 and *Kdm6a cKO* samples using the DESeq2 R package v1.24.0. Cooke's cutoff was applied to exclude outliers.

Chapter 6: Conclusions and Future Directions

The data presented in this dissertation provide novel insights into the molecular and cellular processes governing mouse parturition. In Chapter 2, we provide evidence that gestation length in mice is controlled by an epigenetic timer that operates autonomously within the PDGFRα^{+} fibroblasts of the pregnant uterus. The timer is set in the peri-implantation period via the tuning of appropriate H3K27me3 levels at select loci. After implantation, H3K27me3 levels begin to progressively erode at 4,554 loci, limiting the expression of linked genes until late gestation, when their induction initiates the labor cascade. Overwinding of the timer via genetic ablation of the histone demethylase KDM6B delays parturition. In contrast to other biological timers described to date that drive continuous developmental events, this timer is programmed early in gestation and then appears to run silently in the background to trigger a discrete event in the future. We speculate that other discrete events, such as puberty onset, may be regulated by a similar class of timers.

Chapter 3 was primarily written by Johan Siewiera and Adrian Erlebacher, to which I contributed by performing the eosinophil analyses. This chapter introduces a new model in which mice are manipulated endocrinologically to circumvent luteolysis and oblige them to enter labor through uterus-intrinsic pathways, potentially analogous to those in humans. This model also implicates a role for PDGFRα^{+} fibroblasts in uterus-intrinsic pathways of parturition, via their production of the alarmin IL-33. The data also demonstrates roles for uterine group 2 innate lymphoid cells and eosinophils in controlling the timing of uterus-intrinsic parturition.

Chapter 4 assessed the role of KDM6 demethylases in various mouse models of PTL. These studies took advantage of the well-established LPS injection model of PTB but, for some

experiments, incorporated the additional feature of progesterone administration, which, by sidelining the potential luteolytic effects of LPS, allowed us to assess the uterus-intrinsic components of the response. These experiments demonstrated a requirement for KDM6B within PDGFRα^{+} fibroblasts in these pathways' contribution to PTL. These data raised the possibility that KDM6B, and potentially the H3K27me3 timer presented in Chapter 2, is a common upstream component of both PTL and normal labor pathways.

In Chapter 5, KDM6A was found to be critical for decidualization and pregnancy success in mice. We show that the initial phase of decidualization is intact (embryo attachment, initial proliferation, and vascularization), but *Kdm6a cKO* ESCs fail to fully differentiate into DSCs. The compromised decidualization in *Kdm6a cKO* mice results in complete infertility, highlighting the importance of H3K27me3 demethylation in mouse decidualization and pregnancy.

Together, these results provide insight into how the pregnant uterus, a complex tissue that is constantly evolving over the course of gestation, employs epigenetic pathways within fibroblasts to ensure reproductive success, ranging from early decidualization to parturition. These data present exciting opportunities for future exploration, revealing new questions and hypotheses that we speculate on in the sections below.

How does the fibroblast histone timer induce epithelial COX-1 prior to luteolysis onset?

The exact mechanism whereby uterine fibroblasts induce epithelial COX-1 remains unresolved, but our data certainly suggests a number of possibilities. One possibility involves a role for activin, since *Inhbb*$^{-/-}$ mice show a 1-2 day parturition delay, with some *Inhbb*$^{-/-}$ mice failing to initiate labor altogether resulting in maternal sickness and death of the fetuses in

utero[116]. While the mechanism by which activin induces parturition is still unclear, studies have shown that serum levels of activin increase significantly with advancing gestation in both rats[275] and humans[276,277], that activin stimulates the release of prostaglandins from cultured human amnion cells[278], and that hypothalamic administration of activin into rats leads to a rapid increase in plasma oxytocin levels[279]. While a direct role for activin in inducing *Ptgs1* has not yet been shown, *Inhbb* is expressed in early gestation implantation site fibroblasts adjacent to the uterine luminal epithelial cells expressing COX-1[280]. In mid-to-late gestation PDGFRα$^+$ myo/endo fibroblasts, transcript levels of both *Inhbb* and *Fst*, encoding the activin inhibitor follistatin, increase from GD8.5 to 12.5 (Figure 6.1). While *Fst* transcript levels rapidly decline shortly thereafter in these fibroblasts, they remain elevated in *Kdm6b cKO* fibroblasts, likely antagonizing activin signaling. Collectively these data suggest a potential role for activin signaling in the onset of parturition, but pharmacological studies inhibiting or stimulating the activin pathway in combination with further dissection of genetic mouse models will clarify the exact role of this pathway.

Another possibility involves a role for BMP2 signaling, which has mostly been studied thus far in early pregnancy due to its critical role in decidualization (as discussed in Chapter 5). However, its expression pattern in PDGFRα$^+$ myo/endo fibroblasts is different than that of DSCs. Specifically, PDGFRα$^+$ fibroblast *Bmp2* levels are low in early pregnancy, drastically increase from GD12.5 to 14.5, and remain relatively high throughout the remainder of gestation (Figure 6.1). In contrast, *Kdm6b cKO* fibroblasts fail to reach wildtype *Bmp2* levels until GD18.5. The significant increase in *Bmp2* levels at GD14.5, when *Ptgs1* is also induced in the luminal epithelial cells (see Chapter 2), raises the possibility that fibroblast BMP2 signaling induces

COX-1 in the overlying epithelium. The exact mechanism by which BMP2 induces COX-1 would need to be addressed, but ablation of *Bmp2* in early gestation disrupts *Ptgs2* induction[235].

A third potential pathway involves anthrax toxin receptor 2 (ANTXR2), also known as capillary morphogenesis protein-2 (CMG2), a type I cell surface protein that interacts with extracellular matrix components. *Antxr2* mRNA levels increase in GD14.5 control fibroblasts compared to early gestation and is downregulated in *Kdm6b cKO* cells on GD14.5 (Figure 6.1). Moreover, *Antxr2*$^{-/-}$ mice suffer from progressive uterine fibrosis, disruption of tissue architecture and complete parturition failure[184,281], but are rescued when crossed with *Col6a1*$^{-/-}$, highlighting a role for ANTXR2 as a regulator collagen VI homeostasis. Indeed, *Kdm6b cKO* fibroblasts on GD14.5 express heightened levels of *Col6a1* (Figure 6.1C), raising the possibility that accumulation of collagen VI in the *Kdm6b cKO* myo/endo inhibits epithelial COX-1 induction and delays parturition.

A fourth possibility suggests a role for *Fkbp5*, encoding FK506-binding protein 51, since *Fkbp5*$^{-/-}$ mice exhibit delayed parturition and are completely resistant to stress-induced PTB[269]. FK506-binding proteins are immunophilins that assemble as cochaperones with progesterone receptors (PR)[282]. FKBP51 attenuates PR-mediated transcription and inhibits PR function [283,284]. While the authors attribute the delay of *Fkbp5*$^{-/-}$ mice to a deficiency in "functional P4 withdrawal" within the uterus (due to delayed induction of uterine *Akr1c18* and *Oxtr*), these mice also showed a delayed decline in serum P4 levels suggestive of delayed luteolysis. Future experiments will address the levels of prostaglandins and epithelial expression of *Ptgs1*. Nonetheless, given that *Fkbp5* is an HC1 gene, these data suggest a potential role for our H3K27me3 timer in regulating *Fkbp5*-dependent functional P4 withdrawal within the uterus and luteolysis.

Finally, our finding that the H3K27me3 timer controls *Csf1* expression by uterine fibroblasts (Figure 6.1) suggests a role for macrophages in parturition, and highlights the likely involvement of non-fibroblastic, non-epithelial cell types in the labor cascade in mice, potentially as intermediaries between uterine fibroblasts and epithelial cells. However, given that macrophage-deficient *op/op* mice deliver on time[285], macrophages are not absolutely required for COX-1 induction and/or labor onset. In a similar vein, the probability that a solitary factor produced by uterine fibroblasts induces epithelial COX-1 appears to be minimal. This suspicion stems from the complex nature of labor onset, a process that requires the coordinated action of many different cell types. Rather, and in line with our observation that H3K27me3 erodes at hundreds of loci, we hypothesize that parturition is triggered by a cascading series of events that are each required for the progression and maturation of the uterus. Nevertheless, we anticipate that dissecting each of the above pathways further will bolster this hypothesis and lead to an even greater understanding of parturition.

How is the fibroblast histone timer linked to uterus-intrinsic pathways?

Chapter 2 provides evidence that normal parturition (i.e., luteolysis) in mice is governed by an epigenetic timer that operates autonomously within the fibroblasts of the pregnant uterus. Chapter 3 provides evidence that uterus-intrinsic pathways of mice, unmasked when mice are administered exogenous progestin (DMPA) to circumvent luteolysis, require several components of innate type 2 immunity. Additionally, a post-doctoral fellow in the lab, Dr. Akanksha Onkar, has found that *Pdgfra-cre Kdm6b*$^{f/f}$ mice experience parturition delays when administered DMPA (Figure 6.2). This exciting result suggests that the H3K27me3 timer presented in Chapter

2 may also be upstream of uterus-intrinsic pathways. Given the number of H3K27me3-regulated genes, many different possibilities exist for how this may occur.

One possibility for how the H3K27me3 timer may be upstream of uterus-intrinsic pathways involves the HC4 gene *Gja1*, which encodes connexin 43, a gap junction protein that promotes cell-cell electrical coupling. Gap junctions are most known for increasing in myometrial smooth muscle cells during term and preterm labor and are thought to be essential for the development of uterine contractions[286-290]. Mice lacking expression of *Cx43* in SMCs (i.e., *Cx43$^{fl/fl}$:SM-CreER^{T2}*) are delayed in their labor onset, but interestingly show no changes in other parameters specific to murine parturition including oxytocin receptor expression, prostaglandin F receptor expression or progesterone levels[7]. Thus, *Gja1* expression in fibroblasts may play a distinct role from that of SMCs, perhaps in regulating uterus-intrinsic parturition pathways. Indeed, our data shows that *Cx43* expression increases in fibroblasts 2 days prior to its increase in SMCs, with significantly less induction in *Kdm6b cKO* fibroblasts (Figure 6.3A). Although gap-junctional intercellular channels have been shown to be important in the cell-cell transmission of Ca^{2+} waves (i.e., from SMC to SMC), it is also clear that these waves can spread by paracrine signaling due to the extracellular release of ATP through *Cx43* hemichannels that binds to purinergic receptors (P2X and P2Y). These purinergic receptors are expressed by SMCs but also by a broad range of cell types including eosinophils[291,292], macrophages[293,294], and mast cells[295], the latter of which are activated synergistically by extracellular ATP (eATP) and IL-33[296,297]. Therefore, one potential uterus-intrinsic parturition model involves stretch-induced[298,299] eATP release from uterine fibroblasts acting in a paracrine-manner to both induce SMC contractions[300,301] and activate type 2 immune cells. We anticipate that the P2X7 receptors

(P2X7Rs) are the likely target given that their expression increases throughout pregnancy[300] and their antagonism reduces PTB incidence[302].

Another possibility suggests a role for PGD_2, a type 2 immune regulator with activating and chemotactic effects on ILC2s and eosinophils[171] that is abundantly produced in the prepartum uterus in a COX-1-dependent fashion[154,155]. As presented in Chapter 2, mice harboring a manipulated H3K27me3 timer (i.e., *Kdm6b cKO* mice) exhibit delayed COX-1 induction, and thus likely produce less PGD_2 (although this was not evaluated directly). Although PGD_2 has been shown to directly induce contractions on myometrial tissue strips *in vitro*[155,172], the findings outlined in Chapter 3 suggest that it may also promote labor onset by stimulating type 2 immunity. In this model, PDGFRα^+ fibroblasts would be appropriately timing the induction of COX-1 for both luteolysis and PGD_2-driven activation of type 2 immunity.

A third possibility involves a role for the H3K27me3 timer in regulating IL-33 bioactivity in the late gestation uterus, which is thought to be generated in response to the low-grade inflammation characteristic of late gestation[95,144]. This idea is in line with IL-33 being a nucleus-sequestered alarmin released in response to noxious stimuli, as well as with the ability of inflammation-associated proteases to process IL-33 into more active forms[146,169]. This low-grade inflammation in the late gestation uterus is thought to be associated with the upregulation of proinflammatory cytokines and chemokines[303-305] and cellular adhesion molecules[305,306], inducing localized myometrial inflammation. Both *Ccl2* and *Ccl7*, encoding the chemokines CCL2 and CCL7, attract leukocytes (mostly macrophages and T cells) to tissues and have been found to be markedly increased in laboring compared to quiescent pregnant human myometrium[307]. Most importantly, these genes are regulated by the H3K27me3 timer. While the H3K27me3 at their promoters does not erode with advancing gestation, these loci retain higher

levels of H3K27me3 in *Kdm6b cKO* fibroblasts (i.e., HC2) and are transcriptionally downregulated in *Kdm6b cKO* fibroblasts (Figure 6.3B). Other chemokines regulated by H3K27me3 that may be contributing to the low-grade inflammation prior to labor include *Cxcl10* (HC2) and *Cxcl1* (HC4) (Figure 6.3B).

Is the histone timer relevant for human parturition?

While epithelial COX-1 induction and luteolysis are known to be the proximal triggers of parturition in mice, triggers of human parturition have remained undefined. The field has focused on the idea that signals emanating from the fetus, placenta, or decidua directly induce myometrial maturation, but what times the generation of these signals, or if they are truly relevant, is unknown. Our findings that uterine fibroblasts play an upstream role in controlling uterus-intrinsic and luteolysis-regulated gestation length in mice suggests that parturition timing in humans might also be regulated by this uterine compartment.

As described in Chapter 3, uterine fibroblasts stimulate innate type 2 immune processes to trigger labor onset when mice are hormonally manipulated to model their human counterparts. This type 2 immune pathway seems likely to be downstream of the H3K27me3 gestational timer identified in Chapter 2, given that *Pdgfra-cre Kdm6b*$^{f/f}$ mice also exhibit uterus-intrinsic parturition delays (Figure 6.2). As discussed above, many different potential mechanisms exist to explain how the timer may be regulating type 2 immunity, including roles for gap junctions, PGD_2, and myometrial inflammation.

Directly testing whether these pathways are relevant for human parturition (i.e., without using mouse models) will require future H3K27me3 CUT&RUN and RNA-sequencing experiments on PDGFRα^+ uterine fibroblasts at early, mid and late gestation time points during

human pregnancy. Our observation that some of the genes in uterine fibroblasts we identify as being H3K27me3-regulated have already been implicated in human parturition[81,117-122], including *Inhbb, Csf1, Oxtr, Bmp2, Ngfr,* and *Postn*, suggesting that at least some of these pathways may be relevant. Indeed, loss of H3K27me3 at the promoter of *Bmp2* has been shown to occur in the human amnion in late gestation[308].

What is the mechanism of peri-implantation H3K27me3 tuning and locus-specific H3K27me3 erosion?

Our results also raise questions regarding mechanisms of locus-specific H3K27me3 erosion and peri-implantation H3K27me3 tuning, including how peri-implantation hormones, KDM6B, KDM6A, and EZH2 contribute to the latter process. Indeed, while the H3K27me3 elevations observed in *Kdm6b cKO* mice on GD5.5 suggest a role for KDM6B in peak tuning, our results are also consistent with the possibility that these elevations are present prior to GD0.5. In the scenario where GD0.5 are similar between *cKO* and control mice, this would imply that H3K27me3 levels on select peaks become subject to dynamic regulation in the peri-implantation period, including both methyltransferase and demethylase activity that allows for net H3K27me3 accumulation (winding) and loss (pruning). In the case where winding might entail a moderate reduction in KDM6B-mediated demethylation, *Kdm6b cKO* fibroblasts would likely amass an excess of H3K27me3 by GD5.5. Further investigation into how these loci change during the peri-implantation period will provide insight into whether and how perturbations in early pregnancy (i.e., infections, pollutants, or stress) could alter birth timing.

An alternative scenario is that GD0.5 H3K27me3 levels are already elevated in *Kdm6b cKO* mice, implying that KDM6B functions in the fibroblasts of non-pregnant mice. This would

be interesting in its own regard, since it would suggest that HC1 peaks mark dynamic areas of the uterine fibroblast genome, subject to histone remodeling by the H3K27me3 methyltransferases and demethylases. Exploring the epigenetic changes at these loci throughout the uterine cycle may open up new research avenues, shedding light on how disruptions to the non-pregnant uterine microenvironment (i.e., endometriosis) might influence pregnancy outcomes.

The H3K27me3 erosion mechanism that takes over after implantation is also unclear. Since our data strongly indicates that the erosion occurs in a KDM6B-independent fashion, it seems likely that it could involve activation of KDM6A or locus-specific replicational dilution of H3K27me3. A role for KDM6A would fall in line with the parturition delay we previously observed in GSK-J4-treated mice that were otherwise allowed to deliver via luteolysis, but would contradict a separate study showing mice lacking KDM6A demethylase activity are viable and fertile[256]. If not KDM6A, the erosion could be driven by others in the family of JmjC demethylases, including members of the Kdm4 family which have been shown to exhibit H3K27me3 demethylase activity[309]. Alternatively, it remains possible that a novel family of proteins may actively demethylate H3K27me3 utilizing distinct chemistry. Finally, KDM6-independent loss of H3K27me3 can occur via passive mechanisms, as histones can be turned over multiple times within each cell cycle[310]. The fact that fibroblast proliferation rates likely differ between IS and IIS would discount this hypothesis, but further experiments are required to conclude this.

Concluding Remarks

My dissertation research implicates PDGFRα^{+} uterine fibroblasts as the key cell type driving both luteolysis and uterus-intrinsic parturition pathways in mice, challenging previous notions that this process is controlled by the fetal, placental, or decidual compartments. It moreover reveals the existence and operation of a timer that schedules murine labor onset, the first mechanism of its kind underlying gestation length in any mammalian species. The pan-gestational nature of this timer raises the possibility that disruptions (e.g., infections, pollutants, or stress) to the uterine microenvironment occurring as early as the peri-implantation period could alter birth timing. Whether such perturbations to analogous processes in humans contribute to the pathogenesis of preterm labor remain unknown, but I expect that this work will open up a wealth of new avenues to address this global problem.

Figures

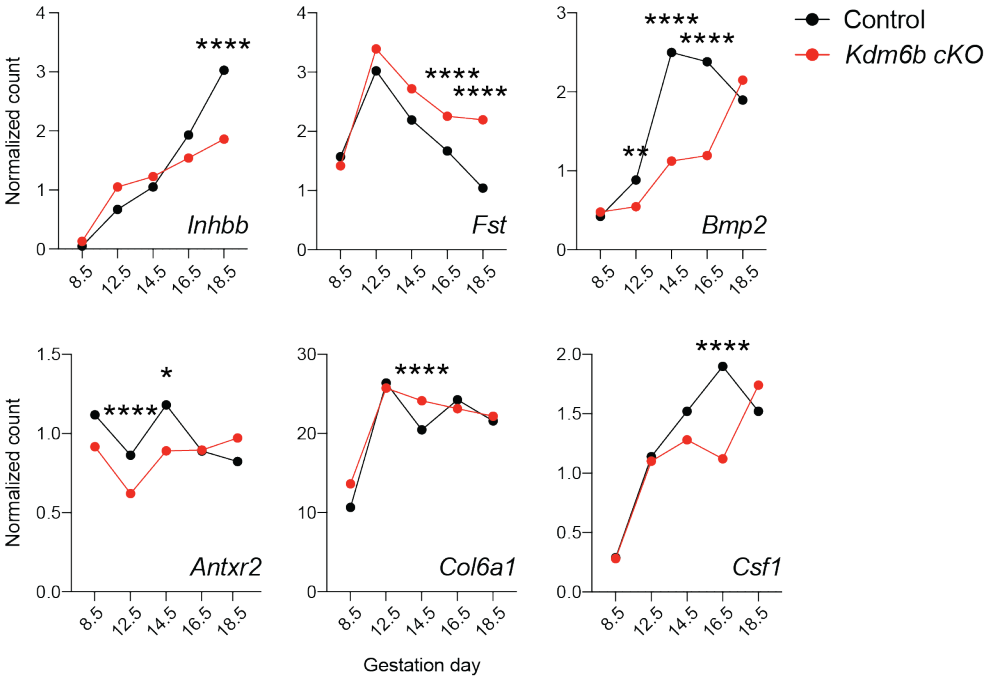

Figure 6.1 Expression patterns of fibroblast genes potentially involved in epithelial COX-1 induction.

Normalized mRNA counts for *Inhbb, Fst, Bmp2, Antxr2, Col6a1,* and *Csf1* in control and *Kdm6b cKO* fibroblasts from GD8.5, GD12.5, GD14.5, GD16.5, and GD18.5 (from the scRNA-Seq analysis shown in Chapter 2 and including data from both IS myo/endo and IIS). *, *FDR*<0.05, ****, *FDR*<0.0001 by a two-sided Wilcoxon rank-sum test.

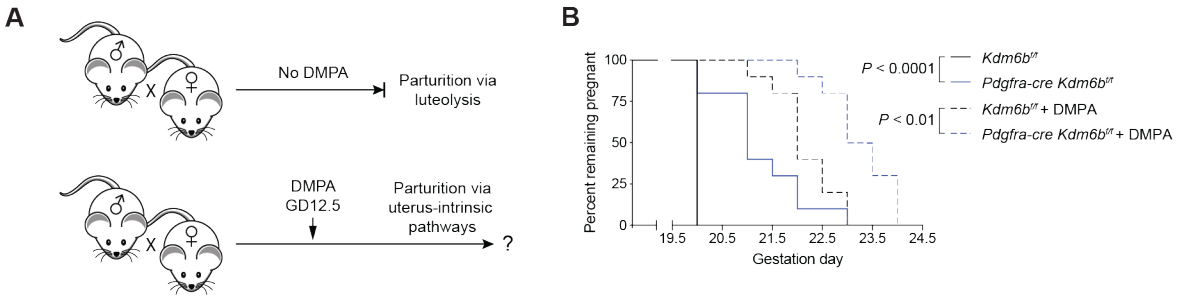

Figure 6.2 KDM6B deficiency in uterine fibroblasts delays labor onset in mice when parturition occurs through uterus-intrinsic pathways.

(A) Schematic of parturition timing experiments. In the absence of DMPA administration, mice enter labor on GD19.5 as the result of luteolysis. Administration of DMPA extends gestation length and allows for parturition to occur via uterus-intrinsic pathways. (B) Parturition timing in *Pdgfra-cre Kdm6b*$^{f/f}$ and control *Kdm6b*$^{f/f}$ mice that were either untreated or injected with DMPA on GD12.5. Groups were compared by the log-rank test (n=10 mice/group). Females were mated with B6 males.

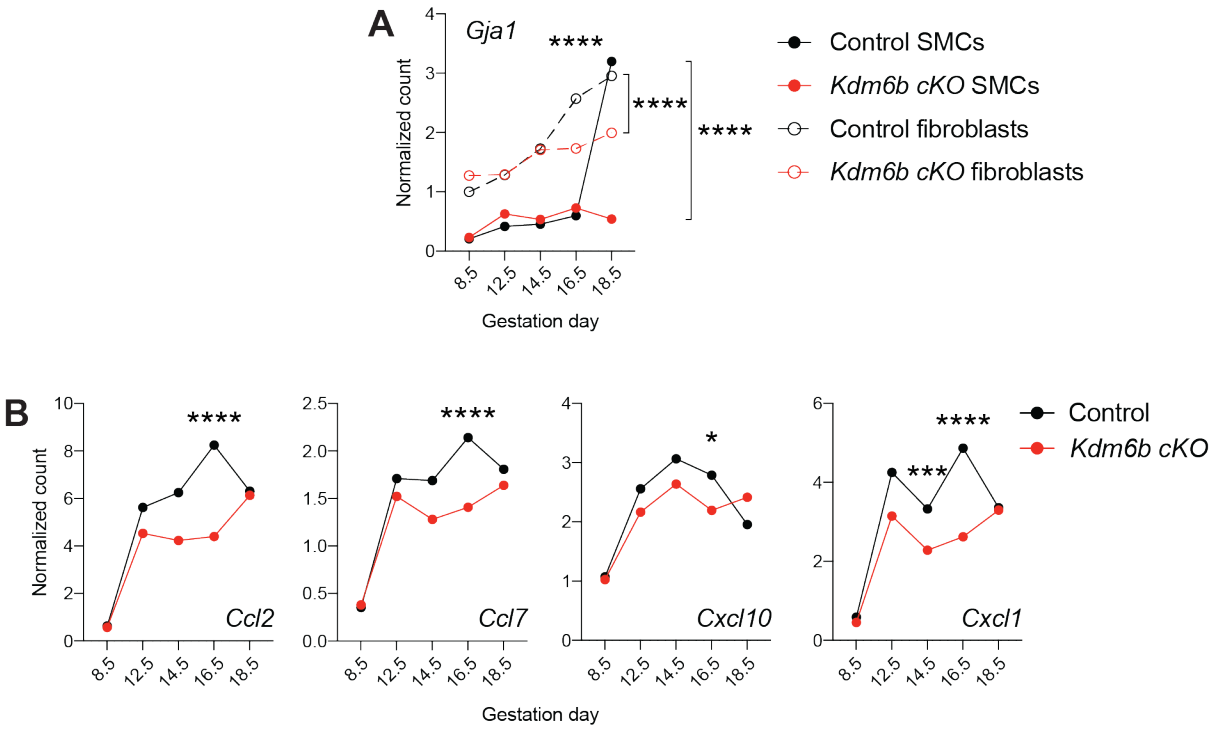

Figure 6.3 Expression patterns of genes potentially linked to uterus-intrinsic pathways of parturition.

(A) Normalized mRNA counts for *Gja1* in control and *Kdm6b cKO* fibroblasts (open circles) and SMCs (closed circles) from GD8.5, GD12.5, GD14.5, GD16.5, and GD18.5 (from the scRNA-Seq analysis shown in Chapter 2). Fibroblast gene expression data includes data from both IS myo/endo and IIS. Note the higher expression of *Gja1* in fibroblasts compared to SMCs prior to GD18.5. ****, *FDR*<0.0001 by a two-sided Wilcoxon rank-sum test. (B) Normalized mRNA counts for *Ccl2, Ccl7, Cxcl10,* and *Cxcl1* in control and *Kdm6b cKO* fibroblasts from GD8.5, GD12.5, GD14.5, GD16.5, and GD18.5 (from the scRNA-Seq analysis shown in Chapter 2 and including data from both IS myo/endo and IIS). *, *FDR*<0.05, ***, *FDR*<0.001, ****, *FDR*<0.0001 by a two-sided Wilcoxon rank-sum test.

References

1. Gross, G.A., Imamura, T., Luedke, C., Vogt, S.K., Olson, L.M., Nelson, D.M., Sadovsky, Y., and Muglia, L.J. (1998). Opposing actions of prostaglandins and oxytocin determine the onset of murine labor. Proc Natl Acad Sci U S A *95*, 11875-11879. 10.1073/pnas.95.20.11875.
2. Langenbach, R., Morham, S.G., Tiano, H.F., Loftin, C.D., Ghanayem, B.I., Chulada, P.C., Mahler, J.F., Lee, C.A., Goulding, E.H., Kluckman, K.D., Kim, H.S., and Smithies, O. (1995). Prostaglandin synthase 1 gene disruption in mice reduces arachidonic acid-induced inflammation and indomethacin-induced gastric ulceration. Cell *83*, 483-492. 10.1016/0092-8674(95)90126-4.
3. Reese, J., Paria, B.C., Brown, N., Zhao, X., Morrow, J.D., and Dey, S.K. (2000). Coordinated regulation of fetal and maternal prostaglandins directs successful birth and postnatal adaptation in the mouse. Proc Natl Acad Sci U S A *97*, 9759-9764. 10.1073/pnas.97.17.9759.
4. Garfield, R.E., Sims, S.M., Kannan, M.S., and Daniel, E.E. (1978). Possible role of gap junctions in activation of myometrium during parturition. Am J Physiol *235*, C168-179. 10.1152/ajpcell.1978.235.5.C168.
5. Garfield, R.E., Blennerhassett, M.G., and Miller, S.M. (1988). Control of Myometrial Contractility - Role and Regulation of Gap-Junctions. Oxford Rev Reprod B *10*, 436-490.
6. G, M.K., and Winterhager, E. (2015). Physiological roles of connexins in labour and lactation. Reproduction *150*, R129-136. 10.1530/REP-15-0134.
7. Doring, B., Shynlova, O., Tsui, P., Eckardt, D., Janssen-Bienhold, U., Hofmann, F., Feil, S., Feil, R., Lye, S.J., and Willecke, K. (2006). Ablation of connexin43 in uterine smooth

muscle cells of the mouse causes delayed parturition. J Cell Sci *119*, 1715-1722. 10.1242/jcs.02892.

8. Kim, S.H., Bennett, P.R., and Terzidou, V. (2017). Advances in the role of oxytocin receptors in human parturition. Mol Cell Endocrinol *449*, 56-63. 10.1016/j.mce.2017.01.034.

9. Kimura, T., Ogita, K., Kumasawa, K., Tomimatsu, T., and Tsutsui, T. (2013). Molecular analysis of parturition via oxytocin receptor expression. Taiwan J Obstet Gynecol *52*, 165-170. 10.1016/j.tjog.2013.04.004.

10. Ohuma, E.O., Moller, A.B., Bradley, E., Chakwera, S., Hussain-Alkhateeb, L., Lewin, A., Okwaraji, Y.B., Mahanani, W.R., Johansson, E.W., Lavin, T., et al. (2023). National, regional, and global estimates of preterm birth in 2020, with trends from 2010: a systematic analysis. Lancet *402*, 1261-1271. 10.1016/S0140-6736(23)00878-4.

11. Dudley, D.J., Branch, D.W., Edwin, S.S., and Mitchell, M.D. (1996). Induction of preterm birth in mice by RU486. Biol Reprod *55*, 992-995. 10.1095/biolreprod55.5.992.

12. Skarnes, R.C., and Harper, M.J. (1972). Relationship between endotoxin-induced abortion and the synthesis of prostaglandin F. Prostaglandins *1*, 191-203. 10.1016/0090-6980(72)90004-4.

13. Mesiano, S., Wang, Y., and Norwitz, E.R. (2011). Progesterone receptors in the human pregnancy uterus: do they hold the key to birth timing? Reprod Sci *18*, 6-19. 10.1177/1933719110382922.

14. Welsh, T.N., Hirst, J.J., Palliser, H., and Zakar, T. (2014). Progesterone receptor expression declines in the guinea pig uterus during functional progesterone withdrawal and in response to prostaglandins. PLoS One *9*, e105253. 10.1371/journal.pone.0105253.

15. Zakar, T., and Hertelendy, F. (2007). Progesterone withdrawal: key to parturition. Am J Obstet Gynecol *196*, 289-296. 10.1016/j.ajog.2006.09.005.

16. Dodd, J.M., Jones, L., Flenady, V., Cincotta, R., and Crowther, C.A. (2013). Prenatal administration of progesterone for preventing preterm birth in women considered to be at risk of preterm birth. Cochrane Database Syst Rev, CD004947. 10.1002/14651858.CD004947.pub3.

17. Zarrow, M.X., Anderson, N.C., Jr., and Callantine, M.R. (1963). Failure of progestogens to prolong pregnancy in the guinea pig. Nature *198*, 690-692. 10.1038/198690b0.

18. Merlino, A.A., Welsh, T.N., Tan, H., Yi, L.J., Cannon, V., Mercer, B.M., and Mesiano, S. (2007). Nuclear progesterone receptors in the human pregnancy myometrium: evidence that parturition involves functional progesterone withdrawal mediated by increased expression of progesterone receptor-A. J Clin Endocrinol Metab *92*, 1927-1933. 10.1210/jc.2007-0077.

19. Mesiano, S., Chan, E.C., Fitter, J.T., Kwek, K., Yeo, G., and Smith, R. (2002). Progesterone withdrawal and estrogen activation in human parturition are coordinated by progesterone receptor A expression in the myometrium. J Clin Endocrinol Metab *87*, 2924-2930. 10.1210/jcem.87.6.8609.

20. Thijssen, J.H. (2005). Progesterone receptors in the human uterus and their possible role in parturition. J Steroid Biochem Mol Biol *97*, 397-400. 10.1016/j.jsbmb.2005.08.011.

21. Mendelson, C.R. (2009). Minireview: fetal-maternal hormonal signaling in pregnancy and labor. Mol Endocrinol *23*, 947-954. 10.1210/me.2009-0016.

22. Euler, V. (1935). A depressor substance in the vesicular gland. J Physiol *84*, 208-218.

23. Goldblatt, M.W. (1935). Properties of human seminal plasma. J Physiol *84*, 208-218. 10.1113/jphysiol.1935.sp003269.

24. Mesiano, S. (2022). Progesterone withdrawal and parturition. J Steroid Biochem Mol Biol *224*, 106177. 10.1016/j.jsbmb.2022.106177.

25. Challis, J.R., Sloboda, D.M., Alfaidy, N., Lye, S.J., Gibb, W., Patel, F.A., Whittle, W.L., and Newnham, J.P. (2002). Prostaglandins and mechanisms of preterm birth. Reproduction *124*, 1-17. 10.1530/rep.0.1240001.

26. Okazaki, T., Sagawa, N., Ban, C., Muneshige, A., and Mori, T. (1985). Regulation of prostaglandin formation during human parturition. Adv Prostaglandin Thromboxane Leukot Res *15*, 617-618.

27. Olson, D.M., Smieja, Z., Zakar, T., MacLeod, E.A., Walton, J., and Milne, K. (1991). Regulation of prostaglandin synthesis in the human amnion. Reprod Fertil Dev *3*, 413-419. 10.1071/rd9910413.

28. Wood, E.M., Hornaday, K.K., and Slater, D.M. (2021). Prostaglandins in biofluids in pregnancy and labour: A systematic review. PLoS One *16*, e0260115. 10.1371/journal.pone.0260115.

29. Haas, D.M., Caldwell, D.M., Kirkpatrick, P., McIntosh, J.J., and Welton, N.J. (2012). Tocolytic therapy for preterm delivery: systematic review and network meta-analysis. BMJ *345*, e6226. 10.1136/bmj.e6226.

30. Mlodawski, J., and Mlodawska, M. (2021). Prostaglandins in the induction of labour – do we have the optimal substance, dose, and route of administration? Literature review. Medical Studies/Studia Medyczne *37*, 162-167. 10.5114/ms.2021.107461.

31. Welsh, T., Mitchell, C.M., Walters, W.A., Mesiano, S., and Zakar, T. (2005). Prostaglandin H2 synthase-1 and -2 expression in guinea pig gestational tissues during late pregnancy and parturition. J Physiol *569*, 903-912. 10.1113/jphysiol.2005.098129.

32. Wu, S.P., Anderson, M.L., Wang, T., Zhou, L., Emery, O.M., Li, X., and DeMayo, F.J. (2020). Dynamic transcriptome, accessible genome, and PGR cistrome profiles in the human myometrium. FASEB J *34*, 2252-2268. 10.1096/fj.201902654R.

33. Kirkwood, P.M., Gibson, D.A., Smith, J.R., Wilson-Kanamori, J.R., Kelepouri, O., Esnal-Zufiaurre, A., Dobie, R., Henderson, N.C., and Saunders, P.T.K. (2021). Single-cell RNA sequencing redefines the mesenchymal cell landscape of mouse endometrium. FASEB J *35*, e21285. 10.1096/fj.202002123R.

34. Saatcioglu, H.D., Kano, M., Horn, H., Zhang, L., Samore, W., Nagykery, N., Meinsohn, M.C., Hyun, M., Suliman, R., Poulo, J., et al. (2019). Single-cell sequencing of neonatal uterus reveals an Misr2+ endometrial progenitor indispensable for fertility. Elife *8*. 10.7554/eLife.46349.

35. Garcia-Alonso, L., Handfield, L.F., Roberts, K., Nikolakopoulou, K., Fernando, R.C., Gardner, L., Woodhams, B., Arutyunyan, A., Polanski, K., Hoo, R., et al. (2021). Mapping the temporal and spatial dynamics of the human endometrium in vivo and in vitro. Nat Genet *53*, 1698-1711. 10.1038/s41588-021-00972-2.

36. Marečková, M., Garcia-Alonso, L., Moullet, M., Lorenzi, V., Petryszak, R., Sancho-Serra, C., Oszlanczi, A., Mazzeo, C.I., Hoffman, S., Krassowski, M., et al. (2023). An integrated single-cell reference atlas of the human endometrium. bioRxiv, 2023.2011.2003.564728. 10.1101/2023.11.03.564728.

37. Cha, J., Sun, X., and Dey, S.K. (2012). Mechanisms of implantation: strategies for successful pregnancy. Nat Med *18*, 1754-1767. 10.1038/nm.3012.

38. Wagner, G.P., Kin, K., Muglia, L., and Pavlicev, M. (2014). Evolution of mammalian pregnancy and the origin of the decidual stromal cell. Int J Dev Biol *58*, 117-126. 10.1387/ijdb.130335gw.

39. Maruyama, T., and Yoshimura, Y. (2008). Molecular and cellular mechanisms for differentiation and regeneration of the uterine endometrium. Endocr J *55*, 795-810. 10.1507/endocrj.k08e-067.

40. Bell, S.C. (1990). Decidualization and relevance to menstruation (Cambridge University Press).

41. Vento-Tormo, R., Efremova, M., Botting, R.A., Turco, M.Y., Vento-Tormo, M., Meyer, K.B., Park, J.E., Stephenson, E., Polanski, K., Goncalves, A., et al. (2018). Single-cell reconstruction of the early maternal-fetal interface in humans. Nature *563*, 347-353. 10.1038/s41586-018-0698-6.

42. Daly, D.C., Maslar, I.A., and Riddick, D.H. (1983). Prolactin production during in vitro decidualization of proliferative endometrium. Am J Obstet Gynecol *145*, 672-678. 10.1016/0002-9378(83)90572-0.

43. Tseng, L., Gao, J.G., Chen, R., Zhu, H.H., Mazella, J., and Powell, D.R. (1992). Effect of progestin, antiprogestin, and relaxin on the accumulation of prolactin and insulin-like growth factor-binding protein-1 messenger ribonucleic acid in human endometrial stromal cells. Biol Reprod *47*, 441-450. 10.1095/biolreprod47.3.441.

44. Suryawanshi, H., Morozov, P., Straus, A., Sahasrabudhe, N., Max, K.E.A., Garzia, A., Kustagi, M., Tuschl, T., and Williams, Z. (2018). A single-cell survey of the human first-trimester placenta and decidua. Sci Adv *4*, eaau4788. 10.1126/sciadv.aau4788.

45. Casey, M.L., and MacDonald, P.C. (1988). Biomolecular processes in the initiation of parturition: decidual activation. Clin Obstet Gynecol *31*, 533-552. 10.1097/00003081-198809000-00005.

46. MacDonald, P.C., Koga, S., and Casey, M.L. (1991). Decidual activation in parturition: examination of amniotic fluid for mediators of the inflammatory response. Ann N Y Acad Sci *622*, 315-330. 10.1111/j.1749-6632.1991.tb37877.x.

47. Romero, R., Dey, S.K., and Fisher, S.J. (2014). Preterm labor: one syndrome, many causes. Science *345*, 760-765. 10.1126/science.1251816.

48. Edey, L.F., O'Dea, K.P., Herbert, B.R., Hua, R., Waddington, S.N., MacIntyre, D.A., Bennett, P.R., Takata, M., and Johnson, M.R. (2016). The Local and Systemic Immune Response to Intrauterine LPS in the Prepartum Mouse. Biol Reprod *95*, 125. 10.1095/biolreprod.116.143289.

49. Ferguson, M.G., Rhodes, P.G., Morrison, J.C., and Puckett, C.M. (1985). Clinical amniotic fluid infection and its effect on the neonate. Am J Obstet Gynecol *151*, 1058-1061. 10.1016/0002-9378(85)90380-1.

50. Gomez, R., Romero, R., Edwin, S.S., and David, C. (1997). Pathogenesis of preterm labor and preterm premature rupture of membranes associated with intraamniotic infection. Infect Dis Clin North Am *11*, 135-176. 10.1016/s0891-5520(05)70347-0.

51. Keelan, J.A. (2018). Intrauterine inflammatory activation, functional progesterone withdrawal, and the timing of term and preterm birth. J Reprod Immunol *125*, 89-99. 10.1016/j.jri.2017.12.004.

52. Kemp, M.W. (2014). Preterm birth, intrauterine infection, and fetal inflammation. Front Immunol *5*, 574. 10.3389/fimmu.2014.00574.

53. Romero, R., Gotsch, F., Pineles, B., and Kusanovic, J.P. (2007). Inflammation in pregnancy: its roles in reproductive physiology, obstetrical complications, and fetal injury. Nutr Rev *65*, S194-202. 10.1111/j.1753-4887.2007.tb00362.x.

54. Romero, R., Mazor, M., Wu, Y.K., Sirtori, M., Oyarzun, E., Mitchell, M.D., and Hobbins, J.C. (1988). Infection in the pathogenesis of preterm labor. Semin Perinatol *12*, 262-279.

55. Yoon, B.H., Romero, R., Moon, J.B., Shim, S.S., Kim, M., Kim, G., and Jun, J.K. (2001). Clinical significance of intra-amniotic inflammation in patients with preterm labor and intact membranes. Am J Obstet Gynecol *185*, 1130-1136. 10.1067/mob.2001.117680.

56. Agrawal, V., and Hirsch, E. (2012). Intrauterine infection and preterm labor. Semin Fetal Neonatal Med *17*, 12-19. 10.1016/j.siny.2011.09.001.

57. Romero, R., Gomez, R., Chaiworapongsa, T., Conoscenti, G., Kim, J.C., and Kim, Y.M. (2001). The role of infection in preterm labour and delivery. Paediatr Perinat Epidemiol *15 Suppl 2*, 41-56. 10.1046/j.1365-3016.2001.00007.x.

58. Elovitz, M.A., Wang, Z., Chien, E.K., Rychlik, D.F., and Phillippe, M. (2003). A new model for inflammation-induced preterm birth: the role of platelet-activating factor and Toll-like receptor-4. Am J Pathol *163*, 2103-2111. 10.1016/S0002-9440(10)63567-5.

59. Gross, G., Imamura, T., Vogt, S.K., Wozniak, D.F., Nelson, D.M., Sadovsky, Y., and Muglia, L.J. (2000). Inhibition of cyclooxygenase-2 prevents inflammation-mediated

preterm labor in the mouse. Am J Physiol Regul Integr Comp Physiol *278*, R1415-1423. 10.1152/ajpregu.2000.278.6.R1415.

60. Migale, R., MacIntyre, D.A., Cacciatore, S., Lee, Y.S., Hagberg, H., Herbert, B.R., Johnson, M.R., Peebles, D., Waddington, S.N., and Bennett, P.R. (2016). Modeling hormonal and inflammatory contributions to preterm and term labor using uterine temporal transcriptomics. BMC Med *14*, 86. 10.1186/s12916-016-0632-4.

61. Motomura, K., Romero, R., Tarca, A.L., Galaz, J., Bhatti, G., Done, B., Arenas-Hernandez, M., Levenson, D., Slutsky, R., Hsu, C.D., and Gomez-Lopez, N. (2020). Pregnancy-specific transcriptional changes upon endotoxin exposure in mice. J Perinat Med *48*, 700-722. 10.1515/jpm-2020-0159.

62. Toothaker, J.M., Presicce, P., Cappelletti, M., Stras, S.F., McCourt, C.C., Chougnet, C.A., Kallapur, S.G., and Konnikova, L. (2020). Immune Cells in the Placental Villi Contribute to Intra-amniotic Inflammation. Front Immunol *11*, 866. 10.3389/fimmu.2020.00866.

63. Willcockson, A.R., Nandu, T., Liu, C.L., Nallasamy, S., Kraus, W.L., and Mahendroo, M. (2018). Transcriptome signature identifies distinct cervical pathways induced in lipopolysaccharide-mediated preterm birth. Biol Reprod *98*, 408-421. 10.1093/biolre/iox180.

64. Hirota, Y., Daikoku, T., Tranguch, S., Xie, H., Bradshaw, H.B., and Dey, S.K. (2010). Uterine-specific p53 deficiency confers premature uterine senescence and promotes preterm birth in mice. J Clin Invest *120*, 803-815. 10.1172/JCI40051.

65. Tsuboi, K., Sugimoto, Y., Iwane, A., Yamamoto, K., Yamamoto, S., and Ichikawa, A. (2000). Uterine Expression of Prostaglandin H2 Synthase in Late Pregnancy and during

Parturition in Prostaglandin F Receptor-Deficient Mice1. Endocrinology *141*, 315-324. 10.1210/endo.141.1.7236.

66. Winchester, S.K., Imamura, T., Gross, G.A., Muglia, L.M., Vogt, S.K., Wright, J., Watanabe, K., Tai, H.H., and Muglia, L.J. (2002). Coordinate regulation of prostaglandin metabolism for induction of parturition in mice. Endocrinology *143*, 2593-2598. 10.1210/endo.143.7.8926.

67. Iino, S., Horiguchi, K., Horiguchi, S., and Nojyo, Y. (2009). c-Kit-negative fibroblast-like cells express platelet-derived growth factor receptor alpha in the murine gastrointestinal musculature. Histochem Cell Biol *131*, 691-702. 10.1007/s00418-009-0580-6.

68. Iino, S., and Nojyo, Y. (2009). Immunohistochemical demonstration of c-Kit-negative fibroblast-like cells in murine gastrointestinal musculature. Arch Histol Cytol *72*, 107-115. 10.1679/aohc.72.107.

69. Kurahashi, M., Zheng, H., Dwyer, L., Ward, S.M., Koh, S.D., and Sanders, K.M. (2011). A functional role for the 'fibroblast-like cells' in gastrointestinal smooth muscles. J Physiol *589*, 697-710. 10.1113/jphysiol.2010.201129.

70. Koh, B.H., Roy, R., Hollywood, M.A., Thornbury, K.D., McHale, N.G., Sergeant, G.P., Hatton, W.J., Ward, S.M., Sanders, K.M., and Koh, S.D. (2012). Platelet-derived growth factor receptor-alpha cells in mouse urinary bladder: a new class of interstitial cells. J Cell Mol Med *16*, 691-700. 10.1111/j.1582-4934.2011.01506.x.

71. Lee, H., Koh, B.H., Peri, L.E., Sanders, K.M., and Koh, S.D. (2013). Functional expression of SK channels in murine detrusor PDGFR+ cells. J Physiol *591*, 503-513. 10.1113/jphysiol.2012.241505.

72. Monaghan, K.P., Johnston, L., and McCloskey, K.D. (2012). Identification of PDGFRalpha positive populations of interstitial cells in human and guinea pig bladders. J Urol *188*, 639-647. 10.1016/j.juro.2012.03.117.

73. Peri, L.E., Koh, B.H., Ward, G.K., Bayguinov, Y., Hwang, S.J., Gould, T.W., Mullan, C.J., Sanders, K.M., and Ward, S.M. (2015). A novel class of interstitial cells in the mouse and monkey female reproductive tracts. Biol Reprod *92*, 102. 10.1095/biolreprod.114.124388.

74. Zhao, H., Wang, Y., Xu, H., Liu, M., Xu, X., Zhu, S., Liu, Z., Cai, H., Wang, Y., Lu, J., et al. (2023). Stromal cells-specific retinoic acid determines parturition timing at single-cell and spatial-temporal resolution. iScience *26*, 107796. 10.1016/j.isci.2023.107796.

75. Challis, J.R.L., S.J. (1994). Parturition (Raven).

76. Fuchs, A.R. (1995). Plasma, membrane receptors regulating myometrial contractility and their hormonal modulation. Semin Perinatol *19*, 15-30. 10.1016/s0146-0005(95)80044-1.

77. Zingg, H.H., Rozen, F., Chu, K., Larcher, A., Arslan, A., Richard, S., and Lefebvre, D. (1995). Oxytocin and oxytocin receptor gene expression in the uterus. Recent Prog Horm Res *50*, 255-273. 10.1016/b978-0-12-571150-0.50015-9.

78. Hidema, S., Fukuda, T., Hiraoka, Y., Mizukami, H., Hayashi, R., Otsuka, A., Suzuki, S., Miyazaki, S., and Nishimori, K. (2016). Generation of Oxtr cDNA(HA)-Ires-Cre Mice for Gene Expression in an Oxytocin Receptor Specific Manner. J Cell Biochem *117*, 1099-1111. 10.1002/jcb.25393.

79. Chan, Y.W., van den Berg, H.A., Moore, J.D., Quenby, S., and Blanks, A.M. (2014). Assessment of myometrial transcriptome changes associated with spontaneous human

labour by high-throughput RNA-seq. Exp Physiol *99*, 510-524. 10.1113/expphysiol.2013.072868.

80. Mittal, P., Romero, R., Tarca, A.L., Gonzalez, J., Draghici, S., Xu, Y., Dong, Z., Nhan-Chang, C.L., Chaiworapongsa, T., Lye, S., et al. (2010). Characterization of the myometrial transcriptome and biological pathways of spontaneous human labor at term. J Perinat Med *38*, 617-643. 10.1515/jpm.2010.097.

81. Stanfield, Z., Lai, P.F., Lei, K., Johnson, M.R., Blanks, A.M., Romero, R., Chance, M.R., Mesiano, S., and Koyuturk, M. (2019). Myometrial Transcriptional Signatures of Human Parturition. Front Genet *10*, 185. 10.3389/fgene.2019.00185.

82. Ji, K., Zhong, J., Cui, L., Wang, X., Chen, L.N., Wen, B., Yang, F., Deng, W., Pan, X., Wang, L., et al. (2024). Exploring myometrial microenvironment changes at the single-cell level from nonpregnant to term pregnant states. Physiol Genomics *56*, 32-47. 10.1152/physiolgenomics.00067.2023.

83. Kane, A.E., and Sinclair, D.A. (2019). Epigenetic changes during aging and their reprogramming potential. Crit Rev Biochem Mol Biol *54*, 61-83. 10.1080/10409238.2019.1570075.

84. Rayon, T. (2023). Cell time: How cells control developmental timetables. Sci Adv *9*, eadh1849. 10.1126/sciadv.adh1849.

85. Dias, J.M., Alekseenko, Z., Jeggari, A., Boareto, M., Vollmer, J., Kozhevnikova, M., Wang, H., Matise, M.P., Alexeyenko, A., Iber, D., and Ericson, J. (2020). A Shh/Gli-driven three-node timer motif controls temporal identity and fate of neural stem cells. Sci Adv *6*. 10.1126/sciadv.aba8196.

86. Soshnikova, N., and Duboule, D. (2009). Epigenetic temporal control of mouse Hox genes in vivo. Science *324*, 1320-1323. 10.1126/science.1171468.

87. Sun, B., Looi, L.S., Guo, S., He, Z., Gan, E.S., Huang, J., Xu, Y., Wee, W.Y., and Ito, T. (2014). Timing mechanism dependent on cell division is invoked by Polycomb eviction in plant stem cells. Science *343*, 1248559. 10.1126/science.1248559.

88. Telley, L., Agirman, G., Prados, J., Amberg, N., Fievre, S., Oberst, P., Bartolini, G., Vitali, I., Cadilhac, C., Hippenmeyer, S., et al. (2019). Temporal patterning of apical progenitors and their daughter neurons in the developing neocortex. Science *364*, 547-+. ARTN eaav2522 10.1126/science.aav2522.

89. Wu, Q., Shichino, Y., Abe, T., Suetsugu, T., Omori, A., Kiyonari, H., Iwasaki, S., and Matsuzaki, F. (2022). Selective translation of epigenetic modifiers affects the temporal pattern and differentiation of neural stem cells. Nat Commun *13*. ARTN 470 10.1038/s41467-022-28097-y.

90. Yang, J.H., Hayano, M., Griffin, P.T., Amorim, J.A., Bonkowski, M.S., Apostolides, J.K., Salfati, E.L., Blanchette, M., Munding, E.M., Bhakta, M., et al. (2023). Loss of epigenetic information as a cause of mammalian aging. Cell *186*, 305-326 e327. 10.1016/j.cell.2022.12.027.

91. Rokas, A., Mesiano, S., Tamam, O., LaBella, A., Zhang, G., and Muglia, L. (2020). Developing a theoretical evolutionary framework to solve the mystery of parturition initiation. Elife *9*. 10.7554/eLife.58343.

92. Mesiano, S. (2015). Chapter 42 - Parturition, Fourth Edition (Academic Press).

93. Gao, L., Rabbitt, E.H., Condon, J.C., Renthal, N.E., Johnston, J.M., Mitsche, M.A., Chambon, P., Xu, J., O'Malley, B.W., and Mendelson, C.R. (2015). Steroid receptor

coactivators 1 and 2 mediate fetal-to-maternal signaling that initiates parturition. J Clin Invest *125*, 2808-2824. 10.1172/JCI78544.

94. McLean, M., Bisits, A., Davies, J., Woods, R., Lowry, P., and Smith, R. (1995). A placental clock controlling the length of human pregnancy. Nat Med *1*, 460-463. 10.1038/nm0595-460.

95. Norwitz, E.R., Bonney, E.A., Snegovskikh, V.V., Williams, M.A., Phillippe, M., Park, J.S., and Abrahams, V.M. (2015). Molecular Regulation of Parturition: The Role of the Decidual Clock. Cold Spring Harb Perspect Med *5*. 10.1101/cshperspect.a023143.

96. Sandman, C.A., Glynn, L., Schetter, C.D., Wadhwa, P., Garite, T., Chicz-DeMet, A., and Hobel, C. (2006). Elevated maternal cortisol early in pregnancy predicts third trimester levels of placental corticotropin releasing hormone (CRH): priming the placental clock. Peptides *27*, 1457-1463. 10.1016/j.peptides.2005.10.002.

97. Sugimoto, Y., Yamasaki, A., Segi, E., Tsuboi, K., Aze, Y., Nishimura, T., Oida, H., Yoshida, N., Tanaka, T., Katsuyama, M., et al. (1997). Failure of parturition in mice lacking the prostaglandin F receptor. Science *277*, 681-683. 10.1126/science.277.5326.681.

98. Nancy, P., Siewiera, J., Rizzuto, G., Tagliani, E., Osokine, I., Manandhar, P., Dolgalev, I., Clementi, C., Tsirigos, A., and Erlebacher, A. (2018). H3K27me3 dynamics dictate evolving uterine states in pregnancy and parturition. J Clin Invest *128*, 233-247. 10.1172/JCI95937.

99. Agger, K., Cloos, P.A., Christensen, J., Pasini, D., Rose, S., Rappsilber, J., Issaeva, I., Canaani, E., Salcini, A.E., and Helin, K. (2007). UTX and JMJD3 are histone H3K27

demethylases involved in HOX gene regulation and development. Nature *449*, 731-734. 10.1038/nature06145.

100. De Santa, F., Totaro, M.G., Prosperini, E., Notarbartolo, S., Testa, G., and Natoli, G. (2007). The histone H3 lysine-27 demethylase Jmjd3 links inflammation to inhibition of polycomb-mediated gene silencing. Cell *130*, 1083-1094. 10.1016/j.cell.2007.08.019.

101. Lee, M.G., Villa, R., Trojer, P., Norman, J., Yan, K.P., Reinberg, D., Di Croce, L., and Shiekhattar, R. (2007). Demethylation of H3K27 regulates polycomb recruitment and H2A ubiquitination. Science *318*, 447-450. 10.1126/science.1149042.

102. Christiaens, I., Zaragoza, D.B., Guilbert, L., Robertson, S.A., Mitchell, B.F., and Olson, D.M. (2008). Inflammatory processes in preterm and term parturition. J Reprod Immunol *79*, 50-57. 10.1016/j.jri.2008.04.002.

103. Shynlova, O., Nedd-Roderique, T., Li, Y., Dorogin, A., Nguyen, T., and Lye, S.J. (2013). Infiltration of myeloid cells into decidua is a critical early event in the labour cascade and post-partum uterine remodelling. J Cell Mol Med *17*, 311-324. 10.1111/jcmm.12012.

104. Soyal, S.M., Mukherjee, A., Lee, K.Y., Li, J., Li, H., DeMayo, F.J., and Lydon, J.P. (2005). Cre-mediated recombination in cell lineages that express the progesterone receptor. Genesis *41*, 58-66. 10.1002/gene.20098.

105. Biggers, J.D., Curnow, R.N., Finn, C.A., and McLaren, A. (1963). Regulation of the Gestation Period in Mice. J Reprod Fertil *6*, 125-138. 10.1530/jrf.0.0060125.

106. Dewar, A.D. (1968). Litter size and the duration of pregnancy in mice. Q J Exp Physiol Cogn Med Sci *53*, 155-161. 10.1113/expphysiol.1968.sp001954.

107. Daikoku, T., Ogawa, Y., Terakawa, J., Ogawa, A., DeFalco, T., and Dey, S.K. (2014). Lactoferrin-iCre: a new mouse line to study uterine epithelial gene function. Endocrinology *155*, 2718-2724. 10.1210/en.2014-1265.

108. Roesch, K., Jadhav, A.P., Trimarchi, J.M., Stadler, M.B., Roska, B., Sun, B.B., and Cepko, C.L. (2008). The transcriptome of retinal Muller glial cells. J Comp Neurol *509*, 225-238. 10.1002/cne.21730.

109. Siewiera, J., McIntyre, T.I., Cautivo, K.M., Mahiddine, K., Rideaux, D., Molofsky, A.B., and Erlebacher, A. (2023). Circumvention of luteolysis reveals parturition pathways in mice dependent upon innate type 2 immunity. Immunity *56*, 606-619 e607. 10.1016/j.immuni.2023.01.005.

110. Aline T. Yamada, J.R.B., Eliano M.O. Lippe, K.Y. Degaki, A.F. Dalmorin, A.K. Edwards, Patricia D.A. Lima, Valdemar A. Paffaro Jr. (2014). Chapter 13. Unique Features of Endometrial Dynamics During Pregnancy (Elsevier Inc.).

111. Erlebacher, A., Zhang, D., Parlow, A.F., and Glimcher, L.H. (2004). Ovarian insufficiency and early pregnancy loss induced by activation of the innate immune system. J Clin Invest *114*, 39-48. 10.1172/JCI20645.

112. Garcia-Flores, V., Romero, R., Peyvandipour, A., Galaz, J., Pusod, E., Panaitescu, B., Miller, D., Xu, Y., Tao, L., Liu, Z., et al. (2023). A single-cell atlas of murine reproductive tissues during preterm labor. Cell Rep *42*, 111846. 10.1016/j.celrep.2022.111846.

113. Salomonis, N., Cotte, N., Zambon, A.C., Pollard, K.S., Vranizan, K., Doniger, S.W., Dolganov, G., and Conklin, B.R. (2005). Identifying genetic networks underlying myometrial transition to labor. Genome Biol *6*, R12. 10.1186/gb-2005-6-2-r12.

114. Shchuka, V.M., Abatti, L.E., Hou, H., Khader, N., Dorogin, A., Wilson, M.D., Shynlova, O., and Mitchell, J.A. (2020). The pregnant myometrium is epigenetically activated at contractility-driving gene loci prior to the onset of labor in mice. PLoS Biol *18*, e3000710. 10.1371/journal.pbio.3000710.

115. Soloff, M.S., Alexandrova, M., and Fernstrom, M.J. (1979). Oxytocin receptors: triggers for parturition and lactation? Science *204*, 1313-1315. 10.1126/science.221972.

116. Vassalli, A., Matzuk, M.M., Gardner, H.A., Lee, K.F., and Jaenisch, R. (1994). Activin/inhibin beta B subunit gene disruption leads to defects in eyelid development and female reproduction. Genes Dev *8*, 414-427. 10.1101/gad.8.4.414.

117. Ackerman, W.E.t., Buhimschi, C.S., Snedden, A., Summerfield, T.L., Zhao, G., and Buhimschi, I.A. (2021). Molecular signatures of labor and nonlabor myometrium with parsimonious classification from 2 calcium transporter genes. JCI Insight *6*. 10.1172/jci.insight.148425.

118. Arrowsmith, S., and Wray, S. (2014). Oxytocin: its mechanism of action and receptor signalling in the myometrium. J Neuroendocrinol *26*, 356-369. 10.1111/jne.12154.

119. Fetalvero, K.M., Zhang, P., Shyu, M., Young, B.T., Hwa, J., Young, R.C., and Martin, K.A. (2008). Prostacyclin primes pregnant human myometrium for an enhanced contractile response in parturition. J Clin Invest *118*, 3966-3979. 10.1172/JCI33800.

120. Lim, R., Barker, G., and Lappas, M. (2014). SLIT3 is increased in supracervical human foetal membranes and in labouring myometrium and regulates pro-inflammatory mediators. Am J Reprod Immunol *71*, 297-311. 10.1111/aji.12181.

121. Mazor, M., Furman, B., and Bashiri, A. (1998). Cytokines in preterm parturition. Gynecol Endocrinol *12*, 421-427. 10.3109/09513599809012845.

122. Pique-Regi, R., Romero, R., Garcia-Flores, V., Peyvandipour, A., Tarca, A.L., Pusod, E., Galaz, J., Miller, D., Bhatti, G., Para, R., et al. (2022). A single-cell atlas of the myometrium in human parturition. JCI Insight *7*. 10.1172/jci.insight.153921.

123. Mackler, A.M., Green, L.M., McMillan, P.J., and Yellon, S.M. (2000). Distribution and activation of uterine mononuclear phagocytes in peripartum endometrium and myometrium of the mouse. Biol Reprod *62*, 1193-1200. 10.1095/biolreprod62.5.1193.

124. Mackler, A.M., Iezza, G., Akin, M.R., McMillan, P., and Yellon, S.M. (1999). Macrophage trafficking in the uterus and cervix precedes parturition in the mouse. Biol Reprod *61*, 879-883. 10.1095/biolreprod61.4.879.

125. Chambers, S.P., and Clarke, A.G. (1979). Measurement of thymus weight, lumbar node weight and progesterone levels in syngeneically pregnant, allogeneically pregnant, and pseudopregnant mice. J Reprod Fertil *55*, 309-315. 10.1530/jrf.0.0550309.

126. Sinha, Y.N., Wickes, M.A., and Baxter, S.R. (1978). Prolactin and growth hormone secretion and mammary gland growth during pseudopregnancy in the mouse. J Endocrinol *77*, 203-212. 10.1677/joe.0.0770203.

127. Kampmann, E., Johann, S., van Neerven, S., Beyer, C., and Mey, J. (2008). Anti-inflammatory effect of retinoic acid on prostaglandin synthesis in cultured cortical astrocytes. J Neurochem *106*, 320-332. 10.1111/j.1471-4159.2008.05395.x.

128. Schneider, N., Lanz, S., Ramer, R., Schaefer, D., and Goppelt-Struebe, M. (2001). Up-regulation of cyclooxygenase-1 in neuroblastoma cell lines by retinoic acid and corticosteroids. J Neurochem *77*, 416-424. 10.1046/j.1471-4159.2001.00264.x.

129. Antonijevic, I.A., Douglas, A.J., Dye, S., Bicknell, R.J., Leng, G., and Russell, J.A. (1995). Oxytocin antagonists delay the initiation of parturition and prolong its active phase in rats. J Endocrinol *145*, 97-103. 10.1677/joe.0.1450097.

130. Takayanagi, Y., Yoshida, M., Bielsky, I.F., Ross, H.E., Kawamata, M., Onaka, T., Yanagisawa, T., Kimura, T., Matzuk, M.M., Young, L.J., and Nishimori, K. (2005). Pervasive social deficits, but normal parturition, in oxytocin receptor-deficient mice. Proc Natl Acad Sci U S A *102*, 16096-16101. 10.1073/pnas.0505312102.

131. Manna, S., Kim, J.K., Bauge, C., Cam, M., Zhao, Y., Shetty, J., Vacchio, M.S., Castro, E., Tran, B., Tessarollo, L., and Bosselut, R. (2015). Histone H3 Lysine 27 demethylases Jmjd3 and Utx are required for T-cell differentiation. Nat Commun *6*, 8152. 10.1038/ncomms9152.

132. Satija, R., Farrell, J.A., Gennert, D., Schier, A.F., and Regev, A. (2015). Spatial reconstruction of single-cell gene expression data. Nat Biotechnol *33*, 495-502. 10.1038/nbt.3192.

133. Korsunsky, I., Millard, N., Fan, J., Slowikowski, K., Zhang, F., Wei, K., Baglaenko, Y., Brenner, M., Loh, P.R., and Raychaudhuri, S. (2019). Fast, sensitive and accurate integration of single-cell data with Harmony. Nat Methods *16*, 1289-1296. 10.1038/s41592-019-0619-0.

134. Meers, M.P., Bryson, T.D., Henikoff, J.G., and Henikoff, S. (2019). Improved CUT&RUN chromatin profiling tools. Elife *8*. 10.7554/eLife.46314.

135. Skene, P.J., Henikoff, J.G., and Henikoff, S. (2018). Targeted in situ genome-wide profiling with high efficiency for low cell numbers. Nat Protoc *13*, 1006-1019. 10.1038/nprot.2018.015.

136. Dobin, A., Davis, C.A., Schlesinger, F., Drenkow, J., Zaleski, C., Jha, S., Batut, P., Chaisson, M., and Gingeras, T.R. (2013). STAR: ultrafast universal RNA-seq aligner. Bioinformatics *29*, 15-21. 10.1093/bioinformatics/bts635.

137. Picard Toolkit. (2019). Broad Institute, Github repository.

138. Zhang, Y., Liu, T., Meyer, C.A., Eeckhoute, J., Johnson, D.S., Bernstein, B.E., Nusbaum, C., Myers, R.M., Brown, M., Li, W., and Liu, X.S. (2008). Model-based analysis of ChIP-Seq (MACS). Genome Biol *9*, R137. 10.1186/gb-2008-9-9-r137.

139. Gu, Z., Eils, R., and Schlesner, M. (2016). Complex heatmaps reveal patterns and correlations in multidimensional genomic data. Bioinformatics *32*, 2847-2849. 10.1093/bioinformatics/btw313.

140. Quinlan, A.R., and Hall, I.M. (2010). BEDTools: a flexible suite of utilities for comparing genomic features. Bioinformatics *26*, 841-842. 10.1093/bioinformatics/btq033.

141. Kent, W.J., Zweig, A.S., Barber, G., Hinrichs, A.S., and Karolchik, D. (2010). BigWig and BigBed: enabling browsing of large distributed datasets. Bioinformatics *26*, 2204-2207. 10.1093/bioinformatics/btq351.

142. Yu, G., Wang, L.G., and He, Q.Y. (2015). ChIPseeker: an R/Bioconductor package for ChIP peak annotation, comparison and visualization. Bioinformatics *31*, 2382-2383. 10.1093/bioinformatics/btv145.

143. Kokubu, K., Hondo, E., Sakaguchi, N., Sagara, E., and Kiso, Y. (2005). Differentiation and elimination of uterine natural killer cells in delayed implantation and parturition mice. J Reprod Dev *51*, 773-776. 10.1262/jrd.17033.

144. Shynlova, O., Nadeem, L., Zhang, J., Dunk, C., and Lye, S. (2020). Myometrial activation: Novel concepts underlying labor. Placenta *92*, 28-36. 10.1016/j.placenta.2020.02.005.

145. Ratajczak, C.K., and Muglia, L.J. (2008). Insights into parturition biology from genetically altered mice. Pediatr Res *64*, 581-589. 10.1203/PDR.0b013e31818718d2.

146. Cayrol, C., and Girard, J.P. (2018). Interleukin-33 (IL-33): A nuclear cytokine from the IL-1 family. Immunol Rev *281*, 154-168. 10.1111/imr.12619.

147. Allen, J.E., and Sutherland, T.E. (2014). Host protective roles of type 2 immunity: parasite killing and tissue repair, flip sides of the same coin. Semin Immunol *26*, 329-340. 10.1016/j.smim.2014.06.003.

148. Markiewicz, L., and Gurpide, E. (1994). Estrogenic and progestagenic activities coexisting in steroidal drugs: quantitative evaluation by in vitro bioassays with human cells. J Steroid Biochem Mol Biol *48*, 89-94. 10.1016/0960-0760(94)90254-2.

149. Terakawa, J., Watanabe, T., Obara, R., Sugiyama, M., Inoue, N., Ohmori, Y., Hosaka, Y.Z., and Hondo, E. (2012). The complete control of murine pregnancy from embryo implantation to parturition. Reproduction *143*, 411-415. 10.1530/REP-11-0288.

150. Word, R.A., Li, X.H., Hnat, M., and Carrick, K. (2007). Dynamics of cervical remodeling during pregnancy and parturition: mechanisms and current concepts. Semin Reprod Med *25*, 69-79. 10.1055/s-2006-956777.

151. Vainchtein, I.D., Chin, G., Cho, F.S., Kelley, K.W., Miller, J.G., Chien, E.C., Liddelow, S.A., Nguyen, P.T., Nakao-Inoue, H., Dorman, L.C., et al. (2018). Astrocyte-derived interleukin-33 promotes microglial synapse engulfment and neural circuit development. Science *359*, 1269-1273. 10.1126/science.aal3589.

152. Dahlgren, M.W., Jones, S.W., Cautivo, K.M., Dubinin, A., Ortiz-Carpena, J.F., Farhat, S., Yu, K.S., Lee, K., Wang, C., Molofsky, A.V., et al. (2019). Adventitial Stromal Cells Define Group 2 Innate Lymphoid Cell Tissue Niches. Immunity *50*, 707-722 e706. 10.1016/j.immuni.2019.02.002.

153. Doisne, J.M., Balmas, E., Boulenouar, S., Gaynor, L.M., Kieckbusch, J., Gardner, L., Hawkes, D.A., Barbara, C.F., Sharkey, A.M., Brady, H.J., et al. (2015). Composition, Development, and Function of Uterine Innate Lymphoid Cells. J Immunol *195*, 3937-3945. 10.4049/jimmunol.1500689.

154. Herington, J.L., O'Brien, C., Robuck, M.F., Lei, W., Brown, N., Slaughter, J.C., Paria, B.C., Mahadevan-Jansen, A., and Reese, J. (2018). Prostaglandin-Endoperoxide Synthase 1 Mediates the Timing of Parturition in Mice Despite Unhindered Uterine Contractility. Endocrinology *159*, 490-505. 10.1210/en.2017-00647.

155. Liu, B., Yang, J., Luo, W., Zhang, Y., Li, J., Li, H., Chen, L., and Zhou, Y. (2017). Prostaglandin D(2) is the major cyclooxygenase-1-derived product in prepartum mouse uteri where it mediates an enhanced in vitro myometrial contraction. Eur J Pharmacol *813*, 140-146. 10.1016/j.ejphar.2017.08.015.

156. Johnston, L.K., Hsu, C.L., Krier-Burris, R.A., Chhiba, K.D., Chien, K.B., McKenzie, A., Berdnikovs, S., and Bryce, P.J. (2016). IL-33 Precedes IL-5 in Regulating Eosinophil Commitment and Is Required for Eosinophil Homeostasis. J Immunol *197*, 3445-3453. 10.4049/jimmunol.1600611.

157. Fettrelet, T., Gigon, L., Karaulov, A., Yousefi, S., and Simon, H.U. (2021). The Enigma of Eosinophil Degranulation. Int J Mol Sci *22*. 10.3390/ijms22137091.

158. Carlens, J., Wahl, B., Ballmaier, M., Bulfone-Paus, S., Forster, R., and Pabst, O. (2009). Common gamma-chain-dependent signals confer selective survival of eosinophils in the murine small intestine. J Immunol *183*, 5600-5607. 10.4049/jimmunol.0801581.

159. Tagliani, E., Shi, C., Nancy, P., Tay, C.S., Pamer, E.G., and Erlebacher, A. (2011). Coordinate regulation of tissue macrophage and dendritic cell population dynamics by CSF-1. J Exp Med *208*, 1901-1916. 10.1084/jem.20110866.

160. Diener, K.R., Robertson, S.A., Hayball, J.D., and Lousberg, E.L. (2016). Multi-parameter flow cytometric analysis of uterine immune cell fluctuations over the murine estrous cycle. J Reprod Immunol *113*, 61-67. 10.1016/j.jri.2015.11.005.

161. Gouon-Evans, V., and Pollard, J.W. (2001). Eotaxin is required for eosinophil homing into the stroma of the pubertal and cycling uterus. Endocrinology *142*, 4515-4521. 10.1210/endo.142.10.8459.

162. Kopf, M., Brombacher, F., Hodgkin, P.D., Ramsay, A.J., Milbourne, E.A., Dai, W.J., Ovington, K.S., Behm, C.A., Kohler, G., Young, I.G., and Matthaei, K.I. (1996). IL-5-deficient mice have a developmental defect in CD5+ B-1 cells and lack eosinophilia but have normal antibody and cytotoxic T cell responses. Immunity *4*, 15-24. 10.1016/s1074-7613(00)80294-0.

163. Park, Y.M., and Bochner, B.S. (2010). Eosinophil survival and apoptosis in health and disease. Allergy Asthma Immunol Res *2*, 87-101. 10.4168/aair.2010.2.2.87.

164. Robertson, S.A., Mau, V.J., Young, I.G., and Matthaei, K.I. (2000). Uterine eosinophils and reproductive performance in interleukin 5-deficient mice. J Reprod Fertil *120*, 423-432. 10.1530/jrf.0.1200423.

165. Dougan, M., Dranoff, G., and Dougan, S.K. (2019). GM-CSF, IL-3, and IL-5 Family of Cytokines: Regulators of Inflammation. Immunity *50*, 796-811. 10.1016/j.immuni.2019.03.022.

166. Grimaldi, J.C., Yu, N.X., Grunig, G., Seymour, B.W., Cottrez, F., Robinson, D.S., Hosken, N., Ferlin, W.G., Wu, X., Soto, H., et al. (1999). Depletion of eosinophils in mice through the use of antibodies specific for C-C chemokine receptor 3 (CCR3). J Leukoc Biol *65*, 846-853. 10.1002/jlb.65.6.846.

167. Menzies, F.M., Khan, A.H., Higgins, C.A., Nelson, S.M., and Nibbs, R.J. (2012). The chemokine receptor CCR2 is not required for successful initiation of labor in mice. Biol Reprod *86*, 118. 10.1095/biolreprod.111.094631.

168. Menzies, F.M., Higgins, C.A., Shepherd, M.C., Nibbs, R.J., and Nelson, S.M. (2012). Mast cells reside in myometrium and cervix, but are dispensable in mice for successful pregnancy and labor. Immunol Cell Biol *90*, 321-329. 10.1038/icb.2011.40.

169. Lloyd, C.M., and Snelgrove, R.J. (2018). Type 2 immunity: Expanding our view. Sci Immunol *3*. 10.1126/sciimmunol.aat1604.

170. Kakkar, R., Hei, H., Dobner, S., and Lee, R.T. (2012). Interleukin 33 as a mechanically responsive cytokine secreted by living cells. J Biol Chem *287*, 6941-6948. 10.1074/jbc.M111.298703.

171. Domingo, C., Palomares, O., Sandham, D.A., Erpenbeck, V.J., and Altman, P. (2018). The prostaglandin D(2) receptor 2 pathway in asthma: a key player in airway inflammation. Respir Res *19*, 189. 10.1186/s12931-018-0893-x.

172. Crankshaw, D.J., and Gaspar, V. (1992). Effects of prostanoids on the rat's myometrium in vitro during pregnancy. Biol Reprod *46*, 392-400. 10.1095/biolreprod46.3.392.

173. Gaynor, L.M., and Colucci, F. (2017). Uterine Natural Killer Cells: Functional Distinctions and Influence on Pregnancy in Humans and Mice. Front Immunol *8*, 467. 10.3389/fimmu.2017.00467.

174. Lutton, E.J., Lammers, W., James, S., van den Berg, H.A., and Blanks, A.M. (2018). Identification of uterine pacemaker regions at the myometrial-placental interface in the rat. J Physiol *596*, 2841-2852. 10.1113/JP275688.

175. Valero-Pacheco, N., Tang, E.K., Massri, N., Loia, R., Chemerinski, A., Wu, T., Begum, S., El-Naccache, D.W., Gause, W.C., Arora, R., Douglas, N.C., and Beaulieu, A.M. (2022). Maternal IL-33 critically regulates tissue remodeling and type 2 immune responses in the uterus during early pregnancy in mice. Proc Natl Acad Sci U S A *119*, e2123267119. 10.1073/pnas.2123267119.

176. Stelzer, I.A., Ghaemi, M.S., Han, X., Ando, K., Hedou, J.J., Feyaerts, D., Peterson, L.S., Rumer, K.K., Tsai, E.S., Ganio, E.A., et al. (2021). Integrated trajectories of the maternal metabolome, proteome, and immunome predict labor onset. Sci Transl Med *13*. 10.1126/scitranslmed.abd9898.

177. Huang, B., Faucette, A.N., Pawlitz, M.D., Pei, B., Goyert, J.W., Zhou, J.Z., El-Hage, N.G., Deng, J., Lin, J., Yao, F., et al. (2017). Interleukin-33-induced expression of PIBF1 by decidual B cells protects against preterm labor. Nat Med *23*, 128-135. 10.1038/nm.4244.

178. Griesenauer, B., and Paczesny, S. (2017). The ST2/IL-33 Axis in Immune Cells during Inflammatory Diseases. Front Immunol *8*, 475. 10.3389/fimmu.2017.00475.

179. Mendes, J., Rodrigues-Santos, P., Areia, A.L., Almeida, J.S., Alves, V., Santos-Rosa, M., and Mota-Pinto, A. (2021). Type 2 and type 3 innate lymphoid cells at the maternal-fetal

interface: implications in preterm birth. BMC Immunol *22*, 28. 10.1186/s12865-021-00423-x.

180. Xu, Y., Romero, R., Miller, D., Silva, P., Panaitescu, B., Theis, K.R., Arif, A., Hassan, S.S., and Gomez-Lopez, N. (2018). Innate lymphoid cells at the human maternal-fetal interface in spontaneous preterm labor. American Journal of Reproductive Immunology *79*, e12820.

181. Romero, R., Kusanovic, J.P., Munoz, H., Gomez, R., Lamont, R.F., and Yeo, L. (2010). Allergy-induced preterm labor after the ingestion of shellfish. J Matern Fetal Neonatal Med *23*, 351-359. 10.3109/14767050903177193.

182. Bytautiene, E., Romero, R., Vedernikov, Y.P., El-Zeky, F., Saade, G.R., and Garfield, R.E. (2004). Induction of premature labor and delivery by allergic reaction and prevention by histamine H1 receptor antagonist. Am J Obstet Gynecol *191*, 1356-1361. 10.1016/j.ajog.2004.06.092.

183. Muzumdar, M.D., Tasic, B., Miyamichi, K., Li, L., and Luo, L. (2007). A global double-fluorescent Cre reporter mouse. Genesis *45*, 593-605. 10.1002/dvg.20335.

184. Reeves, C.V., Wang, X., Charles-Horvath, P.C., Vink, J.Y., Borisenko, V.Y., Young, J.A., and Kitajewski, J.K. (2012). Anthrax toxin receptor 2 functions in ECM homeostasis of the murine reproductive tract and promotes MMP activity. PLoS One *7*, e34862. 10.1371/journal.pone.0034862.

185. Schmitz, T., Souil, E., Herve, R., Nicco, C., Batteux, F., Germain, G., Cabrol, D., Evain-Brion, D., Leroy, M.J., and Mehats, C. (2007). PDE4 inhibition prevents preterm delivery induced by an intrauterine inflammation. J Immunol *178*, 1115-1121. 10.4049/jimmunol.178.2.1115.

186. Bond, C.T., Sprengel, R., Bissonnette, J.M., Kaufmann, W.A., Pribnow, D., Neelands, T., Storck, T., Baetscher, M., Jerecic, J., Maylie, J., et al. (2000). Respiration and parturition affected by conditional overexpression of the Ca2+-activated K+ channel subunit, SK3. Science *289*, 1942-1946. 10.1126/science.289.5486.1942.

187. Pichery, M., Mirey, E., Mercier, P., Lefrancais, E., Dujardin, A., Ortega, N., and Girard, J.P. (2012). Endogenous IL-33 is highly expressed in mouse epithelial barrier tissues, lymphoid organs, brain, embryos, and inflamed tissues: in situ analysis using a novel Il-33-LacZ gene trap reporter strain. J Immunol *188*, 3488-3495. 10.4049/jimmunol.1101977.

188. Nussbaum, J.C., Van Dyken, S.J., von Moltke, J., Cheng, L.E., Mohapatra, A., Molofsky, A.B., Thornton, E.E., Krummel, M.F., Chawla, A., Liang, H.E., and Locksley, R.M. (2013). Type 2 innate lymphoid cells control eosinophil homeostasis. Nature *502*, 245-248. 10.1038/nature12526.

189. Chen, W.Y., Hong, J., Gannon, J., Kakkar, R., and Lee, R.T. (2015). Myocardial pressure overload induces systemic inflammation through endothelial cell IL-33. Proc Natl Acad Sci U S A *112*, 7249-7254. 10.1073/pnas.1424236112.

190. Nancy, P., Tagliani, E., Tay, C.S., Asp, P., Levy, D.E., and Erlebacher, A. (2012). Chemokine gene silencing in decidual stromal cells limits T cell access to the maternal-fetal interface. Science *336*, 1317-1321. 10.1126/science.1220030.

191. Liu, L., Oza, S., Hogan, D., Chu, Y., Perin, J., Zhu, J., Lawn, J.E., Cousens, S., Mathers, C., and Black, R.E. (2016). Global, regional, and national causes of under-5 mortality in 2000-15: an updated systematic analysis with implications for the Sustainable Development Goals. Lancet *388*, 3027-3035. 10.1016/S0140-6736(16)31593-8.

192. Abitbol, C.L., and Rodriguez, M.M. (2012). The long-term renal and cardiovascular consequences of prematurity. Nat Rev Nephrol *8*, 265-274. 10.1038/nrneph.2012.38.

193. Blencowe, H., Lee, A.C., Cousens, S., Bahalim, A., Narwal, R., Zhong, N., Chou, D., Say, L., Modi, N., Katz, J., et al. (2013). Preterm birth-associated neurodevelopmental impairment estimates at regional and global levels for 2010. Pediatr Res *74 Suppl 1*, 17-34. 10.1038/pr.2013.204.

194. Carmody, J.B., and Charlton, J.R. (2013). Short-term gestation, long-term risk: prematurity and chronic kidney disease. Pediatrics *131*, 1168-1179. 10.1542/peds.2013-0009.

195. O'Reilly, M., Sozo, F., and Harding, R. (2013). Impact of preterm birth and bronchopulmonary dysplasia on the developing lung: long-term consequences for respiratory health. Clin Exp Pharmacol Physiol *40*, 765-773. 10.1111/1440-1681.12068.

196. Ream, M.A., and Lehwald, L. (2018). Neurologic Consequences of Preterm Birth. Curr Neurol Neurosci Rep *18*, 48. 10.1007/s11910-018-0862-2.

197. Combs, C.A., Gravett, M., Garite, T.J., Hickok, D.E., Lapidus, J., Porreco, R., Rael, J., Grove, T., Morgan, T.K., Clewell, W., et al. (2014). Amniotic fluid infection, inflammation, and colonization in preterm labor with intact membranes. Am J Obstet Gynecol *210*, 125 e121-125 e115. 10.1016/j.ajog.2013.11.032.

198. Deng, W., Yuan, J., Cha, J., Sun, X., Bartos, A., Yagita, H., Hirota, Y., and Dey, S.K. (2019). Endothelial Cells in the Decidual Bed Are Potential Therapeutic Targets for Preterm Birth Prevention. Cell Rep *27*, 1755-1768 e1754. 10.1016/j.celrep.2019.04.049.

199. Gravett, M.G., Witkin, S.S., Haluska, G.J., Edwards, J.L., Cook, M.J., and Novy, M.J. (1994). An experimental model for intraamniotic infection and preterm labor in rhesus monkeys. Am J Obstet Gynecol *171*, 1660-1667. 10.1016/0002-9378(94)90418-9.

200. Oh, K.J., Kim, S.M., Hong, J.S., Maymon, E., Erez, O., Panaitescu, B., Gomez-Lopez, N., Romero, R., and Yoon, B.H. (2017). Twenty-four percent of patients with clinical chorioamnionitis in preterm gestations have no evidence of either culture-proven intraamniotic infection or intraamniotic inflammation. Am J Obstet Gynecol *216*, 604 e601-604 e611. 10.1016/j.ajog.2017.02.035.

201. Barros, F.C., Papageorghiou, A.T., Victora, C.G., Noble, J.A., Pang, R., Iams, J., Cheikh Ismail, L., Goldenberg, R.L., Lambert, A., Kramer, M.S., et al. (2015). The distribution of clinical phenotypes of preterm birth syndrome: implications for prevention. JAMA Pediatr *169*, 220-229. 10.1001/jamapediatrics.2014.3040.

202. Goldenberg, R.L., Culhane, J.F., Iams, J.D., and Romero, R. (2008). Epidemiology and causes of preterm birth. Lancet *371*, 75-84. 10.1016/S0140-6736(08)60074-4.

203. Romero, R., Espinoza, J., Kusanovic, J.P., Gotsch, F., Hassan, S., Erez, O., Chaiworapongsa, T., and Mazor, M. (2006). The preterm parturition syndrome. BJOG *113 Suppl 3*, 17-42. 10.1111/j.1471-0528.2006.01120.x.

204. Chang, E.Y., Zhang, J., Sullivan, S., Newman, R., and Singh, I. (2012). N-acetylcysteine prevents preterm birth by attenuating the LPS-induced expression of contractile associated proteins in an animal model. J Matern Fetal Neonatal Med *25*, 2395-2400. 10.3109/14767058.2012.697942.

205. Elovitz, M., and Wang, Z. (2004). Medroxyprogesterone acetate, but not progesterone, protects against inflammation-induced parturition and intrauterine fetal demise. Am J Obstet Gynecol *190*, 693-701. 10.1016/j.ajog.2003.10.693.

206. Simmons, D.L., Xie, W., Chipman, J.G., and Evett, G.E. (1991). Multiple cyclooxygenases: cloning of a mitogen-inducible form. Prostaglandins, Leukotrienes, Lipoxins, and PAF: Mechanism of Action, Molecular Biology, and Clinical Applications, 67-78.

207. Smith, W.L., and Dewitt, D.L. (1996). Prostaglandin endoperoxide H synthases-1 and -2. Adv Immunol *62*, 167-215. 10.1016/s0065-2776(08)60430-7.

208. Casey, M.L., and MacDonald, P.C. (1993). Cytokines in the human placenta, fetal membranes, uterine decidua, and amniotic fluid. Molecular aspects of placental and fetal membrane autacoids *361*.

209. Hillier, K., Calder, A.A., and Embrey, M.P. (1974). Concentrations of prostaglandin F2alpha in amniotic fluid and plasma in spontaneous and induced labours. J Obstet Gynaecol Br Commonw *81*, 257-263. 10.1111/j.1471-0528.1974.tb00457.x.

210. Kelly, R.W. (1994). Pregnancy maintenance and parturition: the role of prostaglandin in manipulating the immune and inflammatory response. Endocr Rev *15*, 684-706. 10.1210/edrv-15-5-684.

211. Mijovic, J.E., Zakar, T., Angelova, J., and Olson, D.M. (1999). Prostaglandin endoperoxide H synthase mRNA expression in the human amnion and decidua during pregnancy and in the amnion at preterm labour. Mol Hum Reprod *5*, 182-187. 10.1093/molehr/5.2.182.

212. Mijovic, J.E., Zakar, T., Nairn, T.K., and Olson, D.M. (1998). Prostaglandin endoperoxide H synthase (PGHS) activity and PGHS-1 and -2 messenger ribonucleic acid abundance in human chorion throughout gestation and with preterm labor. J Clin Endocrinol Metab *83*, 1358-1367. 10.1210/jcem.83.4.4692.

213. Fidel, P.L., Jr., Romero, R., Wolf, N., Cutright, J., Ramirez, M., Araneda, H., and Cotton, D.B. (1994). Systemic and local cytokine profiles in endotoxin-induced preterm parturition in mice. Am J Obstet Gynecol *170*, 1467-1475. 10.1016/s0002-9378(94)70180-6.

214. Besinger, R.E., Niebyl, J.R., Keyes, W.G., and Johnson, T.R. (1991). Randomized comparative trial of indomethacin and ritodrine for the long-term treatment of preterm labor. Am J Obstet Gynecol *164*, 981-986; discussion 986-988. 10.1016/0002-9378(91)90569-d.

215. Kurki, T., Eronen, M., Lumme, R., and Ylikorkala, O. (1991). A randomized double-dummy comparison between indomethacin and nylidrin in threatened preterm labor. Obstet Gynecol *78*, 1093-1097.

216. Moise, K.J., Jr., Huhta, J.C., Sharif, D.S., Ou, C.N., Kirshon, B., Wasserstrum, N., and Cano, L. (1988). Indomethacin in the treatment of premature labor. Effects on the fetal ductus arteriosus. N Engl J Med *319*, 327-331. 10.1056/NEJM198808113190602.

217. Norton, M.E., Merrill, J., Cooper, B.A., Kuller, J.A., and Clyman, R.I. (1993). Neonatal complications after the administration of indomethacin for preterm labor. N Engl J Med *329*, 1602-1607. 10.1056/NEJM199311253292202.

218. Elovitz, M.A., and Mrinalini, C. (2004). Animal models of preterm birth. Trends Endocrinol Metab *15*, 479-487. 10.1016/j.tem.2004.10.009.

219. Hirsch, E., and Muhle, R. (2002). Intrauterine bacterial inoculation induces labor in the mouse by mechanisms other than progesterone withdrawal. Biol Reprod *67*, 1337-1341. 10.1095/biolreprod67.4.1337.

220. Carpentier, P.A., Dingman, A.L., and Palmer, T.D. (2011). Placental TNF-alpha signaling in illness-induced complications of pregnancy. Am J Pathol *178*, 2802-2810. 10.1016/j.ajpath.2011.02.042.

221. Liu, W., Xu, C., You, X., Olson, D.M., Chemtob, S., Gao, L., and Ni, X. (2016). Hydrogen Sulfide Delays LPS-Induced Preterm Birth in Mice via Anti-Inflammatory Pathways. PLoS One *11*, e0152838. 10.1371/journal.pone.0152838.

222. Lin, Y., Xie, M., Chen, Y., Di, J., and Zeng, Y. (2006). Preterm delivery induced by LPS in syngeneically impregnated BALB/c and NOD/SCID mice. J Reprod Immunol *71*, 87-101. 10.1016/j.jri.2006.01.005.

223. Gonzalez, J.M., Franzke, C.W., Yang, F., Romero, R., and Girardi, G. (2011). Complement activation triggers metalloproteinases release inducing cervical remodeling and preterm birth in mice. Am J Pathol *179*, 838-849. 10.1016/j.ajpath.2011.04.024.

224. Damdimopoulou, P., Chiang, C., and Flaws, J.A. (2019). Retinoic acid signaling in ovarian folliculogenesis and steroidogenesis. Reprod Toxicol *87*, 32-41. 10.1016/j.reprotox.2019.04.007.

225. Austenaa, L.M., Carlsen, H., Hollung, K., Blomhoff, H.K., and Blomhoff, R. (2009). Retinoic acid dampens LPS-induced NF-kappaB activity: results from human monoblasts and in vivo imaging of NF-kappaB reporter mice. J Nutr Biochem *20*, 726-734. 10.1016/j.jnutbio.2008.07.002.

226. Moon, K.Y. (2007). The chemopreventive effect of retinoids on cellular NF-kappaB activity induced by NMU and NEU in human malignant keratinocytes. Cancer Res Treat *39*, 82-87. 10.4143/crt.2007.39.2.82.

227. Sierra-Mondragon, E., Molina-Jijon, E., Namorado-Tonix, C., Rodriguez-Munoz, R., Pedraza-Chaverri, J., and Reyes, J.L. (2018). All-trans retinoic acid ameliorates inflammatory response mediated by TLR4/NF-kappaB during initiation of diabetic nephropathy. J Nutr Biochem *60*, 47-60. 10.1016/j.jnutbio.2018.06.002.

228. Wang, C., Lee, J.E., Cho, Y.W., Xiao, Y., Jin, Q., Liu, C., and Ge, K. (2012). UTX regulates mesoderm differentiation of embryonic stem cells independent of H3K27 demethylase activity. Proc Natl Acad Sci U S A *109*, 15324-15329. 10.1073/pnas.1204166109.

229. Osokine, I., Siewiera, J., Rideaux, D., Ma, S., Tsukui, T., and Erlebacher, A. (2022). Gene silencing by EZH2 suppresses TGF-beta activity within the decidua to avert pregnancy-adverse wound healing at the maternal-fetal interface. Cell Rep *38*, 110329. 10.1016/j.celrep.2022.110329.

230. Carson, D.D., Bagchi, I., Dey, S.K., Enders, A.C., Fazleabas, A.T., Lessey, B.A., and Yoshinaga, K. (2000). Embryo implantation. Dev Biol *223*, 217-237. 10.1006/dbio.2000.9767.

231. Dey, S.K., Lim, H., Das, S.K., Reese, J., Paria, B.C., Daikoku, T., and Wang, H. (2004). Molecular cues to implantation. Endocr Rev *25*, 341-373. 10.1210/er.2003-0020.

232. Ramathal, C.Y., Bagchi, I.C., Taylor, R.N., and Bagchi, M.K. (2010). Endometrial decidualization: of mice and men. Semin Reprod Med *28*, 17-26. 10.1055/s-0029-1242989.

233. Mori, M., Bogdan, A., Balassa, T., Csabai, T., and Szekeres-Bartho, J. (2016). The decidua-the maternal bed embracing the embryo-maintains the pregnancy. Semin Immunopathol *38*, 635-649. 10.1007/s00281-016-0574-0.

234. Ni, N., and Li, Q. (2017). TGFbeta superfamily signaling and uterine decidualization. Reprod Biol Endocrinol *15*, 84. 10.1186/s12958-017-0303-0.

235. Lee, K.Y., Jeong, J.W., Wang, J., Ma, L., Martin, J.F., Tsai, S.Y., Lydon, J.P., and DeMayo, F.J. (2007). Bmp2 is critical for the murine uterine decidual response. Mol Cell Biol *27*, 5468-5478. 10.1128/MCB.00342-07.

236. Paria, B.C., Ma, W., Tan, J., Raja, S., Das, S.K., Dey, S.K., and Hogan, B.L. (2001). Cellular and molecular responses of the uterus to embryo implantation can be elicited by locally applied growth factors. Proc Natl Acad Sci U S A *98*, 1047-1052. 10.1073/pnas.98.3.1047.

237. Ying, Y., and Zhao, G.Q. (2000). Detection of multiple bone morphogenetic protein messenger ribonucleic acids and their signal transducer, Smad1, during mouse decidualization. Biol Reprod *63*, 1781-1786. 10.1095/biolreprod63.6.1781.

238. Clementi, C., Tripurani, S.K., Large, M.J., Edson, M.A., Creighton, C.J., Hawkins, S.M., Kovanci, E., Kaartinen, V., Lydon, J.P., Pangas, S.A., DeMayo, F.J., and Matzuk, M.M. (2013). Activin-like kinase 2 functions in peri-implantation uterine signaling in mice and humans. PLoS Genet *9*, e1003863. 10.1371/journal.pgen.1003863.

239. Nagashima, T., Li, Q., Clementi, C., Lydon, J.P., DeMayo, F.J., and Matzuk, M.M. (2013). BMPR2 is required for postimplantation uterine function and pregnancy maintenance. J Clin Invest *123*, 2539-2550. 10.1172/JCI65710.

240. Fang, X., Ni, N., Gao, Y., Lydon, J.P., Ivanov, I., Rijnkels, M., Bayless, K.J., and Li, Q. (2020). Transforming growth factor beta signaling and decidual integrity in micedagger. Biol Reprod *103*, 1186-1198. 10.1093/biolre/ioaa155.

241. Peng, J., Monsivais, D., You, R., Zhong, H., Pangas, S.A., and Matzuk, M.M. (2015). Uterine activin receptor-like kinase 5 is crucial for blastocyst implantation and placental development. Proc Natl Acad Sci U S A *112*, E5098-5107. 10.1073/pnas.1514498112.

242. Gellersen, B., and Brosens, J.J. (2014). Cyclic decidualization of the human endometrium in reproductive health and failure. Endocr Rev *35*, 851-905. 10.1210/er.2014-1045.

243. Fullerton, P.T., Jr., Monsivais, D., Kommagani, R., and Matzuk, M.M. (2017). Follistatin is critical for mouse uterine receptivity and decidualization. Proc Natl Acad Sci U S A *114*, E4772-E4781. 10.1073/pnas.1620903114.

244. Candia, A.F., Watabe, T., Hawley, S.H., Onichtchouk, D., Zhang, Y., Derynck, R., Niehrs, C., and Cho, K.W. (1997). Cellular interpretation of multiple TGF-beta signals: intracellular antagonism between activin/BVg1 and BMP-2/4 signaling mediated by Smads. Development *124*, 4467-4480. 10.1242/dev.124.22.4467.

245. Ramsdell, A.F., and Yost, H.J. (1999). Cardiac looping and the vertebrate left-right axis: antagonism of left-sided Vg1 activity by a right-sided ALK2-dependent BMP pathway. Development *126*, 5195-5205. 10.1242/dev.126.23.5195.

246. Yamamoto, M., Beppu, H., Takaoka, K., Meno, C., Li, E., Miyazono, K., and Hamada, H. (2009). Antagonism between Smad1 and Smad2 signaling determines the site of distal visceral endoderm formation in the mouse embryo. J Cell Biol *184*, 323-334. 10.1083/jcb.200808044.

247. Goumans, M.J., Lebrin, F., and Valdimarsdottir, G. (2003). Controlling the angiogenic switch: a balance between two distinct TGF-b receptor signaling pathways. Trends Cardiovasc Med *13*, 301-307. 10.1016/s1050-1738(03)00142-7.

248. Rebbapragada, A., Benchabane, H., Wrana, J.L., Celeste, A.J., and Attisano, L. (2003). Myostatin signals through a transforming growth factor beta-like signaling pathway to block adipogenesis. Mol Cell Biol *23*, 7230-7242. 10.1128/MCB.23.20.7230-7242.2003.

249. Sartori, R., Schirwis, E., Blaauw, B., Bortolanza, S., Zhao, J., Enzo, E., Stantzou, A., Mouisel, E., Toniolo, L., Ferry, A., et al. (2013). BMP signaling controls muscle mass. Nat Genet *45*, 1309-1318. 10.1038/ng.2772.

250. Winbanks, C.E., Chen, J.L., Qian, H., Liu, Y., Bernardo, B.C., Beyer, C., Watt, K.I., Thomson, R.E., Connor, T., Turner, B.J., et al. (2013). The bone morphogenetic protein axis is a positive regulator of skeletal muscle mass. J Cell Biol *203*, 345-357. 10.1083/jcb.201211134.

251. Zhao, L., Yee, M., and O'Reilly, M.A. (2013). Transdifferentiation of alveolar epithelial type II to type I cells is controlled by opposing TGF-beta and BMP signaling. Am J Physiol Lung Cell Mol Physiol *305*, L409-418. 10.1152/ajplung.00032.2013.

252. Zode, G.S., Clark, A.F., and Wordinger, R.J. (2009). Bone morphogenetic protein 4 inhibits TGF-beta2 stimulation of extracellular matrix proteins in optic nerve head cells: role of gremlin in ECM modulation. Glia *57*, 755-766. 10.1002/glia.20803.

253. Abe, Y., Minegishi, T., and Leung, P.C. (2004). Activin receptor signaling. Growth Factors *22*, 105-110. 10.1080/08977190410001704688.

254. Nallasamy, S., Li, Q., Bagchi, M.K., and Bagchi, I.C. (2012). Msx homeobox genes critically regulate embryo implantation by controlling paracrine signaling between uterine stroma and epithelium. PLoS Genet *8*, e1002500. 10.1371/journal.pgen.1002500.

255. Andricovich, J., Perkail, S., Kai, Y., Casasanta, N., Peng, W., and Tzatsos, A. (2018). Loss of KDM6A Activates Super-Enhancers to Induce Gender-Specific Squamous-like Pancreatic Cancer and Confers Sensitivity to BET Inhibitors. Cancer Cell *33*, 512-526 e518. 10.1016/j.ccell.2018.02.003.

256. Faralli, H., Wang, C., Nakka, K., Benyoucef, A., Sebastian, S., Zhuang, L., Chu, A., Palii, C.G., Liu, C., Camellato, B., et al. (2016). UTX demethylase activity is required for satellite cell-mediated muscle regeneration. J Clin Invest *126*, 1555-1565. 10.1172/JCI83239.

257. Gozdecka, M., Meduri, E., Mazan, M., Tzelepis, K., Dudek, M., Knights, A.J., Pardo, M., Yu, L., Choudhary, J.S., Metzakopian, E., et al. (2018). UTX-mediated enhancer and chromatin remodeling suppresses myeloid leukemogenesis through noncatalytic inverse regulation of ETS and GATA programs. Nat Genet *50*, 883-894. 10.1038/s41588-018-0114-z.

258. Morales Torres, C., Laugesen, A., and Helin, K. (2013). Utx is required for proper induction of ectoderm and mesoderm during differentiation of embryonic stem cells. PLoS One *8*, e60020. 10.1371/journal.pone.0060020.

259. Vandamme, J., Lettier, G., Sidoli, S., Di Schiavi, E., Norregaard Jensen, O., and Salcini, A.E. (2012). The C. elegans H3K27 demethylase UTX-1 is essential for normal development, independent of its enzymatic activity. PLoS Genet *8*, e1002647. 10.1371/journal.pgen.1002647.

260. Shpargel, K.B., Sengoku, T., Yokoyama, S., and Magnuson, T. (2012). UTX and UTY demonstrate histone demethylase-independent function in mouse embryonic development. PLoS Genet *8*, e1002964. 10.1371/journal.pgen.1002964.

261. Welstead, G.G., Creyghton, M.P., Bilodeau, S., Cheng, A.W., Markoulaki, S., Young, R.A., and Jaenisch, R. (2012). X-linked H3K27me3 demethylase Utx is required for embryonic development in a sex-specific manner. Proc Natl Acad Sci U S A *109*, 13004-13009. 10.1073/pnas.1210787109.

262. Leng, X., Wang, J., An, N., Wang, X., Sun, Y., and Chen, Z. (2020). Histone 3 lysine-27 demethylase KDM6A coordinates with KMT2B to play an oncogenic role in NSCLC by regulating H3K4me3. Oncogene *39*, 6468-6479. 10.1038/s41388-020-01449-y.

263. Maurya, V.K., Jha, R.K., Kumar, V., Joshi, A., Chadchan, S., Mohan, J.J., and Laloraya, M. (2013). Transforming growth factor-beta 1 (TGF-B1) liberation from its latent complex during embryo implantation and its regulation by estradiol in mouse. Biol Reprod *89*, 84. 10.1095/biolreprod.112.106542.

264. Shooner, C., Caron, P.L., Frechette-Frigon, G., Leblanc, V., Dery, M.C., and Asselin, E. (2005). TGF-beta expression during rat pregnancy and activity on decidual cell survival. Reprod Biol Endocrinol *3*, 20. 10.1186/1477-7827-3-20.

265. Xiao, J.F., Kua, L.F., Ding, L.W., Sun, Q.Y., Myint, K.N., Chia, X.R., Venkatachalam, N., Loh, X., Duex, J.E., Neang, V., et al. (2022). KDM6A Depletion in Breast Epithelial Cells Leads to Reduced Sensitivity to Anticancer Agents and Increased TGFbeta Activity. Mol Cancer Res *20*, 637-649. 10.1158/1541-7786.MCR-21-0402.

266. Jia, Y., Reddy, M.A., Das, S., Oh, H.J., Abdollahi, M., Yuan, H., Zhang, E., Lanting, L., Wang, M., and Natarajan, R. (2019). Dysregulation of histone H3 lysine 27

trimethylation in transforming growth factor-beta1-induced gene expression in mesangial cells and diabetic kidney. J Biol Chem *294*, 12695-12707. 10.1074/jbc.RA119.007575.

267. Afshar, Y., Jeong, J.W., Roqueiro, D., DeMayo, F., Lydon, J., Radtke, F., Radnor, R., Miele, L., and Fazleabas, A. (2012). Notch1 mediates uterine stromal differentiation and is critical for complete decidualization in the mouse. FASEB J *26*, 282-294. 10.1096/fj.11-184663.

268. Daikoku, T., Cha, J., Sun, X., Tranguch, S., Xie, H., Fujita, T., Hirota, Y., Lydon, J., DeMayo, F., Maxson, R., and Dey, S.K. (2011). Conditional deletion of Msx homeobox genes in the uterus inhibits blastocyst implantation by altering uterine receptivity. Dev Cell *21*, 1014-1025. 10.1016/j.devcel.2011.09.010.

269. Guzeloglu-Kayisli, O., Semerci, N., Guo, X., Larsen, K., Ozmen, A., Arlier, S., Mutluay, D., Nwabuobi, C., Sipe, B., Buhimschi, I., et al. (2021). Decidual cell FKBP51-progesterone receptor binding mediates maternal stress-induced preterm birth. Proc Natl Acad Sci U S A *118*. 10.1073/pnas.2010282118.

270. Mizugishi, K., Li, C., Olivera, A., Bielawski, J., Bielawska, A., Deng, C.X., and Proia, R.L. (2007). Maternal disturbance in activated sphingolipid metabolism causes pregnancy loss in mice. J Clin Invest *117*, 2993-3006. 10.1172/JCI30674.

271. Reardon, S.N., King, M.L., MacLean, J.A., 2nd, Mann, J.L., DeMayo, F.J., Lydon, J.P., and Hayashi, K. (2012). CDH1 is essential for endometrial differentiation, gland development, and adult function in the mouse uterus. Biol Reprod *86*, 141, 141-110. 10.1095/biolreprod.112.098871.

272. Reese, J., Binart, N., Brown, N., Ma, W.G., Paria, B.C., Das, S.K., Kelly, P.A., and Dey, S.K. (2000). Implantation and decidualization defects in prolactin receptor (PRLR)-

deficient mice are mediated by ovarian but not uterine PRLR. Endocrinology *141*, 1872-1881. 10.1210/endo.141.5.7464.

273. Shindoh, H., Okada, H., Tsuzuki, T., Nishigaki, A., and Kanzaki, H. (2014). Requirement of heart and neural crest derivatives-expressed transcript 2 during decidualization of human endometrial stromal cells in vitro. Fertil Steril *101*, 1781-1790 e1781-1785. 10.1016/j.fertnstert.2014.03.013.

274. Zhang, C., Large, M.J., Duggavathi, R., DeMayo, F.J., Lydon, J.P., Schoonjans, K., Kovanci, E., and Murphy, B.D. (2013). Liver receptor homolog-1 is essential for pregnancy. Nat Med *19*, 1061-1066. 10.1038/nm.3192.

275. Draper, L.B., Chong, H., Wang, E., and Woodruff, T.K. (1997). The uterine myometrium is a target for increased levels of activin A during pregnancy. Endocrinology *138*, 3042-3046. 10.1210/endo.138.7.5231.

276. Petraglia, F., Florio, P., Gallinelli, A., De Micheroux, A.A., Ferrari, A., De Vita, D., Aguzzoli, L., Genazzani, A.D., and Di Carlo, C. (1994). Secretion and putative role of activin and CRF in human parturition. Ann N Y Acad Sci *734*, 380-386. 10.1111/j.1749-6632.1994.tb21769.x.

277. Petraglia, F., Gallinelli, A., De Vita, D., Lewis, K., Mathews, L., and Vale, W. (1994). Activin at parturition: changes of maternal serum levels and evidence for binding sites in placenta and fetal membranes. Obstet Gynecol *84*, 278-282.

278. Petraglia, F., Anceschi, M.M., Calza, L., Garuti, G.C., Fusaro, P., Giardino, L., Genazzani, A.R., and Vale, W. (1993). Inhibin and activin in human fetal membranes: evidence for a local effect on prostaglandin release. J Clin Endocrinol Metab *77*, 542-548. 10.1210/jcem.77.2.8345060.

279. Vale, W., Hsueh, A., Rivier, C., Yu, J. (1990). The Inhibin/Activin Family of Hormones and Growth Factors (Springer Berlin Heidelberg).

280. McConaha, M.E., Eckstrum, K., An, J., Steinle, J.J., and Bany, B.M. (2011). Microarray assessment of the influence of the conceptus on gene expression in the mouse uterus during decidualization. Reproduction *141*, 511-527. 10.1530/REP-10-0358.

281. Peters, D.E., Zhang, Y., Molinolo, A.A., Miller-Randolph, S., Szabo, R., Bugge, T.H., Leppla, S.H., and Liu, S. (2012). Capillary morphogenesis protein-2 is required for mouse parturition by maintaining uterine collagen homeostasis. Biochem Biophys Res Commun *422*, 393-397. 10.1016/j.bbrc.2012.04.160.

282. Tranguch, S., Smith, D.F., and Dey, S.K. (2007). Progesterone receptor requires a co-chaperone for signalling in uterine biology and implantation. Reprod Biomed Online *14 Spec No 1*, 39-48. 10.1016/S1472-6483(10)61457-5.

283. Ratajczak, T., Ward, B.K., and Minchin, R.F. (2003). Immunophilin chaperones in steroid receptor signalling. Curr Top Med Chem *3*, 1348-1357. 10.2174/1568026033451934.

284. Sanchez, E.R. (2012). Chaperoning steroidal physiology: lessons from mouse genetic models of Hsp90 and its cochaperones. Biochim Biophys Acta *1823*, 722-729. 10.1016/j.bbamcr.2011.11.006.

285. Pollard, J.W., Hunt, J.S., Wiktor-Jedrzejczak, W., and Stanley, E.R. (1991). A pregnancy defect in the osteopetrotic (op/op) mouse demonstrates the requirement for CSF-1 in female fertility. Dev Biol *148*, 273-283. 10.1016/0012-1606(91)90336-2.

286. Chow, L., and Lye, S.J. (1994). Expression of the gap junction protein connexin-43 is increased in the human myometrium toward term and with the onset of labor. Am J Obstet Gynecol *170*, 788-795. 10.1016/s0002-9378(94)70284-5.

287. Kilarski, W.M., Dupont, E., Coppen, S., Yeh, H.I., Vozzi, C., Gourdie, R.G., Rezapour, M., Ulmsten, U., Roomans, G.M., and Severs, N.J. (1998). Identification of two further gap-junctional proteins, connexin40 and connexin45, in human myometrial smooth muscle cells at term. Eur J Cell Biol *75*, 1-8. 10.1016/S0171-9335(98)80040-X.

288. Kilarski, W.M., Rothery, S., Roomans, G.M., Ulmsten, U., Rezapour, M., Stevenson, S., Coppen, S.R., Dupont, E., and Severs, N.J. (2001). Multiple connexins localized to individual gap-junctional plaques in human myometrial smooth muscle. Microsc Res Tech *54*, 114-122. 10.1002/jemt.1126.

289. Orsino, A., Taylor, C.V., and Lye, S.J. (1996). Connexin-26 and connexin-43 are differentially expressed and regulated in the rat myometrium throughout late pregnancy and with the onset of labor. Endocrinology *137*, 1545-1553. 10.1210/endo.137.5.8612484.

290. Ou, C.W., Orsino, A., and Lye, S.J. (1997). Expression of connexin-43 and connexin-26 in the rat myometrium during pregnancy and labor is differentially regulated by mechanical and hormonal signals. Endocrinology *138*, 5398-5407. 10.1210/endo.138.12.5624.

291. Idzko, M., Ferrari, D., and Eltzschig, H.K. (2014). Nucleotide signalling during inflammation. Nature *509*, 310-317. 10.1038/nature13085.

292. Muller, T., Robaye, B., Vieira, R.P., Ferrari, D., Grimm, M., Jakob, T., Martin, S.F., Di Virgilio, F., Boeynaems, J.M., Virchow, J.C., and Idzko, M. (2010). The purinergic receptor P2Y2 receptor mediates chemotaxis of dendritic cells and eosinophils in allergic lung inflammation. Allergy *65*, 1545-1553. 10.1111/j.1398-9995.2010.02426.x.

293. El-Naccache, D.W., Hasko, G., and Gause, W.C. (2021). Early Events Triggering the Initiation of a Type 2 Immune Response. Trends Immunol *42*, 151-164. 10.1016/j.it.2020.11.006.

294. Li, R., Shang, Y., Hu, X., Yu, Y., Zhou, T., Xiong, W., and Zou, X. (2020). ATP/P2X7r axis mediates the pathological process of allergic asthma by inducing M2 polarization of alveolar macrophages. Exp Cell Res *386*, 111708. 10.1016/j.yexcr.2019.111708.

295. Kurashima, Y., Amiya, T., Nochi, T., Fujisawa, K., Haraguchi, T., Iba, H., Tsutsui, H., Sato, S., Nakajima, S., Iijima, H., et al. (2012). Extracellular ATP mediates mast cell-dependent intestinal inflammation through P2X7 purinoceptors. Nat Commun *3*, 1034. 10.1038/ncomms2023.

296. Jordan, P.M., Andreas, N., Groth, M., Wegner, P., Weber, F., Jager, U., Kuchler, C., Werz, O., Serfling, E., Kamradt, T., Dudeck, A., and Drube, S. (2021). ATP/IL-33-triggered hyperactivation of mast cells results in an amplified production of pro-inflammatory cytokines and eicosanoids. Immunology *164*, 541-554. 10.1111/imm.13386.

297. Straus, D.B., Pryor, D., Haque, T.T., Kee, S.A., Dailey, J.M., Jackson, K.G., Barnstein, B.O., and Ryan, J.J. (2022). IL-33 priming amplifies ATP-mediated mast cell cytokine production. Cell Immunol *371*, 104470. 10.1016/j.cellimm.2021.104470.

298. Furuya, K., Sokabe, M., and Furuya, S. (2005). Characteristics of subepithelial fibroblasts as a mechano-sensor in the intestine: cell-shape-dependent ATP release and P2Y1 signaling. J Cell Sci *118*, 3289-3304. 10.1242/jcs.02453.

299. Murata, N., Ito, S., Furuya, K., Takahara, N., Naruse, K., Aso, H., Kondo, M., Sokabe, M., and Hasegawa, Y. (2014). Ca2+ influx and ATP release mediated by mechanical

stretch in human lung fibroblasts. Biochem Biophys Res Commun *453*, 101-105. 10.1016/j.bbrc.2014.09.063.

300. Alotaibi, M. (2018). Changes in expression of P2X7 receptors in rat myometrium at different gestational stages and the mechanism of ATP-induced uterine contraction. Life Sci *199*, 151-157. 10.1016/j.lfs.2018.03.016.

301. Hutchings, G., Gevaert, T., Deprest, J., Nilius, B., Williams, O., and De Ridder, D. (2009). The effect of extracellular adenosine triphosphate on the spontaneous contractility of human myometrial strips. Eur J Obstet Gynecol Reprod Biol *143*, 79-83. 10.1016/j.ejogrb.2008.12.004.

302. Tsimis, M.E., Lei, J., Rosenzweig, J.M., Arif, H., Shabi, Y., Alshehri, W., Talbot, C.C., Baig-Ward, K.M., Segars, J., Graham, E.M., and Burd, I. (2017). P2X7 receptor blockade prevents preterm birth and perinatal brain injury in a mouse model of intrauterine inflammation. Biol Reprod *97*, 230-239. 10.1093/biolre/iox081.

303. Osman, I., Young, A., Ledingham, M.A., Thomson, A.J., Jordan, F., Greer, I.A., and Norman, J.E. (2003). Leukocyte density and pro-inflammatory cytokine expression in human fetal membranes, decidua, cervix and myometrium before and during labour at term. Mol Hum Reprod *9*, 41-45. 10.1093/molehr/gag001.

304. Shynlova, O., Tsui, P., Dorogin, A., and Lye, S.J. (2008). Monocyte chemoattractant protein-1 (CCL-2) integrates mechanical and endocrine signals that mediate term and preterm labor. J Immunol *181*, 1470-1479. 10.4049/jimmunol.181.2.1470.

305. Thomson, A.J., Telfer, J.F., Young, A., Campbell, S., Stewart, C.J., Cameron, I.T., Greer, I.A., and Norman, J.E. (1999). Leukocytes infiltrate the myometrium during human

parturition: further evidence that labour is an inflammatory process. Hum Reprod *14*, 229-236.

306. Ledingham, M.A., Thomson, A.J., Jordan, F., Young, A., Crawford, M., and Norman, J.E. (2001). Cell adhesion molecule expression in the cervix and myometrium during pregnancy and parturition. Obstet Gynecol *97*, 235-242. 10.1016/s0029-7844(00)01126-1.

307. Esplin, M.S., Peltier, M.R., Hamblin, S., Smith, S., Fausett, M.B., Dildy, G.A., Branch, D.W., Silver, R.M., and Adashi, E.Y. (2005). Monocyte chemotactic protein-1 expression is increased in human gestational tissues during term and preterm labor. Placenta *26*, 661-671. 10.1016/j.placenta.2004.09.012.

308. Mitchell, C.M., Hirst, J.J., Mitchell, M.D., Murray, H.G., and Zakar, T. (2019). Genes upregulated in the amnion at labour are bivalently marked by activating and repressive histone modifications. Mol Hum Reprod *25*, 228-240. 10.1093/molehr/gaz007.

309. Williams, S.T., Walport, L.J., Hopkinson, R.J., Madden, S.K., Chowdhury, R., Schofield, C.J., and Kawamura, A. (2014). Studies on the catalytic domains of multiple JmjC oxygenases using peptide substrates. Epigenetics *9*, 1596-1603. 10.4161/15592294.2014.983381.

310. Deal, R.B., Henikoff, J.G., and Henikoff, S. (2010). Genome-wide kinetics of nucleosome turnover determined by metabolic labeling of histones. Science *328*, 1161-1164. 10.1126/science.1186777.

Publishing Agreement

It is the policy of the University to encourage open access and broad distribution of all theses, dissertations, and manuscripts. The Graduate Division will facilitate the distribution of UCSF theses, dissertations, and manuscripts to the UCSF Library for open access and distribution. UCSF will make such theses, dissertations, and manuscripts accessible to the public and will take reasonable steps to preserve these works in perpetuity.

I hereby grant the non-exclusive, perpetual right to The Regents of the University of California to reproduce, publicly display, distribute, preserve, and publish copies of my thesis, dissertation, or manuscript in any form or media, now existing or later derived, including access online for teaching, research, and public service purposes.

DocuSigned by:
TARA MCINTYRE
4F9D5699B025405...
Author Signature

2/23/2024
Date